Adam Mickiewicz University in Poznań, Poland
Institute of Geoecology and Geoinformation

The present-day state of Svenbreen (Svalbard) and changes of its physical properties after the termination of the Little Ice Age

Jakub Małecki

Doctoral Dissertation
June 2013

PhD thesis in geography

The present-day state of Svenbreen (Svalbard) and changes of its physical properties after the termination of the Little Ice Age

by

Jakub Małecki

Supervised by prof. Andrzej Kostrzewski (Adam Mickiewicz University in Poznań)
In collaboration with prof. Douglas I. Benn (University Centre in Svalbard)

Reviewers:
prof. Krzysztof Migała (University of Wrocław)
prof. Grzegorz Rachlewicz (Adam Mickiewicz University in Poznań)

Revised version 2.1

June 2013

Contents

Acknowledgements

This work would not have been possible without help of many people and institutions. First, sincere acknowledgements are addressed to my love Natalia, for sacrifice and patience during my few-year long research. Her endless love, great trust and support gave my energy and motivation at each level of this work, which is fully dedicated to her. Thanks are due to my parents, Iwona and Paweł, for giving me MSc. degree, home and perfect working conditions. Generous funding of the field research and research stays was provided by the Polish National Science Centre (project N N306 062940), by the Research Council of Norway (Yggdrasil personal mobility grant 211133/F11) and by the author's home institution Adam Mickiewicz University in Poznań (AMU), Poland (allowance for research stay at University Centre in Svalbard, UNIS). Cooperation with UNIS is greatly appreciated, as it significantly expanded research possibilities on Svenbreen. Yearly research stay at University of Oslo (UiO) resulted in much wider understanding of numerous problems discussed in this work. Norwegian Polar Institute (NPI), supported the project by providing 1960 and 1990 NPI topography data (particular thanks are due to Anders Skoglund).

I dedicate special thanks to prof. Andrzej Kostrzewski (AMU) for supervision of this work, for his care and for introducing me to the polar world. I deeply appreciate collaboration with prof. Douglas I. Benn (UNIS) for substantial and technical support to this thesis. Prof. Jon Ove Hagen, prof. Thomas Vikhamar Schuler, Thorben Dunse and Christopher Nuth (UiO) are acknowledged for teaching me numerous new research techniques. Nothing could be done in the field without disinterested assistance of many people, including all members of AMU polar expeditions, particularly:

(alphabetically)

Agata Buchwał
Marek Ewertowski
Adam Nawrot
Krzysztof Pleskot
prof. Grzegorz Rachlewicz
Mateusz Strzelecki
Józef Szpikowski
Aleksandra Tomczyk
Tomasz Wawrzyniak

...and colleagues from other institutions:

Alexandra Bernardová
Daniel Binder
Camille Faucherre
Samuel Faucherre
Bernard Hynek
Þorlakur Jon Ingolfsson
Jan Kavan
Steve Lewis

Prof. Grzegorz Rachlewicz is also acknowledged for discussions, sharing his polar enthusiasm and great leadership during the expeditions. Adam Nawrot was my first field-teacher in glaciology. Mateusz Strzelecki constructed and shared 2009 digital elevation models of the study area, being a very important element of this study. Samuel Faucherre and Steve Lewis were doing fantastic work during several winter and summer field campaigns on Svenbreen and nothing could be done without their flair and energy. Valentin gave me shelter while waiting for a delayed ship in Pyramiden town during few stormy days. Sebastian Sikora introduced me to the principles of electronics of the automatic weather station. Many thanks are also due to the reviewers of this work, prof. Krzysztof Migała and prof. Grzegorz Rachlewicz. Since the beginning of my PhD studentship I have been also receiving encouragement and many words of appreciation from my family: brother Michał, aunt Violetta and grandmothers Irena and Aleksandra.

To all of you, please accept my sincere thanks.

D z i ę k u j ę !

The project "Dickson Land ice masses evolution (Svalbard) after the termination of the Little Ice Age and their present-day state and functioning" (N N306 062940) was funded by Polish National Science Centre

Abstract

Melting Svalbard glaciers have been recognized as an early indicator of climate change. Large parts of these arctic islands remain however seldom investigated, including little glacier-covered Dickson Land in the interior of Svalbard. Impact of quasi-continental climate features (relatively low precipitation, humidity and high summer air temperature) on evolution of their physical properties and functioning of small local glaciers is poorly understood. The aim of this thesis is therefore to investigate the present-day state of a small Dickson Land valley glacier, Svenbreen in Petuniabukta (Pyramiden region), in the background of post-Little Ice Age changes of its physical properties. This work brings new fundamental data from many fields of glaciology, concerning volume changes, mass exchange, glacio-meteorology, energy balance, thermal structure, hydrology and dynamics, in many cases being the first from this region.

Analysis of topographic data showed that several Dickson Land glaciers have been thinning at average rates of -49 ± 22 cm a^{-1} between 1960 and 1990, while in the more recent interval 1990-2009 a distinct acceleration of their mass loss was noted (-78 ± 21 cm a^{-1}), linked to progressively warming climate in the region. Svenbreen showed relative resistance to increasing temperature by the least negative changes (-32 ± 19 cm a^{-1} and -61 ± 17 cm a^{-1} respectively for both analysed epochs). Local factors reducing its mass loss were studied in detail. Meteorological and hydrological investigations on the glacier surface were conducted in the period 2009-2012. Relatively high summer air temperature at the sea level does not translate to warmer conditions on the glacier, because of fast cooling with increasing elevation due to limited air moisture. Shortwave radiation incoming to the glacier surface is low, mainly because complex topography surrounding the glacier shades the ice surface, particularly since mid-August. Energy balance structure of Svenbreen shows significant differences when compared to other Svalbard glaciers, due to very low net radiation, negative latent heat flux and low overall melt energy.

Peculiar energy balance conditions shape the present-day structure and functioning of Svenbreen. While many small glaciers in central Svalbard freeze completely under a new, unfavourable climate, on Svenbreen a very small zone of temperate firn has most likely survived few decades of negative mass balance. The glacier is underlain by a thin layer of temperate ice along most of its length. Despite that, glacier flow velocity is very low, as lateral parts are frozen to the valley sides. Warm base makes englacial and subglacial water routing possible, however observations of icing fields suggest, that intraglacial drainage has been most likely experiencing negative changes in the recent years. Mass balance observations from 2008-2012 and direct investigations during three balance years 2010-2012 indicate, that positive net balance on the glacier occurs regularly, in contrast to other small Svalbard glaciers. Stake measurements gave enough data to draw an original temperature-ablation curve for Svenbreen, making it possible to reconstruct its summer balance until 1976. It confirmed much slower melting than on other glaciers in the archipelago.

The study concludes, that quasi-continental climate of central Svalbard, modified by local environmental factors, is well manifested in functioning of Svenbreen and that some small glaciers may be less sensitive to climate change, than it is commonly claimed for Svalbard. Further investigations are however needed to verify representativity of the presented records for regional extrapolations.

Abstrakt

Topniejące lodowce Svalbardu są wczesnym wskaźnikiem zmian klimatycznych. Znaczna część tych arktycznych wysp jest jednak rzadko reprezentowana w literaturze, włącznie ze słabo zlodowaconą Ziemią Dicksona. Region ten leży w wewnętrznych, quasi-kontynentalnych partiach Svalbardu, o bardzo niskich opadach i względnie niskiej wilgotności powietrza oraz stosunkowo wysokiej temperaturze powietrza w ciągu lata. Zagadnienie wpływu tej odmiany klimatu polarnego na ewolucję cech fizycznych i funkcjonowanie małych lodowców środkowego Svalbardu nie zostało do tej pory zbadane. Celem niniejszej rozprawy jest zatem rozpoznanie stanu aktualnego małego lodowca dolinnego Ziemi Dicksona, lodowca Sven (Svenbreen), Petuniabukta (rejon Pyramiden), na tle zmian jego cech fizycznych po Małej Epoce Lodowej. W pracy zawarte są elementarne dane glacjologiczne dotyczące zmian objętości lodowca, wymiany masy z otoczeniem, meteorologii, bilansu energii powierzchni, struktury termicznej, hydrologii i dynamiki, w wielu przypadkach pierwsze w regionie.

Analiza danych topograficznych dla kilku lodowców Ziemi Dicksona wskazuje na wyraźny ubytek ich masy w średnim tempie -49 ± 22 cm a^{-1} w latach (1960-1990) oraz jego przyspieszenie w ostatnich latach do -78 ± 21 cm a^{-1} (1990-2009), co wiązane jest w postępującym ociepleniem klimatu w regionie. Lodowiec Sven wykazał najbardziej powolne zmiany geometrii (-32 ± 19 cm a^{-1} i -61 ± 17 cm a^{-1}). Lokalne czynniki środowiskowe ograniczające negatywne zmiany w jego obrębie poddane zostały szczegółowym badaniom. Względnie wysoka temperatura powietrza w ciągu lata na poziomie morza nie przekłada się na zwiększenie temperatury bezpośrednio nad lodowcem na skutek szybkiego wychładzania powietrza wraz ze wzrostem wysokości, związanego z jego ograniczoną wilgotnością. Promieniowanie krótkofalowe docierające do powierzchni jest niskie, głównie z powodu otaczających lodowiec wysokich ścian skalnych i zacienienia, szczególnie od połowy sierpnia. Bilans energii powierzchni lodowca Sven jest wyjątkowy na tle Svalbardu, wyróżniając się szczególnie niskim udziałem bilansu radiacyjnego, ujemną wartością strumienia ciepła utajonego i ogólnie niską energią dostępną dla topnienia.

Specyficzne warunki bilansu energii kształtują współczesną strukturę i funkcjonowanie lodowca Sven. Podczas gdy wiele małych lodowców środkowego Svalbardu doświadcza zamarzania swoich dotychczas umiarkowanych partii pod wpływem zmian klimatycznych, na lodowcu Sven wciąż istnieje niewielki obszar umiarkowanego firnu oraz lód w punkcie topnienia pod ciśnieniem na kontakcie z podłożem. Pomimo tego, prędkość płynięcia lodowca jest bardzo niska, ponieważ jego partie boczne przymarznięte są do ścian doliny. Obserwacje tworzenia pokryw nalodziowych sugerują jednak o możliwości zmian termiki lodowca w ostatnich latach. Obserwacje bilansu masy z lat 2008-2012 wskazują na to, że dodatni bilans roczny może występować na lodowcu Sven regularnie, wyróżniając go na tle innych lodowców Svalbardu. Przyczyną jest znacznie ograniczone topnienie, na co wskazują m.in. pomiary bilansu energii i temperaturowy model ablacji wykonany dla lat 1976-2012.

Wyniki badań pozwalają stwierdzić, że quasi-kontynentalny klimat środkowego Svalbardu, modyfikowany przez czynniki lokalne, wyraźnie wpływa na funkcjonowanie lodowca Sven, oraz że niektóre małe lodowce Svalbardu mogą być znacząco mniej wrażliwe na zmiany klimatu niż się powszechnie sądzi. Dalsze badania powinny zweryfikować reprezentatywność badanego lodowca na potrzeby ekstrapolacji wyników na większy obszar.

List of figures

List of tables

In appendix:

List of symbols

α	albedo
ε	error term in water balance calculations
$\dot{\varepsilon}$	deformation rate in Glen's flow law
θ	slope
ρ_a	air density
ρ_i	ice density
τ	shear stress in Glen's flow law

A	glacier area in a given year
A_{deform}	rate factor in Glen's flow law
A_n	mass removed from a glacier in a given interval
A_{turb}	exchange coefficient in turbulent heat flux computations
b_n	point net balance in a given balance year
B_n	glacier-wide net balance in a given balance year
b_s	point summer balance in a given balance year
$b_{s\ ext}$	modelled point summer balance in a given balance year
B_s	glacier-wide summer balance in a given balance year
b_w	point winter balance in a given balance year
B_w	glacier-wide winter balance in a given balance year
C	total summer condensation in glacier basin
C_n	mass accumulated on a glacier in a given interval
c_p	specific heat of air
dA	total area change of a glacier in a given interval
dA/dt	area change rate of a glacier in a given interval
DDF_{ext}	modelled degree-day factor
DDF_{obs}	observed degree-day factor
dh	point elevation change on a glacier in a given interval
dH	glacier-wide elevation change in a given interval
dh/dt	point elevation change rate on a glacier in a given interval
dH/dt	glacier-wide elevation change rate in a given interval
dL	total length change of a glacier in a given interval
dL/dt	length change rate of a glacier in a given interval
dS	total change in water storage in glacier basin in a given interval
dV	total volume change of a glacier in a given interval
dV/dt	volume change rate of a glacier in a given interval
E	total summer evaporation in glacier basin
e_a	air vapour pressure
E_{dH}	total error of elevation change
E_g	elevation error of topographic data averaged for individual points inside of a glacier boundary
E_p	average elevation error of topographic data at a given inclination
e_s	surface vapour pressure
g	gravitational acceleration
h	point thickness of a glacier
L	length of a glacier
LW_{bal}	longwave radiation balance
LW_{in}	incoming longwave radiation
LW_{out}	outgoing longwave radiation
M_{ice}	total summer ice melt
M_{slopes}	total summer snow melt from the slopes surrounding the glacier
M_{snow}	total summer snow melt from the glacier
M_{total}	total summer meltwater production in a glacier basin
n	creep exponent in Glen's flow law

N	sample size used in analysis
p	air pressure
PDD_{obs}	positive degree-day sums calculated from direct on-glacier record
PDD_{SVL}	approximated positive degree-day sums calculated from air temperature at Svalbard Lufthavn station
P_{summer}	total summer precipitation in glacier basin
P_{winter}	total winter precipitation in glacier basin
Q	momentary river discharge
Q_G	ground heat flux
Q_H	sensible heat flux
Q_{ice}	ice discharge through a given cross-section
$Q_{Jul\text{-}Sep}$	total water outflow from the glacier basin in July, August and September
Q_{Jun}	total water outflow from the glacier basin in June
Q_L	latent heat flux
Q_M	melt energy
Q_N	net radiation
Q_R	rain heat flux
Q_{total}	total water outflow from the glacier basin during the whole balance year
Q_{winter}	total winter outflow from the glacier basin during winter
r	potential direct solar radiation averaged for the period 15/06-15/09
R	radiation index used in modelling of summer balance distribution
RH	relative humidity of the air
S	snow cover duration index used in modelling of summer balance distribution
s_{slopes}	water reserves in snow cover on slopes surrounding the glacier
s_{Sven}	water reserves in snow cover on the glacier
SW_{bal}	shortwave radiation balance
SW_{in}	shortwave incoming radiation
SW_{out}	shortwave outgoing radiation
T_a	air temperature
T_i	ice temperature
T_s	surface temperature
u	wind velocity
u_{max}	maximum wind velocity
U	ice flow velocity
U_h	horizontal ice flow velocity
U_v	vertical ice flow velocity
V	volume of the glacier
w	empirical coefficient used in used in modelling of summer balance distribution
x	empirical coefficient used in used in modelling of summer balance distribution
y	empirical coefficient used in used in modelling of summer balance distribution

List of acronyms

AAR	accumulation area ratio
AMB	Austre Muninbreen
AMU	Adam Mickiewicz University
AWS	automatic weather station
BLB	Bertilbreen
CTS	cold/temperate transition surface
DDF	degree-day factor
DEM	digital elevation model
ELA	equilibrium line altitude
ELB	Elsabreen
FDB	Ferdinandbreen
GIC	glaciers and ice caps
GIS	Geograhpic Information System
GPR	ground penetrating radar
GPS	Global Positioning System
IRH	internal reflecting horizon
JJA	June-July-August
LIA	Little Ice Age
NNB	NoNamebreen (the unnamed glacier)
NPI	Norwegian Polar Institute
NYA	Ny-Ålesund station
PDD	positive degree-days
PET	Petuniabukta station
RH	relative humidity
RMSE	root mean square error
RTA	Rough Terrain Antenna (Malå Geosystems)
SLR	sea-level rise
SVB	Svenbreen
SVL	Svalbard Lufthavn station
UNIS	University Centre in Svalbard
VMB	Vestre Muninbreen

1

Introduction and thesis objectives

In the age of climate change polar regions are influenced by fast temperature rise and associated changes (ACIA 2005; Styszyńska & Marsz 2007). Fresh-water stored as ice is now rapidly released back to circulation in the environment due to enhanced melt and carries critical consequences for human activities in every climatic zone of the Earth. Water outflow in rivers originating from mountain glaciers has been recently exposed to significant changes. It has been generally rising for the last decades, but after glaciers shrink enough, the water volume will be somewhat reduced. By implication, that may cause serious problems with water supply in densely inhabited regions, as i.e. south and central Asia (Kehrwald et al. 2008; Immerzeel et al. 2010) or with hydro-power potential of mountainous countries (Schaefli et al. 2007). Moreover, glacier melt causes significant changes in functioning of the whole Earth environment, including energy balance issues, sea-water circulation (influencing e.g. sea ice formation), biology etc., both in high latitudes, as well as in tropical zones (e.g. Nihoul & Kostianoy 2008; Bintanja et al. 2013). Last, but not least, melting ice masses significantly contribute to global sea-level rise (SLR) and if melt-out completely, the sea-level would be by 64 m higher than it is today (Lemke et al. 2007). SLR is a complex process involving mainly fresh-water input and thermal expansion of the seas, potentially representing a danger for coastal settlements all over the world. At present, SLR is 2-3 mm a^{-1} (Cazenave et al. 2009; Church et al. 2011), but advanced mathematical models project a continuous increase of glacier melt rates in the 21st century, giving an additional portion of water to the ocean (ACIA 2005). After years of studies it is known that the most sensitive cryospheric indicators of climate shifts are small glaciers and ice caps (GIC), mostly located in the Arctic (Grudd 1990; Oerlemans & Fortuin 1992; Oerlemans 1994; Dyurgerov & Meier 2000). Huge continental ice sheets (in Antarctica and Greenland) show long response time to climate change due to their size and thermal state, so even though the warming is progressing, local air temperature is still well below zero for most of the year. GIC respond to climate fluctuations much faster, as their ice supplies are limited and they comprise of ice that is already relatively warm. Therefore, even though the overall volume of GIC is small, their SLR input is greater than that of huge continental ice sheets (Meier et al. 2007). It is one of the reasons for a great scientific interest in polar glaciers in the last decades.

Large research initiatives such as International Polar (Geophysical) Years (1882-83, 1957-1958 and 2007-09) were all victories of scientific cooperation in the cold regions. Intensive research has brought answers to many problems, but on the other hand it has also raised numerous new questions. Many of them remain unsolved in glaciology, as is the fundamental issue of glacier response to climate change. Some glaciers show a very fast rate of decay while other retreat their fronts very slowly. On the other hand, a small percentage of glaciers behave in contrast to the majority of the world's ice masses and is close to balance or even advance (e.g. Nesje et al. 2008). Sometimes two similar, neighbouring glaciers react differently to similar climatic impulse (Kuhn et al. 1985). After centuries of observation of glacier fluctuations science still have not known all the processes and relations which drive their behaviour. Monitoring and detailed studies of benchmark ice masses in different climatic zones are crucial for our understanding of climate-glacier interactions. There is therefore a strong need for comprehensive elaborations concerning glacier topoclimate, mass balance, dynamics, thermal structure and valley topography among other factors.

Svalbard is the largest ice repository in the Eurasian Arctic, where glaciological research activities have long traditions. However, large parts of the islands remain poorly investigated, particularly their interior regions. Climate of the inner parts of the archipelago has not been well described, but it is considered as relatively unfavourable for glacier development (Hagen et al. 1993). In the summertime it is warmer than at the coast, whereas very little snowfall characterize the winter period. Almost no glacio-meteorological data is available from this peculiar region and not much is known about the present-day state and response of local glaciers to climate change, which have occurred about 100 years ago, terminating the Little Ice Age period of front advances (Nordli & Kohler 2003). This work aims to fill this gap by delivering new, fundamental data from a small, central Svalbard glacier Svenbreen. It covers a wide spectrum of glaciological studies, giving foundations and background for further detailed research from many fields of Earth sciences: glaciology, hydrology, geomorphology, climatology or ecology. That makes the thesis a broad study on how the glacier and its physical properties respond to climate change, what is the structure of its glacial system and of the glacier itself. Its general problem is related to recognition of the present-day state and functioning of Svenbreen, with particular stress on the glacier's geometry changes after the Little Ice Age termination.

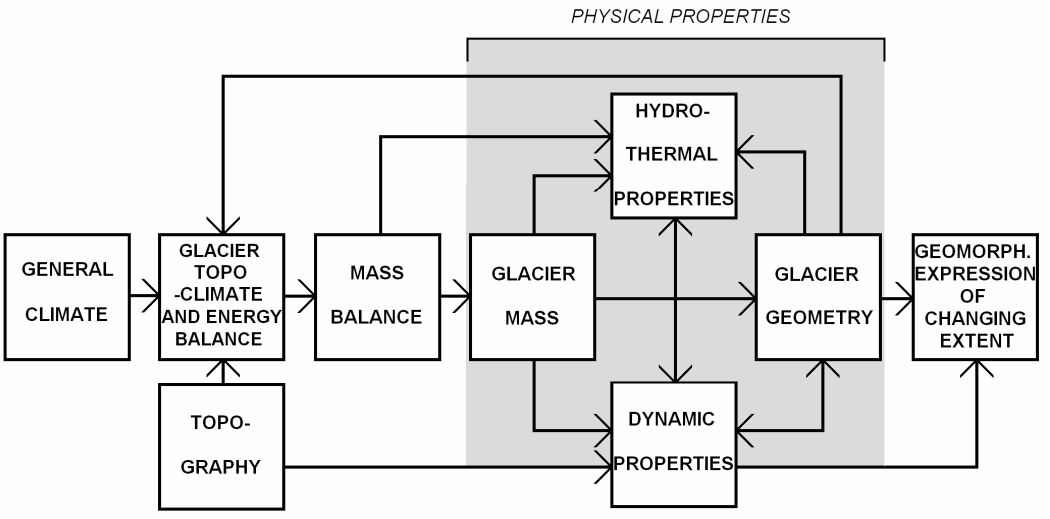

Fig. 1.1 The most important links (arrows) between climate change and physical properties of a glacier

Fig. 1.1 is a basic scheme used in this work, highlighting complex climate-glacier links and interactions between physical properties of a glacier. The work explores a hypothesis, that individuality of a present-day state and functioning of Svenbreen results from quasi-continental climate type and local environmental factors. The main goals of the thesis cover recognition of:

- the present-day geometry and its changes after the Little Ice Age termination,
- variability and spatial distribution of Svenbreen's mass and ice temperature and their drivers,
- selected symptoms of functioning of the glacier and their temporal variability, including mass exchange, surface energy balance as a driver of ablation, meltwater production, runoff and discharge variability
- geomorphological expression of changing glacier physical properties

In this work, 'physical properties' cover glacier parameters, which can be actually measured and have a clear, unambiguous physical meaning, as well as their related characteristics. In this sense, the glacier properties investigated are mass and its fluctuations (seasonal and multiannual - mass balance), ice temperature with its distribution and implications for water routing, motion vectors (flow pattern and velocity) and glacier geometry, describing size of the glacier and being somewhat related to its mass (i.e. length, thickness, volume). 'Present-day state' of Svenbreen covers description of its modern physical properties, treated as a result of changes occurring continuously since the termination of Little Ice Age. 'Functioning' of the glacier is a complex of glacier-environment interactions, which leads to daily, seasonal and multiannual changes of physical properties.

2

Scientific background

A glacier is *a perennial mass of ice, and possibly firn and snow, originating on the land surface by the recrystallization of snow or other forms of solid precipitation and showing evidence of past or present flow* (Cogley et al. 2011). Glaciers are to be found in many cold regions of the world: in high mountains and in circumpolar areas. They are a very important element of Earth's system, covering 11% of land surface and standing for 75% of all fresh water reserves of the planet (Jania 1997). Their fluctuations have a fundamental impact on i.e. local, regional and global landscape, water cycle and climatology. In this chapter some basic information are presented about how glaciers function and how their physical properties evolve under climate influence. The focus is on processes directly related to the contents of this work, particularly on glaciers' growth and decay (mass balance), heat exchange (energy balance), temperature distribution and its implications (thermal regime), water routing (hydrology), motion (flow dynamics) and eventually changes of glacier geometry in response to changing climate. The elements discussed here are essential for full understanding of scientific results from Svenbreen presented in chapters 5-9.

2.1 Glacier mass balance

Glaciers owe their existence to particular climatic conditions in some regions of the world. In order for a glacier to form, winter snow must survive the summer melting season for several years and transform into glacial ice. Sources of winter *mass accumulation* are primarily snowfall, but other factors also play a significant role. Mass loss (*ablation*) is mostly caused by melting, calving (breaking of icebergs into water) and sublimation and is defined as a negative contribution to mass balance. Spatial distribution of both elements shows significant variability, both regional and local. Imposition of these two elements gives a *mass balance* (or *mass budget*), defined as a change in mass of a glacier over a stated time span (Cogley et al. 2011). It stays positive if accumulation exceeds ablation and conversely is negative when ablation is higher than accumulation. The period of consideration in mass budget analysis is often a year or season (winter, summer), whereas the definition of the year depends on the method selected for analysis. Units of the mass balance terms are cm w. eq. (water

equivalent), which inform how much water could be melted from a column of particular medium (snow or ice). Mass budget characterizes health of a glacier and drives changes in its volume. It is therefore a very important parameter, which can be measured for single points on a glacier surface (lower-case symbols: b_w, b_s, b_n) or averaged for the whole glacier (denoted as upper-case symbols: B_w, B_s, B_n, and given here as examples). Processes involved in mass exchange on Svenbreen are a fundamental part of this work (chapter 6).

2.1.2 Accumulation processes and winter mass balance

Mass accumulation on majority of glaciers is characteristic for the winter period. The term *winter balance* (B_w) describes the amount of mass which has been accumulated on a glacier during winter, accounting for the portion of mass removed from its surface (i.e. by winds). The most important process of accumulation is snowfall. Its intensity varies significantly throughout the globe: in maritime mountainous regions in mid-latitudes winter snowfall may exceed few meters, whereas in central parts of Antarctic ice sheet - few centimetres only. Among regional accumulation differences (caused by atmospheric circulation, ocean currents etc.), there are some local externals controlling accumulation. According to Cuffey & Patterson (2010), one of the factors is, that snowfall rises with temperature (to a certain limit) due to rising water vapour content of the overlying atmosphere. Once air is saturated, any cooling (especially rapid, i.e. by orographic lifting) produces cloud droplets or ice particles, which can fall if large enough. Moreover, more precipitation will be formed from a warm air mass rather then from a cold one, what explains low accumulation rates in polar regions and high snowfall in mid-latitude mountains. By implication, snowfall tends to increase with altitude (orography). E.g. in the Alps proportional snowfall contribution to overall precipitation rises by 2.5-3% per 100 m of elevation, so at 3500-4000 m a.s.l. 100% of precipitation is solid (Röthlisberger & Lang 1987). At some point this effect stabilizes, as the air loses its moisture, so accumulation is vastly limited at the highest altitudes. On Greenland and Antarctic ice sheet this effect is visible extremely well. High elevated ice plateaus are distant from any moisture sources, so the observed annual snowfall is on the order of few cm w.eq. (water equivalent), in spite of the altitude exceeding 4000 m in some places.

Direct snowfall is not the only source of mass accumulation: it may also origin from liquid water. In ablation zones meltwater flows downglacier easily, whereas in upper parts (composed of permeable firn layers) percolation and refreezing of water may occur to a large scale, leading to formation of ice layers of high density. This process may be regarded as *internal accumulation* (if occurs within firn layers) or *superimposed ice formation* (if occurs on a glacier surface). Measuring the refreezing water is a serious problem for mass balance studies and sometimes it is the most important source of accumulation, especially in polar areas on extensive, low inclined ice masses. According to Koerner (1968) approximately 90% of ice of Meighen ice cap in Canada originates from superimposed ice, whereas small Storøya ice cap in Svalbard is entirely supplied by refreezing (Jonsson & Hansson 1990). Snow may be also supplied to a given point by wind drift, when some regions are subjected to wind scour and some to deposition. Locally, large amounts of snow may be accumulated by avalanches, which are an important source of mass for some mountain glaciers. Other, sources of ice formation are atmospheric deposition (freezing of water vapour on glacier surface, seldom being significant) and freezing of subglacial water to the bottom of a glacier (often treated as negligible).

2.1.2 Ablation processes and summer mass balance

The end of winter period, which on glaciers of the northern hemisphere occurs approx. with the beginning of May or June, marks the start of strong ablation. *Annual ablation* is a relatively wide concept that covers all the processes removing mass from a glacier in any time of year. However, the great majority of ablation is associated with the warmest part of year on most of the glaciers in the world, so term *summer balance* (B_s) is used most often in the glaciological literature. Melting is usually the most important process of mass loss on land terminating glaciers and may be physically described by energy balance equations (see section 2.2). It generally shows very high correlation with positive air temperature (Ohmura 2001; Hock 2005). It must be however underlined that when some conditions are fulfilled (e.g. high effective solar radiation and low turbulent heat exchange) ice may melt when air temperature is well below zero. The highest melt is observed in the lowest sections of glaciers, at their fronts. In higher zones melting is vastly limited, where air temperature is by few degrees lower than at the snout due to typical lapse rates on the order of 0.5-1.0°C 100 m^{-1}. Other fundamental factor determining the melt rate is exposition to solar radiation. Shaded valleys and cirques are well protected from the sunlight, thus melting in these areas may be twice or more times less effective than in areas of similar altitude, but with higher insolation. Depending on the location of a given glacier, total seasonal melting at a glacier front may be on the order of 1-2 m w.eq. in polar areas up to 10 m w.eq. in mid-latitudes. On the vast majority of Antarctic ice sheet no melting occurs at all (Cuffey & Patterson 2010).

Apart from melting, other important source of mass loss is *calving*. Tidewater glaciers, very common in the polar areas, terminate in the sea with cliffs up to 100 m high. Thermal abrasion of water, together with mechanical forcing of waves, weakens the ice, causing icebergs to fall. The contribution of calving to mass balance of big Arctic ice caps is significant and is on order of 25-40% (i.e. Moholdt et al. 2010b) and may be even more in case of ice sheets. Sublimation is generally not that effective and amounts up to few decimetres w.eq. per year (i.e. Bintanja 1998). It becomes however dominant in arid climates as i.e. in Antarctica or in case of high-altitude tropical glaciers. In these particular regions the contribution of sublimation may reach as much as 40-80% (Lewis et al. 1998). Some ice may also melt at the bottom of a glacier due to bed friction or geothermal heat fluxes. This process is however most often disregarded in mass balance calculations due to its very low efficiency on the order of few mm w. eq. annually, except for areas with active volcanism (Jania 1997).

2.2.2 Net mass balance

Balance year (or *glaciological year*) covers full annual mass turnover cycle: it starts with freeze-up in autumn (often assumed as 1st October on the northern hemisphere), through winter accumulation period, melt-onset in spring, intensive ablation during summer and ends on the last melt day in autumn (often assumed as 30th September, fig. 2.1). *Net mass balance* is a balance at the end of a balance year. Alternatively, it is a change in glacier mass over a period of a balance year and may be presented as a difference between total mass incomes and outcomes. It may be considered for any point (or zone) on a glacier surface (b_n) or averaged for the whole glacier area (B_n).

$$B_n = B_w + B_s \qquad \text{(Eq. 2.1)}$$

If mass incomes (B_w) and outcomes (B_s) equal each other for a longer period, glacier will eventually reach a steady-state. If assumed that a glacier has a zero mass balance, it implies that its volume (geometry) stays unchanged. A prolonged equilibrium of accumulation and ablation is seldom, if ever, found in the nature, but a concept of a steady-state glacier is useful in glaciological considerations as it represents an idealized and simple reality and is used later in this work. To reach a steady-state, a glacier must stay under a uniform climate over decades or hundreds of years. Climate is however variable in time - after a shift in temperature or/and precipitation, one or both mass balance elements will change. An increase in air temperature will cause more melt, while higher precipitation - more mass accumulation. The general warming observed globally in the 20th and 21st century has caused an enhanced ablation at most of the worlds glaciers. After many years of domination of negative B_n, a glacier will respond to new conditions by decreasing its volume (geometry): thinning of its body (more melt than accumulation) will lead to retreat of its front and area decrease. In response, its other properties, such as dynamics, thermal regime and hydrology (all discussed in the next sections) will change as well, what underlines the importance of mass budget and its dominant role in evolution of glacial systems.

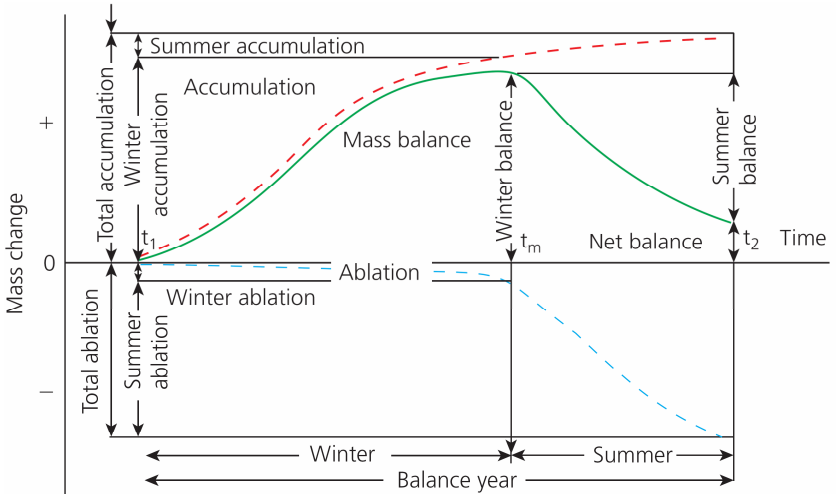

Fig. 2.1 Annual cycle of glacier mass change, showing accumulation, ablation and annual mass balance. After: Benn & Evans (2010)

Specific point mass balance (b_n, note the lower-case symbol) shows great variability over glacier surface. It is the most negative at glaciers' fronts due to thin snow cover in the winter and high melting in the summer. Conversely, it is usually positive in the highest zones, at the foot of rock walls due to high b_w and low b_s. Regions on a glacier where mass is gained and where it is removed are called respectively *accumulation* and *ablation zones*. The so called *accumulation-area ratio* (AAR) is a ratio of the area of accumulation zone to the whole area of a glacier. It ranges from 0 to 1 and is high when B_n is positive and low when B_n is negative. Many years of glacier monitoring in different sites around the globe have shown that the accumulation zone must be slightly larger than ablation zone in order for a glacier to be in balance in particular period, what corresponds to mean equilibrium AAR of 0.5-0.6 (e.g. Zemp et al. 2009). It is however not a universal rule and steady-state AAR may deviate for some glaciers.

The existence of accumulation zone in the higher reaches (where b_n>0) and ablation zone in the lower sections (b_n < 0) implies that at some location between them specific balance is zero

(b_n = 0). This line, or a narrow zone, constitutes an *equilibrium line*. Above the equilibrium line mass is accumulated (snow and superimposed ice survive the summer) and below - all the winter snow is gone, together with some glacial ice. Mean *equilibrium line altitude* (ELA) is a good marker of climatic conditions, as it is highly dependant on the weather on multiannual scale. If ELA is given for one season, it informs how anomalous was this period when compared to average conditions. E.g. after snowy winter and/or cool summer most of the snow will survive the ablation period, implying that ELA will be low and AAR - high, making the overall mass balance B_n positive (fig. 2.2). More information concerning mass balance issues can be found i.e. in Østrem & Brugman (1991), Kaser et al. (2002) and Cogley et al. (2011).

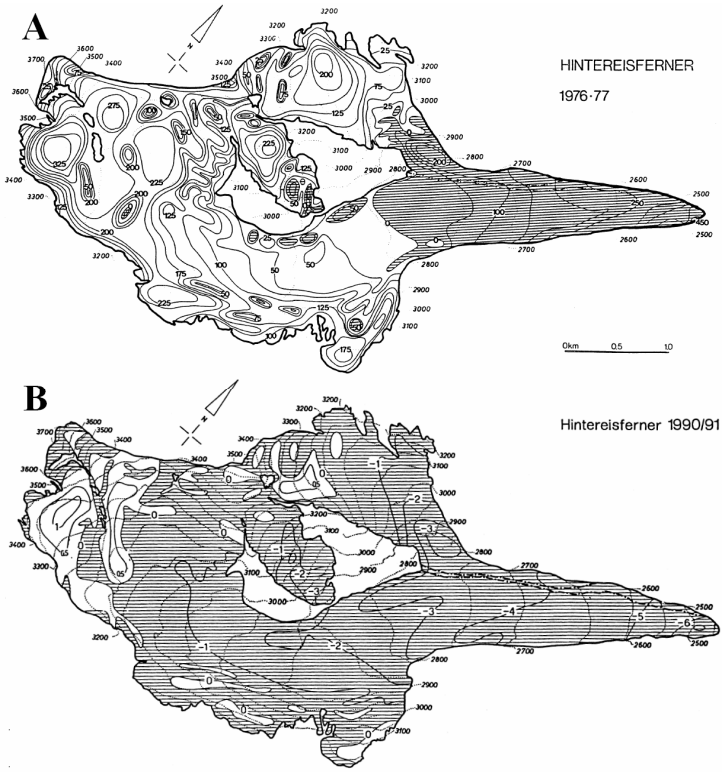

Fig. 2.2 Distribution of specific mass balance on Hintereisferner, Austria. A - a year with positive net balance (map in cm w.eq.), B_n = 76 cm w.eq., ELA = 2840 m and AAR = 0.78; B - a year with negative net balance (map in m w.eq.), B_n = -133 cm w.eq., ELA = 3260 m and AAR = 0.18. White area on the glacier: accumulation zone, dark area: ablation zone, equilibrium line is the boundary between accumulation and ablation zones and glacier flows to the right. Note that low ELA makes the AAR and B_n high. After: Kuhn et al. (1999)

2.2 Energy balance

Melting is the dominant way of mass removal from most of land terminating glaciers. It is not driven by air temperature alone, but it is just closely correlated to this meteorological variable (Ohmura 2001). Melt is regulated by a complex budget of energy of a glacier surface, to which positive (incoming) and negative (outgoing) heat fluxes contribute to an extent driven by weather conditions and surface properties. Structure and variability of summer energy balance shapes individuality of glacier's functioning, as it influences its mass balance, hydrology and thermal regime. Heat budget of Svenbreen was therefore subjected to studies, summarized in chapter 6. In this section sources of energy fluxes are discussed, together with their magnitude and relation with meteorological parameters.

2.2.1 General properties of snow and ice

From all of surface types snow and ice have peculiar properties. Ice and snow cannot exceed temperature above 0°C, what has certain consequences for the overall glacier energy budget. Because every medium showing temperature above the absolute zero emits energy (the warmer the higher), the maximal outgoing energy of ice reaches 316 W m^{-2} and the maximal vapour pressure of the surface is then fixed at 6.11 hPa. The outgoing long-wave radiation of melting ice is relatively high and is stable at this level for most of the ablation season. The maximal surface vapour pressure is low, what favours vapour pressure gradients towards the surface and leads to condensation, giving an important amount of energy to the surface (Hock 2005). Snow and ice are also characterized by high, though variable reflectivity called *albedo*, which is a ratio between reflected and incoming short-wave radiation. High albedo values for snow typically range from 0.4 to 0.9, meaning that only a very small amount of energy may be absorbed by the surface and used for melting. The albedo of ice is generally lower (0.1-0.5; Paterson 1994), so at uniform weather conditions ice melts faster than snow.

Due to mentioned properties glacier cools the overlying air to a significant degree and strong thermal gradients occur within the lowest few metres of atmosphere. Stable air stratification, i.e. cooling of the air when approaching the ice, lasts for most of the summer, so *catabatic winds* (or *glacier winds*) can easily develop, with a characteristic downhill direction (e.g. Oerlemans & Grisogono 2002). Other specific property to mention is transmission of short-wave radiation down to one meter in snow and ten metres in ice, which may contribute to snow heating before melt-onset and cause some melting even when the surface is frozen (Holmgren 1971). In contrast to transmission of short-wave radiation, thermal conductivity of snow is very low and typically amounts to 0.1-0.4 W m^{-1} K^{-1}, which is approximately an order of magnitude lower than that of ice. Snow is therefore a good insulator: in the winter, the external layers of snow are usually the coolest, while the temperature of ice is several degrees higher. Heating of a whole snow column to the melting point may be however a very quick process if liquid water is involved. Specific heat capacity of snow is 2009 J kg^{-1} K^{-1} and it is the amount of energy needed to warm 1 kg of snow by 1 K. Melting of the same amount of snow is very energy-consuming and requires 167 times more energy (334 000 J kg^{-1} K^{-1} which is the latent heat of fusion). After some meltwater (or rainwater) appears on the top of a snowpack, it percolates down and re-freezes when meets sub-zero temperature. This process releases exactly the same amounts of energy as is consumed for melting. Because the amount of energy released by re-freezing is very high, 1 kg of water freezing in a snowpack rises temperature of as much as 160 kg of snow by 1 K.

2.2.2 Surface energy balance components

The energy balance is a sum of all energy fluxes incoming (positive) from surroundings and outgoing from the surface of interest (negative sign). For a glacier surface it may be presented as:

$$Q_N + Q_H + Q_L + Q_G + Q_R - Q_M = 0 \qquad \text{(Eq. 2.2)}$$

where Q_N is net radiation, Q_H is sensible heat flux, Q_L is latent heat flux, Q_G is ground heat flux, Q_R is sensible heat flux of rain and Q_M is energy available for melting. This equality implies that melt energy is simply:

$$Q_M = Q_N + Q_H + Q_L + Q_G + Q_R \quad \text{(Eq. 2.3)}$$

Net radiation, Q_N, is the overall balance of radiation and is usually the most important energy source supplying melting. It consists of shortwave and longwave radiation balances, and may be described as:

$$Q_N = SW_{bal} + LW_{bal} \quad \text{(Eq. 2.4)}$$

where SW_{bal} and LW_{bal} are respectively shortwave and longwave radiation balances. SW_{bal} ranges from 0 to ~500 W m^{-2}, while LW_{bal} from around -350 to 50 W m^{-2}. They are defined as:

$$SW_{bal} = SW_{in} + SW_{out} \quad \text{(Eq. 2.5)}$$

$$LW_{bal} = LW_{in} + LW_{out} \quad \text{(Eq. 2.6)}$$

where SW_{in} is incoming shortwave radiation, SW_{out} is shortwave radiation reflected from the surface, and LW_{in} and LW_{out} are respectively incoming and outgoing longwave radiation fluxes (all outgoing fluxes are negative). SW_{in} is the total (global) shortwave radiation, incoming from several sources: directly from the sun (direct radiation), from sky or clouds (diffuse radiation) and reflected from the surrounding terrain. Its magnitude may reach ~1000 W m^{-2} on clear sky days, 100-300 W m^{-2} on cloudy days and is 0 at night. SW_{out} is dependant on the surface albedo (α, which ranges from 0 to 1) and because no object can reflect as much (or more) energy as it receives, the absolute value of SW_{out} is always lower than SW_{in}:

$$SW_{out} = SW_{in}\,(-1 + \alpha) \quad \text{(Eq. 2.7)}$$

LW_{in} is emitted by the atmosphere and rises with increasing temperature and cloudiness (air humidity). It is relatively stable and usually ranges from 250 to 350 W m^{-2} so on overcast days LW_{in} often exceeds SW_{in}. LW_{out} is governed by glacier surface temperature and is nearly constant during melt season with 316 W m^{-2}, when snow and ice reach their maximal temperature of 0°C. Q_H and Q_L are called *turbulent heat fluxes*, because they use air turbulences above a surface in order to exchange heat. They are difficult to measure in the field, but since they are well correlated with wind speed, moisture and temperature gradients, reasonable approximations have been developed based on these meteorological variables. One of them is the so called bulk aerodynamic approach, given by the following expressions from Patterson (1994):

$$Q_H = \rho_a \cdot c_p \cdot A_{turb} \cdot p \cdot u \cdot (T_a - T_s) \quad \text{(Eq. 2.8)}$$

$$Q_L = 22.2 \cdot A_{turb} \cdot u \cdot (e_a - e_s) \quad \text{(Eq. 2.9)}$$

where ρ_a is air density, c_p is specific heat of air, p is air pressure, A_{turb} is a non-dimensional exchange coefficient, u is wind speed, T_a stands for air temperature (at standard height of 2 m above ice), T_s is surface temperature, e_a and e_s are vapour pressure (of air at 2 m above ice and at the surface respectively). The importance of turbulent heat fluxes is usually of the second order when averaged over longer timescales and when compared to net radiation. In shorter intervals however (measured in hours or days), as well as in maritime regions, their contribution may be dominant. Sensible heat flux, Q_H, is an energy transfer of the air's heat to the surface. Q_H is zero during no-wind weather or when air temperature is lower than T_s.

Conversely, it is high when wind velocity and temperature gradient are high. Latent heat flux, Q_L, is the energy released or required to change phase and applies to condensation, evaporation, sublimation and resublimation. Again, Q_L is the highest with high wind speed and high gradient of vapour pressure. Because vapour pressure of melting ice is fixed at 6.11 hPa, the gradient rises with air temperature, as it drives the maximal vapour pressure of the air. The gradient may be negative and in such case energy is used not for melting but for evaporation or sublimation. The remaining heat fluxes, ground heat flux (Q_G) and rain energy (Q_R), do not contribute significantly to the overall melt energy. During melt season Q_G is slightly negative (glaciers with cold surface layer) or zero (temperate glaciers). In the first case, some energy which could be used for melt is lost for heating of the surface. Q_R is often disregarded in energy balance melt models because of its negligible contribution when compared to other fluxes. As demonstrated by Hock (2005), daily precipitation of 10 mm at 10°C delivers a heat flux of only 2.4 W m^{-2}, being enough for melting of only 0.6 mm w.eq. day^{-1}. The role of liquid precipitation may however influence energy balance conditions in an indirect way. It is significant for heating of a snowpack after winter period to a melting temperature (see previous section) and it may significantly change the albedo of snow and ice. Throughout the globe contribution of particular elements of glacier energy balance varies significantly. Generally, Q_N contributes to melt energy in 50-90% and Q_H in 10-50%. Q_L represents a minor contribution and ranges from negative values (indicating sublimation) up to ~30%, when condensation dominates (Jania 1997). A comprehensive review of surface energy balance of glaciers can be found in Hock (2005) and Armstrong & Brun (2008).

2.2.3 Basal and internal heat sources

The components of energy balance described above operate on a glacier surface. Some amount of energy may be however produced beneath a glacier and inside of it. Due to inaccessibility of these zones they are poorly understood. The processes involved in an internal energy balance are heat conductivity from the surface and from the bed, transformation of kinetic energy into heat due to internal friction and water percolation and refreezing in firn zones. At a glacier base, the additional heat sources are geothermal flux, friction at bed (including incorporated debris) and phase changes of subglacial water (Jania 1997). The geothermal flux is variable in space and is the largest in geologically active areas of the world. It is generally very low with average of 60 W m^{-2} a^{-1}. Depending on temperature gradients in an ice mass, the basal and internal heat may be conducted up to the surface or be consumed for melt. For Svenbreen, no directly inferred data about its internal energy balance is available, but the role of the mentioned heat sources must be considered, as they may play a crucial role in shaping glacier's thermal structure.

2.3 Thermal structure of glaciers

Distribution of temperature in a glacier body is its crucial property: it regulates glacier flow, hydrology and geomorphological impact on the landscape to a large extent. Ice temperature depends on a number of factors and is variable along a glacier flowline and cross-profiles, it also changes with depth. Heat budget of individual zones and glacier flow history determine the thermal layering of the whole ice mass. Its importance has been recognized decades ago and has been a basis for many general glacier classifications (i.e. Lagally 1932; Ahlmann 1933; Baranowski 1977). In modern glaciology the widest use has been gained by a clear, threefold classification, which distinguishes glaciers that are *cold*, *temperate* (also called

warm) or glaciers that consist of ice both cold and warm. The latter ice masses are known as *polythermal* and are the most geographically widespread (Blatter & Hutter 1991; Benn & Evans 2010). Thermal state of ice evolves constantly, but while deep parts of glaciers may change their temperature relatively slowly in response to long-term climatic changes (Kelvins per decades), external layers (to a depth of 10-20 m) change their temperature in seasonal cycles. Thermal structure and its role in mass balance and dynamics have been also recognized for Svenbreen: for its both shallow and deep sections (see chapter 7).

2.3.1 Near-surface temperature distribution

Temperature of the uppermost part of glaciers is strictly related to processes of heat exchange (surface energy balance, heat conduction, water refreezing). Winter snow cover isolates the ice from a very cold air but still heat exchange occurs. Temperature gradient favours cooling of glacier surface (ice is warmer than air) in the form of a *cold wave*, gradually penetrating to deeper sections of a glacier. The greatest winter-summer temperature amplitudes (on the order of 10°C or more) occur directly at the surface. They gradually decay downwards and completely vanish at 15-20 m (Patterson 1981; Jania & Pulina 1990). At 10 m depth ice temperature is fairly stable throughout the year (amplitude <1°C) and it is a valuable information for analysis of glacier thermal regime. The lowest yearly ice temperature at 10 m depth occurs few months after a minimal air temperature, what is related to propagation time of a cold wave. Mean ice temperature at 10 m below the surface is often close to the mean annual air temperature, with a reservation that no melting occurs (Jania 1997).

When summer temperature is positive, percolating meltwater refreezes in a snowpack and firn, rising their temperature to a melting point. After summer season some snow in accumulation zone, having relatively high temperature, may be buried and insulated under a fresh snow-cover, if winter accumulation is high. Such a cyclic, repeated year after year process may eventually lead to formation of temperate ice in accumulation area. In contrast, when no melting occurs there, higher reaches will remain cold. The size of either warm or cold layer is extended by glacier flow, which transports the ice (together with its properties) from accumulation area down to ablation zone. In the lower sections of a glacier winter cold content in ice is removed, first by water refreezing in snow and then by ice ablation. If melt intensity is low and some cold ice survives the summer season, cold layer gets thicker during next winter. Conversely, it may be completely melted out if summer melting is high enough, exposing ice with relatively high temperature, from deeper sections not affected by winter cold wave. Interactions of the mentioned factors are important for shaping thermal structure of near-surface ice and together with internal and basal heat sources give multiple combinations of possible thermal structures.

2.3.2 Thermal classification of glaciers

In the light of considerations from the previous section, glaciers functioning under very cold climate (where limited or no melting occurs even in the summer) produce cold ice. Their temperature is below pressure melting point throughout their body (fig. 2.3A). Borehole profiles in ice are characterized by a slow temperature increase with depth (due to geothermal heat flux and ice flow energy) and carry information about past climate conditions. At the bottom their temperature is still below melting point so they are frozen to the bed. Cold glaciers flow very slowly due to low deformation rates of ice at low temperature (see section

2.5) and are 'impermeable' to water what limits water circulation possibilities, mostly to surface runoff. They are common i.e. in the mountains of Antarctica or in cold Arctic areas.

Temperate glaciers form in the regions where winter cold content is completely removed in the following summer season. It is possible when ablation is intensive and accumulation is high, because thick winter snow cover insulates the ice from cool air, while high melting in spring and summer delivers large amounts of water, which may refreeze and warm-up the surface. Last, effective ablation melts the near-surface ice layers, which still may show some winter cold-content. In effect the whole ice mass (including ice-bed contact) stays at temperature near the pressure melting point (fig. 2.3B). Warm ice conditions carry important consequences for glacier flow, as they enable an ice mass to slide on water saturated bed and greatly increase deformation rates and thus - flow velocity (section 2.5). Moreover, glaciers with warm bed have high geomorphological potential as they may efficiently incorporate material from the bed and overdeepen their valleys. Such glaciers can be found in numerous maritime mountain ranges, i.e. in Norway, New Zealand, southern Iceland, North America or the Alps.

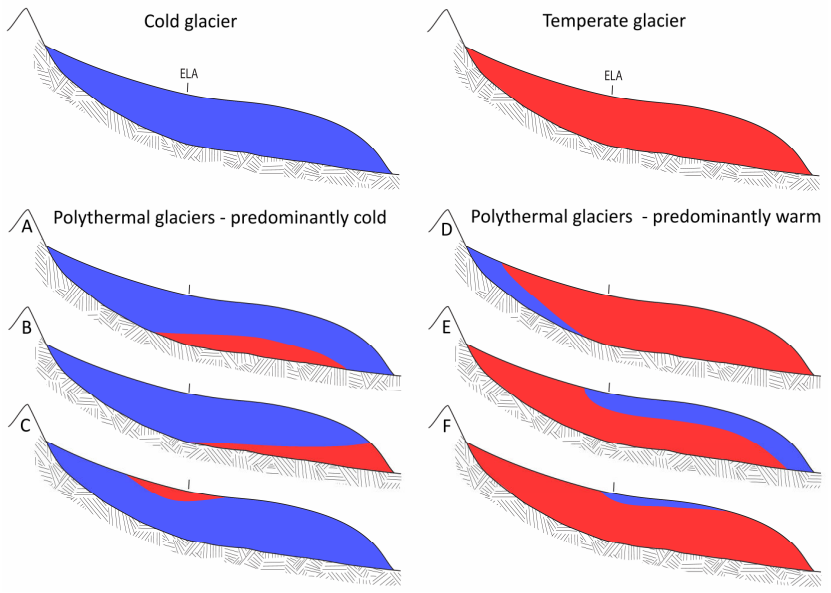

Fig. 2.3 Main thermal structure of glaciers discussed in text. Blue colour - cold ice, red - temperate ice. Polythermal glacier types after Blatter & Hutter (1991). Modified from Pettersson (2004)

Under a wide spectrum of climates and subsurface heat transfer patterns polythermal glaciers, consisting of cold and warm ice, may form (Baranowski 1977; Blatter & Hutter 1991). The polythermal glacier regime often develops in regions characterized by relatively low temperature and precipitation and thus: low mass turnover. Depending on the continentality of climate different polythermal structures may occur, ranging from almost entirely cold to nearly completely warm throughout their mass. Polythermal structure may be further divided into six main subtypes showed on fig. 2.3 (types *A*-*C* and *D*-*F*), as distinguished by Blatter & Hutter (1991). Intermediate types may however result from different climatic and dynamic glacier peculiarities. The first group of polythermal glaciers, predominantly cold (subtypes *A*-*C*), exist in cool climates with very limited melt even in the highest glacier reaches. Types *A* and *B* origin from accumulation zones where only cold ice is formed, due to no (or almost no) melt, and thus no snow heating by latent heat release of refreezing water. Warm ice in the deepest glacier zones origins from strain heating of flowing ice under high pressure and is

mostly located along main flowline, with margins frozen to the bed. In case of type *C* only the lowest sections of accumulation zone experience significant melting, what favours formation of some temperate ice which may be transported some way down to ablation zone. Predominantly warm glaciers (*D*-*F*) are typical for slightly more maritime climates where intensive melt is found in most of accumulation zones forming temperate ice. In type *D* however the highest zones are cool enough to produce limited amount of cold ice. Types *E* and *F* are characterized by cold surface layer in the ablation zone, created by near-surface winter chilling. If ablation is low even at the front, the cold layer will not be removed (type *E*). When melting at the margin is sufficient, cold layer will be restricted only to the upper ablation zone where melting is the lowest (*F*).

Polythermal glaciers are relatively common in glacierized regions. Many of them can be found e.g. in the Alps and continental mountains of Asia. Also in high latitudes they experience favourable conditions for development. The largest ice masses on Earth - Antarctic and Greenland ice sheets - also belong to polythermal type, with ice-bed interface being temperate in some areas. Svalbard is a well known region of occurrence of polythermal glaciers of types A and E, having temperate bed conditions that greatly influence their dynamics and hydrology. Recognition of thermal regime of Svenbreen was therefore of special interest.

2.4 Glacier hydrology

Water is an essential component of every glacier. In solid state, as snow and ice, it constitutes its mass. As a liquid, it is a medium of heat and sediment transfer and it influences many glacier characteristics. Conversely, character of hydrology and runoff may be used to conclude about internal properties of a glacier. Such approach has been used on Svenbreen (section 7.2).

Thermal regime affects general glacier hydrology in a number of ways. Water may penetrate temperate glaciers down to bed by moulins and crevasses on a glacier surface and flow through englacial channels inside and subglacial channels beneath it. Cold ice is a barrier for water as it soon refreezes when in contact with sub-zero ice temperature. Cold glacier margins may also act as dams for subglacial water, eventually leading to catastrophic floods (Skidmore & Sharp 1999). Presence and pressure of subglacial waters play a crucial role in glacier dynamics. The knowledge of water discharge variations in glacial rivers is of great interest in many regions of the world, as it carries information about superficial, internal and subglacial processes, but also for practical reasons, like flood forecasting, fresh-water supply and hydro-power consumption. For these reasons glacier hydrology is often a basic issue to be studied, also in this work (chapter 7). In this section only a very brief introduction to basic glacio-hydrologic terms is presented, more detailed literature is suggested in the end and in the text.

Glacial water origins primarily from melt of snow and ice and from rainfalls. As soon as it appears on a glacier surface it may be stored in snow or drained downglacier (*supraglacial drainage*). Water in a snowpack may refreeze or form *slush* (water-saturated snow). Water flowing down on a glacier surface tends to focus in *supraglacial channels*, often being very stable for many decades. Because ablation zone is often convex along its cross-profile, supraglacial streams tend to direct the water to the lateral glacier margins. If a crevasse or a *moulin* dissects a stream, water falls down, rapidly passing from supraglacial to *englacial*

drainage system. Another possible pattern of water migration to englacial environment is via closing of supraglacial channels (*cut-and-closure conduits*, Gulley et al. 2009) and percolation between firn grains or through small veins between ice crystals (0.001-1 m of water column a^{-1}), observed in temperate ice (Jania 1997). Inside of glacier body water creates complex systems of horizontal and vertical channels, subjected to continuous evolution caused by ice deformation and thermal erosion of water. These *glacier caves* may eventually reach glacier bed. Water transferred beneath a glacier body becomes a part of its *subglacial drainage*, poorly understood due to inaccessibility of this zone. In early melt-season, water flow in englacial and subglacial systems is limited, but it evolves towards fast meltwater transfer as the summer progresses and cavities are widened or unblocked by flowing water. Subglacial flow may occur efficiently in different forms of channels, from which the most important are *R-channels* (incised in ice) and *N-channels* (incised in bedrock). Other option of water transfer under a glacier body is via *linked-cavities*. It is a system of constantly evolving shallow subglacial conduits connected with narrow passages, which is much less efficient than canalised flow and prone to blocking. Both systems may however operate simultaneously. Blockage of linked-cavities may drastically increase basal water pressure. Presence of large amounts of subglacial water may have a huge impact on basal sliding and hence on glacier flow (i.e. Kamb 1987; Zwally et al. 2002).

Thermal regime of ice determines many hydrological characteristics of glaciers. Cold ice masses are characterized by modest supraglacial drainage. Low melting creates limited amount of meltwater drained only surficially, because as soon as water gets inside of a glacier, sub-zero temperature of its body causes water to refreeze. At temperate glaciers large amounts of water are usually found due to intensive ablation. Water is easily removed from the surface: it finds way to englacial and subglacial drainage by percolating through veins between crystals or by supraglacial runoff via sparse stream network and moulins. Drainage of polythermal glaciers is complex due to many possible thermal structures and not well studied. Individual glacier zones are characterized by different thermal (and hence: hydrological) properties. Supraglacial channels are numerous when surface cold layer exists. Englacial and subglacial drainage may develop in warm zones, so polythermal conditions enable some water circulation even in the winter period. Winter outflow of such water leads to formation of *icings* - characteristic ice patches in the glacier forefield, up to few metres thick, created from refreezing of winter discharge outside of a glacier.

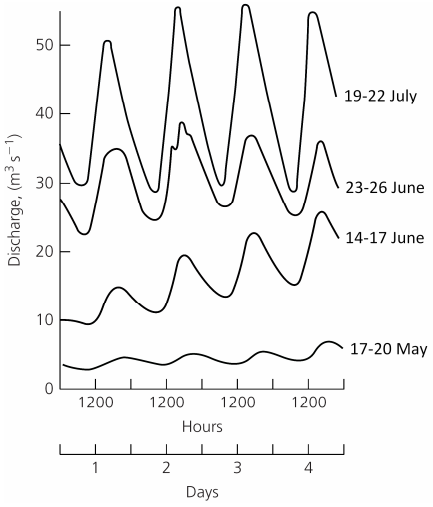

Fig. 2.4 Variability of discharge in proglacial river of Gornegletscher, Switzerland, in 1959 (modified after Benn & Evans 2010). Note the daily periodicity and discharge increase as the summer progresses

In case of a typical mountain glaciers it is common that all glacial water is focused in one stream, flowing from one portal at a glacier front, whereas larger ice masses usually develop multiple equivalent *proglacial rivers*. Water discharge in such streams starts typically in spring after melt onset (often in a form of a flood, called *the spring event*), reaches maximum in mid-summer due to the greatest melt intensity and gradually ceases in late-summer and autumn until freeze-up. Daily discharge cycle is well pronounced (fig. 2.4) and is primarily related to meltwater production: it is the lowest at night and the highest in the afternoon, usually 2-4 hours after daily melt maximum (i.e. Nienow et al. 2005). Daily discharge amplitudes are low when snow still covers a glacier due to meltwater storage in a snowpack. Conversely, after most of the snow is melted out in mid-summer, amplitudes increase. These cycles are imposed on *base flow* - water discharge occurring even after a sudden freeze-up. According to Röthlisberger and Lang (1987) base flow origins from different sources: subglacial meltwater; water which is continuously and steadily released from snow, firn, englacial and subglacial cavities or from groundwater supplies. Water in proglacial streams may be also supplied from rainfalls, but it plays significant role only occasionally, during the most intensive rain events (Jania, 1997) or on glaciers functioning under peculiar climatic conditions such as monsoon-dominated Himalayas (Hasnain 1999). More about general glacier hydrology can be found in Fountain & Walder (1998), Benn & Evans (2010) and Cuffey & Patterson (2010). For detailed information see i.e. Skidmore & Sharp (1999), Jansson et al. (2003), Nienow et al. (2005), Hubbard & Nienow (1997), Bingham et al. (2005).

2.5 Glacier flow and its variability

Motion of ice is a fundamental glacier property, as highlighted in a glacier definition by Cogley et al. (2011), mentioned in the beginning of this chapter. It is strictly dependant on bedrock geometry, ice properties and characteristics of interface of both these elements. Glacier motion is a complex branch of glaciological studies, so again only some basic concepts are sketched in this introduction to ease the receipt of further scientific results from Svenbreen (sections 5.3 and 8.3).

2.5.1 Glacier motion

On a steady-state glacier mass gain from higher zones should be transported down to replace mass losses. It implies that ice discharge through a cross-profile along equilibrium line should be equal to mass gained above ELA (net mass accumulation, C_a) and to mass removed below ELA (net ablation, A_a) to remain in a steady-state (Sugden & John 1976, fig. 2.5). Therefore, glaciers with high mass turnover (with high C_a and A_a, e.g. in maritime regions) flows much faster than glaciers with low mass turnover (e.g. in continental climate), because they must transport more mass from upper to lower elevations. Arrows in fig. 2.5 represent two flow components: *horizontal* and *vertical*. The horizontal component is an obvious planimetric result of a downglacier ice motion direction (the arrows are pointing generally to the right). The vertical component is directed to the bottom of a glacier in its accumulation zone, as it compensates the pressure of new firn layers (*submergence velocity*). Conversely, in the ablation zone motion vectors are directed towards the surface (*emergence velocity*) to compensate the ice losses due to ablation. Overall ice velocities required to balance accumulation and ablation are known as *balance velocities*. In the nature they are found seldom, as the observed ice velocities are very variable on different timescales (hourly, daily,

seasonal, multiannual). Flow speed ranges from less than a metre per year (small cold glaciers, as i.e. mountain glaciers in the Antarctic) to thousands of metres annually (ice streams draining huge ice caps or ice sheets, as i.e. Jakobshavn Isbrae in west Greenland), with normal velocities ranging from 1 to 100 m a^{-1} for many glaciers in the world.

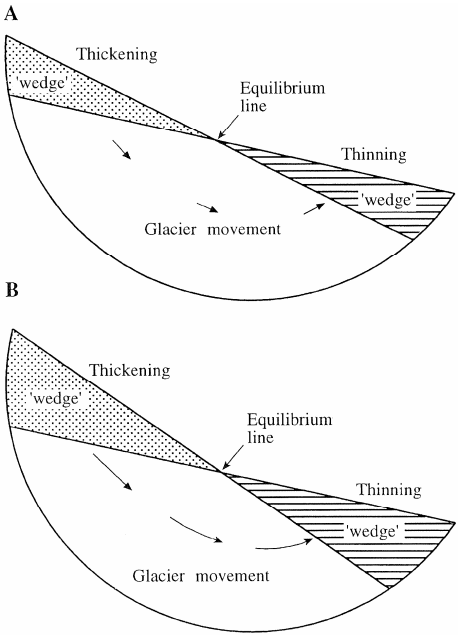

Fig. 2.5 An idealized scheme showing ice discharge (indicated by length of the arrows) on glaciers with A - low mass turnover and B - high mass turnover. After: Sudgen & John (1976)

Two main types of flow are distinguished in glaciology: *ice deformation* (in response to stress) and *basal motion*. In the first mechanism, ice motion occurs due to deformation induced by *driving stress* (force gradients exerted by the ice) and is described by *Glen's flow law* (Glen, 1955; Nye, 1957). It may be presented in a simplified form (with shear stress only) as:

$$\dot{\varepsilon} = A_{deform}\,\tau^{n} \qquad \text{(Eq. 2.10)}$$

where $\dot{\varepsilon}$ denotes deformation rate, τ is a shear stress, A_{deform} is a rate factor and n stands for an empirical parameter, most often set as 3. Eq. 2.10 clearly shows that deformation rate rises exponentially with applied stress. Rate factor A_{deform} is strictly temperature dependant, but debris content, presence of water or crystal fabric may also modify it to a lower extent. For temperate ice A_{deform} equals to 3.4 x 10^{-16} being 16 times higher than for ice at -10°C, 68 times more when compared to ice at -20°C and 340 times higher than for ice at -30°C. Cold glaciers are therefore very poorly deformable and hence flow much slower, but little shifts in ice temperature may result in significant changes in deformation rates. From Glen's flow law ice velocities may be derived (Benn & Evans, 2010):

$$U = \frac{2A_{deform}}{n+1}(\rho_i\, g \tan\theta)^{n}\, h^{n+1} \qquad \text{(Eq. 2.11)}$$

where U is velocity, ρ_i is ice density, g stands for gravitational acceleration, θ for slope and h is ice thickness. This simplified version relies on some assumptions, so its results may slightly

deviate from observations, but it underlines the importance of ice temperature, slope inclination and ice thickness in deformative flow velocity. The higher these parameters are, the faster deformative ice motion.

Another flow mechanism is basal motion. It is an important component for warm-based glaciers, while it is almost zero in case of cold-bedded ice masses (millimetres annually). Basal motion is extremely difficult to study and very few reliable data is available. Several different processes are involved in this mechanism depending on the bed quality. *Basal sliding* applies to hard solid beds with no sediment cover. Bed obstacles provide resistance to sliding, so to surmount small bumps basal ice melts on the stoss side of a bump (due to increased stress) and refreezes on the lee side (*regelation*). Larger obstacles are primarily crossed due to ice deformation around them (*enhanced creep*). Many glaciers are underlain by a layer of loose sediments covering the actual bedrock. In response to relatively low stresses the, so called, soft beds may easily deform providing an additional motion component. A glacier may also slide over sediments (*ploughing*) so the effective soft-bed motion is most likely a mixture of these two processes.

2.5.2 Flow dynamics

Glacier flow speed is not constant because stresses in an ice body and subglacial properties change in time due to different external and internal factors. All of the motion mechanisms described in the previous section may be variable in different time scales: daily, seasonal and multiannual. Basal sliding is responsible for most of the observed velocity fluctuations and is strictly related to basal water pressure (Jania 1997). As melting changes in a daily and seasonal rhythm, variable amounts of water may penetrate down to the bed and minimize the basal drag. Acceleration of a glacier after a period of more intensive melting has been observed on many glaciers in the world and first demonstrated by Müller & Iken (1973). Recently a lot of scientific attention has been paid to the Greenland ice sheet where this process is known as *'Zwally effect'*. Zwally et al. (2002) have observed rapid flow increase at the beginning of each melt season, meaning that meltwater must have travelled 1 200 m through mostly cold ice down to the bed in very short time to increase basal lubrication. Water pressure beneath a glacier may also rise due to re-organisation of subglacial drainage, as i.e. narrowing of subglacial channels due to ice creep (Hooke et al. 1990) or due to external forcing such as tides or rainwater transfer to subglacial zone (Krimmel & Vaughn 1987).

The most spectacular aspect of changing flow velocities is a *glacier surge*: a cyclic rapid mass transfer from higher to lower elevated zones, accompanied by fast flow period (10^1-10^2 higher than velocity in a normal mode, called the *quiescent phase*) and, most often, a significant front advance. Surges are not a common phenomenon: only 1% of world glaciers show surge-character (Jiskoot et al. 1998), but they are very common in several regions of the world, including Alaska, Pamirs, Iceland and Svalbard among others. The length of a quiescent phase varies throughout the globe, from ~10 to few hundred years, while the active phase of a surge is much shorter, from 1 to 10 years long. Temperate and warm-bedded polythermal glaciers show different surge character and no single surge mechanism has been developed yet, but there is general agreement that they are not related directly to climate. The widest recognition has been gained by *hydrologic switch* and *thermal switch* models. The first explains surge occurrence in warm ice masses by changes in basal hydrology (Kamb 1987), while the latter attributes surges of polythermal glaciers to switch of basal thermal regime (Murray et al. 2000; Fowler et al. 2001). On multiannual scale glacier velocities are mainly

driven by climate change and may act as two contradictory effects. First, the warming climate causes glacier thinning and often a shift from a warm to a cold-based glacier, both decreasing ice velocities (reduction of driving stress and basal motion). On the other hand, more intensive summer melt may lubricate the bed and hence speed the glacier up.

As showed in this section, glacier flow velocity depends on a number of factors, including local ice thickness, surface inclination and ice-bed characteristics. On Svenbreen, spatial variability of flow rates is responsible for its geomorphological activity and partly - for its geometry changes. For further information see glacier flow processes' reviews: Hooke (2005), Greve & Blatter (2009), Schulson & Duval (2009) and general glaciological handbooks (Jania 1997; Cuffey & Patterson 2010; Benn & Evans 2010).

2.6 Geometry changes as an effect of mass balance, dynamics and topography

Glacier geometry is understood as its size and shape and thus covers mainly its volume, thickness (surface elevation), length amd area. As visible in fig. 1.1, it is an end-product of complex climate-glacier interactions, hence in this work rate of changing geometry of Svenbreen is treated as an indicator of magnitude its overall changes and relative resistance to climate shifts (chapter 5).

A mass balance-flow concept of Sugden & John (1976) presented in section 2.5.1 is very illustrative when considering geometry changes of glaciers (fig. 2.5). On an idealized steady-state glacier, net accumulation C_n occurs in its upper parts, while mass loss (net ablation, A_n, negative sign) occurs at lower elevations. To stay in a steady-state, mass equal to C_n and $-A_n$ must be transported through a cross-profile at the equilibrium line (ice discharge, Q_{ice}). Such situation may be described as:

$$C_n + A_n = B_n = 0 \qquad \text{(Eq. 2.12)}$$

$$Q_{ice} = C_n = -A_n \qquad \text{(Eq. 2.13)}$$

When equations 2.12 and 2.13 are valid for a longer period, a glacier will remain in a steady-state and no geometry change will occur. When one of the conditions is not fulfilled, geometry change (thinning or thickening) results.

Globally glaciers show a clear tendency of decreasing their mass due to warming climate (Kaser et al. 2006), so this case is now considered. On a steady-state glacier thinning may occur from three situations: a) B_n changes to negative (A_n rises and/or C_n decreases) while Q_{ice} is constant, b) A_n and C_n are stable but ice flow is enhanced (section 2.5.2) or c) a mosaic of these two situations occurs, with different possible magnitudes of both effects. Further glacier response may be complex and may carry significant long-term consequences: a change in subglacial hydrological properties and/or a change in temperature distribution in ice. When initial thinning is significant, the surface is progressively lowered to warmer zones, so A_n increases. As a result, ice temperature and meltwater production rise. Warming of the ice makes the strain rates higher (section 2.5.1) and more water may eventually reach the bed. In effect, flow velocities and hence discharge increase, due to faster deformations and basal sliding, making it a positive feedback accelerating thinning. On the other hand, initial thinning may considerably reduce thickness and basal temperature and switch thermal regime from a

warm-based to a cold-based glacier (see section 2.3). Together with reduction of driving stress it will decelerate both the glacier motion and thinning. The potential response to any change in eqs. 2.12 and 2.13 will depend on the magnitude of mass balance or dynamic shifts, as well as on the initial state of a glacier. Variations of mass balance and ice discharge are the fundamental factors responsible for glacier geometry changes and they stay in complex relations to each other. On a typical mountain glaciers the mass balance plays however the primary role.

Geometry changes manifest in several different ways. Variations in glacier volume (thickness) entail changes of their area, best visible as front (length) fluctuations. Glacier *advance* occurs by terminus transgression (length increase), while *front retreat* is a process of glacier length reduction. Length fluctuations may occur throughout the year: as ablation reaches zero (e.g. in the winter) some glaciers distinctly advance, but soon they retreat again due to normal summer melting and/or calving. Net length reduction is mostly related to periods warmer than average, when enhanced melting of marginal ice causes retreat of the terminus (faster for flat ice surfaces than for steep fronts). Advances occur via high accumulation input together with limited ablation and are not immediately visible in the glacier morphometry. The time lag between occurrence of a mass balance signal and first signs of advance is known as *reaction time*, while the theoretical period between two steady-states resulting from an impulse is known as *response time* (Chorley & Kennedy 1971; Bahr et al. 1998). Johannesson et al. (1989) developed a simple estimation of a glacier response time using its maximal thickness and balance rates at the front and obtained values ranging from 10 to100 years for parameters typically observed on mountain glaciers. The mass balance impulse of additional volume travels from accumulation zone downglacier as a *kinematic wave* (a bulge of increased ice velocities, Nye 1960; van de Wal & Oerlemans 1995) and may eventually lead to an advance if it reaches the front after few or few tens of years. Such process is often blurred by many different climatic impulses acting one after another and by diffusion of the wave.

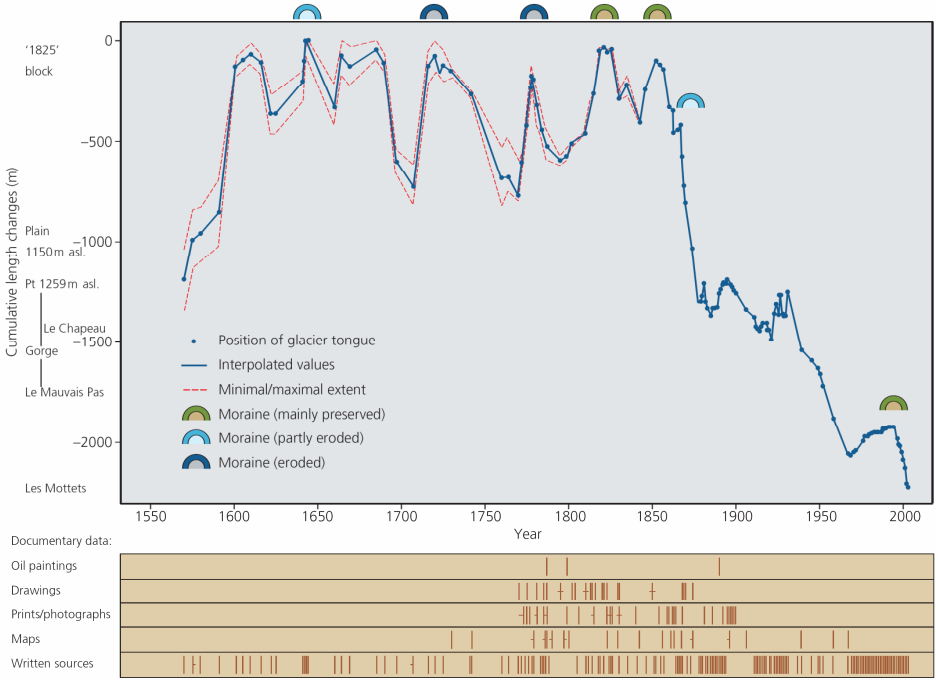

Fig. 2.6 Reconstructed length changes of Mer de Glace, Alps, in the last ~400 years. Note the Little Ice Age advance (before 1600) and retreat after its termination (after 1850). After: Nussbaumer et al. (2007); Benn & Evans (2010)

If accounting for some restrictions, glacier geometry changes are a very sensitive marker of climate (e.g. Oerlemans 2005). Many efforts have been made to reconstruct them with use of different historical sources to interpret climate changes from the past. The longest records were achieved for length fluctuations, as they have been the easiest to observe (fig. 2.6). Not all ice masses are however useful as past-climate indicator: in case of tidewater and surge-type glaciers there is no straight-forward relation between climate and length, with dynamics and fracture distribution playing the fundamental role (e.g. Mann 1986). In the length record from fig. 2.6, greater glacier size clearly corresponds to the so called "Little Ice Age" - a cold period favourable for glaciers' growth. After its termination the glacier has been generally decaying. Front retreat is usually caused by negative mass balance, general volume decrease and thinning on majority of glacier area and is accompanied by steepening of a glacier (fig. 2.7A). During cold and snowy periods glaciers switch to positive mass balance mode and increase their thickness. The extra volume is eventually transferred to the front causing an advance (fig. 2.7B). Surge-type glaciers are a special case of geometry changes. In a quiescent phase their flow speed is lower than balance velocities, so ice lost by ablation in the lower sections is replaced by ice flow only partially. In result, surface lowering occurs at the front and some thickening (*building-up*) in the higher zones (*reservoir area*, fig. 2.7C). At some critical point, the mass from reservoir area is released to the receiving area downglacier and ice discharge rises by one or two orders of magnitude. In response to fast flow, the reservoir area is drained from mass and lowers significantly, while the lower zone receives this volume, thickens and the front advances (fig. 2.7D).

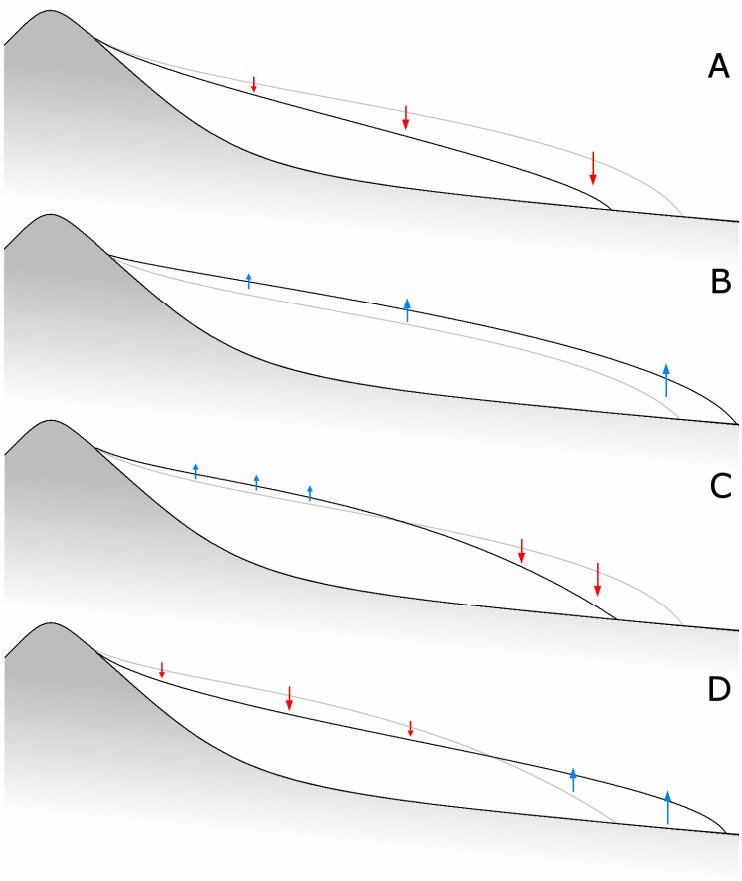

Fig. 2.7 Typical geometry change patterns of mountain glaciers. Grey line indicates initial glacier profile, black line - new profile resulting from a geometry change. Arrow size represents magnitude of thinning (red) or thickening (blue). A - glacier thinning and retreat; B - thickening and advance; C - quiescent phase of a surge; D - active phase of a surge

An important factor shaping the basic geometry change patterns is topography of a glacier valley and of a glacier itself. Aspects such as ratio between glacier and valley widths, glacier hypsometry (area-altitude distribution) or bedrock shape (especially near the terminus) all modify the general glacier response to changing conditions. Narrow glacier tongues in wide valleys melt and retreat fast due to heat exchange from warmer slopes to the ice (Oerlemans 1986). Steep ice masses with large portion of their area in higher elevation bands (e.g. mountain glaciers) are more resistant to warming climate than poorly inclined glaciers with less favourable area-altitude distribution, because on flat ice masses every ELA rise significantly reduces the AAR (section 2.1). Near-front bedrock relief plays a fundamental role during glacier advance and retreat, particularly in case of tidewater glaciers. Water depth and fjord relief is crucial for calving processes in a larger extent than climate shifts. It is therefore its main control (Hanson & Hooke 2000; Oerlemans & Nick 2005).

The presented in this chapter scientific background highlights complexity of glacier systems and multiple feedbacks between their individual elements. All of them were studied on Svenbreen for the purpose of this work, though with different level of detail and temporal coverage (see chapter 4 for methods). Results of the investigations are presented in chapters 5-7.

3

Study area

The Arctic region covers vast areas of Arctic Ocean and lands situated around the north pole. It is characterized by peculiar insolation conditions, with large annual energy supply contrasts, related to its location inside of the northern polar circle. It results in harsh climatic conditions with very low air temperature. According to Baird (1967), the characteristic marks of polar regions are their high latitude, long winter and short summer periods, low precipitation, occurrence of frozen ground, lakes and seas and almost complete lack of trees. Many attempts of Arctic delimitation exist (e.g. Kostrzewski et al. 2007a). The most commonly used are the climatic border (10°C isotherm of July) and the botanical border (with tree line being the southern limit of the region). In many works an astronomical criterion is used - the Arctic is assumed to lay within the northern polar circle (66°33' N). Such described extent of the Arctic is not precise, as it includes also regions having only some of the characteristic marks of polar regions, such as Scandinavia. Different authors have been however using it as it is clearly and elegantly defined. The region may be further divided into the Low and the High Arctic. The Low Arctic comprises the northern rims of Eurasia and North America. The latter subregion covers the most barren islands situated on the Arctic Ocean: Greenland, Canadian Arctic Archipelago, Russian arctic islands (Novaya Zemlya, Franz Josef Land, Severnaya Zemlya and New Siberian Islands) and Svalbard.

3.1 Geographical and climatic setting of Svalbard

The study area in this work is located in central Svalbard. It is a mountainous High Arctic archipelago, situated between the latitudes of 74° - 81°N and longitudes of 10° - 35°E, with Longyearbyen in its central part as the main town. Total area of Svalbard is $62 \cdot 10^3$ km^2, with Spitsbergen being the largest island ($38 \cdot 10^3$ km^2). The remaining area is focused in Nordaustlandet ($15 \cdot 10^3$ km^2), Edgeøya ($5.2 \cdot 10^3$ km^2), Barentsøya ($1.3 \cdot 10^3$ km^2) and other small islands (fig. 3.1, Liestøl 1993). From the west Svalbard neighbours a warm West Spitsbergen Current (Greenland Sea), which is the reason of relatively high air temperature in Svalbard when compared to other High Arctic sites. In the period 1981-2010 at Svalbard Lufthavn station (SVL, in Longyearbyen) average air temperature of the coldest month

(February) was -13.5°C, of the warmest month (July) 6.4°C and the annual mean was -5.1°C, based on data from Norwegian Meteorological Institute. Eastern parts of Svalbard are influenced by cool East Spitsbergen Current (Barents Sea), resulting in distinct thermal gradients across the archipelago. Interior of Svalbard, where the studied glacier is situated, shows distinct quasi-continental climate features, making it a unique region, underrepresented in the glaciological literature.

Annual precipitation sums are low, usually ranging from 400 to 600 mm along the coasts and about twice less in the interior (e.g. 412 mm in Ny-Ålesund at the western coast against 188 mm at SVL, 1981-2010). Precipitation measurements in polar regions suffer however from severe errors, related mainly to gauges' undercatch at high wind speeds and snow drift, so the real precipitation is considerably higher than measured (Førland & Hanssen-Bauer 2000; Killingtveit et al. 2003). Another climate characteristic of the archipelago are strong winds, especially during winter when weather in Svalbard is controlled by migration of cyclones from above Iceland, with dominant eastern atmospheric circulation. During summer, Svalbard stays under the influence of higher pressure originating from Greenland area and contribution of eastern air inflow is reduced, although still dominant. Regional climate is significantly modified in Svalbard by mountainous relief, distance from the seas and surface characteristics (e.g. Migała et al. 2005; Sikora et al. 2009, 2010; Bednorz & Kolendowicz 2010; Araźny et al. 2010).

Fig. 3.1 Map of Svalbard. Square - Petuniabukta region, the study area. Black circles - settlements with acronyms of meteorological stations given in brackets where relevant. White areas - glaciers. Numbers indicate some of glaciers mentioned in the manuscript: 1 - Svenbreen, 2 - Bertilbreen, 3 - Midre Lovénbreen, 4 - Austre Brøggerbreen, 5 - Kongsvegen, 6 - Waldemarbreen, 7 - Irenebreen, 8 - Werenskioldbreen, 9 - Hansbreen

In the 20th century climate of the Arctic has been experiencing significant changes, influencing functioning of all polar terrestrial environments (ACIA 2005; Kostrzewski et al. 2007a,b; Przybylak 2007; Zwoliński et al. 2008). The so called Little Ice Age (LIA) was a

post-medieval, globally cool period, strongly reflected also in the north Atlantic sector (e.g. Overpeck et al. 1997; Grove 2001). LIA onset in Svalbard was dated for 13th-14th century, while its termination for early-20th century by sedimentological and ice core investigations (Gordiyenko et al. 1980; Svendsen & Mangerud 1997; Isaksson et al. 2003, 2005). These studies revealed low air temperature during LIA, although recent work by D'Andrea et al. (2012) suggests relatively mild conditions in Svalbard in that period, though with increased precipitation. The earliest instrumental air temperature record from the study area, spanning since 1911, indicates a sharp temperature increase around 1920, however some doubts remain about the quality of the earliest data (Kohler et al. 2002; Nordli & Kohler 2003). Air temperature rise is very well pronounced particularly since 1960's, and more recently since 1990's (fig. 3.2) and is linked to wide-scaled changes in circulation patterns, ocean temperature and sea-ice extent (e.g. Hanssen-Bauer & Førland 1998; Førland et al. 2002; Niedźwiedź 2004, 2006; Kruszewski 2005). Climate scenarios predict further warming in the region in the 21st century (Benestad et al. 2002; Førland et al. 2012).

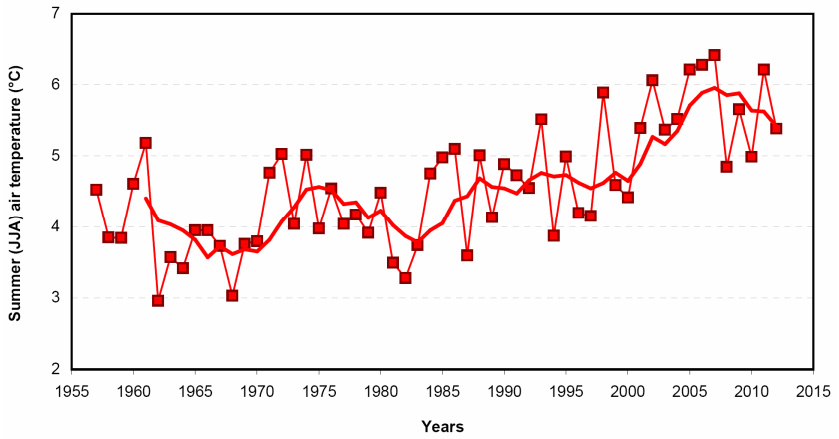

Fig. 3.2 Summer (June-August) air temperature at SVL based on Norwegian Meteorological Institute data. Thick red line indicates a 5-year running mean

3.2 Svalbard glacier cover

Glaciers in Svalbard cover at present approximately 60% of its area ($35 \cdot 10^3$ km^2) and stand for volume of $7 \cdot 10^3$ km^3 (Hagen et al. 1993; Moholdt et al. 2010a). They are one of the greatest ice reservoirs in Eurasia and constitute 15% of the total ice area of arctic islands (Dyurgerov & Meier 1997). Four large glaciation centres of Svalbard may be distinguished: three on Spitsbergen and one on Nordaustlandet (fig. 3.1). Heavy glacier cover occurs also on smaller eastern islands of Barentsøya, Edgeøya and Kvitøya. In Spitsbergen ice is primarily focused in mountainous regions in the south, north-west and north-east of the island. These glacier cover centres consist of multiple connected ice caps and ice fields, drained by long (up to 40 km) outlet glaciers, with individual ice streams separated by nunatak ridges. Arid central regions of Spitsbergen are less favourable for glaciers' development, hence are relatively poorly glacier-covered (in 10-30%) and dominated by local, mountain glaciation (cirque and valley glaciers). On the second largest island, Nordaustlandet, extensive ice caps occur: Vestfonna and Austfonna, the latter being the largest glacier of Europe and one of the largest in the Arctic ($8 \cdot 10^3$ km^2). Due to regional climate gradients (mainly precipitation and summer air temperature distribution) glaciation has developed at different levels. It is well reflected by distribution of theoretical, steady-state equilibrium line altitudes (ELA, fig. 3.3),

being the lowest along the coasts (100-300 m a.s.l.) and much higher in arid, quasi-continental interior of Spitsbergen (up to 800-900 m a.s.l.).

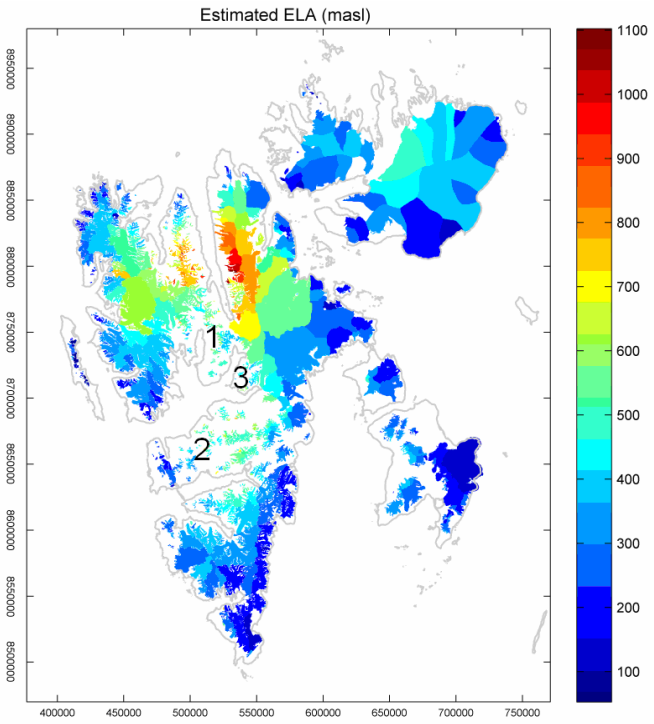

Fig. 3.3 Theoretical steady-state equilibrium line altitude in Svalbard after König et al. (2013). Numbers indicate the regions of central Spitsbergen: 1 - Dickson Land; 2 - Nordenskiöld Land; 3 - Bünsow Land. Note the lowest ELA along the coasts and high ELA in the interior of Spitsbergen

Most of Svalbard glaciers are polythermal, with temperate deeper layers (type A from fig. 2.3) and often also accumulation zones (type E, e.g. Schytt 1969; Gokhman & Khodakov 1983; Ødegård et al. 1992; Bjornsson et al. 1996; Jania et al. 1996; Moore et al. 1999; Pälli et al. 2003a). Glaciers smaller than ~5 km^2 are rather cold throughout their mass, with minor patches of temperate ice-bed interface (e.g. Hodgkins et al. 1999; Etzelmüller et al. 2000; Machío et al. 2007; Bælum & Benn 2011). Activity of small glaciers is generally low in Svalbard, due to low mass balance gradients (average of 41 cm w.eq. · 100 m^{-1}, Pelto et al. 1990), low inclination and cold ice presence. Small land-terminating glaciers flow at typical velocities of 1-15 m a^{-1} (e.g. Baranowski 1977; Melvold & Hagen 1998; Hagen et al. 2003a; Sund & Eiken 2004; Nutall & Hodkins 2005; Neumann 2006; Rachlewicz 2009a). Larger tidewater glaciers show significantly faster ice motion, typically on the order of 30-300 m a^{-1} (e.g. Vieli et al. 2004; Błaszczyk et al. 2009), which in extreme cases may reach mean long-term velocity of few metres daily (Kronebreen, Hagen et al. 2003a).

During relatively short periods similarly high flow speed has been achieved by many other glaciers during surges (e.g. Hagen 1988; Murray et al. 1998; Dowdeswell & Benham 2003). Surge-type glaciers are generally very common in Svalbard (e.g. Schytt 1969; Dowdeswell 1986; Hagen 1987, 1988; Dowdeswell et al. 1991; Lefauconnier & Hagen 1991; Jiskoot et al. 2000; Sund et al. 2009). Their share in the local population is uncertain, but it is relatively high: it has been estimated as 13% (Jiskoot et al. 1998), 36% (Hamilton & Dowdeswell 1996) or as much as 90% (Lefauconnier & Hagen 1991). Svalbard surges are different from those observed in other regions of the globe, as they are characterized by a very long quiescent

phases (50-500 years, attributed to low build-up rates; e.g. Hagen 1987; Solheim 1991; Liestøl 1993; Murray et al. 1998), as well as long active phase duration (3-10 years; Dowdeswell et al. 1991). Surges in Svalbard are expected to be triggered due to a thermal switch at the bed, from cold to temperate conditions (Fowler et al. 2001; Murray et al. 2000, 2003). Distinct short-term glacier speed-ups, though much weaker than a surge, are also observed in Svalbard in response to increased basal lubrication caused by increased surface water availability by summer melting (e.g. Vieli et al. 2004; Nutall & Hodgkins 2005; Dunse et al. 2012).

Melting in Svalbard is dominated by radiative fluxes (shortwave and longwave), although there is a limited sample of energy balance investigations, likely due to difficult maintenance of measuring stations in remote polar conditions. One of the first studies of energy balance issues in Svalbard were performed on Werenskioldbreen (S Spitsbergen) in the period 1957-1960 and later, mainly by Polish researchers from University of Wrocław (Baranowski 1977), and recently continued (Ignatiuk 2012). Modern records from different glaciers in Svalbard reveal average summer shortwave radiation flux (SW_{in}) on the order of 150-200 W m^{-2} and incoming longwave flux (LW_{in}) of 280-290 W m^{-2} (Hodson et al. 2005; Arnoldt et al. 2006; Migała et al. 2006; Krismer 2009; Østby 2010). Mean summer sensible heat flux (Q_H) is generally similar at each site (11-13 W m^{-2}), whereas latent heat flux (Q_L) is low or even negative. In general, summer energy balance along the coasts of Svalbard is dominated in 72-83% by net radiation (Q_N) and sensible heat flux (9-19%), while latent heat flux is of the lowest overall importance (from -12 to 9%).

According to Hagen et al. (2003a) the cryosphere of Svalbard is very sensitive to climate changes and ocean shifts, due to its relatively mild conditions and proximity to oceanic heat transfer zone. Hence, its extent has changed in time considerably, particularly in the last millennium. A broad study by Svendsen & Mangerud (1997) argues that a small glacier Linnebreen in W Spitsbergen (and probably many other small glaciers as well) has started to form just 4,400 years BP, when climate became favourable for glacier development. The same authors conclude that Svalbard glaciers have reached their maximum Holocene extents during the late-LIA (around year 1900 AD). The reason for these glacier advances is attributed to low air temperature and/or increased winter precipitation, but their relative importance is still debated (e.g. Isaksson et al. 2001, 2003; D'Andrea et al. 2012).

The general warming observed in Svalbard since the early-20th century (Nordli & Kohler 2003) has a distinct negative impact on local ice masses, with small glaciers showing the fastest response to changing climate (e.g. Johanneson et al. 1989; Grudd 1990). Glaciological investigations on small, land-terminating glaciers are well developed in Svalbard, mainly around human settlements Ny-Ålesund, Hornsund and Longyearbyen. Midre Lovénbreen and Austre Brøggerbreen in Ny-Ålesund area (fig. 3.1) are objects of long-term mass balance programme by Norwegian Polar Institute. Their direct records span since the 1960's and indicate an average net balance of -38 and -48 cm w.eq. respectively (WGMS 2012). Despite progressive climate warming, their records (being among the longest in the Arctic) do not reveal any clear trend. Hagen et al. (1991) reconstructed their mass balance and announced net mass loss since at least 1912. A similar finding has been recently reported by Grabiec et al. (2012) for Werenskioldbreen in the area of Polish Polar Station in Hornsund. In the more recent years Werenskioldbreen and neighbouring Ariebreen have been showing very negative net balance (3-year averages of -87 and -68 cm w.eq. respectively, Nawrot 2011; Ignatiuk 2012). Waldemarbreen, Irenebreen and recently also Elisebreen (NW Spitsbergen) are covered with direct studies since mid-1990's or early 2000's by Nicolaus Copernicus

University in Toruń, Poland, and show slightly higher mass loss rates than glaciers in nearby Ny-Ålesund area (about -60 to -70 cm w.eq., e.g. Sobota 2007a, b, c, 2009; WGMS 2012). Several small glaciers were also studied near the Russian town Barentsburg, i.e. Aldegondabreen and Grønfjordbreen, which have been showing an extremely high mass deficit exceeding -120 cm w.eq. between 2003 and 2006 (Solovyanova & Mavlyudov 2007). Russian measurements from several central and east Spitsbergen glaciers revealed their average net balance of -32 to -70 cm w.eq. in the 1970's and 1980's (Troitskiy 1988). Mass loss from small Svalbard glaciers has been also confirmed indirectly by analysis of their geometry changes (e.g. Baranowski 1977; Jania et al. 1984; Bukowska-Jania & Jania 1988; Jania 1988; Etzemüller et al. 1993; Lankauf 2002; Nuth et al. 2007, 2010; Kohler et al. 2007; Rachlewicz et al. 2007; Zagórski et al. 2008a,b; Barrand et al. 2010; Moholdt et al. 2010a,b; James et al. 2012). The negative changes have caused partial or total decay of their firn zones and at numerous sites exposed bare ice. Hence, meltwater can not penetrate to lower layers anymore, so no latent heat release and warming occurs. This process has important consequences: there are strong evidences for changing hydro-thermal regimes of Svalbard glaciers by freezing up of their bodies (e.g. Hodgkins et al. 1999; Hambrey et al. 2005; Willis et al. 2007).

Response of larger glaciers to climate change is disturbed by bedrock topography (in case of tidewater glaciers) and often also by dynamics (surges). Field-based studies in Svalbard show that their mass balance may be either slightly negative, as seems e.g. for Hansbreen and Nordenskiöldbreen (-35 and -39 cm w.eq. respectively; WGMS 2012; Van Pelt et al. 2012), or near-zero or positive (e.g. Kongsvegen and Austfonna, Hagen et al. 2003a; Moholdt et al. 2010b). Direct and indirect studies on other larger glacier systems in Svalbard confirm this regularity and attribute it to their size and hypsometry, excluding actively surging glaciers (e.g. Melvold & Hagen 1998; Pinglot et al. 2001; Hagen et al. 1999, 2003a, 2005; Bamber et al. 2004, 2005; Raper et al. 2005; Nuth et al. 2007, 2010; Kääb 2008; Moholdt et al. 2010a, b). Large ice masses drive the overall mass balance of Svalbard. Despite its significant decrease by calving of tidewater glaciers (Błaszczyk et al. 2008; Dowdeswell et al. 2008), modern Svalbard-wide estimates range from -12 cm w.eq. to -55 cm w.eq. (Dowdeswell et al. 1997; Hagen et al. 2003b). The most recent estimate of -19 cm w.eq. a^{-1} (including calving) corresponds to 1% of cryospheric sea-level rise contribution (0.013 mm a^{-1} for 2003-2008, Moholdt et al. 2010a). Negative mass balance mode significantly prolonged quiescent phases of Svalbard surge-type glaciers, leading to reduction of their activity (Hodgkins 1994; Dowdeswell et al. 1995; Melvold & Hagen 1998).

Only very few glaciers in central Svalbard have been well ellaborated yet and most of them remain completely uninvestigated. Mass balance records from three glaciers in central Spitsbergen suggest lower snow accumulation and similar ablation as elsewhere in the archipelago (Troitskiy 1988). Nuth et al. (2007) announced slow average thinning of glaciers in central Nordenskiöld Land (-26 cm a^{-1}, 1936-1990). Kohler et al. (2007) and James et al. (2012) measured long-term thinning of Slakbreen and reported -32 cm a^{-1}, with a net thickening until 1960. Bælum & Benn (2011) measured -60 cm a^{-1} for Tellbreen. Due to rather low initial area of local glaciers, their post-LIA area changes may exceed -50% or more (Ziaja & Pipała 2007). Thermal structure of local ice masses seems to be predominantly cold with only small patches of temperate bed, although for some of them evidence exists for polythermal regime earlier in the 20th century (e.g. Hodgkins et al. 1999; Etzelmüller et al. 2000; Rutter et al. 2011; Bælum & Benn 2011). Present-day polythermal structure seems to be restricted to larger glaciers, as i.e. Slakbreen and Gruvefonna (Schuler & Melvold 2004).

To sum up, due to climate warming Svalbard ice reserves have been showing negative mass balance and wide-spread thinning over the last decades. These changes are much more pronounced in case of small valley glaciers, than larger ice caps and ice fields. Although changes in larger systems are often related to their dynamics, small glaciers respond mainly to a mass balance change, due to progressively warming ablation seasons, particularly after 1990. It must be however noted, that the glaciological research is biased towards the coastal areas of Svalbard, leaving many central Spitsbergen regions poorly investigated, i.e. Dickson Land. Their climatic conditions differ from those found along the coasts and are likely to significantly affect glaciers' functioning.

3.3 Climate and glaciology of Petuniabukta basin

The studied glacier, Svenbreen, is located in Petuniabukta, Pyramiden region, Dickson Land. Petuniabukta is the northernmost bay of Billefjorden (figs. 3.1 and 3.6A), situated far from the oceanic influence. It is a sub-basin of relatively high glacier cover as for its region (33%), surrounded by seven main glaciers, including Ebbabreen - the largest glacier of Dickson Land (22 km^2). In Ebbadalen (Ebba valley) the Adam Mickiewicz University Polar Station (AMUPS) operates since 2011, being a logistical base of research activities presented in the following work.

Meteorological data was collected in the study area since 2000 and is sufficient to sketch the main elements of local climate. Previous research in this region showed that summer periods are relatively warm when compared to coastal areas (e.g. Przybylak et al. 2006, 2007b) and that air temperature, T_a, at PET station (5 m a.s.l., close to AMUPS, see fig. 3.6B) shows very high correlation with conditions at SVL station in Longyearbyen (Rachlewicz & Styszyńska 2007; Láska et al. 2012). Further in text, PET dataset is also compared to Ny-Ålesund station (NYA) in NW Spitsbergen (see fig. 3.1). Unfortunately, due to the expeditionary character of AMU research and equipment malfunctions, continuous PET records are limited, e.g. full annual records are available only for 2002 and 2010 (fig. 3.4, tab. 3.1). Therefore, data from each year was used to caclulate a multiannual mean for each day of the year (fig. 3.5A). Any statistics given in this section (averages or totals for given periods) refer to the baseline curve from fig. 3.5A, unless otherwise stated. It must be underlined that the values presented in this section were not derived using climatological standards and are only used to give a general picture of climatic individuality of the study area.

The annual T_a cycle in Petuniabukta reflects well its high latitude location, with long winter and short summer seasons. As mentioned in section 3.1 climate in Svalbard is mild as for its latitude (79° N), what is best visible as relatively high winter air temperature. In the period 2000-2012 mean daily T_a has never dropped below -30°C at SVL and there were several winter seasons when it was generally not lower than -20°C (fig. 3.4). Winter T_a course is characterized by high day-by-day variability due to common advection of warm air masses to Svalbard, what makes mid-winter thawing events typical for the archipelago. In the comparison period the coldest month at PET was March (-17.0°C on average). Midnight sun period lasts from mid-April to late-August and positive air temperature occurs between mid-May and late-September (± 2 weeks). Average summer T_a (June-July-August, JJA) is 6.1°C, being slightly higher than calculated for SVL (5.5°C, if the same days are used for computations) and NYA (4.3°C, tab. 3.1). The warmest month of the year is July with mean of 7.6°C.

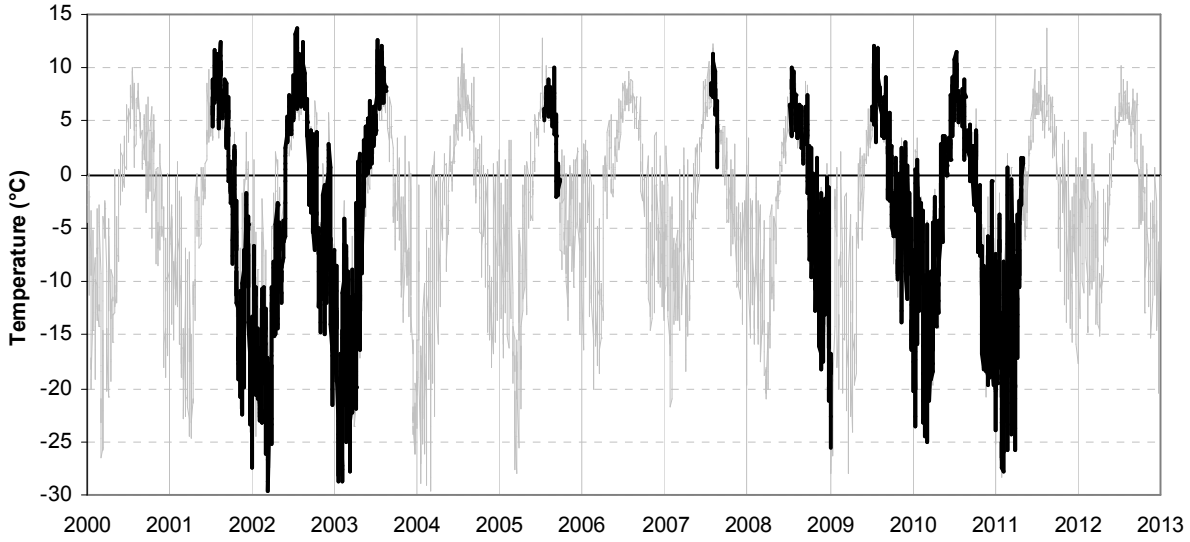

Fig. 3.4 Available temperature record from PET station (black) against temperature variations at SVL (grey). Data from SVL after Norwegian Meteorological Institute

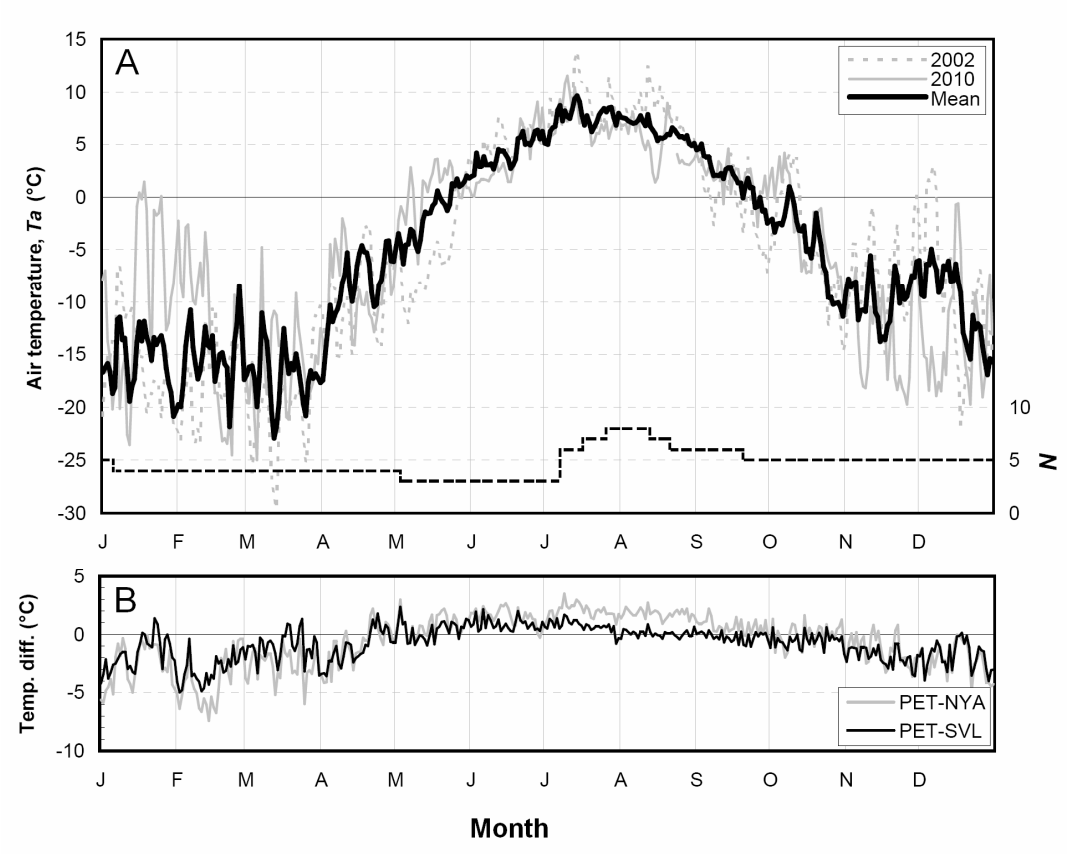

Fig. 3.5 A - Annual air temperature cycle in Petuniabukta, central Svalbard. Thick line - mean daily temperature (averaged from discontinuous data from 1710 days between 2001 and 2011). Gray lines - examples of yearly temperature records showing typical variability range; black dashed line (*N*) - sample size (number of seasons with a record for a given day); B - temperature differences between PET, SVL and NYA. Positive values indicate periods when air temperature at PET is higher than at a station of comparison. Data from SVL and NYA after Norwegian Meteorological Institute

Tab. 3.1 Mean monthly temperature (in °C) at PET, SVL and NYA obtained for the averaged dataset and for example years 2002 and 2010 (the only years with full annual record). Note increased thermal contrasts at PET, particularly the warmer ablation seasons. Data from SVL and NYA after Norwegian Meteorological Institute

	AVERAGE*			2002			2010		
Month	**PET**	**SVL**	**NYA**	**PET**	**SVL**	**NYA**	**PET**	**SVL**	**NYA**
January	-15.5	-13.8	-12.8	-15.7	-12.7	-11.7	-9.8	-7.2	-8.0
February	-15.3	-12.2	-11.3	-17.2	-13.5	-12.4	-12.5	-10.3	-10.6
March	-17.0	-15.9	-14.4	-20.0	-18.1	-14.5	-15.8	-15.8	-14.0
April	-8.4	-7.3	-7.4	-9.5	-6.1	-7.1	-9.0	-7.7	-7.7
May	-1.5	-1.9	-2.3	-5.4	-3.4	-3.9	0.4	0.0	-0.3
June	4.2	3.3	2.7	5.1	3.7	3.0	3.7	3.5	2.8
July	7.6	6.8	5.6	8.4	7.0	5.8	7.3	6.6	5.7
August	6.4	6.3	4.6	7.8	7.5	5.5	5.1	4.9	3.4
September	1.7	1.9	1.0	-0.3	0.1	-0.9	1.9	2.0	1.2
October	-4.6	-4.1	-4.5	-4.1	-3.0	-3.3	-2.9	-2.9	-3.4
November	-9.5	-7.6	-8.2	-7.7	-5.6	-5.4	-13.0	-11.0	-11.6
December	-10.2	-8.3	-7.9	-9.4	-7.5	-6.9	-13.1	-11.7	-10.9
MEAN annual temp.	**-5.1**	**-4.3**	**-4.5**	**-5.7**	**-4.3**	**-4.3**	**-4.8**	**-4.1**	**-4.4**
MEAN summer (JJA) temp.	**6.1**	**5.5**	**4.3**	**7.1**	**6.1**	**4.8**	**5.4**	**5.0**	**4.0**
Annual PDD sums	**631**	**581**	**443**	**722**	**682**	**541**	**609**	**595**	**456**
PDD summer sums (JJA)	**559**	**508**	**395**	**649**	**590**	**439**	**489**	**461**	**369**

*Average conditions in the comparison period stacked from 1710 days between 2001 and 2011

The new composite record confirms previous findings of Rachlewicz (2003a, 2009a; Rachlewicz & Styszyńska 2007), reporting quasi-continental climate in Petuniabukta, although some doubts remain about its reliability, as the measuring sensor was not calibrated. Hence, the presented results may be treated only as an approximation: typical error of monthly means lies probably within ± 1°C and is expected to be the highest during summer. In any case, high JJA T_a makes PET one of the stations with the warmest ablation seasons in Svalbard. However, local mountainous topography modifies T_a to a significant extent, both vertically and horizontally, so automatic air temperature sensors installed at other sites in the study area show different seasonal and daily T_a course pattern (Bednorz & Kolendowicz 2010; Láska et al. 2012). Because Petuniabukta is situated 100 km from the open seas, air moisture advection is limited. Therefore, relative humidity (*RH*) observed at PET in the summertime is typically only about 70-75% (Rachlewicz 2003a; Małecki et al. 2011), although Láska et al. (2012) reported mean *RH* exceeding 80% on the other side of Petuniabukta. No year-round precipitation measurements were performed in the study area yet. Rachlewicz (2009a) indirectly estimated its annual sums to be 150-170 mm, being even lower than at measured at SVL. Short campaigns of July-August precipitation measurements seem to confirm reduced summer rainfalls (15-33 mm) when compared to other sites on Spitsbergen (35-115 mm, Przybylak et al. 2006, 2007).

The object of research in this work, Svenbreen, has not been studied yet, although glaciological investigations in the study area were intensive in 1970's and 1980's. For practical reasons detailed studies were performed on Bertilbreen: a water supply for a nearby Russian town and coal mine Pyramiden, neighbouring Svenbreen from the south and having a similar size (fig. 3.6). The works covered mass balance measurements, radio-echo soundings, borehole drilling and hydrological monitoring. Between 1976 and 1985 the glacier has shown average winter balance of only 41 cm w.eq. (Troitskiy 1988), being the lowest in Svalbard, likely reflecting arid climate of the region. Summer balance of Bertilbreen was very similar as noted elswhere (-115 cm w.eq.), suggesting that increased summer air temperature has no

distinct effect on ablation rates. Average net balance of the glacier was -74 cm w.eq. and was the most negative from all glaciers surveyed in Svalbard at that time. The glacier volume was estimated as 0.46 km^3 by Macheret et al. (1985), with maximum ice thickness of about 150 m (Zhuravlev et al. 1983). Bertilbreen has a cold surface layer, with 10 m ice temperature of about -4.5°C (Jania et al. 1996) and a temperate basal layer along its centre line (Zhuravlev et al. 1983). In a borehole drilled down to 50 m depth measurements revealed no liquid water phase despite pressure melting point conditions, while at a site located just 200 meters from the centreline temperature at 100 m depth was only -1.1°C (Ueda & Talalay 2007). The temperate core of Bertilbreen was subjected to a distinct decay due to the retreat of firn line (Gokhman 1987a,b; Gokhman et al. 1982). Predominantly cold regime causes relatively low ice velocity of Bertilbreen on the order of 2.5 m a^{-1} (Mavlyudov 2010). Russian investigations were terminated in 1985, but since 2010 the glacier is again under observation of Czech researchers (e.g. Hanaček et al. 2011; CPE 2012).

Researchers from Adam Mickiewicz University in Poznań, Poland, have been conducting glaciology-related studies in Petuniabukta area since 1980's. Karczewski (1989) argued an early-20th century surge activity of Hørbyebreen, being a rare feature in Dickson Land, indirectly confirmed later by Gibas et al. (2005). Direct glacial research covered mainly past and present geomorphological processes and controls of sedimentation by local glaciers and was summarized by i.e. Kłysz (1985); Karczewski (1989, 1995), Karczewski et al. (1987), Karczewski & Rygielski (1989), Kostrzewski & Zwoliński (2003); Rachlewicz (2007, 2009a); Kasprzak & Ewertowski (2007); Ewertowski et al. (2010, 2011) and Szuman & Kasprzak (2010). Glacio-hydrological research was conducted on several glaciers in the area (e.g. Kostrzewski et al. 1989; Kostrzewski & Zwoliński 1995; Rachlewicz 2003b, 2009a, b; Strzelecki 2007, 2009). Visual synthesis of geomorphological research has been illustrated as maps by Kłysz et al. (1987), Karczewski et al. (1990) and recently by Evans et al. (2011). Melting and motion of three local ice masses (Hørbyebreen, Ebbabreen and Ragnarbreen) were investigated in detail by Rachlewicz (2009a). His direct ablation measurements revealed very high summer surface lowering between 2001 and 2003 at their fronts (200-250 cm a^{-1}) and at ~500 m a.s.l. (100-150 cm a^{-1}). Maximum flow velocities recorded for these glaciers were 10-12 m a^{-1}, with a ~30% increase during the melt season. River discharge was dominated by supraglacial drainage, as suggested by high correlation with air temperature. Character of water outflow after freeze-ups and during winter periods was interpreted as an evidence of their polythermal regime. Similarly as in other Svalbard regions, Petuniabukta glaciers also have been experiencing fast decay. Mean long-term rates of their front retreat vary between 5 and 15 m a^{-1}, though locally they may exceed 150 m a^{-1} over shorter timescales (Rachlewicz et al. 2007). Until now, no research has been conducted on Svenbreen, chosen as object of detailed studies in this work.

3.4 Svenbreen

Svenbreen (ID 145 12, Hagen et al. 1993) is a small (3.7 km^2) land-terminating valley glacier, spanning from 170 m to 750 m a.s.l., with relatively high median elevation of 470 m, typical for central Spitsbergen. Despite its small size it is characterized by a complex ice supply pattern. It has a well developed main glacier cirque (500-750 m a.s.l.) and three tributaries, given in this study unofficial names: *Poznańskaret*, *Nataliaskaret* and *Hannabreen* (fig. 3.6). The first is a north-western branch of the glacier, connected with a neighbouring glacier Hoelbreen at 650 m a.s.l. Nataliaskaret is a southern pass (630 m a.s.l.) between Svenbreen and Ferdinandbreen, from which two steep ice streams origin. Hannabreen is an individual

small glacier (300-400 m a.s.l.) located close to the present-day front of Svenbreen, in a deeply incised, well shaded cirque and is treated as a separate unit, hence not included into the Svenbreen area. The only information in the literature about the glacier relevant for its further studies was the occurrence of icings in its forefield (Gokhman 1987b), significant retreat of the front in the period LIA-1960 and slow since then (Rachlewicz et al. 2007). The glacier is not known to surge. Its theoretical steady-state ELA is at about 420 m a.s.l., if equilibrium accumulation area ratio is assumed as 0.6.

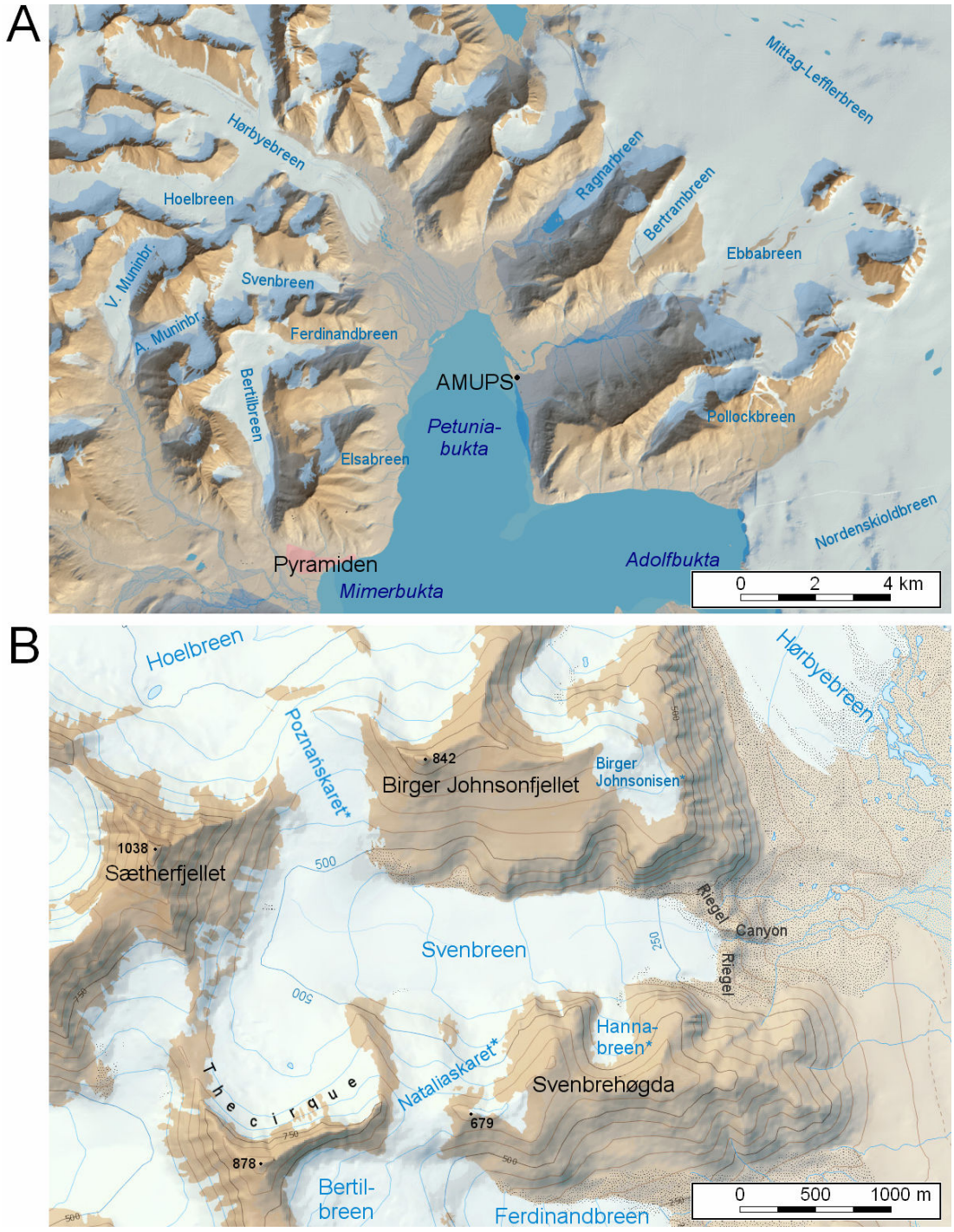

Fig. 3.6 Location of the study area. A - Petuniabukta region (AMUPS - Adam Mickiewicz University Polar Station); B - Svenbreen basin. Names marked with an asterisk are unofficial. Glacier geometry is valid for 1990, contour interval is 50 m. Maps are a courtesy of Norwegian Polar Institute

The Svenbreen area is very diversified. The present-day glacier snout is hidden behind a huge roche moutonée riegel, projecting for ~50 m above the front on the up-glacier side, and for as much as ~200 m above moraine zone from the steeper down-glacier side. The riegel is dissected by a deep short canyon, occupied by a rapid proglacial stream and blocks of icings. The Svenbreen valley (*Svendalen*) is deeply incised between Birger-Johnsonfjellet in the north (842 m), Sætherfjellet in the west (1038 m), the cirque in the south-west (878 m) and Svenbrehøgda in the south (679 m). In the upper zones of Svendalen sedimentary mountain slopes are moderately inclined, with exception of the main glacial cirque. They become very steep in the lowest sections of Svendalen, where metamorphic Hecla Hoek rocks are exposed. Relief of the glacier-covered parts of the valley remained unknown until detailed geophysical field investigations with ground-penetrating radar (*GPR*) for the purpose of this work (section 5.2.1). Some of the basic characteristics of basin and glacier geometries were inferred from a 2009 DEM. Total area of the basin is 8.66 km^2 and 45% is covered with ice (Svenbreen, Hannabreen and Birger-Johnsonisen). The glacier surface is even and poorly inclined (8° on average, fig. 3.7a), although its aspect is very variable over short distances, with areas exposed mainly towards east, north and south (fig. 3.7b). Together with complex surrounding topography it causes large spatial variability of potential direct solar radiation (fig. 3.7c). Southern rims of Svenbreen tongue and the main cirque are very well shaded and protected from sunshine, while along the northern rims (and especially on southerly exposed Poznańskaret) potential insolation is relatively high.

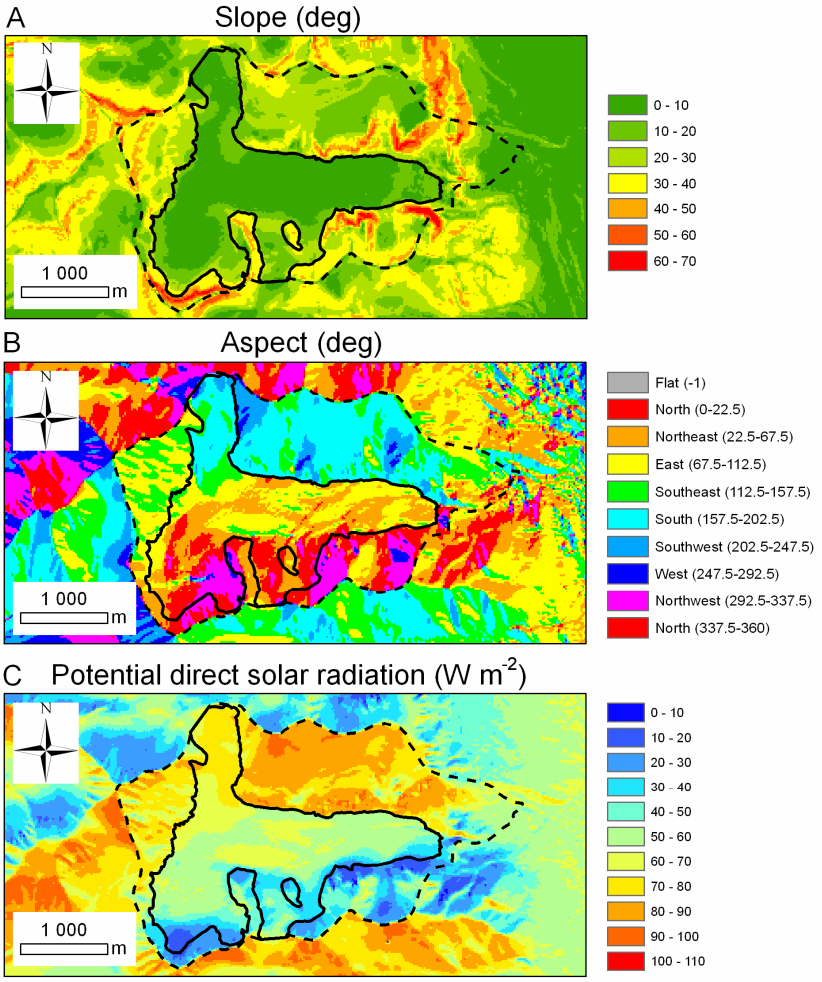

Fig. 3.7 Selected surface properties in Svenbreen basin (dashed line) for its 2009 geometry: A - slope inclination; B - aspect; C - potential direct solar radiation averaged for 15/06-15/09. Solid line - Svenbreen outline

The introduction to the literature presented in this chapter shows, that data concerning response of central Svalbard glaciers to climate change is patchy and is a mosaic of selected issues, rather than a general and coherent picture. It is still unclear if average mass loss of local glaciers is fast or slow (in relation to small ice masses elsewhere in Svalbard). Peculiar quasi-continental climatic conditions are generally poorly elaborated yet. Almost no glacio-meteorological data from Spitsbergen interior has been discussed in the literature, so understanding of the influence of warm and dry summer seasons on melt and runoff processes is poor. Thermal regime of most glaciers in the region may be only guessed from their size, presence of icing fields or sparse hydrological records. Hence, there was a strong need to perform a broad research in this region and Svenbreen was chosen as the object of detailed investigations.

4

Methods and errors

To solve the main scientific problem, dealing with impact of quasi-continental climate of central Spitsbergen on the present-day state, functioning and changes of Svenbreen (chapter 1), a wide variety of methods was selected. They may be generally divided into fieldworks and cameral (office) works. The first group aimed to collect data directly from the glacier. The performed activities covered installation and maintenance of originally designed, comprehensive and integrated monitoring network, mass balance measurements, geodetic and geophysical surveys. The second part of the work covered analysis, interpretation and intercomparison of the collected information and available topographic data. As an effect of intensive research in the last years, data for each of the elements presented in fig. 1.1 is available (for results see chapters 5-7). For the key elements of the methodology, an error assessment has been carried out. It must be here underlined, that the presented work is the first such broad glaciological study in Dickson Land, after Russian research programme on Bertilbreen was terminated in 1985.

4.1 Geomorphometric and geodetic measurements

Geomorphometric and geodetic studies aimed to recognize geometry of glaciers in the study area for 1960, 1990, 2009, 2010 and 2012, and its changes between these years. 1960 geometry was obtained from a 1: 100 000 topographic map with 50 m contour interval. The map was constructed by Norwegian Polar Institute (NPI) with use of 1: 50 000 vertical aerial images. Glacier topography in 1990 was recognized from a NPI digital elevation model (*DEM*) with 20 m resolution, constructed from vertical images (1: 15 000). A new, 2009 DEM with 20 m cell size was created by Strzelecki (2013) from vertical photographs of ~0.5 m ground resolution and was been used in the analysis. To check for misalignments between all datasets, a universal co-registration correction, described in details by Nuth and Kääb (2011), was used. The datasets were iteratively aligned to 1990 DEM until the computed misalignments in x, y and z directions were lower than 0.2 m. Glacier outlines were digitized from the described data sources, disregarding elongated snow-patches adhered to the surrounding rock walls. Glacier outline for the Little Ice Age maximum was obtained by

simple addition of the area of lateral and frontal moraine complex to the oldest available outline (1960). Length of Svenbreen was measured along 3 profiles, spreading from the highest point on the glacier to the front and parallel on its tongue. Results were then averaged for LIA, 1960, 1990 and 2009.

Geometry changes for the 1990-2009 epoch were measured by subtracting co-registered and aligned 2009 DEM from 1990 DEM. To measure elevation differences between 1960 map and 1990 DEM, 1960 contours were exported to point format and interpolated into the cells of 1990 DEM by bilinear interpolation, so local elevation difference, *dh*, between the two years could be measured. A map of surface elevation changes of 20 m resolution was then created using 'Topo to Raster' tool (a discretized thin plate spline technique available in ESRI ArcGIS software) and *dh* value at each point. Manually drawn contours of equal elevation change at the glaciers' fronts were introduced to improve the performance of the interpolation, because high gradients of *dh* and sparse data produced unrealistic patterns, i.e. closed zones of high surface lowering along the contours, with areas of modest thinning between them. In order to evaluate performance of this method, it was used to calculate *dH* for the 1990-2009 period, for which DEMs are yet available. The results of the tests were in good agreement with those obtained by DEM differencing. Residuals ranged from -0.62 to 0.55 m. If weighted by area of the studied glaciers, the mean difference in *dH* between the method and DEM differencing was -0.24 m, with standard deviation of 0.42 m. When measured in %, method A gave on average more negative values by 2%, with differences ranging from -5% to 4% for individual glaciers in relation to DEM-obtained results. It may be therefore stated that the method gives similar results as DEM differencing. To calculate total volume change of a glacier (*dV*), *dh* at each cell of the final rasters was multiplied by the area it covers (400 m^2) and the results were further summed up. From *dV* an average glacier surface lowering (*dH*) was inferred by dividing *dV* by mean glacier area in a given period.

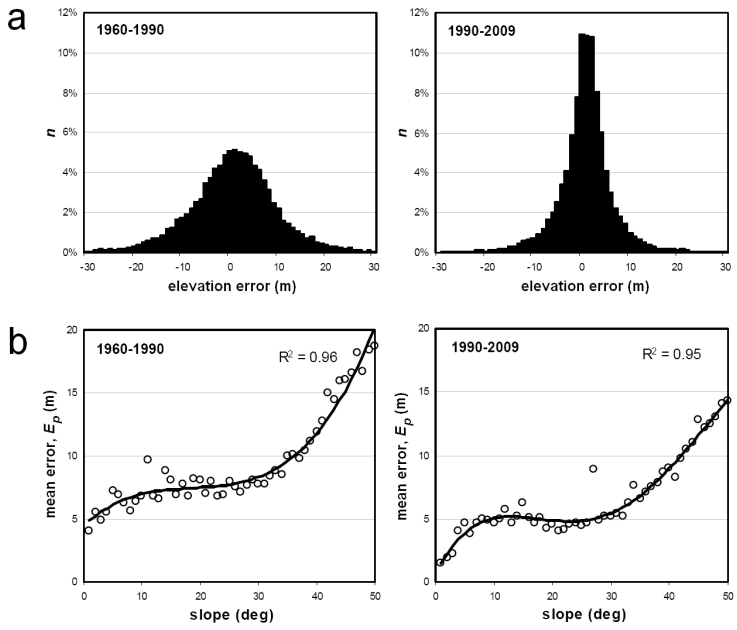

Fig. 4.1 Errors of topography datasets used in this study: A - frequency distribution of elevation errors over non glacier-covered terrain and B - elevation error against slope for stable ground and glacier ice.

To estimate the mean error of the analysis, elevation differences between individual topographic datasets from non glacier-covered terrain were investigated using over 18 000

(1960-1990) and 35 000 points (1990-2009). Standard deviation of elevation difference in the whole populations of points was 10.8 m and 7.3 m, respectively for 1960-1990 and 1990-2009 (fig. 4.1A). However, the points used in this test represent mountainous terrain, characterized by high angle of slopes, where even low misalignments translate to distinct elevation errors. Ice masses in Svalbard are gently inclined (typically 10° for small valley glaciers), so the expected errors should be adequately lower. To investigate this relation, points were grouped in 1° slope bins and in these clusters root mean square error was calculated, representing mean elevation error of an individual point at a given slope (E_p). As a result, a relationship of E_p rising with slope was obtained, well described by third order polynomial functions (fig. 4.1B). Further, the error also depends on surface type: snow surfaces are characterized by greater elevation errors than stable terrain due to low radiometric contrast on aerial images. In this study glacier ice with good contrast has error characteristics similar to that of non glacier-covered terrain, while for snow covered parts the errors from fig. 4.1B are assumed to be doubled (Nuth et al. 2010).

With use of a DEM, a slope histogram of the glacier could be extracted and applied to a respective function in order to convert slope bins to E_p bins. Then, for each epoch a weighted mean of E_p was calculated to obtain a typical elevation error for the whole population of points located on the glacier (E_g). The total error of the elevation change measurement (E_{dH}) was calculated by dividing E_g by a square root of sample size (N):

$$E_{dH} = \frac{E_g}{\sqrt{N}} \qquad \text{(Eq. 4.1)}$$

As the elevation errors are spatially autocorrelated to a certain level, correlation scale of 1 000 m was adopted from the literature, so N became the glacier area in km^2 (Nuth et al. 2007; James et al. 2012). Volume estimate error is simply E_{dH} multiplied by the area of the glacier in a studied period.

GPS surveys on Svenbreen were carried out on 27/07/2010 and 23/07/2012 with Leica equipment in order to measure location of ablation stakes and their displacement. Base station was installed on a stable ground close to the front of Svenbreen, while the actual surface was measured by placing a rover antenna into the snow, thus neglecting the snow surface. Real point elevation change $dh_{2010\text{-}2012}$ accounts for surface slope along motion vectors. Accuracy of GPS measurements depends on many factors, such as: precision of installation of the base station above a fixed point with known coordinates (assumed accuracy ± 1 cm), precision of measurement itself (± 5 cm) or re-measuring exactly the same point as in the earlier survey (± 2 cm). For the purpose of this study, a conservative overall error for stake locations has been set as ± 10 cm, propagating to ± 14 cm for raw elevation changes 2010-2012 and horizontal stake displacements calculated from GPS data. In case of annual rates of surface lowering and horizontal flow ($dh/dt_{2010\text{-}2012}$ and U_h respectively) the error is twice lower (± 7 cm), as the data covers two years. Rates of ice emergence/submergence (U_v) carry a slightly higher uncertainty (± 8 cm), as they are computed from $dh/dt_{2010\text{-}2012}$ and point net balance (with error ± 3 cm explained below).

4.2 Mass balance measurements

To investigate mass balance of Svenbreen direct glaciological method was used. Following eq. 2.1, net balance at each location (b_n) was separated into winter (b_w) and summer (b_s)

components. In reality, the elements measured at stakes are winter and net balances, while local summer balance is calculated from b_w and b_n. From measurements at stakes, glacier-wide balance values (B_w, B_s and B_n) were calculated in the second order.

4.2.1 Point mass balance measurements and errors

Winter surveys on Svenbreen were carried out on 29/03/2010, 4/05/2011 and 15/04/2012, while April and early-May are commonly assumed as the period of the maximum accumulation. Spatial distribution of snow depth was determined by 130-180 depth soundings all over the glacier (only 43 in the preliminary study in 2010) with avalanche probe. Ideally, snow probings should be coupled to last summer surface investigations. However, since very little snow survived summer seasons directly before the winter surveys, the effect of extra thickness introduced by previous-winter snow was assumed to be negligible. In order to convert snowpack thickness into water equivalent, snow density studies were performed in 2011 and 2012 at two sites in the lower (270-360 m a.s.l.) and upper part (515 m) of Svenbreen. Each 10 cm column of a snow pit was collected into a tube and weighted by Winter Engineering snow density gauge. Density at both pits was then averaged and the result was used as a uniform value for the whole glacier area.

In the summer season of 2010 a network of 14 ablation stakes were installed. Stakes were inserted for 8 m into glacier ice along the main flow-line, in 2011 two additional stakes have extended the network as a cross-sectional transect in the ablation zone (tab. 4.1, fig. 4.2). It must be pointed out that steep, high elevated zones are underrepresented by the stake network for safety reasons. Ablation measurements assume that stakes are fixed in ice (do not sink), so changes in their length exposed above glacier surface represent ablation of the surrounding ice and snow. To convert a layer lost by ablation to water equivalent, a fixed density of each medium was assumed. Density of melting snow was taken as 0.50 g cm^{-3}, superimposed ice as 0.80 g cm^{-3} and ice as 0.90 g cm^{-3}. Stake inspections were performed every 5-7 days in July and August 2010, 4 times in July 2011, 2 times in September 2011, July 2012 and September 2012. Short-term ablation rates were calculated for 14 summer periods for 3-16 stakes, giving in total 139 readings. In order to measure net balance at stakes, final inspections were carried out in mid-September (13/09/2010, 18/09/2011 and 10/09/2012). As showed by meteorological records, ablation after the final readings must have been very low (< 3 cm w.eq. in the middle of the glacier). Point summer balance was obtained by subtraction of b_w from b_n.

Tab. 4.1 Altitude of ablation stakes on Svenbreen in July 2012

Stake	Altitude (m a.s.l.)	Stake	Altitude (m a.s.l.)
S10	185	S70	391*
S20	222	S80	424*
S30	277	S90	463
S40	304	S100	513
S41	302	S110	541
S42	314	S120	625*
S50	331	S130	507
S60	358	S140	565

*July 2010

Mass balance investigations with direct glaciological method are known to suffer from many random and systematic errors (e.g. Andreassen 1999; Cox & March 2004). It is very difficult to quantify them accurately, so the following considerations are based on assumed error values. Winter balance measurements are associated with inaccuracies of snow depth probing (due to surface roughness and non-vertical snowpack penetration by a probe, here assumed as ± 5%) and density measurement (a conservative ± 10% error assumed). In conditions found on Svenbreen it corresponds to an error of 3-8 cm w.eq. of point mass accumulation estimate, the higher the greater snow depth. Further uncertainties arise from probing sample size and number of snow density data. In case of point net balance even more inaccuracies are involved. First, error of single stake length measurement or summer snow depth may be assumed as ± 2 cm (due to surface roughness and tilting of a stake), so it propagates to ± 3 cm when measuring length difference between two moments. Density of ice used in the literature varies, so in reality it may be slightly different than 0.90 g cm^{-3} used in this study (± 0.03 g cm^{-3} assumed). Similarly, assumed snow and superimposed ice density may carry an inaccuracy of ± 0.05 g cm^{-3}, resulting in b_n error for individual sites on Svenbreen ranging from 2 to 9 cm w.eq., rising with more negative mass balance. Local summer balance, b_s, is calculated from b_w and b_n, both suffering from multiple errors, so b_s uncertainty propagates to 5-9 cm w. eq. for individual stakes in both studied balance years.

4.2.2 Glacier-wide mass balance extrapolation and its errors

Local mass balance values were used as an input data to construct maps (rasters) of glacier-wide winter balance (B_w), summer balance (B_s) and net balance (B_n). Overall B_n was calculated by a simple summation of winter and summer balance rasters, both computed in the first order. In case of winter balance, the sample for map construction was relatively high and consisted of 130-180 points containing snow accumulation data. They were then interpolated to the entire glacier area using spline technique ('spline with barriers' tool in ESRI ArcGIS software). In contrast to B_w, input data for B_s raster was limited only to 14-16 ablation stakes, mainly along the glacier's centreline. Complex topography of the glacier made it unlikely that a single elevation-ablation curve would be valid for all its zones. For this reason, a new technique is here proposed for an automatic extrapolation of ablation data from stakes to entire glacier area.

It is commonly accepted that ablation decreases with increasing elevation, but other variables also play a significant role in mass loss processes (e.g. solar radiation, albedo etc., see section 2.2). Svenbreen consists of several high elevated zones of different aspect and hence - different incoming solar radiation and ablation intensity. The main concept of the new scheme origins from temperature-index modelling methods, as it rests on calculating spatially distributed degree-day factor (DDF): a factor of proportionality between ablation and air temperature (expressed as a sum of positive degree-days at each location, PDD_{obs}). In this study, the observed degree-day factor, DDF_{obs}, is averaged for each stake for the whole ablation season and is expressed as:

$$DDF_{obs} = \frac{b_s}{PDD_{obs}} \qquad \text{(Eq. 4.2)}$$

where b_s is the observed summer mass balance at a given stake (negative value) and PDD_{obs} is a sum of positive degree-days since May until the end of observations, calculated from direct meteorological record. The idea of the presented model assumes that average seasonal DDF

shows great spatial variability (e.g. Hock 2003, 2005), mainly driven by incoming solar radiation and length of snow cover presence. In reference to DDF_{obs}, modelled degree-day factor is given by a following expression:

$$DDF_{ext} = R + S \quad \text{(Eq. 4.3)}$$

where DDF_{ext} is an extrapolated value of DDF at any site on the glacier, R is a radiation term and S is a snow cover duration term. Local R depends on potential direct solar radiation at each site, r, calculated from a DEM in GIS software (average for the period 15/06-15/09, in W m^{-2}). S represents length of snow cover presence: the lower winter mass balance at each location (b_w, in cm w.eq.) and higher PDD_{obs}, the faster snow cover melts out from the site and the higher DDF_{ext} becomes.

$$R = w \cdot r \quad \text{(Eq. 4.4)}$$

$$S = (x \cdot PDD_{obs}) - (y \cdot b_w) \quad \text{(Eq. 4.5)}$$

Empirical coefficients w, x and y are tuning parameters calculated in reference to DDF_{obs} for each ablation season by least square minimalization. Parameter values used in this study are given in tab. 4.2. Both investigated summer seasons 2011 and 2012 were distinctly different in case of evolution of snow conditions during the summer season. In contrast to 2011, snow cover duration in 2012 had only a little effect on melt differentiation between individual stakes, because snow conditions were relatively even throughout the whole summer. It is clearly manifested by low absolute value of y for this year.

Tab. 4.2 Values for parameters w, x and y used for 2011 and 2012 ablation seasons

	2011	**2012**
w	-3.04	-3.42
x	-0.67	-0.42
y	-2.33	0.27

Using rasters of r, b_w and PDD_{obs}, together with empirical coefficients w, x and y, a glacier-wide maps of DDF_{ext} have been then computed for each ablation season, with its minimum and maximum values fixed at the level of extreme DDF_{obs}. As a final step, raster of DDF_{ext} multiplied by a PDD_{obs} raster gave a map of $b_{s\ ext}$ (extrapolated summer balance).

$$b_{s\ ext} = DDF_{ext} \cdot PDD_{obs} \quad \text{(Eq. 4.6)}$$

For warm summer of 2011 differences between $b_{s\ ext}$ and observed b_s for individual stakes on the glacier ranged from -9.4 cm w.eq. to 7.4 cm w.eq., with average difference of 0.5 cm w.eq. and R^2 = 0.99. For cooler and rainy summer season in 2012 differences were significantly larger (from -19.4 to 16.1 cm w.eq.), with 0.6 cm w.eq. as an average and R^2 = 0.95. If expressed in percentages, errors of modelling are low for 2011 (5% standard deviation), but considerably higher for 2012 (12%), however still acceptable (tab. 4.3).

The overall performance of final $b_{s\ ext}$ rasters was tested against rasters obtained from simple logarithmic altitude-ablation relationship. As to be expected, in both cases logarithmic solution gave slightly more negative glacier-wide values (by 8 and 5 cm w. eq., or 7% and 8% respectively), as it relied only on stake readings, thus neglecting large shaded zones at the foot

of rock walls, underrepresented by the stake network due to safety reasons (rock falls, avalanching). The author finds the new tool very promising in extrapolation of summer balance values from stakes to the entire glacier, as it is automatic, objective and based on strong theoretical background, although locally it may produce considerable errors (tab. 4.3) and fails to reproduce ablation inversions. Accounting for uncertainties associated with interpolation and extrapolation of point data, error bars of discussed glacier-wide mass balance estimates have been arbitrarily set at a higher level than point values, with ± 10 cm w.eq. for B_w and ± 15 cm w.eq. for B_s, propagating to an error of ± 18 cm w.eq. for B_n.

Tab. 4.3 Differences between observed summer balance b_s and modelled $b_{s\ ext}$ for 2011 and 2012

	2011		**2012**	
	Difference ($b_{s\ ext}$ - b_s)		**Difference ($b_{s\ ext}$ - b_s)**	
Stake	**cm w.eq.**	**%**	**cm w.eq.**	**%**
S10	5.1	2%	8.7	5%
S20	2.9	1%	5.4	3%
S30	-5.4	-3%	-4.8	-4%
S40	-7.2	-4%	-16.1	-18%
S41	-	-	-13.0	-13%
S42	-	-	-8.0	-10%
S50	1.1	1%	2.2	2%
S60	-9.4	-6%	2.2	2%
S70	-1.7	-1%	19.4	20%
S80	4.8	3%	-9.3	-17%
S90	0.5	0%	-1.8	-3%
S100	-0.6	-1%	-1.3	-3%
S110	0.2	0%	4.0	10%
S120	7.4	13%	3.6	18%
S130	6.0	5%	10.9	18%
S140	3.5	3%	6.8	15%
Mean	**0.5**	**1%**	**0.6**	**2%**
Std. dev.	**5.1**	**5%**	**9.3**	**12%**

4.2.3 Temperature index reconstruction of summer balance

Reconstruction of summer balance of Svenbreen (section 8.1.2.2) was attempted in this work with an empirical model, based on air temperature data from Svalbard Lufthavn station (SVL). To each day of the record between May and September a constant temperature gradient of -1.0°C · 100 m^{-1} (typically observed between SVL and the glacier, section 6.1.1) was used to obtain maps of approximated positive degree-day distribution for Svenbreen for different years (PDD_{SVL}). Glacier geometry was based on 1990 and 2009 DEMs. For each year in between these two dates an elevation update was introduced from a raster of annual elevation change rate to simulate changing geometry. To compute total melt the method used a linear relation between summer balance at each stake and PDD_{SVL} computed for this stake (fig. 8.3, eq. 8.1). Due to availability of two reference years only, it was impossible to calculate reliable error statistics, so ± 25 cm w.eq. uncertainty was assumed.

4.3 Integrated monitoring system

Reference climate records used in this work are a courtesy of and have been collected by Norwegian Meteorological Institute at low-altitude stations Svalbard Lufthavn (SVL, near

Longyearbyen town, 28 m a.s.l., 60 km SSW from Svenbreen) and Ny-Ålesund (NYA, western coast of Spitsbergen, 8 m a.s.l., 100 km W from Svenbreen). In the study area several measuring instruments have been operating continuously in the period of research. In the early stage of investigations a portable air temperature (T_a) and relative humidity (RH) sensor was used (WatchDog 2000 Series) at the riegel close to the front (July 2009-August 2010) and on the glacier at site S60 (358 m a.s.l., August 2010-September 2011), together with an external wind sensor (HOBO S-WCA-M003). Since 13/09/2011 weather parameters and energy balance of the surface are measured at S60 by a Campbell Scientific automatic weather station (AWS). Comparison of T_a and RH record from both stations showed that data collected by WatchDog sensor is reliable and from both these parameters air vapur pressure (e_a) is calculated. Additional stations in the lower ablation zone (at front in July-September 2011 and at S30 since then, 277 m) and in the accumulation zone (S100, 513 m), were equipped with Onset HOBO MicroStation data loggers, S-THB air temperature and humidity sensors and S-TMB ice thermistors, installed 2, 4 and 8 m below the ice surface (in glacier ice at S30 and superimposed ice at S100). Ice temperature, T_i, was interpolated between measuring points using a linear gradient between two neighbouring sensors. Map of the monitoring network is showed in fig. 4.2. A list of the measured parameters and the equipment used is to be found at the end of this section in tab. 4.4.

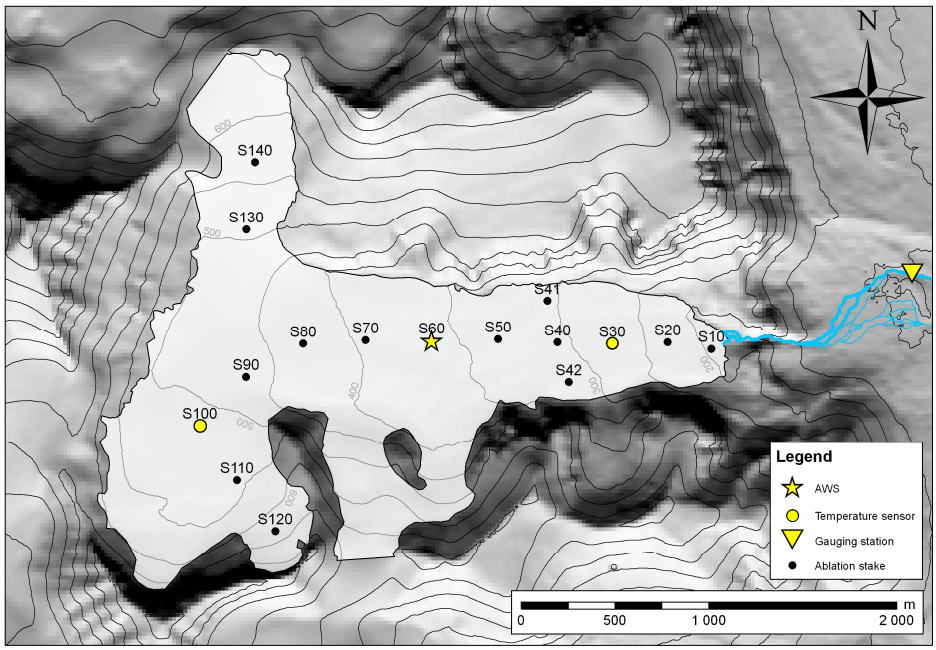

Fig. 4.2 Monitoring network on Svenbreen and location of ablation stakes. Symbols refer to stake names. Contour interval is 50 m (2009 geometry)

Several corrections were introduced to the original AWS data in energy balance calculations. RH was measured by Vaisala HMP155 thermohygrometer (in MET21 radiation shield) with respect to water, so it was corrected for ice with expression of Curry and Webster (1999). Shortwave radiation balance, SW_{bal} (eqs. 2.5 and 2.7), was measured with Hukseflux LP02 pyranometer and its results were corrected using the accumulated albedo method (being a ratio between running mean of shortwave incoming radiation, SW_{in}, and running mean of reflected radiation, SW_{out}, over 24 hours) to remove daily albedo cycle, strongly influenced by tilt of the radiation sensors and their poor cosine response (Van der Broeke et al. 2004; Andreassen et al. 2008). Net radiation, Q_N, was measured by a domeless net radiometer Kipp

& Zonnen NR-Lite, so its record was corrected for wind velocity (inferred from Young Wind Monitor 05103), with formulation provided by the manufacturer (detailed analysis of its performance can be found in Brotzge & Duchon 2000). Longwave radiation balance, LW_{bal}, was calculated from Q_N and SW_{bal}. For the melt season (15/06-10/09/2012) a constant LW_{out} was set at 315.6 W m^{-2}, being a longwave emission of black body at 0°C, thus making it possible to compute LW_{in}. Other simplifying assumptions were also included in the model: negligible rain and ground heat fluxes. Sensible and latent heat fluxes (Q_H and Q_L) were calculated with Brock & Arnold (2000) energy balance model, which turned to be useful in energy balance computations on many glaciers in the world (e.g. Peliciotti et al. 2005; Brock et al. 2007), including Svalbard (Hodson et al. 2005). It uses the bulk aerodynamic approach, suitable when measurements at only one screen level are available. The model is based on Monin-Obukhov similarity theory, includes stability corrections and assumes logarithmic vertical profiles of u, T_a and e_a. Roughness of the surface is specified as constant, in this case as 5 mm for melting snow and ice. Further, the model accounts for limitation of energy transfer during conditions of low wind speed and strong stability. Turbulent fluxes are set as zero when $u < 2$ m s^{-1} and $u/T_a < 0.3$ or when $u < 1.5$ m s^{-1} and -1°C < T_a < 1°C.

Fig. 4.3 Automatic weather station on Svenbreen in autumn 2011

In the proglacial stream, approximately 1 km from the front, a barometric water level logger HOBO U20 was operating during summer seasons (22/07-30/08/2009, 23/07-23/08/2010, 2/07-18/09/2011 and 1/07-10/09/2012), with a similar sensor measuring air pressure for compensation. The choice of the instrument location was limited, mainly due to braiding of the stream, but also due to river curvature and presence of an icing field. The stream is characterized by heavily turbulent flow conditions, having a negative impact on data quality, both of water level and discharge. Multiple manual water level inspections were performed at a fixed watermark as a control for barometrically inferred water stage information. Manual inspections have been then used to correct data from water level sensors, because continuous accumulation of dense sediments inside of a sensor tube significantly increased pressure

reading and thus - overestimation of actual water level. Moreover, turbulent flow causes at the sampling point formation of waves (~5 cm high at level of 30 cm, ~10 cm high at higher levels), which obviously influence the pressure reading. This effect is partly eliminated by high sampling frequency in 2009-2011 (5 min), but in 2012, when most discharge measurements were taken, it was only 1 h. Average error of water level measurement was estimated as ± 5 cm. Discharge measurements have been performed in 2011 and 2012 with an acoustic Doppler velocimeter Sontek Flowtracker with accuracy of ± 20%. Eight out of ten measurements were used to investigate water level-discharge relationship (rating curve). Exponential curve gave the highest correlation ($R^2 = 0.81$), but resulted in unrealistically high discharge during high stages. Therefore, power regression was chosen to represent the rating curve with $R^2 = 0.74$ (fig. 4.4).

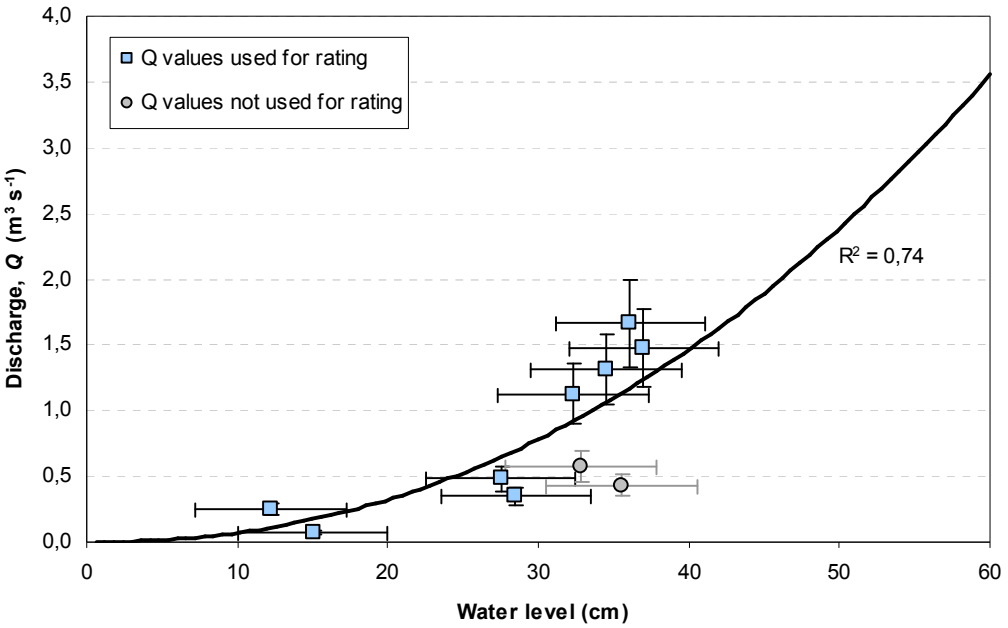

Fig. 4.4 Rating curve used for stage-discharge conversion for Svenbreen river (with 60 cm water level being about the highest ever observed). 5 cm error bars marked for water level, 20% for discharge measurements

Water balance of Svenbreen basin was estimated with the following equation modified from Hodson et al. (2005):

$$P_{winter} - B_n + P_{summer} + C = Q_{total} + E - (dS + \varepsilon) \quad \text{(Eq. 4.7)}$$

Here, P_{winter} and P_{summer} are winter and summer precipitation, B_n denotes net balance of Svenbreen, C is condensation, Q_{total} is total runoff, E stands for evaporation and $(dS + \varepsilon)$ is water storage and error term, together being a balance residual. Further relations are:

$$P_{winter} = s_{Sven} + s_{slopes} = B_w + s_{slopes} \quad \text{(Eq. 4.8)}$$

$$P_{winter} - B_n = M_{ice} + M_{snow} + M_{slopes} = B_s + M_{slopes} = M_{total} \quad \text{(Eq. 4.9)}$$

$$Q_{total} = Q_{winter} + Q_{Jun} + Q_{Jul\text{-}Sep} \quad \text{(Eq. 4.10)}$$

where: B_w and B_s - winter and summer balance of Svenbreen, s_{slopes} and s_{Sven} - winter snow cover on surrounding ice-free slopes and on the glacier respectively, M_{total} - total meltwater

production, M_{ice} and M_{snow} - meltwater produced from glacier ice and snow cover directly on Svenbreen, M_{slopes} - water from melting snow surrounding the glacier, Q_{winter} - winter runoff, Q_{Jun} - early melt season runoff occurring before the measurements, $Q_{Jul\text{-}Sep}$ - runoff measured in July, August and September. The fundamental formula is then derived:

$$Q_{total} = M_{total} + P_{summer} + C - E + (dS + \varepsilon) \quad \text{(Eq. 4.11)}$$

Water masses are quantified in two units: m^3 (absolute volume) and m (specific volume, normalized for the whole basin area). Calculations of water balance are based on several assumptions. Some parameters were not measured directly and they were given fixed values after previous works from Svalbard (summarized in Killingtveit et al. 2003). Summer precipitation data (since June until the end of observations each season) was obtained from Norwegian Meteorological Institute for Svalbard Lufthavn station (SVL), 60 km from Svenbreen. Previous research has shown that precipitation measurements at SVL suffer from considerable undercatch and should be multiplied by a factor of 1.15 for rain and 1.75 for snow. To extrapolate these corrected sums to higher areas of the catchment, precipitation gradient inferred from winter mass balance measurements (30% · 100 m^{-1}) was used. C accounts only for the glacier area and was computed using 2012 energy balance data, when summer condensation was only 3 mm (point measurements at S60, see section 6.2). Daily rate of E was fixed at 1.5 mm d^{-1} and applied only to ~0.5 km^2 of the glacier forefield over three summer months, based on measurements performed in the study area (Marciniak et al. 2007; Mazurek et al. 2012). The term ($dS + \varepsilon$) is unknown and is calculated as a residual to close the water balance. As an estimate of s_{slopes} it was assumed that average initial snow thickness on surrounding slopes was 60 cm in 2011 and 70 cm in 2012 (the year with generally higher accumulation), with the same density as measured on the glacier in a given year. Q_{winter} is very low and is taken as twice the early-July volume of the icing field in the glacier forefield. No Q_{Jun} data is available, so cumulative discharge in June was set so it accounts for 18% of Q_{total}, as observed in Bayelva - a similar catchment in NW Spitsbergen. Accounting for significant uncertainties of the assumptions above, it must be stressed that the water balance study is only a rough approximation.

Tab. 4.4 Equipment specifications of Svenbreen monitoring network provided by manufacturers

	Parameter (height against surface/sampling interval)	Equipment	Accuracy
S60 (summer 2011):	Air temperature, T_a (2 m/30 min)	Spectrum WatchDog 2700	±0.6°C
	Relative humidity, RH (2 m/30 min)	Spectrum WatchDog 2700	±3%
	Wind speed, u (2.3 m/5 min)	Onset S-WCA-M003	±0.5 m s^{-1}
	Wind direction (2.3 m/5 min)	Onset S-WCA-M003	±5°
S60 (AWS 2011/12):	Air temperature, T_a (2 m/10 min)	Vaisala HMP155A	±0.2°C
	Relative humidity, RH (2 m/10 min)	Vaisala HMP155A	±2%
	Wind speed, u (2.3 m/10 min)	Young Wind Monitor 05103	±0.3 m s^{-1}
	Wind direction (2.3 m/10 min)	Young Wind Monitor 05103	±3°
	Net radiation, Q_N (2 m/10 min)	Kipp & Zonnen NR-LITE	±5%
	Shortwave radiation, SW_{in} & SW_{out} (2 m/10 min)	Hukseflux LP02	±10%
S30 & S100:	Air temperature, T_a (2 m/10 min)	Onset HOBO S-THB	±0.2°C
	Relative humidity, RH (2 m/10 min)	Onset HOBO S-THB	±3%
	Ice temperature (-2, -4 & -8 m/10 min)	Onset HOBO S-TMB	±0.25°C
Gauging station:	Water level (-/5 min 2009-11, 1h 2012)	Onset HOBO U20-001-004	±0.03 m
	Water discharge (-/-)	Sontek Flowtracker	±20%*

*assumed total uncertainty

4.4 Ground penetrating radar survey

Ground penetrating radar (GPR) investigation on Svenbreen was carried out on 15/04/2012 during dry-snow conditions. Malå RTA system was used with ProEx control unit and 100 MHz antenna. The antenna was pulled by a snow scooter driving with average speed of 20-30 km h^{-1} and the data points were collected approximately every 1-2 m. The glacier was covered by a network of longitudinal and transverse profiles of 20 km length in total (fig. 5.2). Processing of the data was carried out in ReflexW software and considered reflection picking, static correction, dewow and gain functions, but no migration was possible for this dataset due to non-equidistant sampling. For travel-time/depth conversion wave propagation velocity for ice of 0.170 m ns^{-1} was used. Because snow depth on the glacier was known, post-processing of the data accounted for it and its extra-thickness effect could be removed (wave velocity of 0.220 m ns^{-1} used for snow after Murray et al. 2007). A simple hand-held GPS device was connected to the control unit and its readings of horizontal position were used in the analysis. From a network of points a map of ice thickness was interpolated using 'Topo to Raster' tool (ESRI ArcGIS), with additional manual improvements in zones of the poorest data coverage. Total volume of the glacier was obtained by integration of all cells of the thickness raster. Map of subglacial topography was achieved by subtraction of ice thickness raster from a DEM. The DEM used was based on 2009 model, but it accounted for geometry changes occurring since 2009 until 2011, by a double addition of annual surface elevation change raster, averaged for the 1990-2009 period.

Accuracy of single thickness measurement by a GPR depends on a number of factors, including quality of subjective interpretation of radargrams, wave propagation velocities used for snow and ice or snow cover thickness estimate. Because bedrock reflection is mostly poorly visible in the deepest sections of Svenbreen, the uncertainties may locally be as high as ±10 m in these areas. To illustrate errors associated with picking reflections, 92 crossing points have been extracted from independent profiles and their ice thickness estimates have been compared. In 33% of cases, difference between them was lower than 1 m, while 50% of points have shown thickness difference lower than 1.7 m. 10% of cross-points differed by more than 5 m, with 7.4 m being the maximum noted. Standard deviation in the population of crossing points was 1.8 m, while mean difference was 2.3 m. Wave propagation velocity also has a significant impact on thickness estimate. Velocity most often used in the literature is 0.168 m ns^{-1}, but for other Svalbard glaciers higher values were reported (e.g. 0.173 m ns^{-1}, Zhuravlev et al. 1983). Use of these two values corresponds to an uncertainty of ± 3 m at 100 m thickness. Snow depth is known at probing sites with accuracy of ± 5%, but error is higher between them. Interpolation of GPR data into an ice thickness map (also covering not surveyed areas) introduces further inaccuracy. Therefore, for the purpose of this work, a ± 5 m error of thickness measurement seems to be reasonable and is used further.

The adopted methodology presented in this chapter gave possibility to collect data relevant for each element from the diagram on fig. 1.1. The only case when directly collected data origins from a single point only, is the energy balance study performed at S60 (from obvious technical, logistical and economical reasons). The presented measuring system and procedures involved may be therefore assumed as representative for Svenbreen, because they considered functioning of the glacier as a whole.

5

Post-Little Ice Age glacier geometry changes in Petuniabukta basin

5.1 General trends of geometry changes, 1960-1990-2009

In order to investigate whether Svenbreen (in this section called SVB) shows any unique behaviour, long-term elevation changes of six neighbouring glaciers have been analysed as well. Those are Bertilbreen (BLB), Vestre Muninbreen (VMB), Austre Muninbreen (AMB), Ferdinandbreen (FDB), Elsabreen (ELB) and an unnamed glacier called in this study No Namebreen (NNB, ID number 16819 in Hagen et al. 1993), located approximately 4 km NE from SVB. Because no elevation data for LIA maximum is available, a comprehensive analysis of thickness and volume changes is limited to periods 1960-1990 and 1990-2009.

The results of detailed geomorphometric study show high thinning at fronts of all investigated glaciers, with very limited thickening (1960-1990) or no thickening at all, even in their highest parts (1990-2009). The greatest magnitude of elevation changes (*dH/dt*) was observed on VMB, with -66 and -96 cm a^{-1}, respectively for the first and the second analysed epoch, giving in total -39.3 m of glacier-wide elevation change. NNB thinned by 35.3 m, with high *dH/dt* rates of -68 and -81 cm a^{-1}. Other glaciers have been lowering their surface slightly slower, from -32 to -53 cm a^{-1} in 1960-1990 and from -61 to -82 cm a^{-1} between 1990 and 2009. It must be underlined that the latter period is characterized by a significantly higher thinning rates than the first epoch. The mean *dH/dt* weighted by area of each elevation band in 1960-1990 is -49 cm a^{-1}, with zero-elevation change line at 575 m, above which some thickening occurred, while after 1990 *dH/dt* decreased by 54% to -78 cm a^{-1} and no further elevation increase was observed.

As a result of thickness loss the volume of all glaciers dropped significantly. VMB volume change (*dV*) since 1960 was the most prominent with $-134 \cdot 10^6$ m^3 with relatively little decrease in volume change rate (*dV/dt*) between the two epochs (-20%), being adequate to a slight acceleration of volume loss rate. BLB volume drop was similar ($133 \cdot 10^6$ m^3), with decrease in *dV/dt* of -26%. SVB lost $84 \cdot 10^6$ m^3 of ice in total and after 1990 it experienced

the volume change rate decrease of 80% - the greatest acceleration of volume loss rate from all of the observed ice masses. For AMB *dV* of -72 · 10^6 m^3 and *dV/dt* decrease of -45% was measured. The three smallest glaciers decreased their volume by *dV*=-50 · 10^6 m^3 (NNB), *dV*=-31 · 10^6 m^3 (FDB) and *dV*=-13 · 10^6 m^3 (ELB). Two of them, NNB and ELB, showed a certain deceleration of volume loss due to decrease of glacier area exposed for melt (*dV/dt* increase by +5% and +2% respectively) while for FDB a 75% acceleration of volume loss was noted. The total *dV* of all glaciers was estimated to be -517 · 10^6 m^3 since 1960, with a 33% acceleration of mass loss after 1990. It stands for roughly 39% volume loss based on 1960 volume estimates by Hagen et al. (1993).

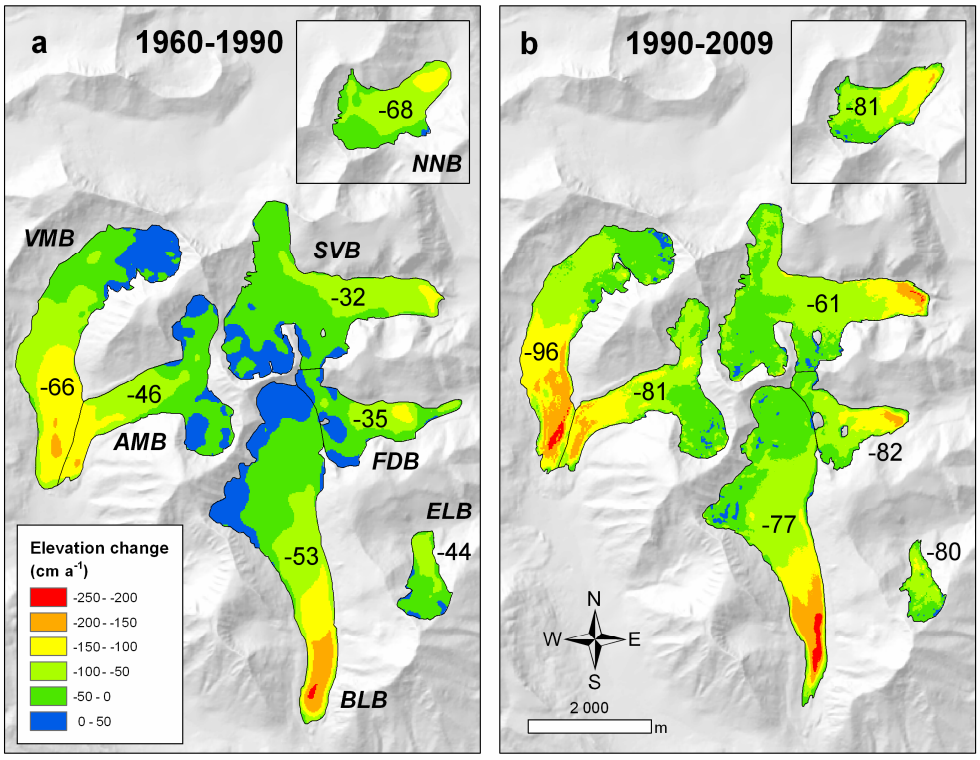

Fig. 5.1 Annual surface elevation change rate, *dh/dt,* of glaciers in the study area. a - 1960-1990, b - 1990-2009. Numbers indicate glacier-wide annual surface elevation change in cm a^{-1} (*dH/dt*)

Tab. 5.1 Elevation and volume changes in the two studied periods. Note different units used

	BLB	SVB	VMB	AMB	NNB	FDB	ELB	Overall
Elevation change, *dH* 1960-1990 (m)	-15.8 ± 5.0	-9.5 ± 5.6	-19.7 ± 5.4	-13.9 ± 6.9	-20.3 ± 8.8	-10.5 ± 9.6	-13.2 ± 15	-14.8 ± 6.5
Elevation change, *dH* 1990-2009 (m)	-14.6 ± 3.0	-11.7 ± 3.3	-18.2 ± 3.1	-15.3 ± 4.2	-15.3 ± 5.7	-15.6 ± 6.6	-15.2 ± 10	-14.8 ± 3.9
Elevation change, *dH* 1960-2009 (m)	-30.4 ± 5.7	-20.9 ± 6.3	-39.3 ± 6.1	-29.9 ± 7.8	-35.3 ± 9.8	-24.6 ± 11	-29.7 ± 17	-29.8 ± 7.3
Annual elev. change, *dH/dt* 1960-1990 (cm a^{-1})	-53 ± 17	-32 ± 19	-66 ± 18	-46 ± 23	-68 ± 29	-35 ± 32	-44 ± 50	-49 ± 22
Annual elev. change, *dH/dt* 1990-2009 (cm a^{-1})	-77 ± 16	-61 ± 17	-96 ± 16	-81 ± 22	-81 ± 30	-82 ± 35	-80 ± 55	-78 ± 21
Annual elev. change, *dH/dt* 1960-2009 (cm a^{-1})	-62 ± 12	-43 ± 13	-80 ± 12	-61 ± 16	-72 ± 20	-50 ± 22	-61 ± 34	-61 ± 15
dH/dt change after 1990 (%)	-45%	-94%	-46%	-74%	-19%	-136%	-82%	-58%
Volume change, *dV* 1960-2009 (10^6 m^3)	-133.3 ± 28	-84.5 ± 27	-133.9 ± 25	-72.2 ± 22	-49.8 ± 17	-30.5 ± 17	-13.0 ±12	-517 ±149
Annual volume change, *dV/dt* 1960-2009 (10^6 m^3 a^{-1})	-2.72 ± 0.6	-1.72 ± 0.6	-2.73 ± 0.5	-1.47 ± 0.5	-1.02 ± 0.3	-0.62 ± 0.3	-0.26 ± 0.2	-10.55 ± 3
dV/dt change after 1990 (%)	-26%	-80%	-20%	-45%	+5%	-75%	+2%	-33%

5.2 Geometry changes of Svenbreen

All glaciers investigated in the previous section have been losing mass in the studied period and all experienced a distinct acceleration of thinning rates after 1990, mostly accompanied by an increased volume loss. One of the glaciers, Svenbreen, has been clearly showing significantly slower downwasting than other ice masses. Its 1960-2009 thinning rate was lower than noted on the neighbouring glaciers by about 30%, what makes it a perfect object to study how local factors affect functioning of the glacier and its mass exchange. Little Ice Age (LIA) in Svalbard (14^{th}-19^{th} century, see section 3.1) was a period when local glaciers reached their maximal Holocene extents, in most cases well marked by lateral and frontal moraine ridges, used in this study to approximate its maximum size in 1900. In this section post-LIA geometry changes of Svenbreen are presented, with analysis of its drivers discussed in section 5.2.3. For methods see section 4.1.

5.2.1 Length and area variations against geometry of the valley, 1900-1960-1990-2009

Length variations are the most prominent sign of changes occurring on/in glaciers (see section 2.6). Front position is altered by many factors, such as mass balance and dynamics history or topography of the bed. To investigate the latter, in April 2012 Svenbreen was covered with over 20 km of longitudinal and cross-sectional GPR profiles (fig. 5.2). Radargrams from this survey, together with interpretation of ice structures, are to be found in section 7.1.2, while here only subglacial relief maps are presented. The study revealed that Svendalen is of U-shaped type, with the exception of minor ice patches spreading between the main glacier and mountain passes Nataliaskaret and Poznańskaret. A slight asymmetry of the valley can be noted - its axis is shifted 50-150 m south from the glacier centre-line.

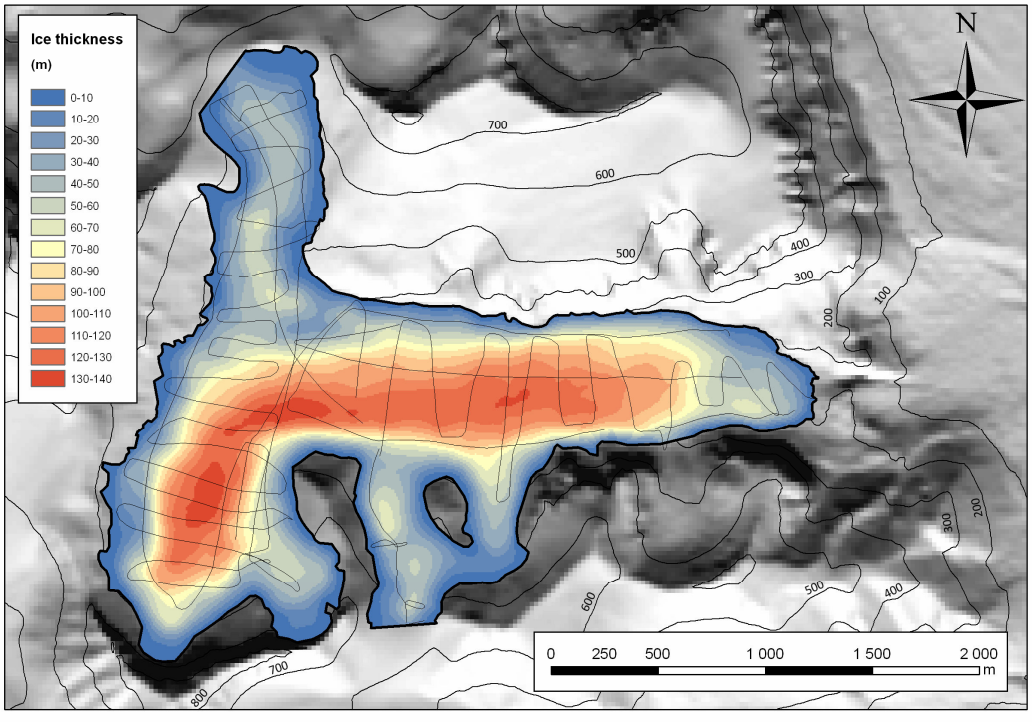

Fig. 5.2 Svenbreen 2011 ice thickness. Zig-zag lines on the glacier represent GPR profiles

Bedrock reflections from all profiles were picked and converted to points so it was possible to construct maps of glacier thickness and bedrock relief (figs. 5.2 and 5.3). Due to the valley shape, ice thickness increases very rapidly when moving towards the glacier centreline. The glacier typically reaches thickness of 100-120 m in the ablation zone and up to 138 m in the main glacier cirque. The mean glacier thickness was determined to be 58 m, what corresponds to the total volume of the glacier equal to 0.216 km^3 for the end of 2011 ablation season and 0.221 km^3 for 2009, to keep consistent years with surface lowering analysis. The valley floor is generally smooth with only few irregularities of the relief. The present-day front rests on a flat area on the up-glacier side of distinct riegel, which used to be ice-covered until ~1960's.

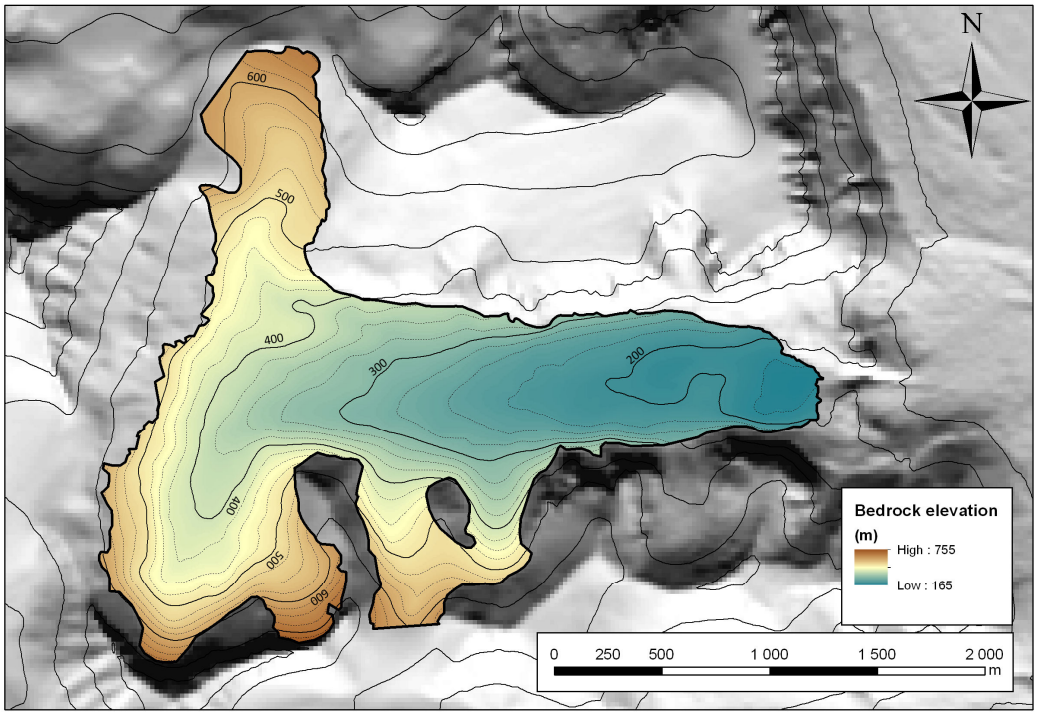

Fig. 5.3 Svenbreen subglacial topography. Thick contour lines are drawn every 100 m, thin dashed contours - 25 m

In the maximum phase of LIA Svenbreen was thick enough to surpass the riegel. This tectonic threshold is very steep from the downglacier-side, what must have significantly accelerated the advancing frontal ice when moving downhill. Such a situation led to formation of a peculiar front zone, in a form of a crevassed expanding foot resting on a flat terrain and staying in contact with neighbouring Hørbyebreen snout. In effect, the LIA length (L_{LIA}) of the glacier was 5 201 m, with area (A_{LIA}) of 5.61 km^2. The foot was most likely thin due to limited ice supply caused by discharge blockage by the riegel. The early 20th century temperature rise had therefore dramatic consequences for its existence.

The first known information about Svenbreen is available from the 1920's. Slater (1925) visited the glacier in 1921 and noted that moraines have been yet developing, indicating that the glacier already entered the post-LIA decay period. Unfortunately, the front position has not been mapped in his work, but the photographs indicate that the foot is most likely not far from the maximal glacier extent, similarly as a photograph from 1933 (Glen et al. 1934). The front zone of Svenbreen is visible on 1949 map by Harland (1953), but it is of insufficient quality for reliable geometry change estimates. An intensive down-wasting of the lowest

Svenbreen section is however well visible. Until 1960 the front retreated to the summit of the riegel and remnants of the ice foot have been melting away beneath it as blocks of dead ice, as visible on Norwegian aerial photographs. In result, the glacier shortened since the LIA maximum by $dL_{LIA\text{-}1960}$ = -1 247 m to L_{1960} = 3 954 m and its area decreased to A_{1960} = 4.34 km^2. Most of the retreat occurred probably between ~1920 and 1960, but in this work the LIA maximum was assumed to occur in year 1900, giving the mean annual retreat rate $dL/dt_{LIA\text{-}1960}$ = -20.8 m a^{-1}. Such fast decay resulted most likely from geometry of the front zone - it was thin and flat, so even a small initial climate change could have caused its complete melt-out.

For the next 30 years the front has been retreating further. Between 1960 and 1990 Svenbreen decreased its length by 124 m, giving an average length change rate of $dL/dt_{1960\text{-}1990}$ = -4.1 m a^{-1}, total length of L_{1990} = 3 830 m and area A_{1990} = 3.98 km^2. Until present, the terminus behaviour seems to be stable and it is still slowly retreating. In the period 1990-2009 dL/dt was equal to -5.0 m a^{-1}, so L_{2009} and A_{2009} decreased to 3 734 m and 3.73 km^2 respectively. Stable decay was confirmed by year-by-year front position measurements between 2007 and 2012, which have shown continuous interannual retreat of similar magnitude each summer (not presented here for greater clarity). The total post-LIA front retreat was relatively high with $dL_{LIA\text{-}2009}$ = -1 467 m (28% length reduction until 2009). In the upper parts of the valley the glacier outlines have not changed significantly, so the decay of the front zone was the main cause of glacier area decrease, which reached in total $dA_{LIA\text{-}2009}$ = -1.89 km^2 (-34%).

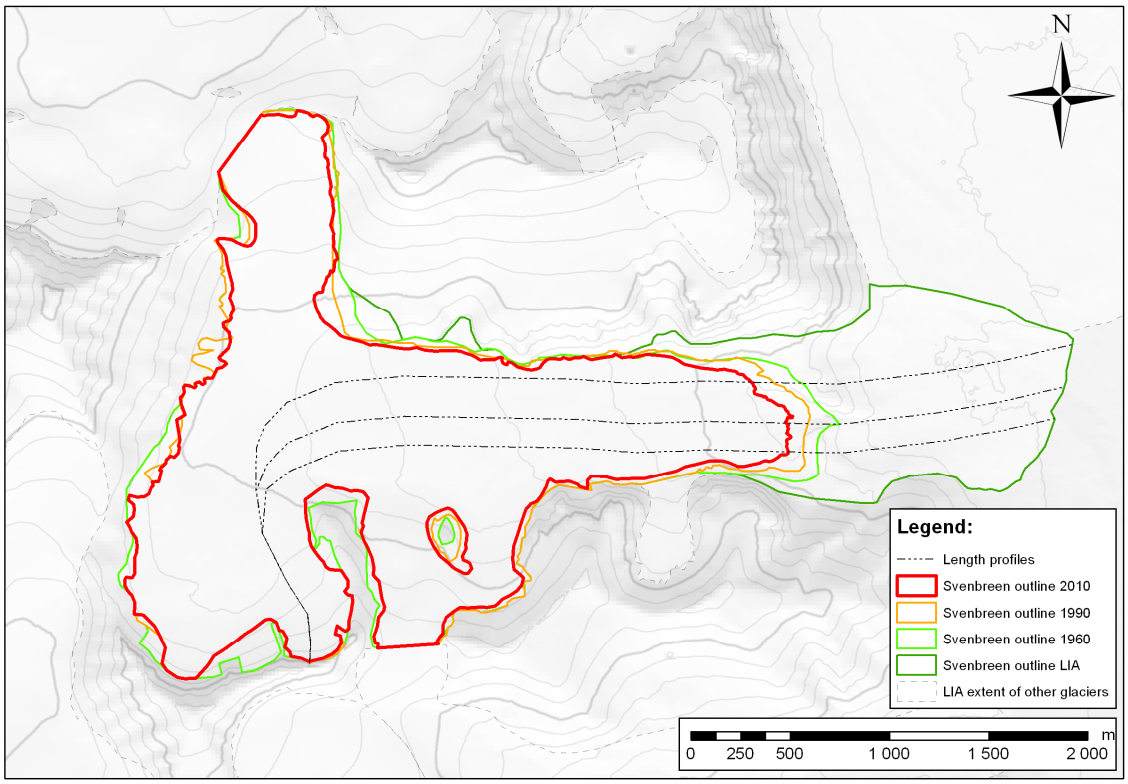

Fig. 5.4 Svenbreen length and area changes after Little Ice Age (*LIA*). Contour lines (2009) are drawn every 50 m

5.2.2 Long-term surface elevation variations and associated changes, 1960-1990-2009

Surface lowering and front fluctuations described in previous sections are a clear indication that Svenbreen glacial system has been experiencing significant changes for the last ~100 years. Spatial variability of thickness losses is significant on the glacier, with zones of extra thinning and minor thickness gains. Detailed analysis of geometry change of Svenbreen was an important part of this work, as its spatial variability carries some information about the surface mass balance of the glacier and its dynamic activity.

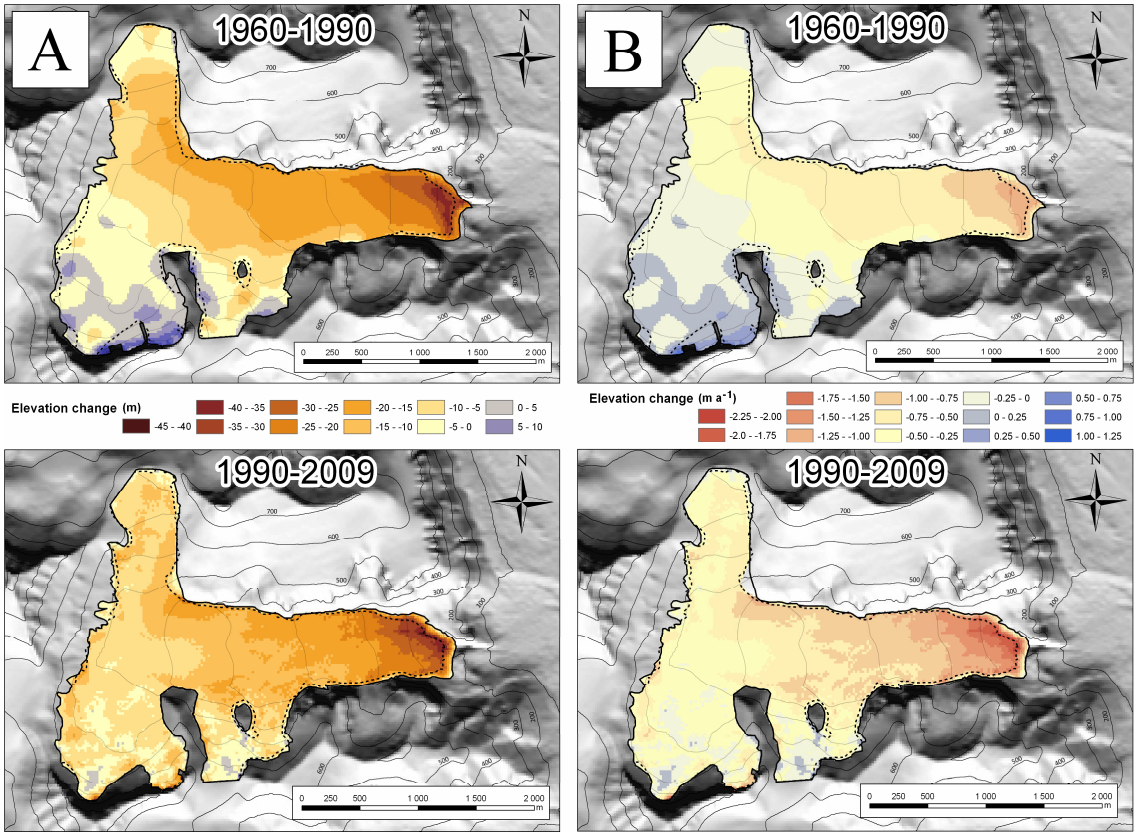

Fig. 5.5 Elevation changes of Svenbreen: A - total elevation change in metres; B - normalized elevation change in metres per year. Contour lines on the glacier and solid glacier outlines are valid for 1960 (upper images) and 1990 (lower images). Dashed outlines are valid for 1990 and 2009 (respectively for upper and lower images). Vertical contour spacing is 50 m on the glacier and 100 m on the surrounding terrain

Results of the analysis clearly show that Svenbreen has been thinning in almost every elevation band for at least five decades (fig. 5.6A). Surface lowering shows a clear pattern to decrease with elevation, but it does not explain the observed spatial variability fully. In both periods Poznańskaret, with its southern aspect, has been experiencing much faster thinning than the main cirque and Nataliaskaret tributary branches in the mid-sections, even though they are characterized by similar vertical extent. In the 30-year period from 1960 to 1990, the front experienced thinning of up to dh = -38 m. The highest zone above 550 m was close to zero elevation change, with some thickening on the order of ~5 m being also noted (fig. 5.5). In the steep highest sections however, even more pronounced thickening is visible, but it may be an artefact introduced by errors in the available datasets, increasing with slope inclination

(see section 4.1). The overall elevation change in the first period 1960-1990 was clearly negative (-9.1 m). In the second, shorter period, 1990-2009, the total surface elevation loss had a greater magnitude, with $dH_{1990\text{-}2009}$ = -11.3 m, similarily as was the case for maximum thinning at the front (43 m). No build-up was noted anymore, except for very small isolated patches of weak positive elevation change. In the early period the glacier has been thining on average by $dH/dt_{1960\text{-}1990}$ = -32 cm a^{-1}, while after 1990 it was almost twice faster, with $dH/dt_{1990\text{-}2009}$ = -61 cm a^{-1}. (figs. 5.5B and 5.6A, tab. 5.3).

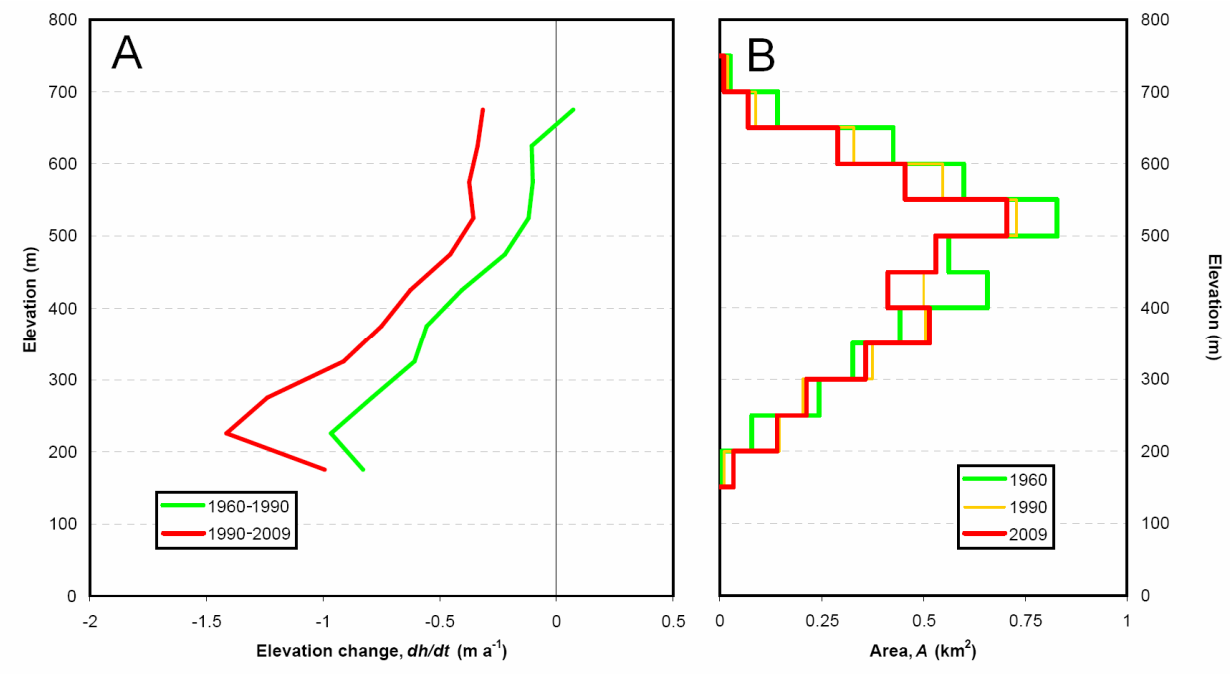

Fig. 5.6 A - Mean annual elevation change of Svenbreen in periods 1960-1990 and 1990-2009 within 50 m elevation bins; B - area-altitude distribution in 50 m elevation bands in different years. Note a decrease at higher elevations and an increase in the lowest sections

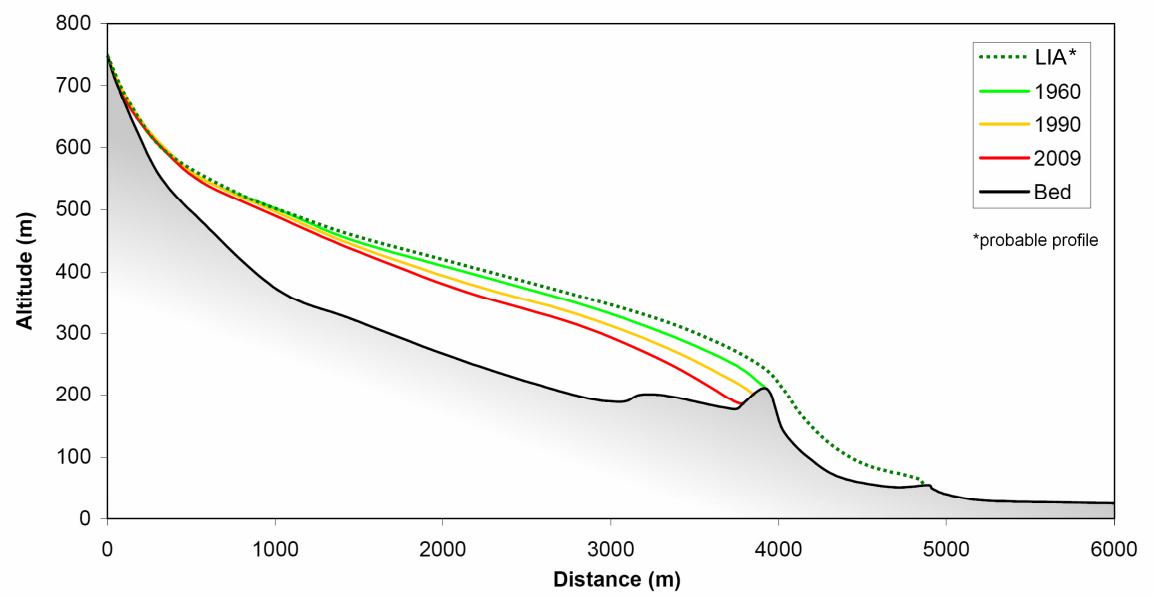

Fig. 5.7 2-dimensional illustration of post-Little Ice Age volume changes of Svenbreen. Note that the presented longitudinal profile slightly deviates from length profiles to highlight the role of the riegel in front retreat

Thickness decrease has a direct impact on many other geometry properties, with volume (V) being the most important (fig. 5.7). Between 1960 and 1990 the glacier lost $dV_{1960\text{-}1990}$ = -39.5 · 10^6 m^3 while in the more recent period it was $dV_{1990\text{-}2009}$ = -45.0 · 10^6 m^3. Due to enhanced thinning after 1990, recent annual volume change rate, $dV/dt_{1990\text{-}2009}$, is by 80% more negative than observed between 1960 and 1990 (-1.3 · 10^6 m^3 a^{-1} vs. -2.4 · 10^6 m^3 a^{-1}, respectively for the early and the recent analysed period). The total volume of Svenbreen has been therefore continuously decreasing in the analysed time span. In 1960 it was equal to 0.305 km^3, 30 years later it diminished to 0.265 km^3, while in 2009 it was only 0.221 km^3, giving a 28% volume decrease since 1960 (tabs. 5.2 and 5.3). Another effect of surface lowering is a decrease of total glacier area (described in the previous section) and change in glacier area-altitude distribution. In the highest elevation bands area losses are very well pronounced, while minor area gains were noted in the ablation zone. Therefore, evolution of the glacier hypsometry transfers area from higher to lower zones, being an extra boost for ablation (fig. 5.6B). In result, median elevation of Svenbreen has been consequently lowering. In 1960 half of Svenbreen area was situated above 488 m a.s.l., while in 2009 the same portion was located above 470 m.

Tab. 5.2 Main geometry parameters of Svenbreen in different years

Geometry parameter	1900	1960	1990	2009
Length, L (m)	5 201	3 954	3 830	3 734
Area, A (km^2)	5.61	4.34	3.98	3.73
Volume, V (km^3)	-	0.305	0.266	0.221
Median elevation (m)	-	488	475	470
Approximate average front elevation (m)	60	200	200	200
Min. front elevation (m)	30	150	165	170

Tab. 5.3 Change of Svenbreen geometry parameters in the studied epochs. Note different units

	1900-1960	1960-1990	1990-2009	1900-2009	1960-2009
Length change, dL (m)	-1 247	-124	-95	-1 467	-220
Length change, dL (%)	-24.0%	-2.4%	-1.8%	-28.2%	-4.2%
Annual length change, dL/dt (m a^{-1})	-20.8	-4.1	-5.0	-13.5	-4.5
Annual length change, dL/dt (% a^{-1})	-0.40%	-0.08%	-0.10%	-0.26%	-0.09%
Area change, dA (km^2)	-1.27	-0.36	-0.26	-1.89	-0.61
Area change, dA (%)	-22.7%	-6.3%	-4.6%	-33.6%	-10.9%
Annual area change, dA/dt (10^3 m^2 a^{-1})	-21.2	-11.9	-13.5	-17.3	-12.5
Annual area change, dA/dt (% a^{-1})	-0.38%	-0.21%	-0.23%	-0.31%	-0.22%
Thickness change, dH (m)	-	-9.5 ±5.6	-11.7 ±3.3	-	-20.9 ±6.3
Annual thickness change, dH/dt (cm a^{-1})	-	-32 ± 19	-61 ± 17	-	-43 ± 13
Volume change, dV (10^6 m^3)	-	-39.5 ±24.2	-45.0 ±13.0	-	-84.5 ±27
Volume change, dV (%)	-	-12.9%	-14.8%	-	-27.7%
Annual volume change, dV/dt (10^6 m^3 a^{-1})	-	-1.32 ± 0.81	-2.37 ± 0.69	-	-1.72 ± 0.56

5.2.3 Elevation changes against ice motion, 2010-2012

Because surface elevation changes are a direct result of mass budget and flow pattern, one needs both information to properly interpret changing geometry. In July of 2010 and 2012 direct GPS measurements were performed on the glacier surface to measure stake locations.

From their positions horizontal velocity of stakes could be computed, while vertical components of ice motion were inferred from measured *dh* and ablation data. The first survey was performed on 12 stakes along the longitudinal transect (Małecki et al. 2011), while the latter campaign two years later coincided with snowy conditions, so some of the stakes were buried under the snow and could not be remeasured. In effect data of horizontal shift 2010-12 is available for 9 stakes and elevation change information for 8 points along the main flowline. Measurement error of annual flow velocities was estimated as ± 7 cm a^{-1} (see section 4.1).

Results of the survey show generally low horizontal flow velocity (U_h) of Svenbreen. Maximum flow speed was measured in the middle zone of the glacier and in the entrance to the cirque (fig. 5.8, tab. 5.4). Stake S60 has been moving at rate of U_h = 2.48 m a^{-1}, S90 at U_h = 3.21 m a^{-1} and S100 at U_h = 2.92 m a^{-1}. The lowest velocity was noted in the front zone. Displacement of stake S20 gave flow speed of only U_h = 0.38 m a^{-1}, while S10 was almost stagnant with U_h = 0.10 m a^{-1}. Motion velocity measured at other sites was 1.05-1.31 m a^{-1}. Flow direction at each measured stake was consistent with general flow pattern and surface inclination. The only exception was stake S60 moving towards NE, while other stakes in the ablation zone have shown eastern direction. Such pattern could result either from strong influence of Nataliaskaret ice stream flowing from S to N, or from a faulty measurement.

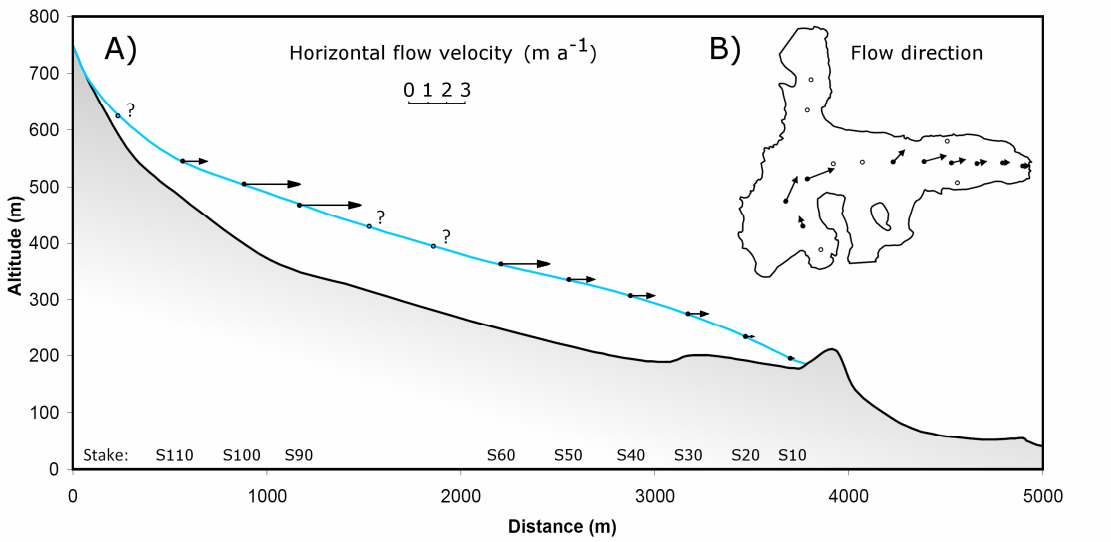

Fig. 5.8 A - flow velocity of Svenbreen along longitudinal profile; B - flow direction at surveyed stakes

Tab. 5.4 Horizontal (U_h) and vertical flow velocity (U_v), elevation change ($dh_{2010\text{-}2012}$) and mass balance (b_n) at individual stakes on Svenbreen between 07/2010 and 07/2012

Stake	2012 elevation (m a.s.l.)	U_h (m a^{-1})	$dh_{2010\text{-}2012}$ (m a^{-1})	b_n (m a^{-1})	U_v (m a^{-1})
S10	185	0.10	-1.82	n/d	n/d
S20	222	0.38	-1.55	-1.69	0.14
S30	277	1.05	-1.06	-1.25	0.19
S40	304	1.24	-0.93	-0.98	0.05
S50	331	1.31	-0.72	-0.91	0.19
S60	358	2.48	-0.73	-0.90	0.17
S90	463	3.21	-0.37	-0.47	0.10
S100	513	2.92	-0.27	-0.30	0.02
S110	541	1.23	-0.08	-0.09	0.01

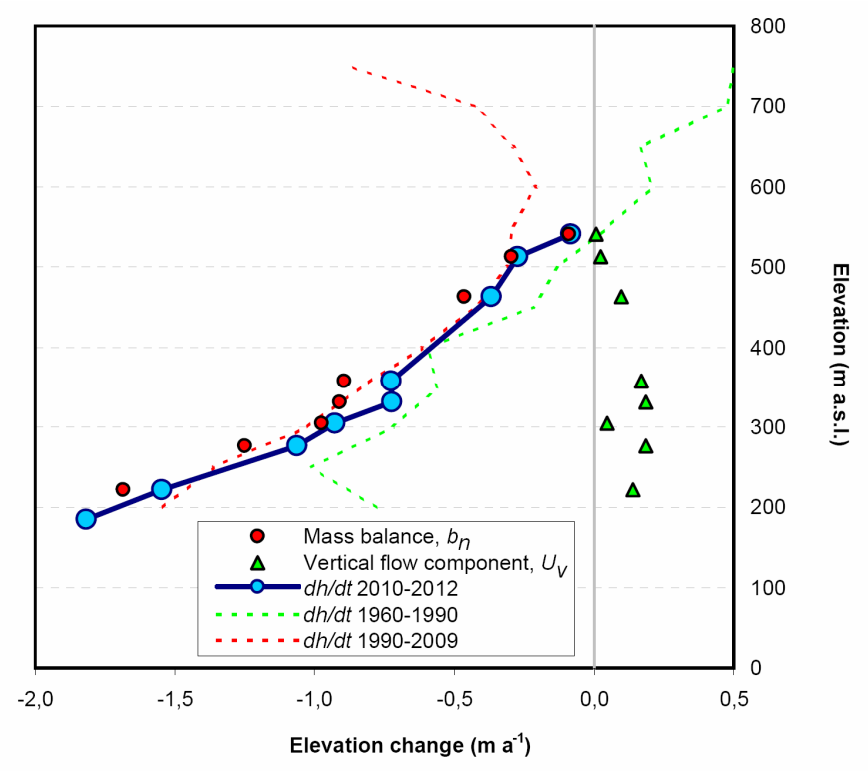

Fig. 5.9 Annual elevation changes ($dh/dt_{2010\text{-}2012}$), mass balance (b_n) and vertical flow component (U_v) at individual stakes on Svenbreen in the period 2010-2012, against centreline elevation changes in the periods 1960-1990 ($dh/dt_{1960\text{-}1990}$) and 1990-2009 ($dh/dt_{1990\text{-}2009}$)

Flow velocity and surface slope along motion vectors were used to compute corrected $dh/dt_{2010\text{-}2012}$. The survey provides an evidence of continuation of surface lowering in the studied period, similarly as observed in 1960-2009. The rate of recent, GPS-derived changes agrees very well with centreline thinning calculated from DEM-differencing method for the period between 1990 and 2009. The most interesting finding of the geodetic flow survey is a negligible role of dynamics in surface elevation changes of Svenbreen. In tab. 5.4 and on fig. 5.9 mass balance data was used to decompose surface lowering into ablation (b_n) and vertical flow contribution (U_v). Fig. 5.9 shows that thinning of Svenbreen (blue dots) is in good agreement with surface ablation (red dots) and that ice emergence velocity (positive U_v, green triangles) is low or near-zero, with maximum value of 19 ± 7 cm a^{-1}. Positive sign of U_v agrees with the theory of glacier motion, as in ablation zones mass emerges towards the surface, while accumulation areas of glaciers are characterized by ice submergence (negative U_v, compare e.g. with fig. 2.5).

Findings from this chapter provide an evidence for long-term surface lowering of glaciers in Dickson Land. Svenbreen has been showing the slowest thinning, suggesting operation of certain mechanisms reducing its mass loss. Negative mass balance was found to be responsible for glacier-wide thinning, but net ablation is also the main driver of point-surface lowering.

6

Topoclimate and mass balance of Svenbreen

6.1 Topoclimate

Meteorological investigations in Svenbreen area have been carried out since summer 2009. The first air temperature (T_a) and relative humidity (RH) measurements were taken at the summit of the riegel (220 m a.s.l.), close to the front of the glacier. A portable weather station has been operating for the whole winter 2009/10 and in summer 2010 it was moved to the middle section of Svenbreen to stake S60 (358 m a.s.l.). In September 2011 old sensors were replaced by an automatic weather station (AWS), measuring also surface energy balance components. The fundamental dataset discussed in this section covers T_a, RH, e_a (air vapour pressure) and u (wind velocity) record from ablation seasons 2011 and 2012 and energy balance of the glacier surface for the whole glaciological year 2011/12. Here, only the results are presented, with glaciological implications discussed in chapter 8. Basic graphic display of the data shows mostly the warmer part of year, with 2011 records showed in red (the warmer summer season) and 2012 in blue (the cooler summer season). Daily values of individual components of the glacier topoclimate are to be found in the appendix, in tabs. A1-A7.

6.1.1 Air temperature

Because low altitude T_a record from PET station is available only for 2009 and 2010 (section 3.5), with no coverage in 2011 and 2012, continuous data from Svalbard Lufthavn station (SVL) is used here as a general reference for interannual comparative studies. To make data collected in 2009 and 2010 comparable with later on-glacier records, they were recalculated to altitude of S60, using a uniform lapse rate of -1°C · 100 m^{-1}, typical for Svenbreen. Data gaps in 2009 and 2010 are filled using SVL data and the same temperature gradient. It must be underlined that 2009-2010 record recalculated for S60 is only an approximation, presented here as a background for 2011 and 2012 *in situ* data.

Summer (JJA) T_a at SVL is on average 4.9°C (1981-2010), while in 2009 it was 5.7°C (warm summer) and 5.0°C in 2010 (normal summer). Temperature at S60 was obviously

significantly lower than at SVL (by about 3°C) due to elevation difference and glacier surface properties. In the summer season of 2009 it was 2.8°C and 2.3°C in 2010. Positive degree-day sums calculated for S60 were respectively 285 and 231 PDD (for more details see tab. 6.1). In 2009 at SVL period of continuous occurrence of positive T_a lasted since late-May to mid-September. The probable 2009 temperature course at S60 showed oscillations around 0°C in June, suggesting melting and refreezing conditions until July. Negative air temperature occurred most likely in mid-September. Ablation season of 2010 was characterized by warm May with positive temperature at SVL in its latter half, lasting almost continuously until 11/10. At S60 positive temperature onset occurred in mid-June, and the freeze-up in late-August, being relatively early.

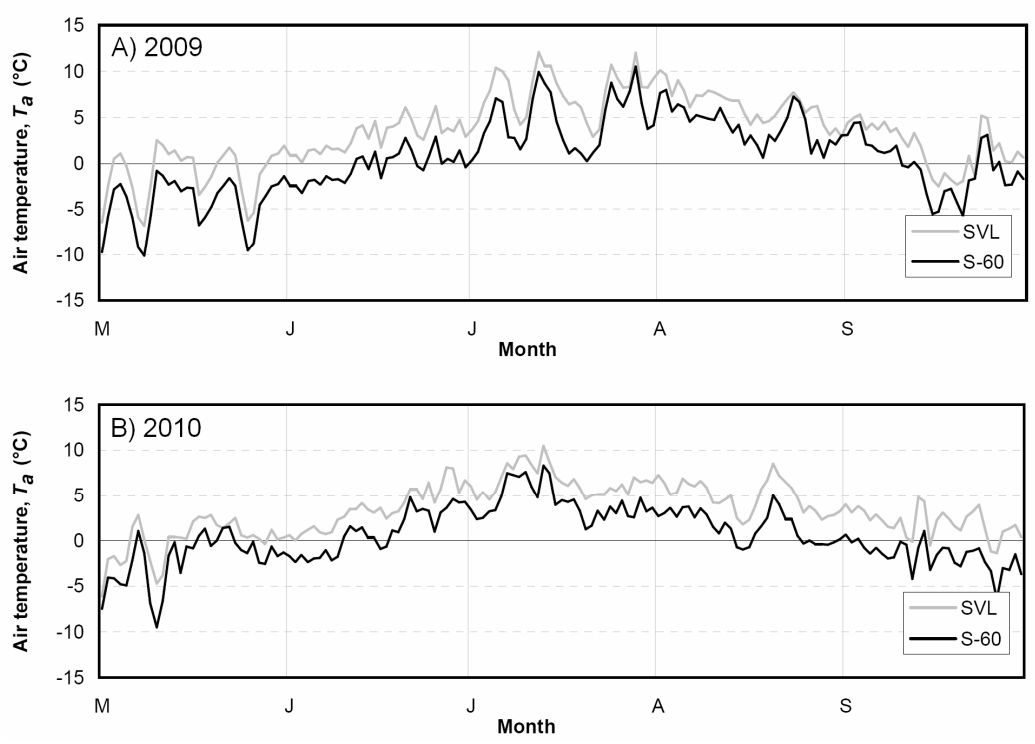

Fig. 6.1 Mean daily summer air temperature at S60 (approximated, black line) and at SVL (grey line) in the summer season of A - 2009; B - 2010

Data for 2011 and 2012 are based on direct measurements at S60. In general, mean daily temperature values in the mid-zone of Svenbreen show very high correlation with records from low-altitude stations PET and SVL. The only cold period fully covered with data is the winter 2011/12. It was extremely mild, even as for Svalbard (figs. 3.4 and 6.2). Average multiannual air temperature of the coldest months at SVL is -12.9°C for January, -13.5°C for February and -13.2°C for March (1981-2010). In 2012 it was respectively -3.4°C (the second warmest January noted), -5.6°C and -5.3°C (the warmest February and March in SVL record). At S60 it was -7.0°C, -9.8°C and -10.1°C for January, February and March respectively. Summer T_a at SVL in 2011 and 2012 was respectively 6.2°C (one of the warmest ever recorded) and 5.4°C. Both ablation seasons were therefore significantly warmer than average. Mean air temperature of 2011/12 balance year at SVL was -1.7°C and -5.5°C at S60 (10/09/2011-9/09/2012). Full air temperature record from S60 spanning from 05/2011 to 09/2012 is to be found in the appendix in tab. A1.

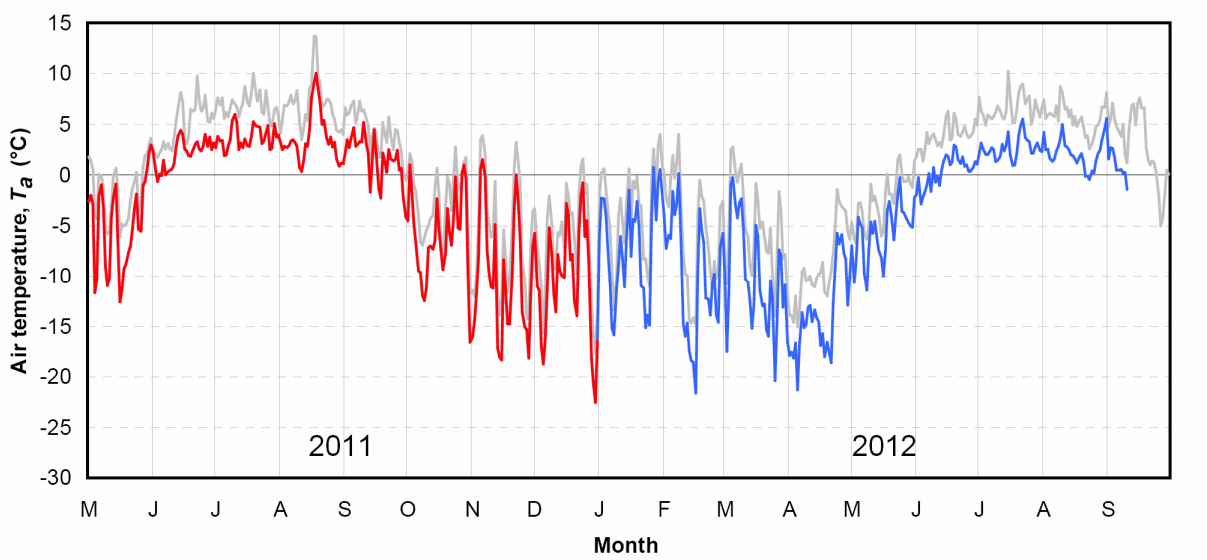

Fig. 6.2 Mean daily air temperature at S60 (colour bold lines) and at SVL (grey line) in 2011 and 2012. Note a very mild winter period

Air temperature course at SVL was relatively similar in 2011 and 2012. The only significant difference was an extremely warm pentade 15-20/08 in 2011, with mean T_a of 10.6°C and peak values reaching nearly 14°C on 17-18/08. The actual start of both melt-seasons occurred at SVL in late-May, but the 2011 was slightly longer: the freeze-up occurred on the 4/10, while in 2012 - on the 25/09. In case of Svenbreen, the difference between thermal conditions of both summer periods was much more pronounced. In 2011 ablation season positive temperature was occurring at S60 between 29/05 and 29/09. In 2012 this period was much shorter, as the onset of positive temperature fell on 13/06 and the freeze-up occurred most likely in mid-September (no *in situ* data available after 10/09).

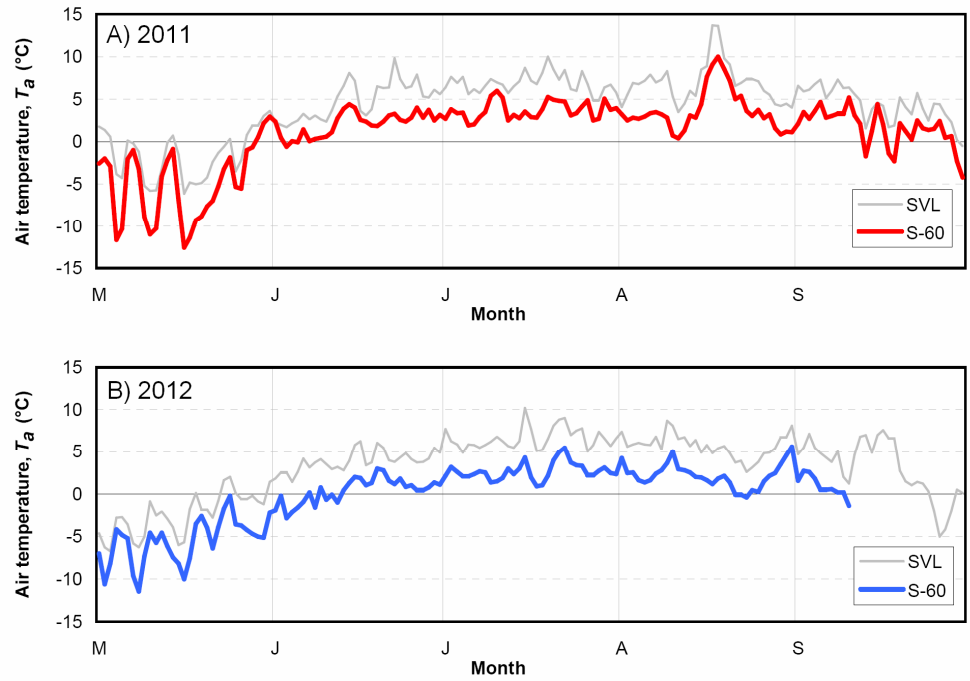

Fig. 6.3 Mean daily summer air temperature at S60 (colour bold lines) and at SVL (grey line) in the summer season of A - 2011; B - 2012

Atmospheric conditions prevailing in 2011 and 2012 have led to a distinct difference of average summer lapse rates between SVL and S60. The two sites are however located 60 km apart, so the following considerations about T_a gradient are presented only to show the general picture of its variability in particular years. As visible on fig. 6.4, SVL-S60 temperature gradient was slightly more negative in the more recent melt-season than in the earlier one. In result, average JJA temperature difference between S60 and SVL was -3.1°C in 2011, but in 2012 it was greater with -3.6°C. Therefore, the generally cooler conditions of 2012 were even strengthened on the glacier: JJA temperature was 3.2°C in 2011, but only 1.8°C in 2012. This considerable difference resulted in significantly reduced PDD sums in 2012 (293 PDD in 2011 vs. 176 PDD in 2012, tab. 6.1). The difference was most likely caused by different circulation patterns and associated air properties dominating each of the ablation seasons, such as air stratification or moisture content. According to Niedźwiedź (2013), the JJA proportion of cyclonic, anticyclonic and unclassified circulation was 40%:58%:2% in 2011 and 61%:39%:0% in 2012.

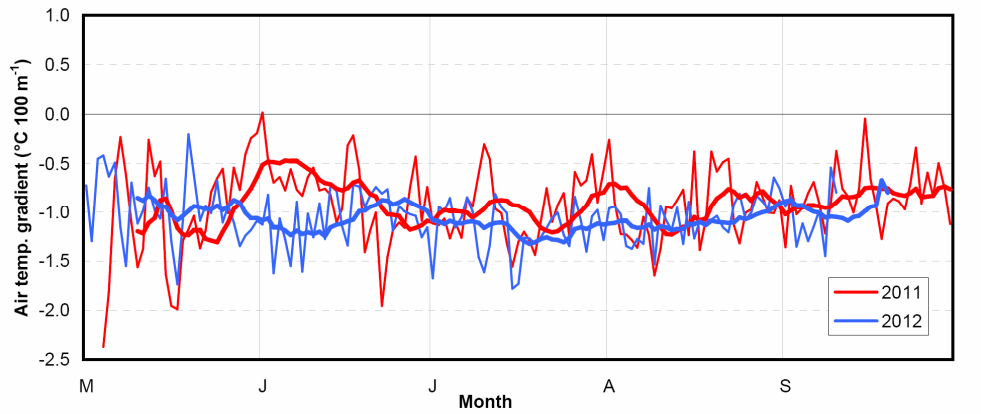

Fig. 6.4 Mean daily air temperature gradients along transect SVL-S60 in the summer seasons 2011 and 2012. Bold line - 10 days running means

Tab. 6.1 Mean monthly air temperature at SVL and S60 and positive degree-day sums in June-August (PDD JJA)

	2009		2010		2011		2012	
	SVL	**S60**	**SVL**	**S60**	**SVL**	**S60**	**SVL**	**S60**
May	-1.0	-4.4*	0.0	-2.1*	-1.6	-5.0	-2.4	-5.6
June	3.0	-0.4*	3.5	0.9*	4.8	2.1	3.9	0.4
July	7.7	4.6*	6.6	4.3*	6.9	3.7	6.6	2.7
August	6.3	4.1*	4.8	1.6**	6.9	3.7	5.7	2.2
September	1.7	-0.5*	2.0	-1.7*	4.4	1.6	3.0	-0.5**
Mean JJA	5.7	2.8*	5.0	2.3*	6.2	3.2	5.4	1.8
PDD JJA	523	285*	461	231*	573	292	497	176

*computed using entirely modelled data
**computed using partly modelled data

For 2011 and 2012 summer periods data from an additional temperature sensor in the lower ablation zone was available. In 2011 the sensor was installed at the front (190 m a.s.l.), while in 2012 at S30 (275 m). On-glacier temperature gradient showed a similar pattern as along

transect SVL-S60. During a common measurement period, the average gradient observed in 2011 was -0.70°C · 100 m^{-1} (14/07-10/09/2011) and showed high day-by-day variability, ranging from -1.26°C · 100 m^{-1} to positive values during inversive weather days (maximum of 0.76°C · 100 m^{-1}). In 2012 melt-season thermal gradients were more negative than in 2011. Average on-glacier lapse rate between S30 and S60 was -0.95°C · 100 m^{-1} (14/07-10/09/2012), with minimum of -1.60°C · 100 m^{-1}. No air temperature inversions were noted along this transect in 2012 summer season and the maximum gradient was -0.27°C · 100 m^{-1}.

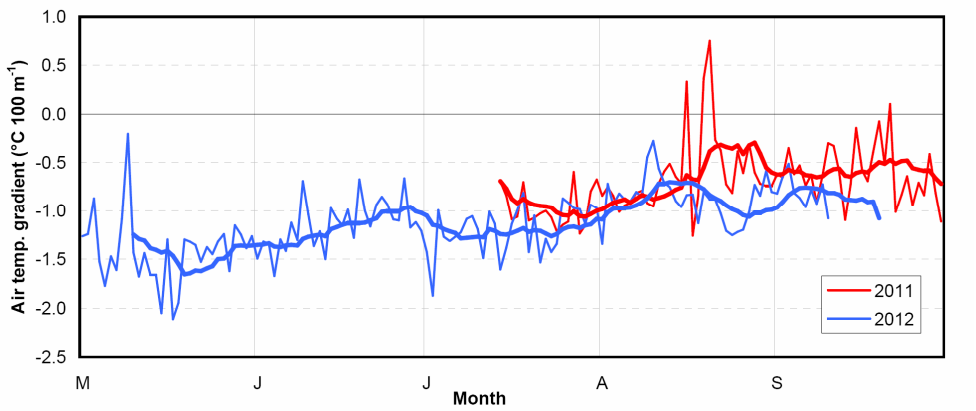

Fig. 6.5 Mean daily air temperature gradients in the ablation zone of Svenbreen in the summer seasons of 2011 (transect front-S60) and 2012 (S30-S60). Bold lines - 10 days running means

6.1.2 Air moisture

Moisture content of air in the study area is limited. At the sea-level PET station relative humidity (*RH*) in the summer is typically about 75% (Rachlewicz 2003a; Przybylak et al. 2006, 2007; Małecki et al. 2011), but in the middle of Svenbreen it is higher by about 10% (fig. 6.6). General seasonal courses of *RH* on Svenbreen in 2011 and 2012 were considerably different, as they reflected temperature variability to a certain degree (fig. 6.7). The warmer summer season in 2011 resulted in lower *RH* (JJA mean of 77.1%). The minimum daily humidity noted at S60 was as low as 40.8% (the absolute minimum dropped to 26.2%) and coincided with the warmest day of the year (10°C). Conversely, cooler ablation season in 2012 caused higher overall relative humidity (with 84.0% as JJA average). Air vapour pressure, e_a, was low and has been exceeding 600 Pa only sporadically during both seasons (fig. 6.8), having important consequences for energy balance of the surface, sublimation and evaporation (see section 6.2). JJA air vapour pressure was 592 Pa in 2011 and 567 Pa in 2012.

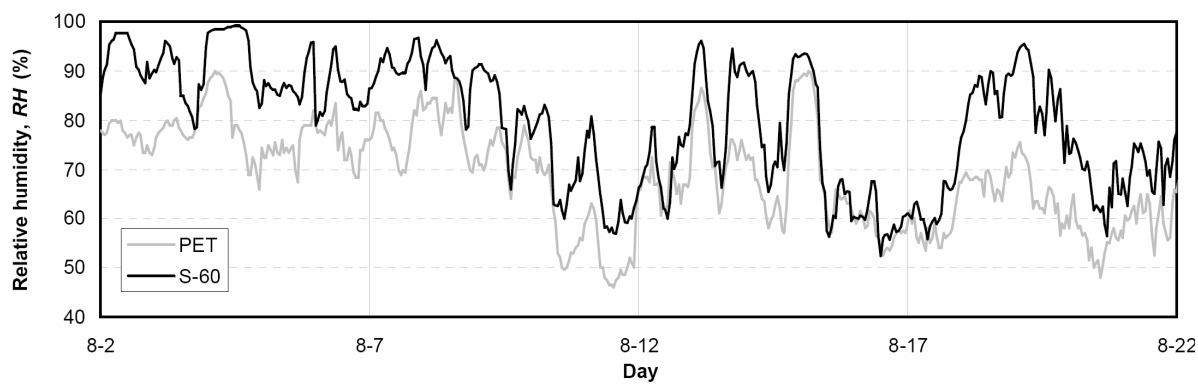

Fig. 6.6 An example of mean hourly relative humidity course at S60 (black line) and at PET (grey line) in August 2010

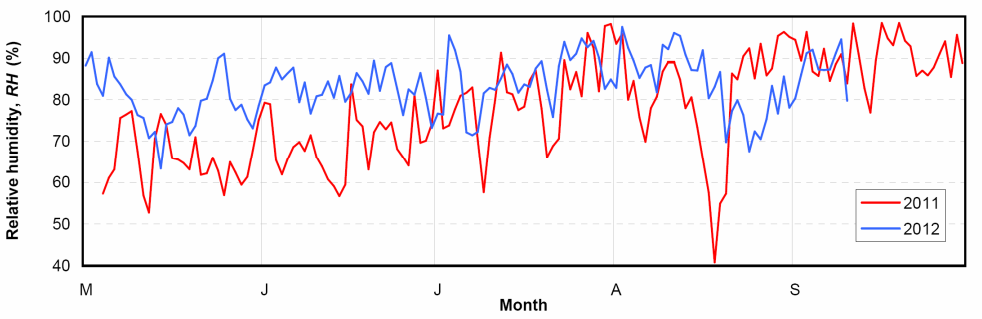

Fig. 6.7 Mean daily relative humidity on Svenbreen at S60 in 2011 and 2012

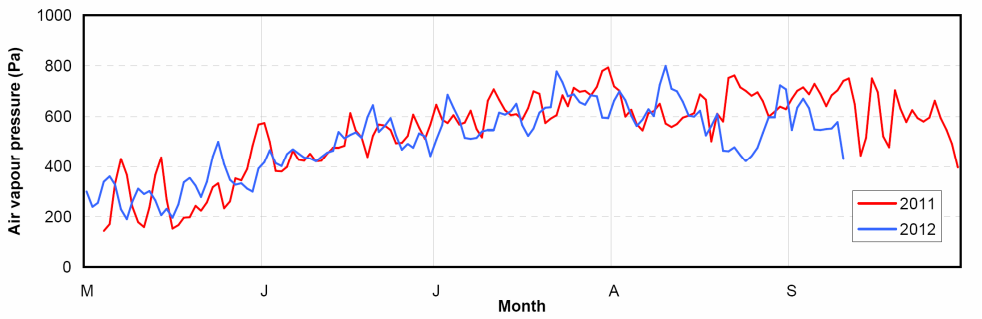

Fig. 6.8 Mean daily air vapour pressure on Svenbreen at S60 in 2011 and 2012

6.1.3 Wind conditions

Preliminary wind measurements at S60 performed in August 2010 indicated that summer wind velocity, *u*, observed on Svenbreen is much lower (1.5 m s^{-1} on average) than at the sea-level (PET station, 4.3 m s^{-1}). Further 2011 and 2012 summer campaigns confirmed that wind speed on the studied glacier is very low indeed (figs. 6.9 and 6.10), with averages of 1.3 m s^{-1} (1/06-13/07/2011, discontinuous data) and 1.7 m s^{-1} (1/06-31/08/2012). Maximum daily *u* values (defined as the highest daily velocity averaged over 5 or 10 minutes) rarely reach 10 m s^{-1}. Momentary gust speeds exceeding >15 m $s^{-1}$are very seldom.

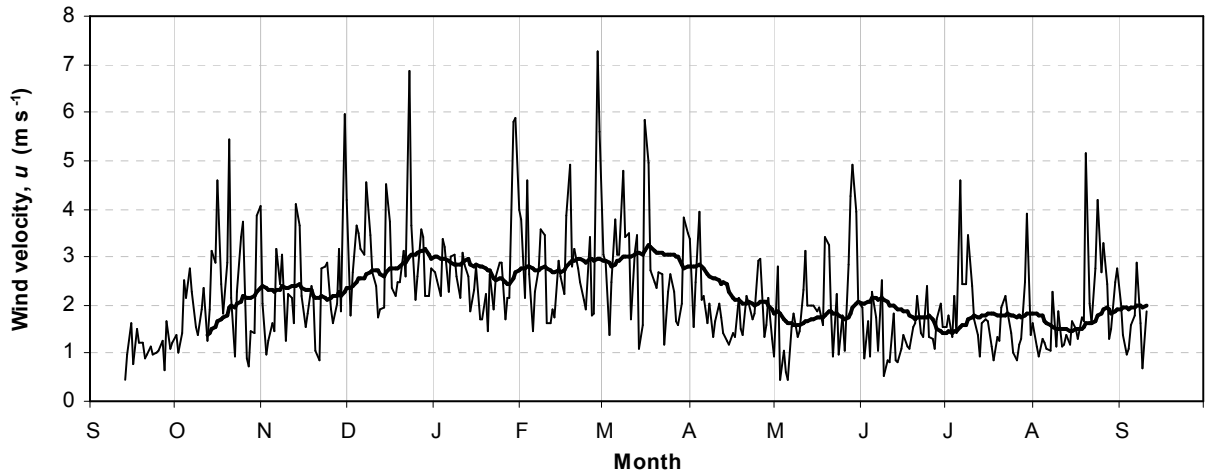

Fig. 6.9 Mean daily wind velocities (thin line) in balance year 2011/12. Thick line - 30 day running mean. Note higher wind velocity in the winter than in the summer season

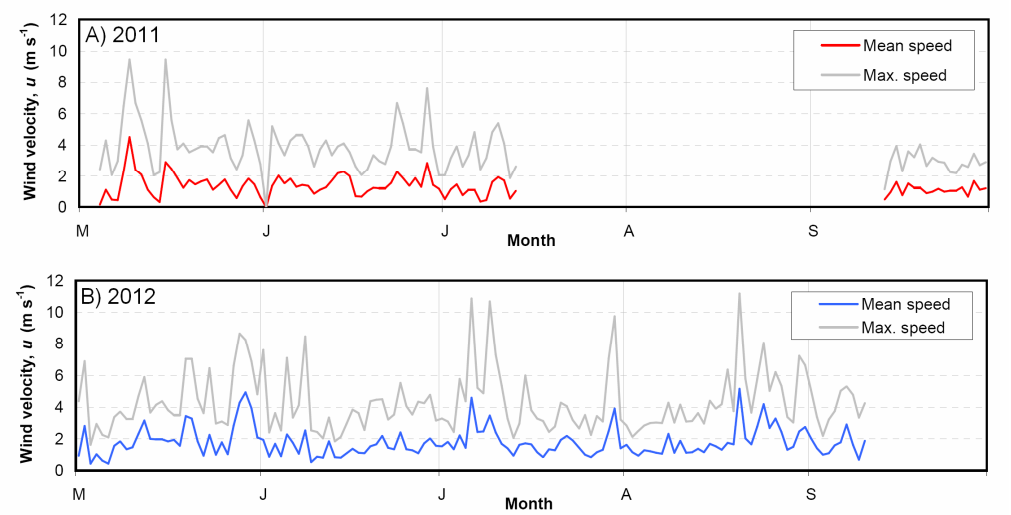

Fig. 6.10 Mean daily wind velocities at S60 in summer seasons of 2011 and 2012

The only year-round record of wind speed, measured by the AWS between 13/09/2011 and 10/09/2012 (fig. 6.9), shows a distinct seasonal variability, with higher *u* in the winter, typical for the archipelago (e.g. Kruszewski 2009). After the 2011 melt-season has ceased, *u* has been staying at a relatively higher level in the winter (~3 m s^{-1}, maximum daily average of 7.3 m s^{-1}). However, wind speed noted during the winter was still relatively low, as their daily maxima exceeded 10 m s^{-1} only on 5 days (absolute momentary maximum 15.5 m s^{-1}). After the midnight-sun season has begun in mid-April, *u* has dropped to 1.5-2 m s^{-1} (maximum 5.1 m s^{-1}) and this calmer period lasted until the end of observations. Annual *u* was 2.2 m s^{-1}.

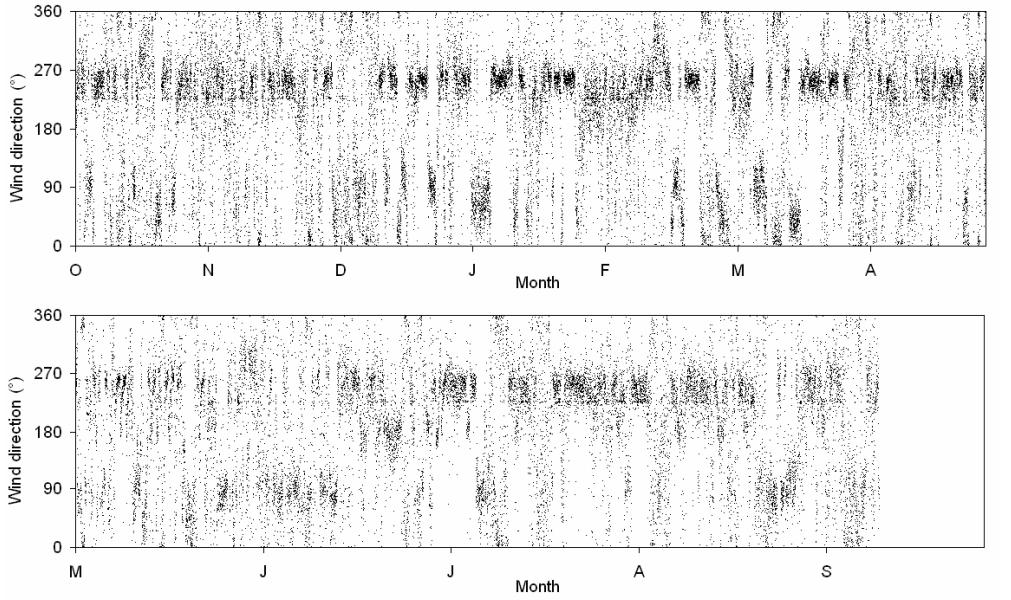

Fig. 6.11 Scatter of 10 min wind direction for winter 2011/12 (upper panel) and summer 2012 (lower panel)

In contrast to velocity, wind direction showed no distinct intra-annual shifts (fig. 6.11). Both in cold (October-April) and warmer part of year (May-September) the most frequent winds have been blowing down-glacier from the western sector (overall contribution of WSW direction - 19%, W - 14% and SW - 10%), with little share of eastern, up-glacier winds (E -

7%, ENE - 6%, NE - 5%), as visible on fig. 6.12. General circulation above Svalbard is however dominated by eastern air inflow (42%, overall from SE, E and NE), while western advection (NW, W and SW) contributes only in 15% (after Niedźwiedź 2007). These results clearly show that wind direction on Svenbreen is local and is mostly independent against the general circulation pattern, as could be expected for a mountainous terrain. Down-glacier direction is often observed on glaciers and is related to catabatic flow of the air.

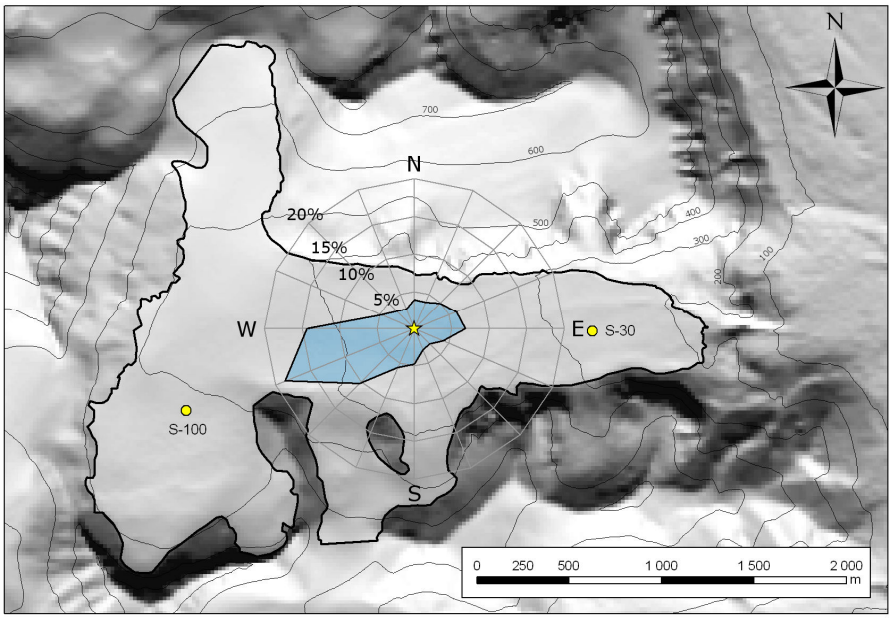

Fig. 6.12 Average annual wind direction for 2011/12 balance year at AWS site at S60 (asterisk). Yellow circles - S-30 and S-100 (additional monitoring stations). Contour lines drawn every 100 m

Strong wind events ($u_{max} \geq 10$ m s^{-1}) are important for melt processes during ablation season as they enhance turbulent heat exchange between air and surface. On Svenbreen they occur very seldom. They have not been observed during summer (JJA) in 2010 and 2011 (though the data is discontinuous), while in 2012 summer season there were four such events (on 6/07, 9/07, 30/07 and 20/08, fig. 6.13). A well visible *RH* change, together with a clear wind direction shift, occurred at the beginning and end of each event. The described winds were all dry and they have been blowing from different directions: from the east, north and west. From early morning of 6/07 (fig. 6.13A), an eastern, up-glacier wind has been slowly increasing its velocity until afternoon and has caused a temperature drop from 4°C to 1°C and *RH* decrease from 85 to 65%. A cool wind, though 1°C warmer than air before the event, occurred on 9/07 (fig. 6.13B) and was most likely a foehn-like wind from the north, weakened after surpassing several mountain massifs on its way from Austfjorden. Strong western winds occurred twice: on 30/07 (fig. 6.13C) and 20/08 (fig. 6.13D). Again, they have caused a well visible cooling (by 1-2°C) and sharp *RH* decrease (by 20-30%). According to Niedźwiedź (2013) atmospheric circulation above Svalbard during the described events (in all cases cyclonic) was SE on 6/07, N on 9/07 and NW on 30/07 and 20/07. In contrast to days with normal wind velocity, strong winds on Svenbreen have therefore shown a good agreement with the general synoptic situation.

Concluding, wind speed on Svenbreen shows seasonal variability, with the greatest u in the winter season (~3 m s^{-1}) and lower velocity in the summer (~1.5 m s^{-1}). In 2011/12 balance year wind direction has shown no variability and in both cool and warmer season of the year

the prevailing direction was from the west (down-glacier), being independent of general circulation. Seldom stronger winds occurred during cyclonic weather, bringing cool and dry air from different directions and originated from general synoptic situation above Svalbard. Wind is an important element of surface energy budget of a glacier surface, as it shapes heat exchange between air and ice. As demonstrated for Svenbreen, local wind conditions are potentially unfavourable for extra melt production.

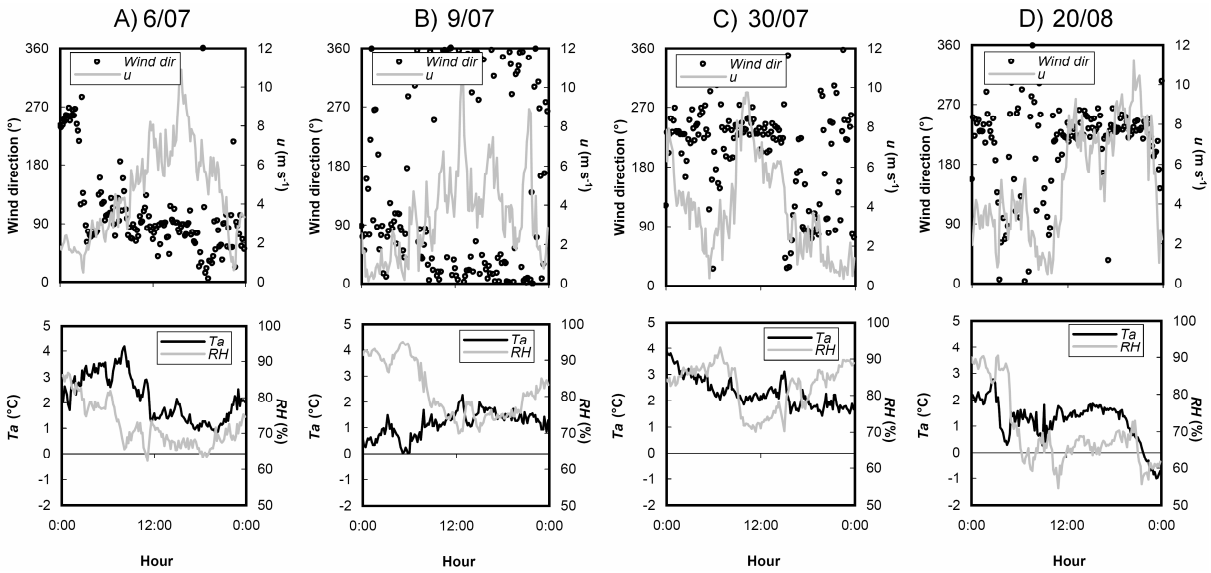

Fig. 6.13 Strong wind events at S60 in summer 2012 and their characteristics: wind speed (u) and direction, air temperature (T_a) and relative humidity (RH). Data interval is 10 min. Note a clear RH drop at the onset of each event

6.2 Surface energy balance

Energy balance investigations of a glacier surface are very rare in Svalbard and no such measurements were taken previously on small glaciers in its arid central regions. The parameters directly observed on Svenbreen in the period 13/09/2011-10/09/2012 were incoming and outgoing shortwave radiation (SW_{in} and SW_{out}) and balance of shortwave and longwave radiation (Q_N). Energy fluxes modelled are sensible and latent heat (Q_H and Q_L). For the need of energy balance computations several corrections and assumptions were introduced to the AWS data and the model (for more details see chapter 'Methods and errors'). In the previous section the main period of comparison was June-August, but since the first half of June in the investigated 2012 season was rather cool, a conservative date of 15/06 was adopted as the day when surface temperature reached T_s = 0°C and melting begun. The time span of the analysis was however expanded until the end of observation campaign (10/09/2012), so in this section 'summer' refers to nearly 3 months from mid-June to mid-September 2012.

6.2.1 Seasonal rhythm of energy fluxes

Winter months are the time of a polar night on Svenbreen and no solar radiation is available between November and mid-February. In late-winter/spring the weather in Svalbard is usually sunny and that was the case for Svenbreen area in 2012, as suggested by smooth rhythm of

hourly SW_{in} values in March, April and May (fig. 6.14). The highest daily means of SW_{in} in 2012 were noted in May and June (maximum 361 W m^{-2} on 30/06/2012), but the maximum hourly value was noted on 8/07 (783 W m^{-2}). Greater cloudiness in the summer season and lower sun angles caused generally lower insolation and its daily amplitudes, so daily peaks of only 100-300 W m^{-2} were noted on many days in June, July and August. The mean SW_{in} for the summer period was relatively low with 140 W m^{-2}.

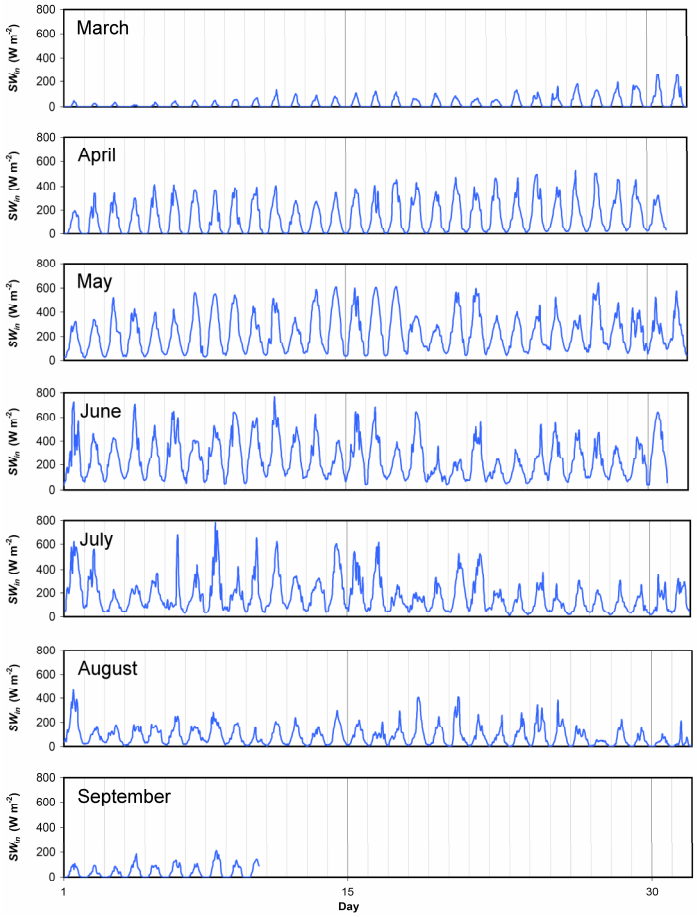

Fig. 6.14 Hourly incoming shortwave radiation (SW_{in}) in period March-September 2012 at S60. Note a relatively smooth SW_{in} course from March to May (frequent sunny days) and disturbed course since June (mainly overcast weather)

Due to continuous snow cover with relatively high albedo, α, most of this energy was however reflected (fig. 6.15). Albedo course at AWS showed a continuous decrease from mid-March (~90%, typical for fresh snow) to mid-August, when ice was eventually exposed, as indicated by ~35% albedo (fig. 6.16). In the latter half of August α increased to 80%, suggesting presence of a fresh snow on the surface, and then dropped to 22% after it melted-out during the warmest day of the season (30/08). A similar α rise was observed in early-September. Average summer albedo of the surface was 61% (when calculated from average summer SW_{in} and SW_{out}) or 56% (when averaged from daily α means), significantly reducing shortwave radiation which could contribute to melt. SW_{bal} was zero during the polar night and positive since its termination in mid-February. Even though the incoming solar radiation has been decreasing since June, SW_{bal} in July and August was still relatively high due to greater energy absorption of the surface. The maximum daily SW_{bal}, noted on 30/06, reached 124 W m^{-2}, with summer mean of 54 W m^{-2}.

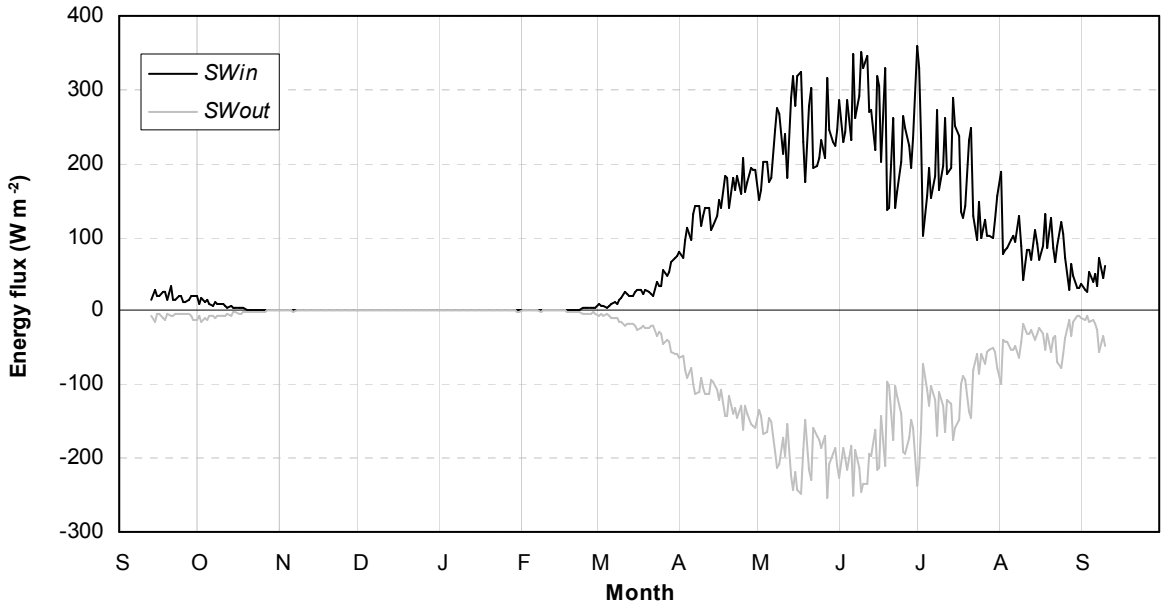

Fig. 6.15 Mean daily incoming (SW_{in}) and reflected (SW_{out}) shortwave radiation at S60 in balance year 2011/12

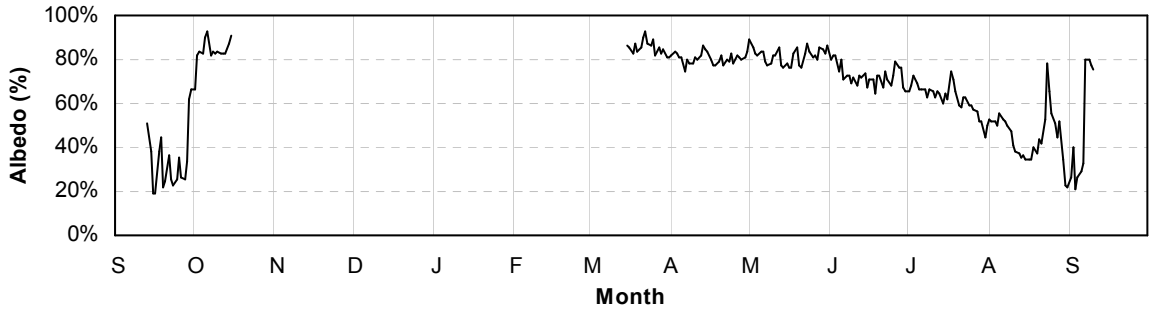

Fig. 6.16 Mean daily albedo at S60 in balance year 2011/12

Longwave outgoing radiation, LW_{out}, of a melting glacier is fixed, so incoming longwave radiation LW_{in} could also be calculated for the summer season from the available data. This parameter was relatively stable in the studied period, and its summer mean reached only 282 W m^{-2}, with its daily averages varying from 217 W m^{-2} to 312 W m^{-2}. It was however significantly lower than LW_{out}, being 316 W m^{-2} for a melting ice surface. Therefore, longwave balance LW_{bal} has been continuously negative for all of the year (-33 W m^{-2} on average). Generally, LW_{bal} oscillated between -5 and -50 W m^{-2} in the winter and reached the lowest daily values in April, May and June (minimum of -99 W m^{-2}). In July-September LW_{bal} returned to its winter level and overall summer average was -33 W m^{-2}. Due to the nature of shortwave and longwave radiation fluxes, net radiation, Q_N, was negative in the winter as it was governed by LW_{bal}, while in the summer period it reflected variability of SW_{bal} and was positive between June and September (summer mean of only 21 W m^{-2}, fig. 6.17). The annual average of Q_N was negative with -10 W m^{-2}.

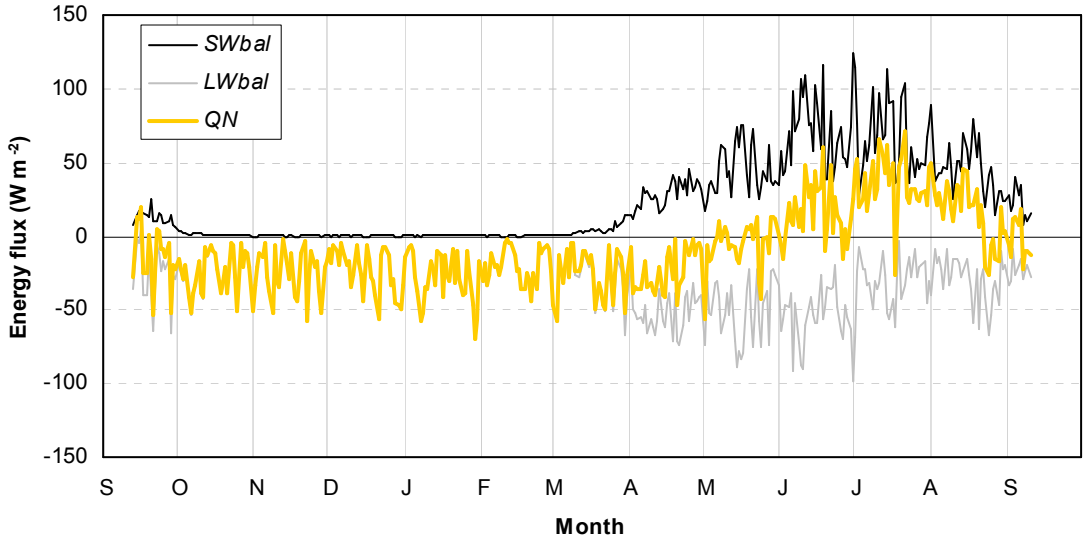

Fig. 6.17 Annual course of radiative heat fluxes in balance year 2011/12. Mean daily intensity of shortwave radiation balance (SW_{bal}), longwave radiation balance (LW_{bal}) and net radiation (Q_N). Note that Q_N is positive only from June to August

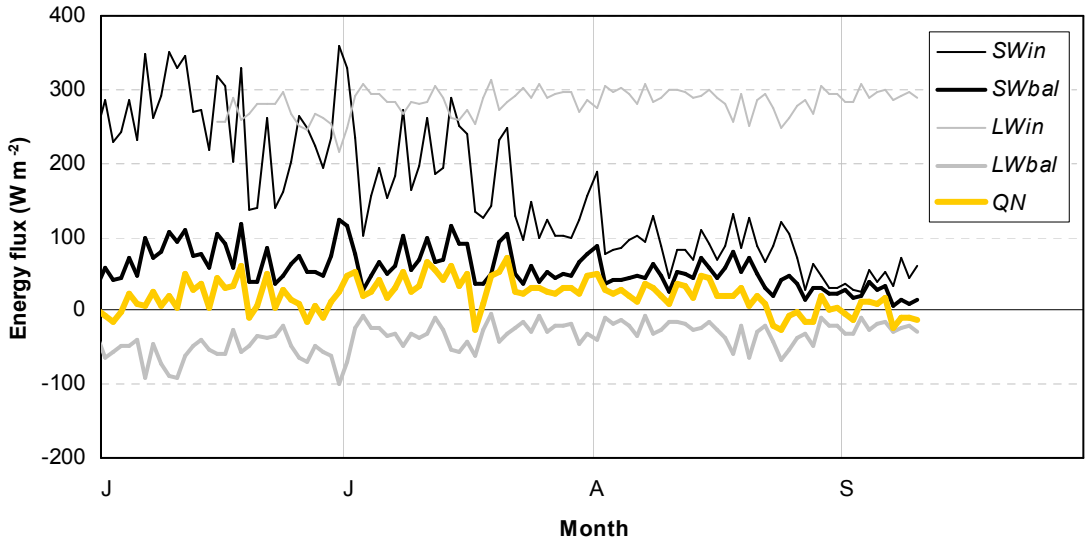

Fig. 6.18 Radiative fluxes in the summer season of 2012. Note a distinctly decreasing trend of SW_{in} (incoming shortwave radiation), relatively stable SW_{bal} due to decreasing surface albedo and stable LW_{in} (incoming longwave radiation)

Turbulent fluxes of sensible (Q_H) and latent heat (Q_L) were computed only for the summer period using Brock & Arnold (2000) energy balance model. It uses u, T_a (in case of Q_H) and e_a (in case of Q_L) as input data, so the estimated values are correlated to these parameters (fig. 6.19). Q_H was on average 6.7 W m^{-2} and ranged from -3.6 W m^{-2} on the coolest day in the studied summer period up to 28 W m^{-2} on the warmest day. Q_L oscillated mostly around zero, with extreme values of -32 W m^{-2} and 10 W m^{-2}. Latent heat flux has shown negative average contribution to the overall energy balance (-2.5 W m^{-2}), indicating net evaporation (sublimation) from the surface in the summer.

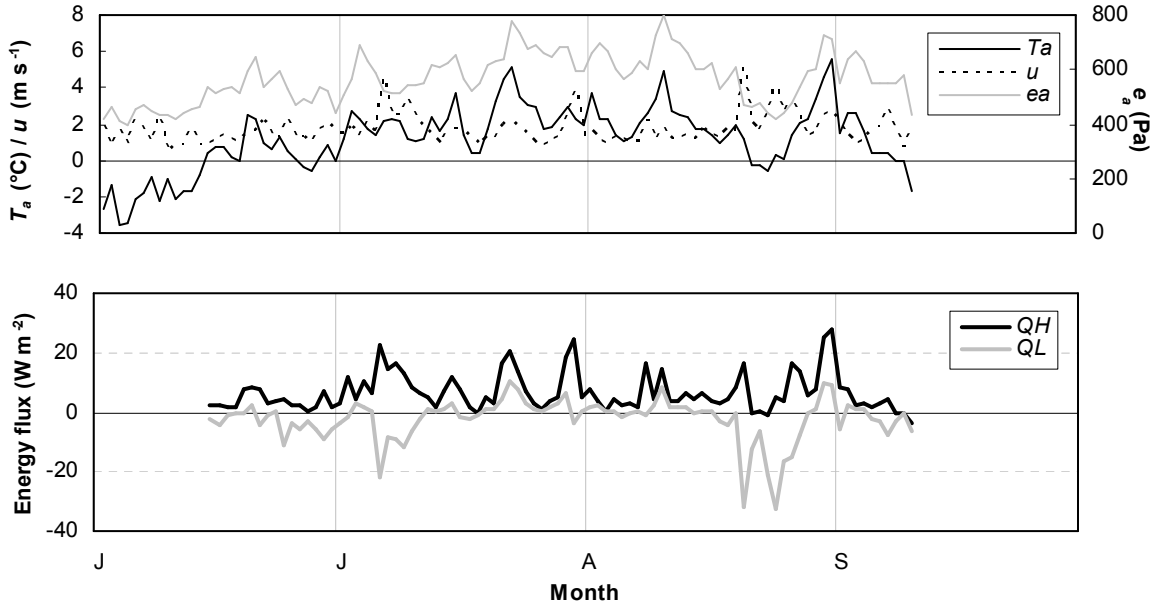

Fig. 6.19 Mean daily values of turbulent heat fluxes against main meteorological elements in summer 2012. Upper panel - air temperature (T_a), air vapour pressure (e_a) and wind speed (u). Lower panel - sensible (Q_H) and latent heat fluxes (Q_L)

6.2.2 Surface ablation as a result of energy balance

By summation of the modelled energy balance components, Q_N, Q_H and Q_L, overall ablation (including melt and sublimation) is calculated, together with associated ablation rates for the whole studied summer season. Manual inspections of local mass balance were carried out at stake S60 situated 15 m from AWS and the collected data is used as a reference for the melt model. Melting snow density was assumed as 0.50 g cm^{-3}, density of superimposed ice as 0.80 g cm^{-3} and glacier ice - 0.90 g cm^{-3}. Mass accumulated at S60 on the first day of the model run, 15/06, was assumed to be the same as on 18/04 (winter balance survey), as suggested by sub-zero T_a in the period between these two dates (fig. 6.3). Results of the modelling show reasonable agreement with ablation observed at S60 (fig. 6.20). The model however slightly underestimates the mass loss. The total ablation calculated for the studied period is 74.6 cm w.eq., while the observed summer balance at S60 was -89.0 cm w.eq. Ablation rates computed for 2012 ranged from 0 to 2.4 cm w.eq. d^{-1}, with average seasonal rate of 0.85 cm w.eq. d^{-1}.

In the whole studied summer season LW_{in} was the primary incoming energy flux (tab. 6.2). SW_{in} was also an important source of heat, although twice lower, while Q_H represented only a minor (though important in an overall heat budget) income, when compared to LW_{in} and SW_{in}. These positive fluxes were not balanced by outgoing heat transfer, generally lower than incoming energy, with LW_{out} playing the dominant role and followed by SW_{out} and Q_L. The average energy available for melt, Q_M, was 25 W m^{-2} and reached daily maximum of 92 W m^{-2}. Q_N contributed to the overall melt-energy in 70%, together with relatively high share of Q_H (22%). Q_L was generally reducing Q_M, as the energy was consumed for evaporation and sublimation (-8%).

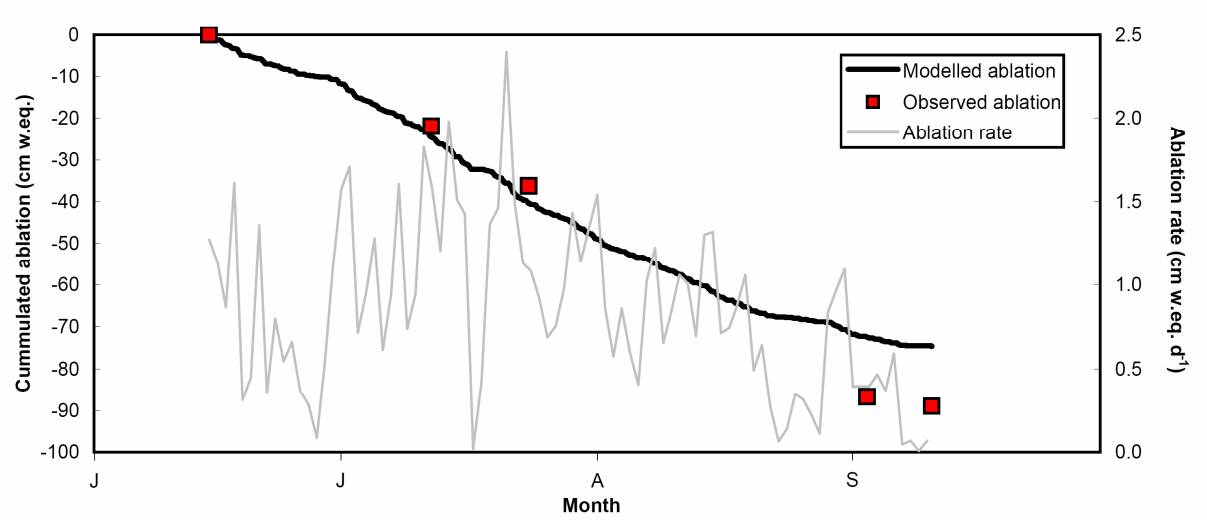

Fig. 6.20 Calculated cumulated melt at S60 in 2012 (bold black line) against ablation measured in the field (squares) and modelled daily melt rates (grey line)

Tab. 6.2 Meteorological elements and components of the surface energy balance of Svenbreen in 2012

	T_a	RH	e_a	u	SW_{in}	SW_{out}	SW_{bal}	α	LW_{in}	LW_{out}	LW_{bal}	Q_N	Q_H	Q_L	Q_M
	°C	%	Pa	m s^{-1}	W m^{-2}	W m^{-2}	W m^{-2}	%	W m^{-2}	W m^{-2}	W m^{-2}	W m^{-2}	W m^{-2}	W m^{-2}	W m^{-2}
15-30 Jun	1.4	83%	531	1.5	232	-163	69	70%	264	-316*	-51	18 (71%)	3.6 (15%)	-3.5 (-14%)	18 (86%)
1-15 Jul	2.5	82%	577	2.1	211	-137	74	65%	282	-316*	-34	40 (75%)	9.5 (18%)	-3.6 (-7%)	46 (93%)
16-31 Jul	2.9	88%	642	1.6	144	-85	59	59%	288	-316*	-28	31 (75%)	8.5 (21%)	1.9 (5%)	41 (100%)
1-15 Aug	2.7	90%	654	1.3	95	-44	50	47%	294	-316*	-22	29 (81%)	5.5 (16%)	1.2 (3%)	36 (100%)
16-31 Aug	1.7	78%	542	2.4	77	-36	41	47%	279	-316*	-37	4.1 (20%)	8.7 (41%)	-8.2 (-39%)	4.6 (61%)
1-10 Sep	0.9	88%	570	1.6	44	-23	22	51%	292	-316*	-24	-2.0 (-28%)	2.6 (37%)	-2.5 (-35%)	-2.3 (37%)
TOTAL	**2.1**	**85%**	**587**	**1.8**	**139.7**	**-85.4**	**54.3**	**61%**	**282.4**	**-315.6***	**-33.2**	**21.1 (70%)**	**6.7 (22%)**	**-2.5 (-8%)**	**25 .0 (92%)**

*assumed constant surface temperature at 0°C

Energy balance structure was averaged over half-month intervals to illustrate seasonal variability of its portioning, mainly related to lowering of the sun angle (tab. 6.2, fig. 6.22). Net radiation, the dominant energy source, has been continuously decreasing since mid-July and in September Q_N eventually turned its sign to negative. Therefore, contribution of Q_N to melt-energy suddenly dropped from a stable level of ~75% to 20% in the second half of August and then to -28% in September. At the same time, the relative role of sensible heat flux has been consequently rising with decreasing Q_N, so in the last weeks of observations melting was mainly driven by Q_H, even though its absolute magnitude was low. Latent heat, Q_L, has also shown distinct variability in the studied period. Although generally negative, it has been contributing to melting for about a month, between mid-July and mid-August, when air vapour pressure reached its maximum values (>600 Pa).

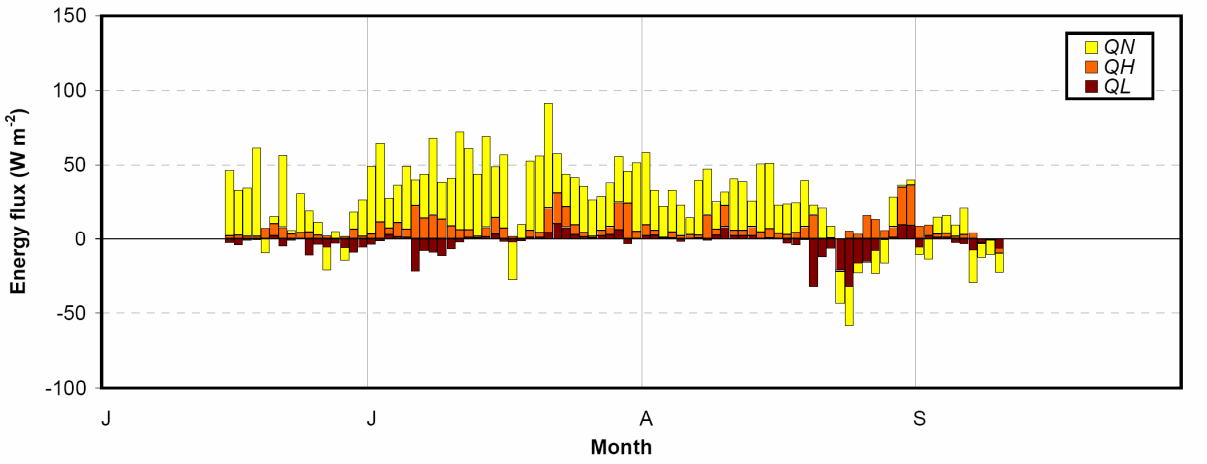

Fig. 6.21 Daily means of net radiation (Q_N), sensible heat flux (Q_H) and latent heat flux (Q_L) in the summer season of 2012

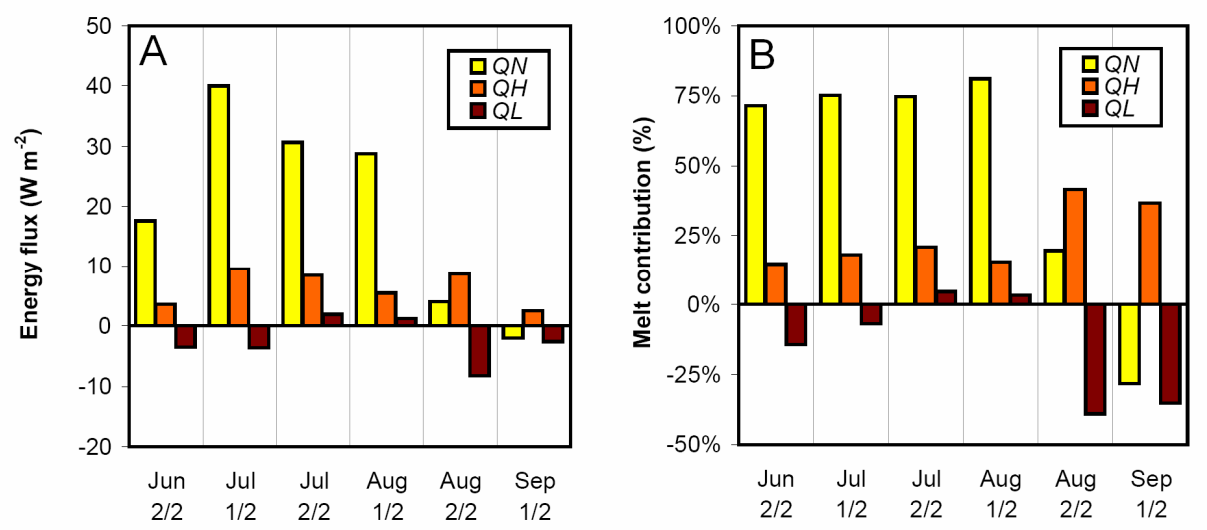

Fig. 6.22 A - Absolute and B - relative half-monthly means of net radiation (Q_N), sensible heat flux (Q_H) and latent heat flux (Q_L) in the summer season of 2012. Note a decreasing relative role of Q_N and increasing role of Q_H

Intra-seasonal and sub-daily changes of melt-rates and energy budget portioning were directly related to daily atmospheric conditions above the glacier. In the earliest period of melt, contribution of net radiation to Q_M was the greatest. SW_{in} was the highest in June and July, its momentary values reached 500-700 W m^{-2} on sunny days, with maximum hourly SW_{bal} on the order of 200 W m^{-2} (e.g. 30/06-2/07 on fig. 6.23; 15-16/07 on fig. 6.24). Midnight-sun has been causing low air temperature amplitudes, so daily variability of longwave emission of the atmosphere was largely driven by its moisture content, cloudiness and e_a. During overcast periods and nights SW_{in} was generally low (30-200 W m^{-2}), with simultaneous high longwave contribution (~300 W m^{-2}, e.g. 3/07). Therefore, LW_{in} was the greatest energy source during early summer, even though the solar angle was high. The only exception were seldom sunny mid-days (e.g. 30/06-2/07, 15/07-16/07). Net radiation ranged from about -50 to 150 W m^{-2} and the role of turbulent heat fluxes was generally low in the first period of melt season and restricted to rare windy days few days of increased wind speed (e.g. 4/07).

In the latter half of the summer insolation was greatly reduced. On fair weather days SW_{in} has been exceeding 100 W m^{-2} only for 8-10 hours a day in August and 2-4 hours daily in September, with maximum values reaching 100-400 W m^{-2}. Hence, domination of LW_{in} as an incoming heat flux (150-300 W m^{-2}) was nearly constant in this period. Q_N oscillated around zero or was only slightly positive at mid-days (e.g. 30/08-3/09 on fig. 6.26). Turbulent heat fluxes became therefore relatively more important in an overall energy budget, although still low (e.g. 2/09). In some situations however, their role was superior, as e.g. during a strong wind event on 20/08 (fig. 6.25) or on the warmest days of the summer (30-31/08). In the first case, a relatively strong and dry wind from the west (see also fig. 6.13D) resulted in a very negative latent heat flux (down to -83 W m^{-2}) due to intensive evaporation from the surface, not compensated by an increased sensible heat flux due to low T_a (similar situation occurred e.g. on 6/07, 9/07, 30/07 from fig. 6.13). In the end of August air temperature has exceeded 6°C (30/08) and 9°C (31/08), with simultaneous modest wind speed and e_a. It caused high Q_H and Q_L (reaching 89 and 37 W m^{-2} respectively), making turbulent heat fluxes the main drivers of melting in this period, as the net radiation oscillated around zero. It underlines that high T_a is insufficient to trigger extra melt on Svenbreen, because considerable wind velocity is crucial.

From the examples above, figs. 6.14-6.26 and previous considerations several regularities concerning surface energy balance of Svenbreen have been found. In the summer season of 2012, melting was generally governed by net radiation, but with well pronounced progressing evolution of energy portioning. Change in relative contribution to melt of individual components was mostly related to continuous SW_{in} decrease, while variability of LW_{in} was of much lower magnitude, which for all summer oscillated between 250 and 300 W m^{-2}, making it the main heat income. A distinct inverse proportionality of the major melt-energy sources, LW_{in} and SW_{in}, could be observed on Svenbreen during the entire summer, i.e. periods of low SW_{in} (overcast days and nights) corresponded to periods of higher LW_{in}. In June and July SW_{in} reached its maximum values, during few sunny days being even higher than LW_{in}, but high albedo has limited daily peaks of Q_N to ~100 W m^{-2}. In mid-August SW_{in} was greatly decreased, however lower α of old snow and ice kept SW_{bal} at a similar level as in the first part of ablation season. In late-August and September, when midnight-sun period was already over and low insolation resulted in near-zero net radiation, generally weak turbulent heat fluxes were playing the major role in shaping the energy budget of the surface, especially when momentary wind velocity was higher than 4 m s^{-1}. Turbulent fluxes were low mainly due to low wind speed. Efficiency of Q_H was limited also due to low air temperature above Svenbreen in 2012. Relatively low humidity in the study area has resulted in mostly negative Q_L values due to evaporation from the surface. Average energy available for melt in the studied summer period, 25 W m^{-2} (tab. 6.2), was enough to melt only 75 cm w.eq. (modelled value) or 89 cm w.eq. (measured) of snow and ice at AWS site. Daily parameters of energy balance are presented in the appendix in tabs. A2-A7.

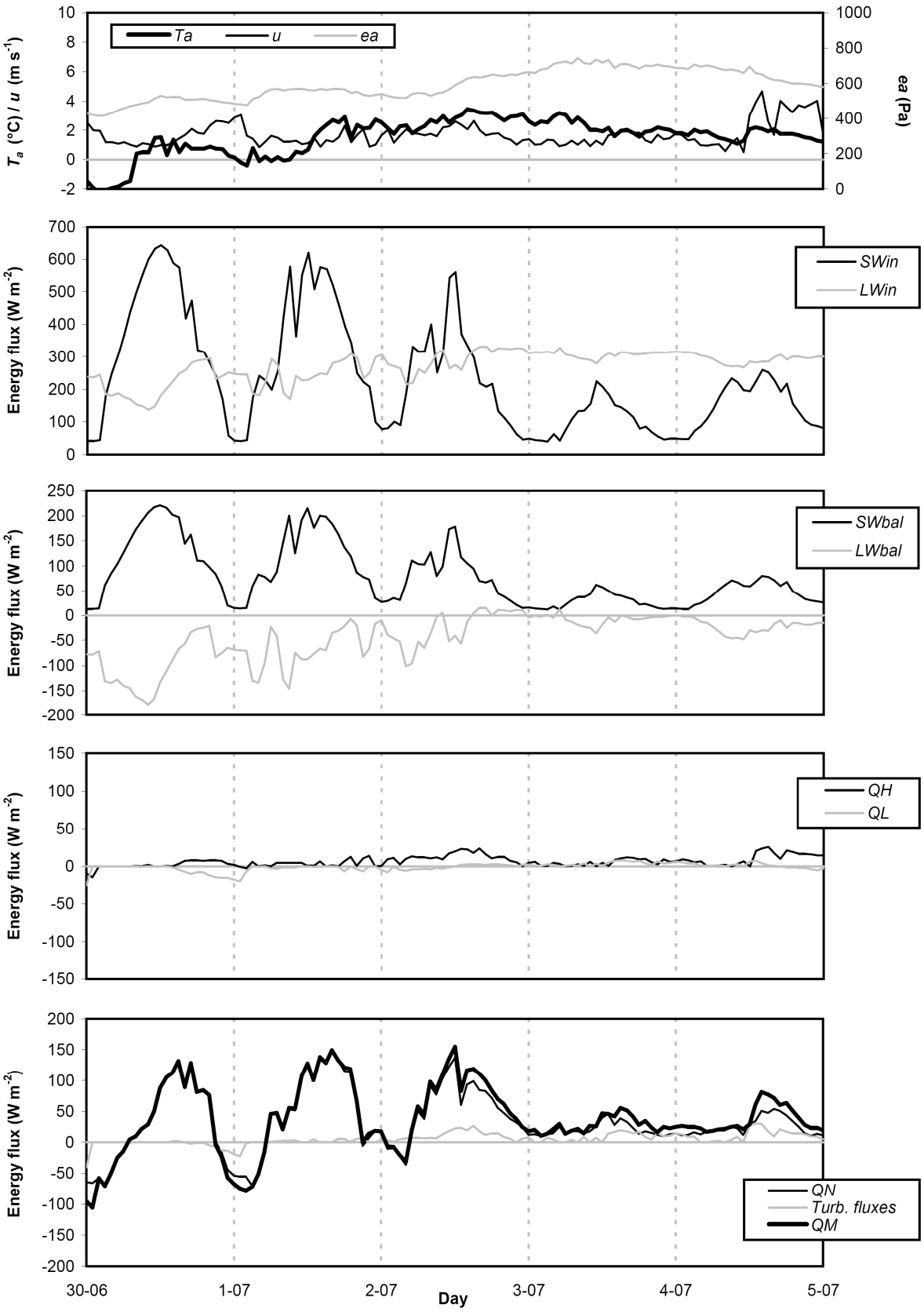

Fig. 6.23 Surface energy balance of Svenbreen in early-July of 2012

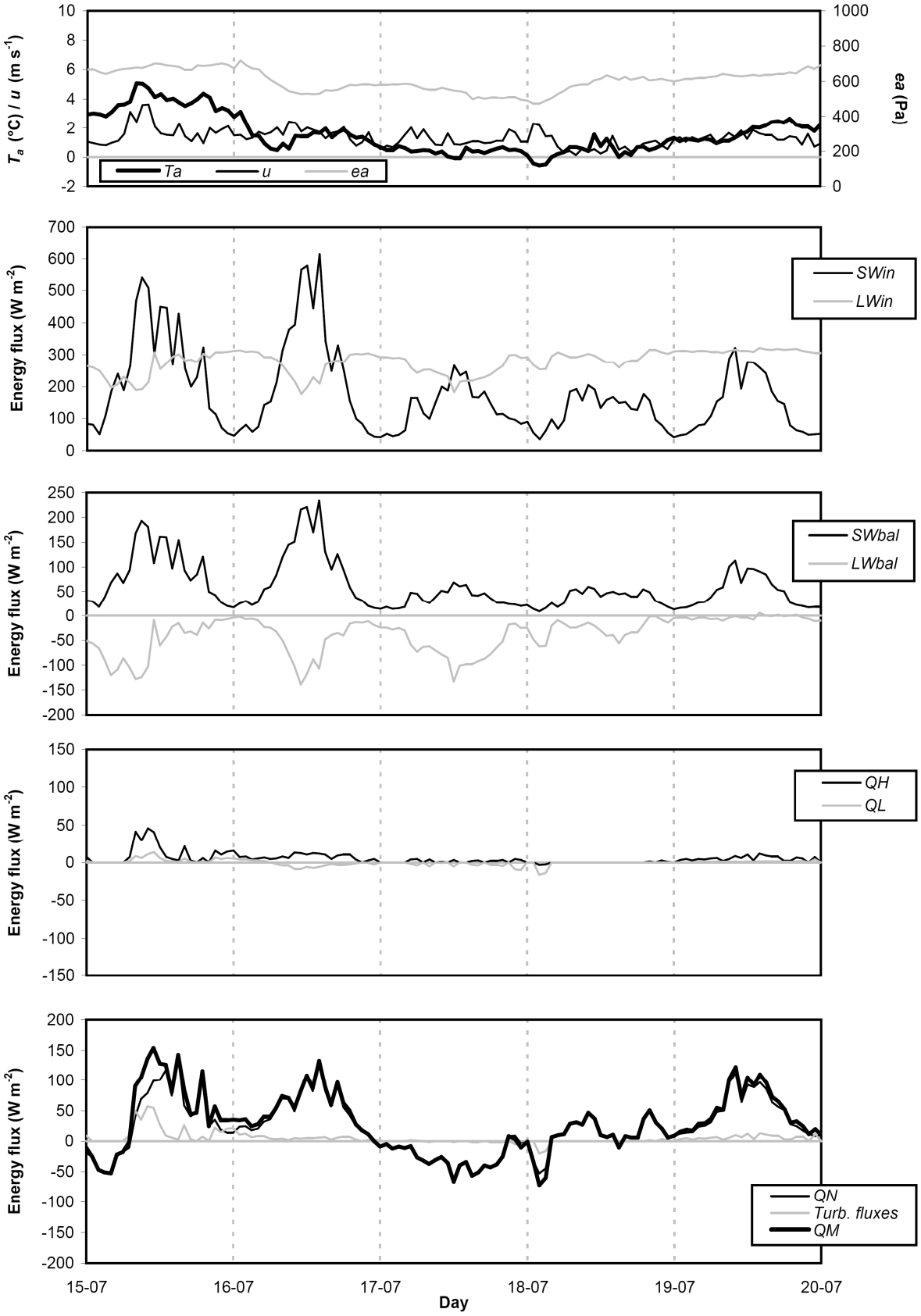

Fig. 6.24 Surface energy balance of Svenbreen in mid-July of 2012

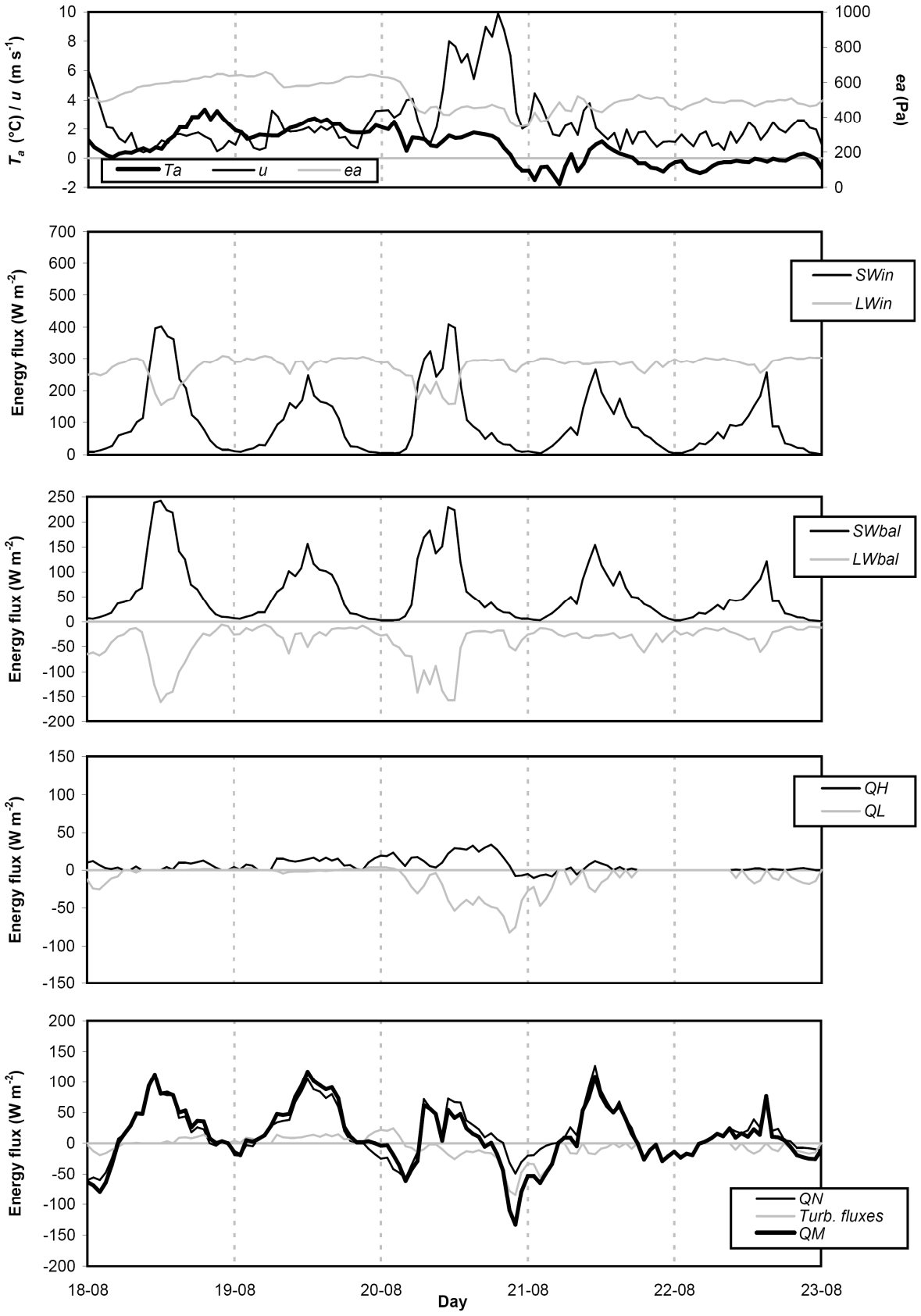

Fig. 6.25 Surface energy balance of Svenbreen in mid-August of 2012

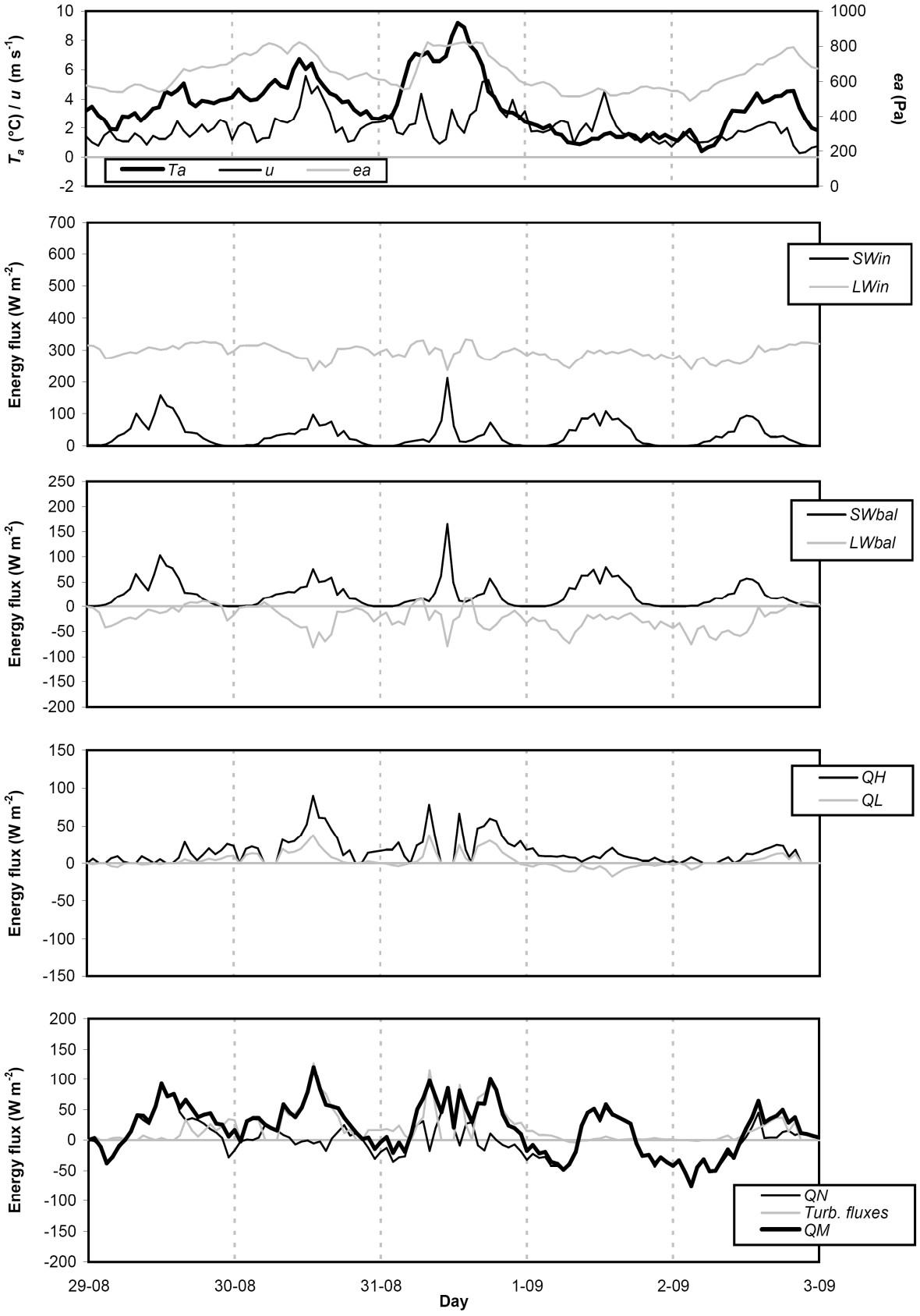

Fig. 6.26 Surface energy balance of Svenbreen in late-August of 2012

6.3 Mass balance

In the previous section point energy-balance study performed in the mid-glacier zone is presented, together with its impact on ablation at S60. Surface energy budget (and thus ablation) is however variable along glaciers, what is mainly related to altitude and topography, which influence temperature, humidity and pressure of the air, radiation and wind conditions. Snow accumulation pattern is the other factor shaping the spatial variability of glacier's mass budget. Direct observations of Svenbreen with direct glaciological method begun in 2010, when limited studies of snow accumulation and ablation were performed, but the full information was obtained for 2010/11 and 2011/12 balance years. This is the first direct mass balance data from this region since 1985, after systematic survey on neighbouring Bertilbreen was terminated (see sections 3.5). Detailed tables regarding mass balance parameters of Svenbreen are presented in the appendix (tabs. A9-A11).

6.3.1 Winter mass balance

Central Spitsbergen is generally considered as relatively dry (Hagen et al. 1993; Winther et al. 1998; Humlum 2002), so accumulation on the order of 40-50 cm w.eq. was expected on Svenbreen before the field campaign has started (see section 3.4). In the first year of direct measurements, 2010, only preliminary information of snowpack thickness was collected in late-winter. Snow depth was probed at 43 sites on the glacier surface (12 points km^{-2}), but even though the sample size was relatively low, it was sufficient to sketch the main pattern of snow accumulation on Svenbreen (fig. 6.27). Clearly, snow depth observed on 30/03/2010 was low: in the front zone it was less than 100 cm, but it gradually increased up-glacier, locally reaching 200 cm in the main glacier cirque. Mean snow depth, as calculated from the interpolated raster, was 130 cm, but it is most likely slightly underestimated (no information from the highest zones). No data from snow pits is available for this year, but subjective estimates indicate generally low snow density. It must be underlined here that accumulation period in Svalbard lasts usually until May, so some snow could be supplied to the surface after the survey was performed.

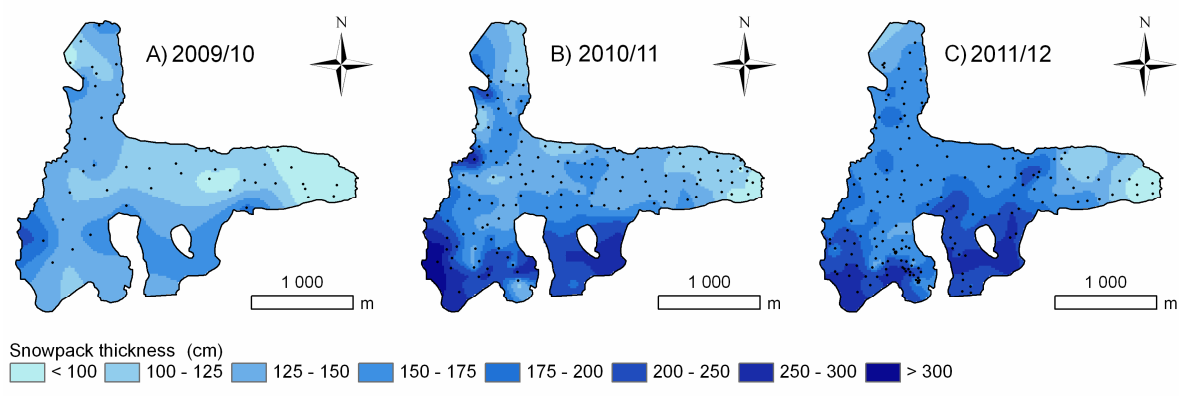

Fig. 6.27 Winter snowpack thickness on Svenbreen on A - 30/03/2010; B - 4/05/2011; C - 15/04/2012. Black dots - snow depth probing locations. Note that map on panel A is interpolated from sparse data and no direct information is available for steep high elevated zones

On 4/05/2011 the field campaign was much more detailed. The snow thickness was probed at 130 points (35 points km^{-2}) and two snow-pits were dug in order to measure snow density.

General snow distribution pattern was relatively similar as in 2010: steeper frontal part experienced low snow accumulation (minimum snowpack thickness was 80 cm), while the maximum depth was observed in the main glacier cirque and exceeded 300 cm at the foot of steep rock walls. Average snow thickness was much higher than in the previous year with 170 cm. Snow pit studies performed at S-30 and S-100 (277 m and 513 m a.s.l. respectively) revealed low average snow density of only 0.29 g cm^{-3} and 0.35 g cm^{-3}. Assuming a uniform density of the entire snowpack on Svenbreen, obtained by averaging of the two values from S-30 and S-100 (0.32 g cm^{-3}), glacier-wide winter balance, B_w, was calculated as 54 ± 10 cm w.eq. for 2010/11 winter season (fig. 6.28A).

Winter survey for 2011/12 balance year was carried out on 16/04/2012. Snowpack thickness was measured at 180 locations (49 points km^{-2}). As in previous years, snow depth at the front was lower than 100 cm. Mean thickness of the snowpack was the greatest from analysed winter seasons with 180 cm and again the greatest thickness (270 cm) was noted close to the rock walls in the main cirque and on steep ice slopes of southern tributaries originating from Nataliaskaret (partly surveyed for the first time). Snow density measured at S-100 (183 cm, 0.36 g cm^{-3}) was again higher than at lower elevations (180 cm and 0.32 g cm^{-3} at S60, 360 m a.s.l.). The reason for such situation in 2011 and 2012 may be attributed to increased wind action in the higher reaches of Svenbreen, resulting in greater wind-packing. Average density of the 2011/12 snow was set as 0.34 g cm^{-3} and the calculated B_w was 61 ± 10 cm w.eq. (fig. 6.28B).

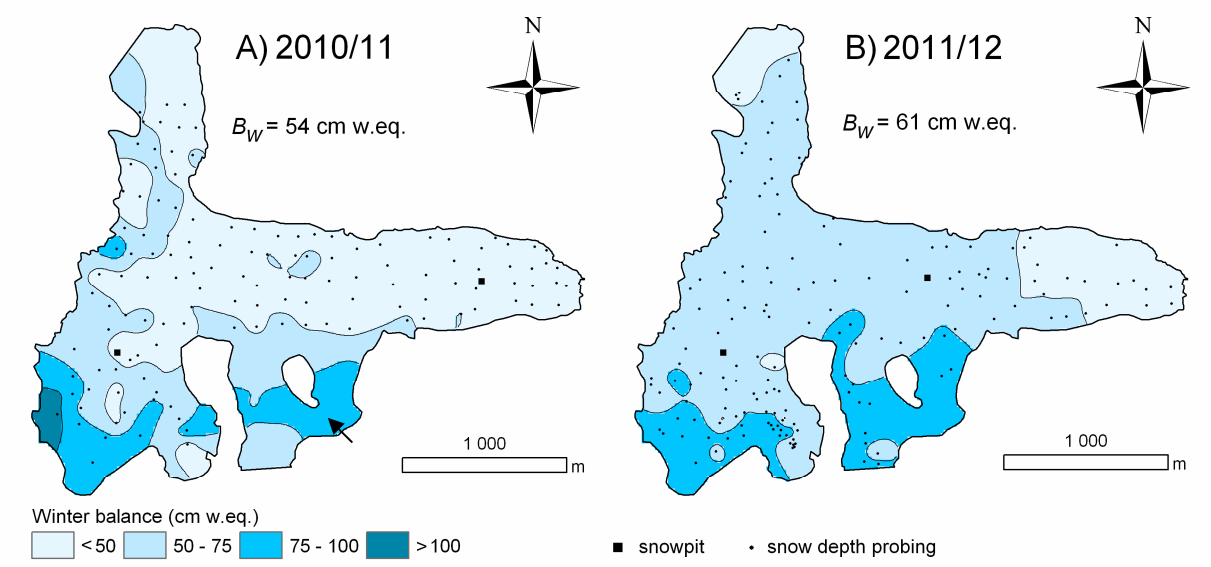

Fig. 6.28 Winter balance of Svenbreen in winter seasons of A) 2010/11 and B) 2011/12. Arrow on panel A marks zone where no direct data was available and for which a general snow distribution pattern observed in 2012 was used (with adequately lower snow depth, due to generally lower accumulation than in 2012)

As visible on fig. 6.27 the lowest snow depths are noted at the front (<100 cm). In mid-sections of Svenbreen thickness of the snowpack is relatively even and generally ranges from 100 to 175 cm. In the main glacier cirque large variability occurs, snowpack thickness may change by 50-100 cm within a short distance and the highest zone, close to S120, is characterized by distinctly lower snow depth. At steep slopes under the rock walls snow accumulation is the highest and locally may reach 300 cm. High snow depth was also noted on Nataliaskaret, though data from this area is available only for one season. Accumulation

was the highest in an elevation band 550-600 m a.s.l. in both studied seasons, while higher up a decreasing trend was pronounced due to high inclination of slopes. Because snow redistribution on flat tongue of Svenbreen is limited due to low wind velocity (see section 6.1.3) snow data could be used to infer a general gradient of precipitation. If measured from the front to the upper tongue (450-500 m a.s.l.) it results in 8.1 cm w.eq. · 100 m^{-1} for 2010/11 and 10.5 cm w.eq. · 100 m^{-1} for 2011/12, translating to 28-32% · 100 m^{-1}. Different values result from measuring the gradient up to the highest glacier parts, influenced by high inclination. Accumulation gradients calculated by linear fit are 5.0 and 6.4 cm w.eq. · 100 m^{-1}, respectively for 2010/11 and 2011/12 balance years.

6.3.2 Summer mass balance

Mass loss on Svenbreen was a subject of studies in summer seasons of 2010, 2011 and 2012. Since 26/07/2010 ablation measurements were carried out on the glacier using 11-16 ablation stakes, installed along the main flowline (2010), with one (2011) or two cross-transects (2012, see chapter 4 and fig. 4.2). Surface melting is by far the most important ablation process on Svenbreen and its drivers have been discussed in detail in section 6.2. Another observed process of mass loss of low importance is sublimation (~1 cm w.eq. at S60 in 2012). Locally in the front area, above a glacial portal, several cubic metres are lost by dry calving. Some melting may occur at the bottom of the glacier, but the mass lost by subglacial melting is generally considered as negligible when compared to surface losses (section 2.1).

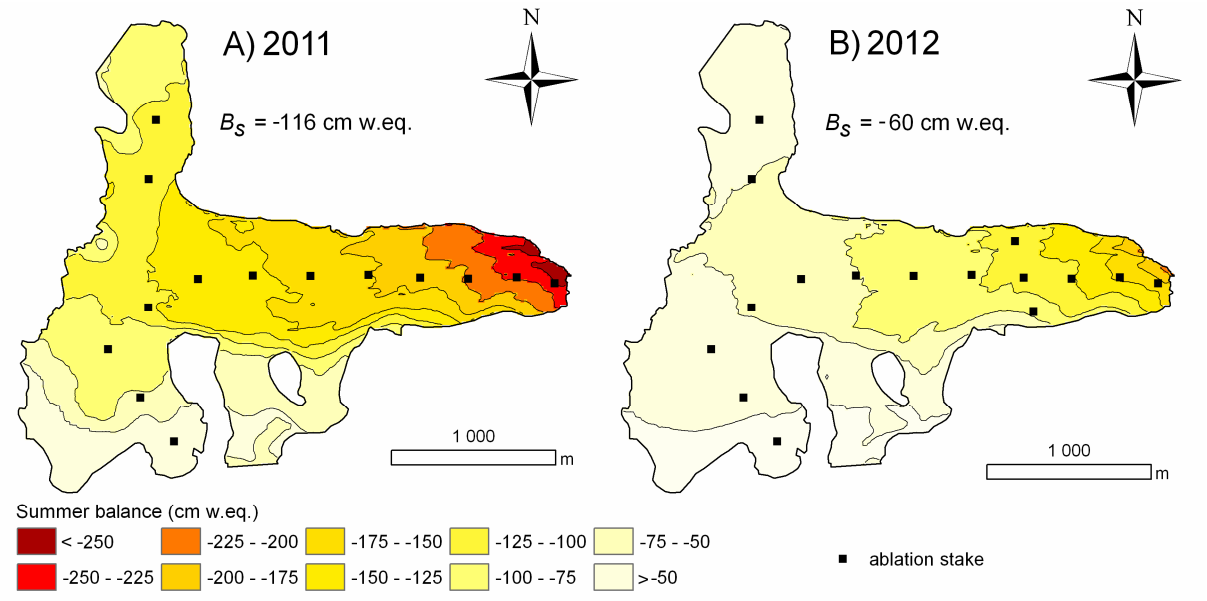

Fig. 6.29 Summer balance of Svenbreen in summer seasons of A) 2011 and B) 2012. Note that the spatial distribution of summer balance is modelled using data from ablation stakes and spatial distribution of average potential direct solar radiation, winter balance and positive degree-day sums, hence may slightly deviate from observed point b_s values

Ablation measurements in summer of 2010 begun in late-July and lasted until 13/09, so complete summer balance data is unavailable for this year. In 2011 and 2012 several stake inspections were performed in July and September and full B_s information was obtained. Final inspections of stakes were carried out on 18/09 in 2011 and on 10/09 in 2012. In the summer season of 2011 (one of the warmest at SVL) Svenbreen experienced high melting (fig.

6.29A). At the lowest stake, S10 (185 m a.s.l.), total summer balance was b_s = -259 cm w.eq. Even in the highest zones of Svenbreen ablation was intensive. Investigations along a cross-profile in the accumulation zone (stakes S90-S140) revealed a significant variability of melting. In the well shaded cirque, at S120 (625 m a.s.l.), b_s was -55 cm w.eq., while on Poznańskaret ablation was even higher: at S140 (565 m) summer mass balance was -109 cm w.eq. Summer season of 2012 was characterized by significantly reduced mass loss (fig. 6.29B). Total summer ablation reached only -175 cm w.eq. at the front (S10), -20 cm w.eq. at S120 and -46 cm w.eq. at S140. Observations along a transect crossing the lower ablation zone (stakes S40-S42, ~310 m a.s.l.) has shown that in the shaded area, close to the steep rock walls of Svenbrehøgda, melting was distinctly slower than along the northern rim of the snout (-99 cm w.eq. at S41 vs. -78 cm w.eq. at S42). Linear ablation gradients noted in both seasons were 38.7 cm w.eq. · 100 m^{-1} and 29.3 cm w.eq. · 100 m^{-1}, while overall summer balances were B_s = -116 ± 15 cm w.eq. and B_s = -60 ± 15 cm w.eq. respectively for 2010/11 and 2011/12 balance years.

6.3.3 Net mass balance

Net balance of a glacier, B_n, as a result of winter and summer balances, is a measure of its annual mass exchange and is the most important parameter describing the state of a glacier in a given period. In balance year 2010/11 mass accumulated during the winter on Svenbreen was twice lower than mass lost in the summer (B_w = 54 ± 10 cm w.eq., B_s = -116 ± 15 cm w.eq.), resulting in a highly negative net balance (B_n = -62 ±18 cm w.eq., fig. 6.30A). ELA was at 560 m a.s.l., giving accumulation area ration (AAR) equal to 22%. Most of the accumulated mass formed superimposed ice and almost no snow survived the ablation season, except for narrow area close to the rock walls of the main cirque and little snow on Nataliaskaret. The only stake with positive balance was S110 (b_n = 6 cm w.eq.), while at the highest stake, S120, net balance was slightly negative (-10 cm w.eq.) due to lower snow accumulation in the winter period. Stake S10 at the front of the glacier has experienced net loss of -233 cm w.eq. Overall net balance gradient was 43.7 cm w.eq. · 100 m^{-1}.

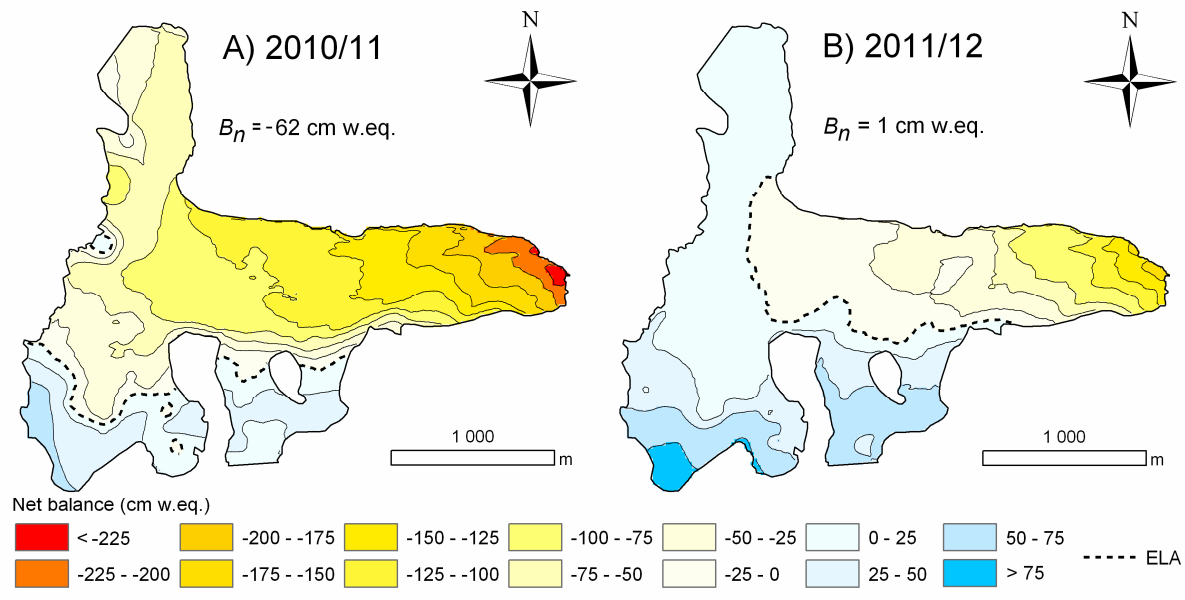

Fig. 6.30 Net balance of Svenbreen in balance year A) 2010/11 and B) 2011/12. ELA - equilibrium line altitude

In 2011/12 larger B_w (61 ± 10 cm w.eq.) and greatly reduced ablation in the summer (B_s = -60 ± 15 cm w.eq.) gave a near-zero net balance (B_n = 1 ±18 cm w.eq., fig. 6.30B). In mid-September 2012 large part of Svenbreen was covered with superimposed ice, with maximum measured thickness of 24 cm at S100. Last-winter snow, mostly underlain by superimposed ice, occupied the upper parts of the cirque (fig. 6.33B) and small tributary ice streams originating from Nataliaskaret. At the frontal stake S10 b_n was -145 cm w.eq., while at the highest, S120, 17 cm thick superimposed ice and 48 cm of snow survived the ablation season, giving b_n = 38 cm w.eq. In contrast to the previous year, Poznańskaret has also contributed to accumulation: at S140 b_n was positive with 10 cm w.eq. Equilibrium line was located between S80 (b_n = -1 cm w.eq.) and S90 (b_n = 2 cm w.eq.). Average ELA was significantly lower than in the previous season, at 410 m a.s.l., corresponding to 60% AAR. Average net balance gradient was slightly lower than in the previous year, with 35.7 cm w.eq. · 100 m^{-1}.

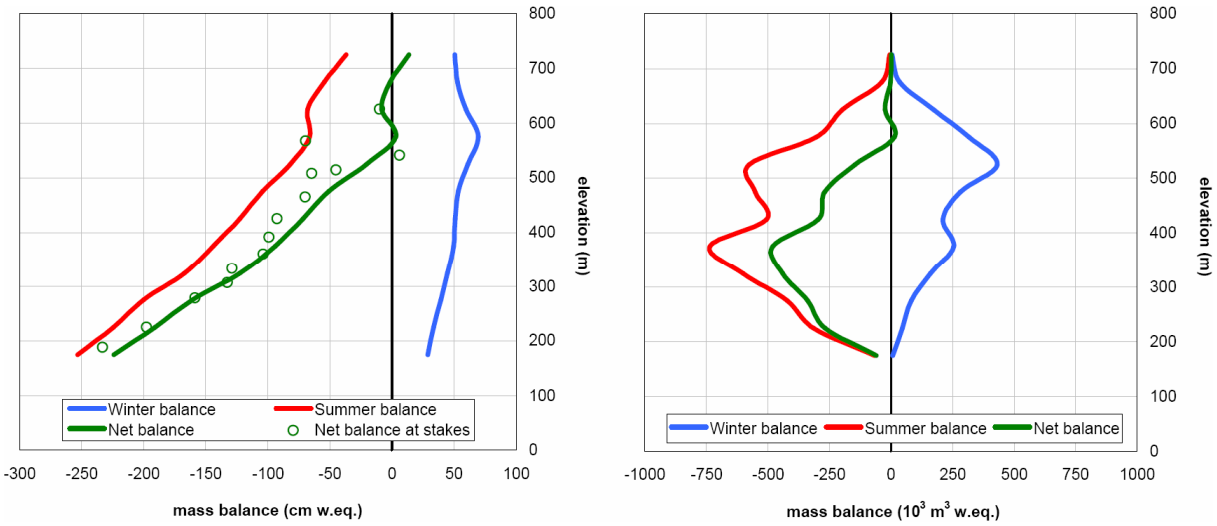

Fig. 6.31 Svenbreen mass balance diagram for 2010/11 balance year, showing specific balance (left) and volume balance (right panel)

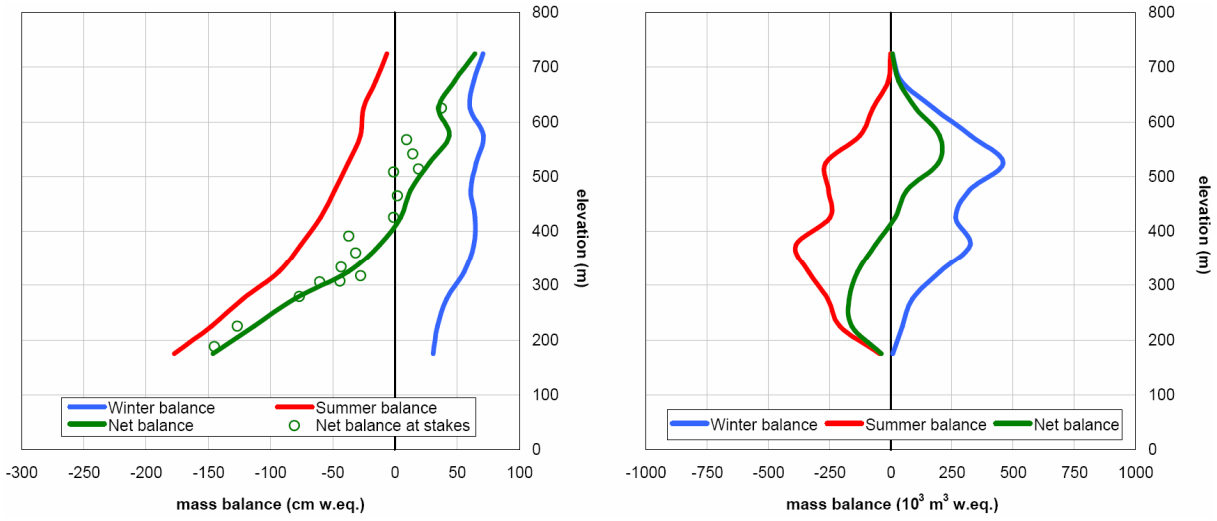

Fig. 6.32 Svenbreen mass balance diagram for 2011/12 balance year, showing specific balance (left) and volume balance (right panel)

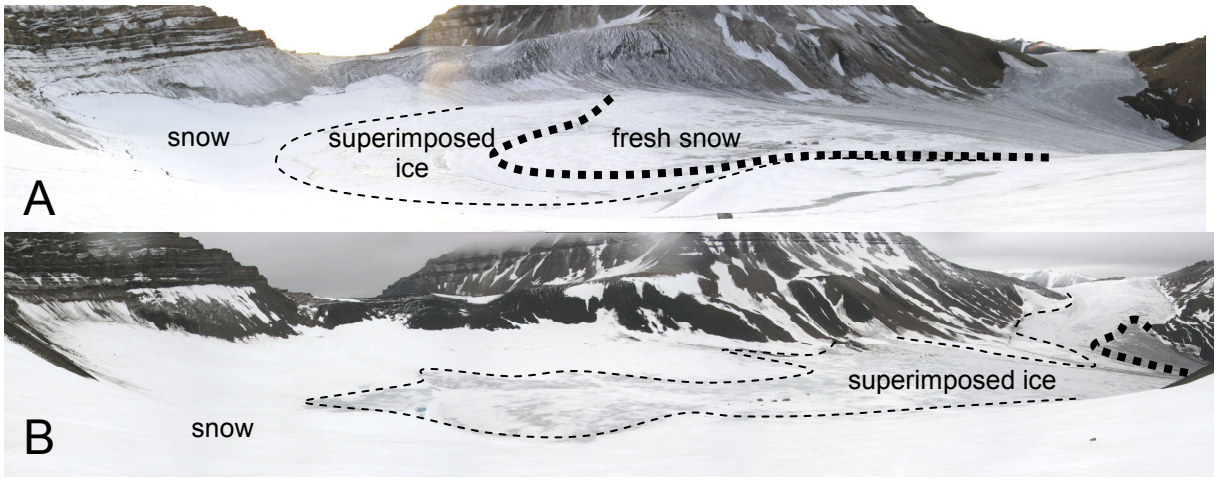

Fig. 6.33 Panoramas of accumulation zone of Svenbreen in the end of A - 2010/11, B - 2011/12 balance years, as seen from stake S120. Thick dashed line - equilibrium line, thin dashed line - snow line. On panel A borders between glacial zones are only approximated due to presence of fresh snow, covering the actual surface type. Main glacier cirque is to the left, Poznańskaret is to the right

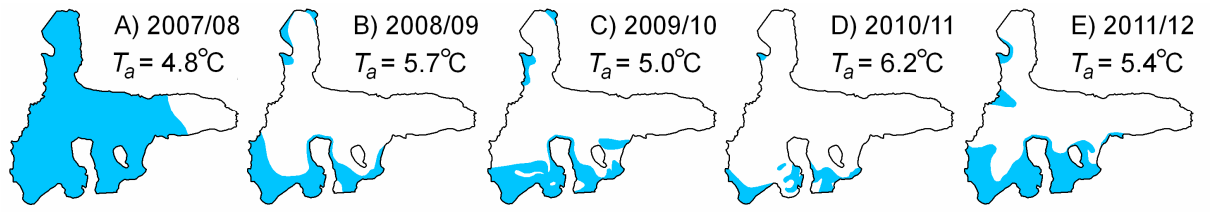

Fig. 6.34 Last-winter snow cover extent (blue colour) on Svenbreen observed on: A - 26/08/2008; B - 30/08/2009; C - 9/08/2010 (soon before first snowfalls); D - 13/09/2011; E - 2/09/2012. T_a - summer air temperature at Svalbard Lufthavn station. Note that equilibrium line is situated below the snowline

No detailed mass balance studies have been performed in the first stage of investigations on Svenbreen, but late-summer observations from 2008-10 reveal high variability of late-summer snowpack extent (fig. 6.34). Although end-of-season snowline in Svalbard is not equivalent to ELA due to superimposed ice occurrence (e.g. fig. 6.33B), it is still a valuable proxy of glacier's mass balance. Last-winter snow extent shows obviously a correlation with average summer temperature - it is greater in cooler periods (e.g. fig. 6.34A & E) and lower after warm summers (e.g. fig. 6.34D). However, in the end of 2007/08 balance year, when JJA T_a (4.8°C at SVL) was only slightly lower than average (4.9°C, 1981-2010), snow has survived the ablation season on 85% of the glacier's area, being an evidence of highly positive B_n in that particular year. Other studied summer seasons were warmer than long-term mean. Despite this fact, after each of them some accumulation has occurred in the upper zones of the main cirque and Nataliaskaret, even after a very warm summer in 2011 (6.2°C).

As a summary, mass balance of Svenbreen is driven by factors related to its unique location in quasi-continental central Spitsbergen. Topoclimatic conditions above the glacier clearly show the effect of climate continentalization. It is manifested not by increased air temperature (as observed at the sea-level), but primarily by reduced air moisture, causing frequent dry adiabatic lapse rates and evaporation from the glacier, which considerably reduces the energy available for melt. Shortwave radiation reaching the ice surface is greatly reduced by surrounding topography, so overall melt energy on Svenbreen is relatively low. Mass balance

of the glacier and its structure was substantially different in the two studied balance years. Winter balance was similar in both cases (54 and 61 cm w.eq. in 2010/11 and 2011/12 respectively). B_s was -116 cm w.eq. in 2011 and only -60 cm w.eq. in 2012, despite the fact, that summer of the latter year was by 0.5°C warmer than average. The main form of accumulation is superimposed ice, exceeding 15-20 cm thickness in the cirque. Five seasons of observation of Svenbreen suggest, that its mass balance is negative, but years with steady-state or positive net balance may occur on regular bases.

7

Hydrothermal properties of Svenbreen

7.1 Thermal structure

Temperature distribution within an ice mass influences its dynamics and hydrology. It is prone to fundamental changes in small Svalbard glaciers, so it may be used as an indicator of their mass balance conditions. Seasonal temperature variability of external layers of Svenbreen was monitored continuously for the whole balance year 2011/12, while thermal conditions in the deepest sections of the glacier were deduced from radargrams. Monthly ice temperature values from ice thermistors are to be found in the appendix in tab. A12.

7.1.1 Near-surface thermal regime

Ice temperature (T_i) of the near-surface layer of Svenbreen was monitored in the balance year 2011/12. Two stations were installed: in the lower ablation zone (S30, 277 m) and in the higher zone at S100 (513 m). At the latter site net accumulation of snow was observed in balance year 2007/08 and formation of superimposed ice in 2008/09, 2009/10 and 2011/12, so it may be assumed that this location represents typical accumulation area conditions of Svenbreen. Full-year observation cycle covered monitoring of ice temperature at 2, 4 and 8 m depth below 2011 summer surface. Due to annual mass balance changes the actual depth of thermistors varied considerably. In 2011/12 winter season S30 site was covered by 1.3 m of snow, while S100 by 1.8 m. On the last day of observations (10/09/2012) the depth of thermistors at S30 was lower than originally by 85 cm due to negative net balance (1.15 m, 3.15 m and 7.15 m), while at S100 sensors were deeper by 24 cm due to superimposed ice formation (2.24 m, 4.24 m and 8.24 m).

After the summer period of 2011 has ended an autumn cold wave reached the sensors at 2 m depth in early-October. Despite a very mild (even as for Svalbard) air temperature during the 2011/12 winter (figs. 3.4 and 6.2) cooling of the ice was significant. Surface temperature measured manually during snow pit investigations in mid-April 2012 was -7.0°C and -7.5°C, respectively at S60 and S100, assumed to be the lowest annual T_i of the surface. At 2 m depth

at S30 two T_i minima of -5.3°C were noted: in late-January and mid-May, with relatively higher T_i in between. In contrast, 2 m sensor at S100 has shown continuous temperature decrease with minimum of -6.2°C in mid-May. At both measuring sites the lowest T_i at 4 m and 8 m depth occurred respectively 29-33 and 59-60 days after minimum T_i at 2 m. Hence, progressive warming up of the ice occurred in the studied period since May at 2 m, since June at 4 m and since July at 8 m depth. However, T_i reached melting point only on the surface. Maximum 2 m temperature after the summer season of 2012 was -0.7°C at S30, while at S100 it was -2.0°C.

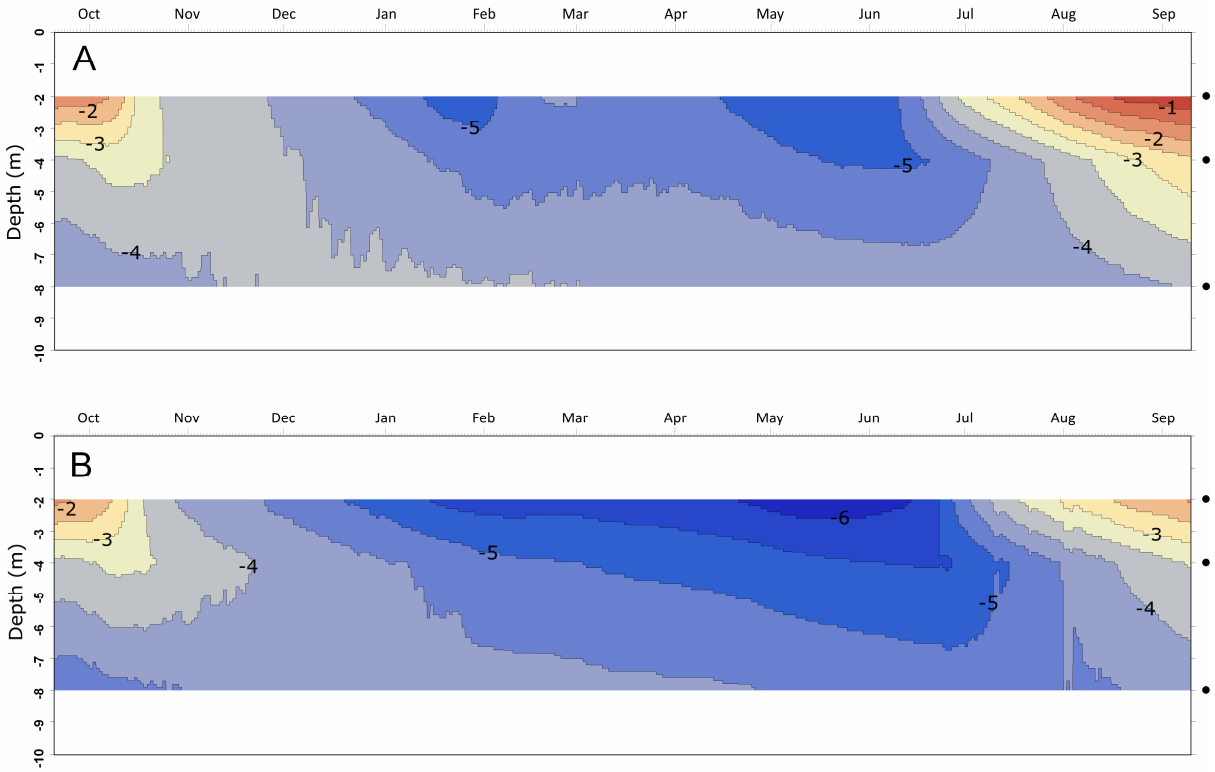

Fig. 7.1 Near-surface ice temperature variability of Svenbreen in its: A - ablation zone (S30, 277 m); and B - accumulation zone (S100, 513 m) in 2011/12 balance year. Black dots on the right axis indicate original depth of the sensors. Temperature values given in °C. For air temperature course see fig. 6.2

Surface of a glacier experiences obviously much greater T_i fluctuations during the year than its deeper zones. In 2011/12 balance year annual T_i amplitude on Svenbreen was about 7°C on its surface, while at 2 m temperature differences reached 4.3-4.6°C and 2.2-2.4°C at 4 m depth. 8 m beneath the surface T_i was almost stable, with annual amplitudes of only 0.6°C and average temperature of -4.1°C (S30) and -4.5°C (S100), being higher than mean annual (2011/12) air temperature (-4.8°C at S30 and about -6.7°C at S100). The results of thermal monitoring of external Svenbreen layers bring clear evidences that it is characterized by sub-zero temperature throughout the year, except for the first ~1 m of ice, seasonally warmed up to the melting point, and may be considered as generally cold. The higher of measuring points revealed lower ice temperature than at the site in the ablation zone. However, in accumulation areas of many Svalbard glaciers T_i is often higher than in ablation zones due to refreezing water percolating through firn (e.g. Sobota 2009), so newly formed ice is often at the melting point (e.g. Baranowski 1977; Ødegård et al. 1992; Jania et al. 1996; Pälli et al. 2003a). This is not the case on Svenbreen, where cool conditions in its high zones and impermeable

superimposed ice (the main form of mass accumulation) lead to formation of new ice that is already cold, carrying important consequences for overall thermal regime of the glacier.

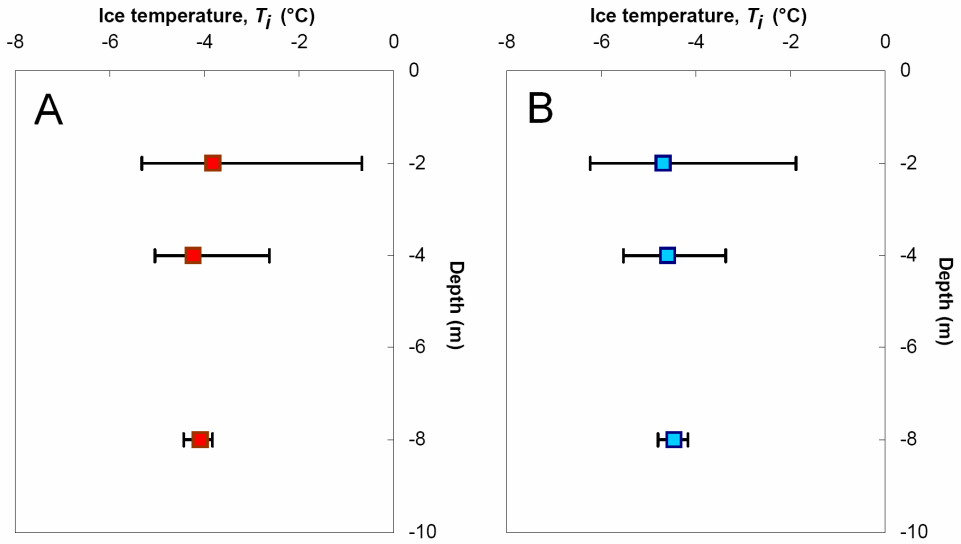

Fig. 7.2 Mean annual ice temperature (squares) in shallow boreholes on Svenbreen in: A - ablation zone (S30, 277 m) and B - accumulation zone (S100, 513 m) in 2011/12 balance year. Bars show annual temperature range

7.1.2 Thermal structure - interpretation of GPR survey

To investigate hydro-thermal structure of Svenbreen a geophysical survey with ground penetrating radar (GPR) was carried out in April 2012 (20 km of profiles in total). Thickness of Svenbreen and its bedrock topography are presented in section 5.2.1, so here only results relevant to thermal regime of the glacier are discussed. Location of GPR profiles mentioned in text is showed on fig. 7.3. It must be noted in advance that interpretation of unmigrated GPR profiles from valley glaciers is not straightforward, mainly due to artefacts and side-reflections from steep topography. Interpretation attempt applied in this section is therefore general, with some comments given to unambiguous elements visible on radargrams.

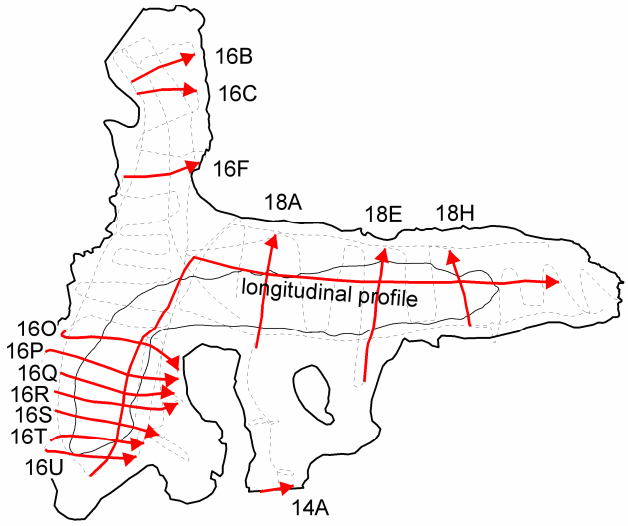

Fig. 7.3 Location of radar transects discussed in text. Arrows point direction of profiles' display on figs. 7.4-7.7. Dashed line - full radar track. Solid line inside of the glacier boundary indicates a 100 m thickness contour

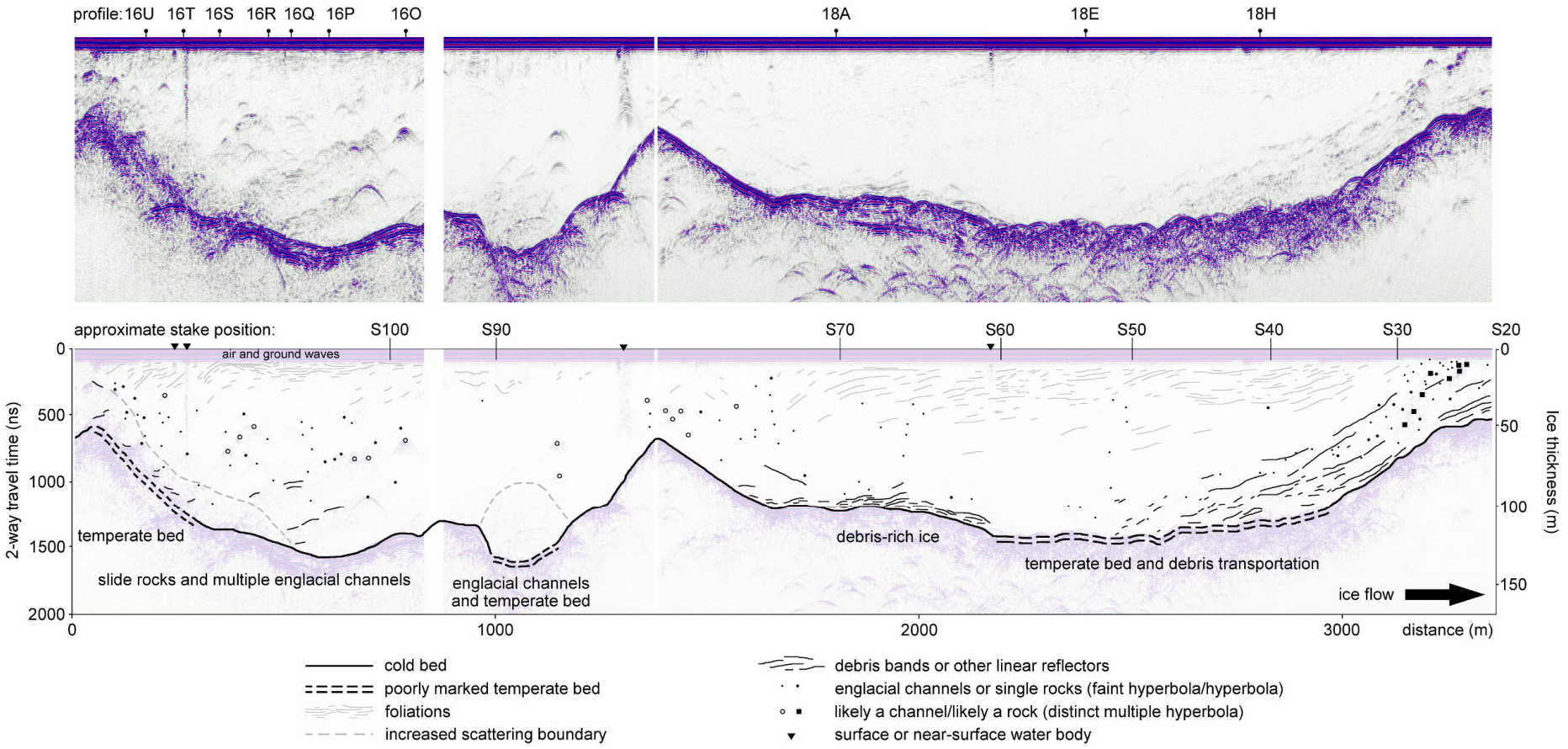

Fig. 7.4 Longitudinal profile along Svenbreen, with accumulation zone to the left and ablation zone to the right. Markers at the top of the upper radargram indicate cross-points with transverse profiles from figs. 7.5-7.7. Positions of ablation stakes at the lower radargram are only approximated. Note that bedrock rise in the middle of the profile is an effect of a slight off-track, as the profile did not follow the line of the greatest ice thickness

Radargrams of Svenbreen delivered by 100-MHz antenna suggest it is mostly cold, with some zones of temperate ice. Fig. 7.4 shows longitudinal profile of the glacier, together with general interpretation key used in this study. Scatter visible on the left-hand side (accumulation area) may origin from three situations: from water infiltrating through numerous cracks or firn, from slide rocks (falling from walls surrounding the cirque) or from side-reflections (artefacts). Considerable water content seems however the most probable source of increased scattering, as indicated by transverse profiles across accumulation area (discussed later in this section). Distinct hyperbolae in the wider zone from 0 to 800 m are interpreted as rocks and englacial channels. Around 1000 m distance the profile crosses the thickest axis of the glacier, where a faint scatter is visible beneath 100 m depth. It is distinctly structured in some places, suggesting multiple small englacial channels. It was classified as ice warmer than the surroundings: not necessarily at the pressure melting point, but most likely with temperate ice-bed interface.

At about 2000 m of the profile horizontal bands occupy the lowest ~10 m of ice, indicating debris-rich basal layers. Further downglacier the bed is not visible clearly due to strong hyperbolic reflections below 100 m depth. Such pattern could potentially result from artificial side-reflections from steep subglacial slopes, but it appears only under the glacier tongue and not beneath i.e. Poznańskaret (discussed later). This unambiguous feature was also noted during the same GPR survey on neighbouring Bertilbreen. Considering the previous hydro-thermal record of the latter glacier (e.g. Zhuravlev et al. 1983), no liquid phase detected during 50-100 m deep borehole drillings (Ueda & Talalay 2007) and recent geophysical survey by the author, the occurrence of 'blurred' bottom reflection on Svenbreen and Bertilbreen is interpreted as temperate bed conditions with low liquid water content. Warm-based conditions of Svenbreen are in line with thrust faults, visible on the radargram from 2500 m. Large boulders are transported from beneath ablation stake S50 and melt out close to S20, as confirmed by direct observations. The occurrence of debris transport is related to compressive stress due to decreasing sliding at the front, because from about 3000 m of the profile snout is frozen to the bed, as the reflection is continuously clear.

Apart from longitudinal GPR transect, Svenbreen was also surveyed by multiple transverse profiles. The main accumulation zone in the cirque was covered by seven transects (fig. 7.5), giving an opportunity to study spatial variability of its structure. Distinct changes may be observed when moving up-glacier. For lower profiles (16O-16Q) near-surface temperature of about -4.5°C was measured at 8 depth at S100, close to the middle of profile 16P. Meanwhile in their deepest zones some weak scatter occurs, interpreted using the same key as scatter on fig. 7.4 (ice warmer than surroundings, with small englacial channels and only slightly increased water content). With rising elevation the scatter becomes more intensive (profiles 16R-16U) and hyperbolae more numerous. On the two highest transects (at about 550 m a.s.l.) distinct water inflow can be observed from the surface. On profile 16T a crevasse filled with water near the beginning of the profile is apparent, as well as multiple small englacial water features and/or slide rocks (fig. 7.5F). The highest transect, 16U (fig. 7.5G), reveals temperate conditions, spanning locally from the surface down to the bed, as interpreted from strong (random to a large extent) noise on the left-hand side of the profile (west). It is probably the last remnant of water-saturated firn zone of Svenbreen.

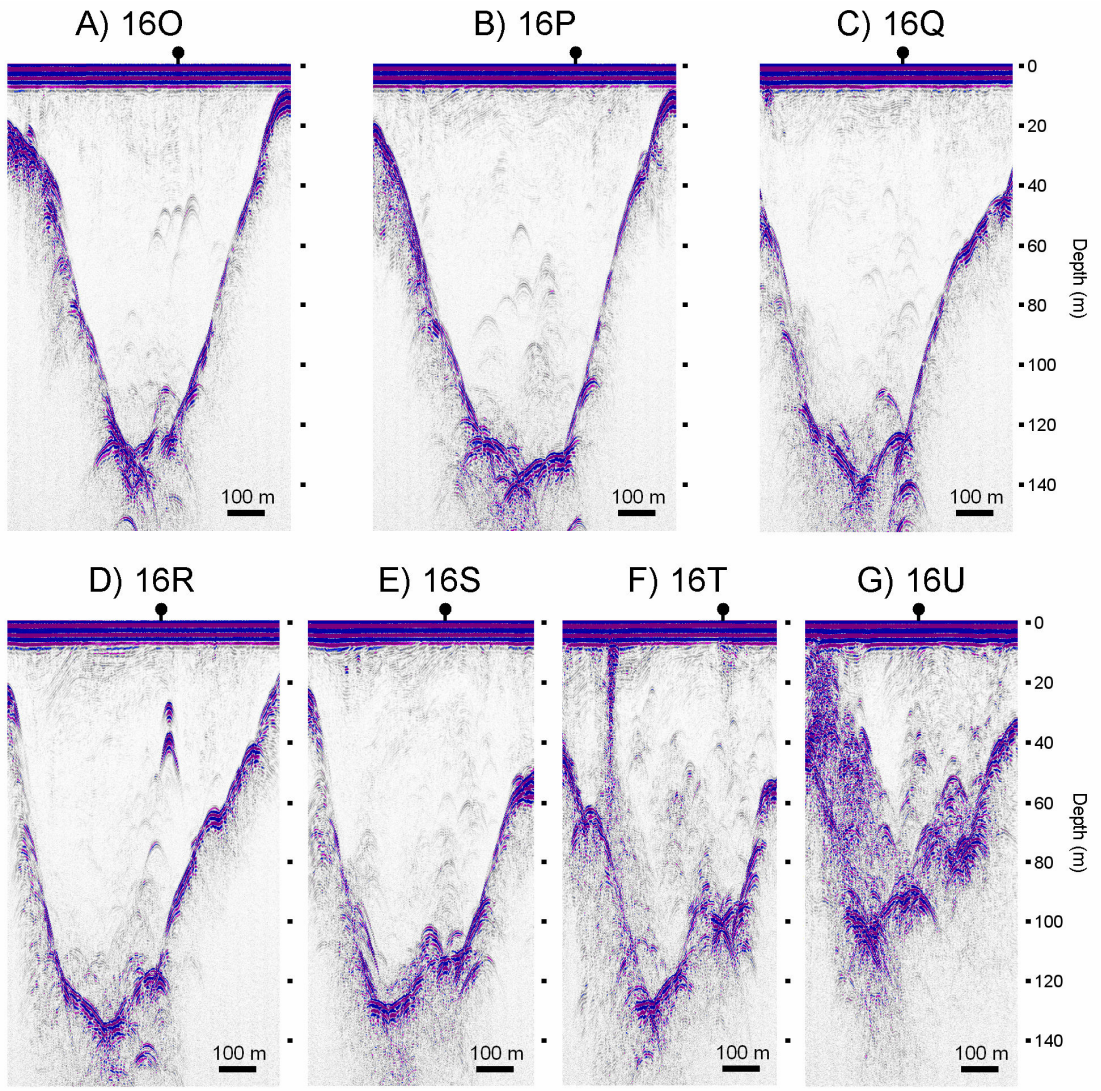

Fig. 7.5 Transverse profiles across the accumulation zone of Svenbreen. Markers at the top of each radargram indicate a cross-point with longitudinal profile from fig. 7.4. West to the left, east to the right

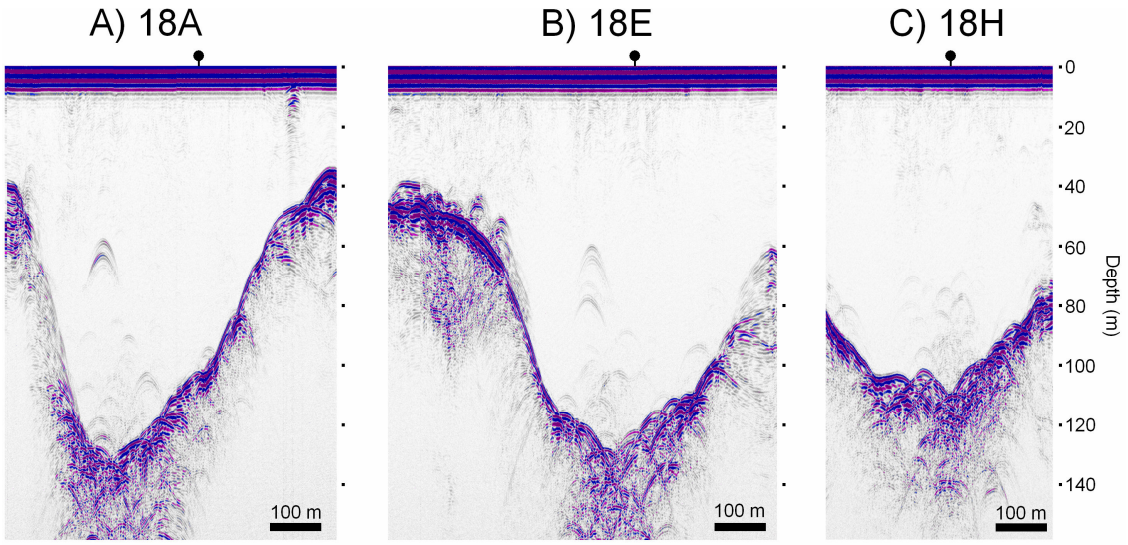

Fig. 7.6 Transverse GPR profiles across Svenbreen tongue. Markers at the top of each radargram indicate a cross-point with longitudinal profile from fig. 7.4

Middle and lower sections of Svenbreen are relatively more transparent to radio-waves than ice in the cirque, implying minimum water and/or debris content (fig. 7.6). On the longitudinal profile no scatter is visible beneath the glacier tongue, but transverse profiles 18A-18H bring a clear evidence of its continuous extent from the glacier cirque. Moreover, transect 18H crosses the zone of debris incorporation, manifested in the same manner as weak scatter on the profiles 18A and 18E. They also show the 'blurred' bedrock reflection beneath 100 m depth, possibly indicating temperate bed conditions. Distinct reflections at 60-100 m depth suggest presence of small englacial drainage features.

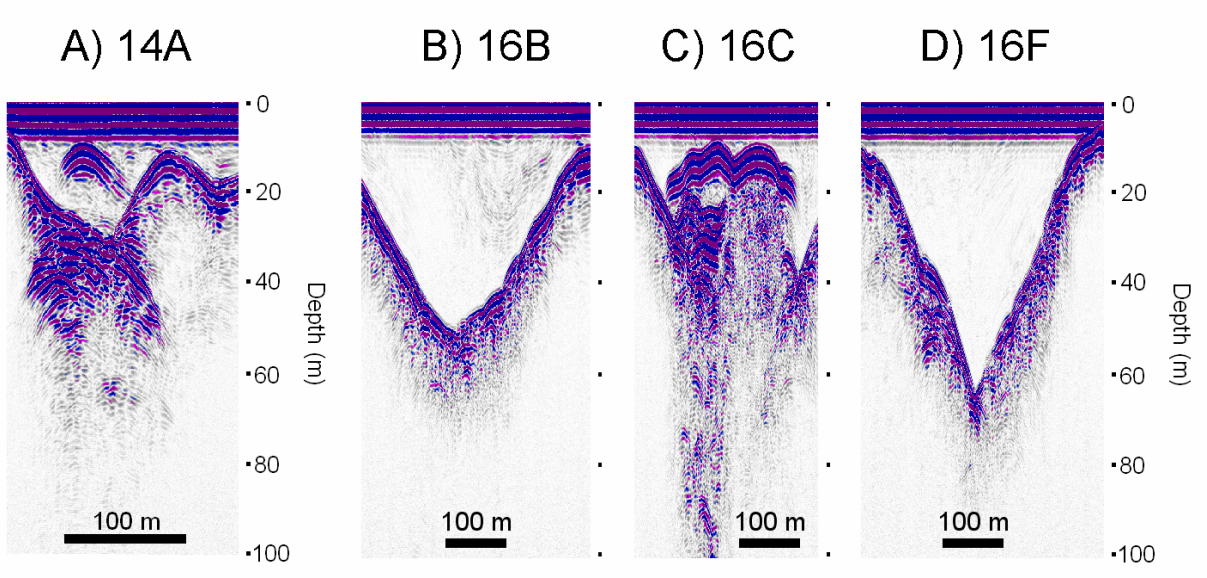

Fig. 7.7 Transverse GPR profiles across A) Nataliaskaret and B-D) Poznańskaret

On fig. 7.7 selected transverse profiles from Nataliaskaret and Poznańskaret are presented. Nataliaskaret pass is located at ~630 m a.s.l. (well above the ELA). Several englacial reflections are apparent on the GPR data from this zone, as the one visible on profile 14A (fig. 7.7A), most likely being a near-surface water body or englacial cavity. The reflector is surrounded by a weak scatter, but shallow ice limits interpretation possibilities. Hence thermal structure of this area is unambiguous, though it most likely contains some liquid phase. Poznańskaret spans in the same elevation bands, but experiences more negative mass balance (see section 6.3), so no firn is present in this zone. Profiles 16B and 16F (fig. 7.7B and D) show cold, transparent ice with a clear bedrock reflection. Exactly along profile 16C (fig. 7.7C) a very strong internal reflecting horizon (IRH) was detected at depth of 10-15 m, spanning for 200 m across a considerable width of the valley. Other profiles carried out in this area reveal that the IRH has a linear character. Absorption of the bottom echo suggests that the IRH is caused by water stored in ice. Summer photographs reveal a distinct linear feature on the surface along the profile, so presence of the reflector is interpreted as a water-filled crevasse.

GPR data revealed interesting information about hydro-thermal structure of Svenbreen, but still some doubts remain. Mass balance investigations and thermal monitoring of near-surface layer show that most of new mass is accumulated as impermeable superimposed ice, resulting in cold ice formation. However, in a limited, well protected zone of the main glacier cirque some firn survived few decades of negative mass balance. Hence, limited amount of water may locally penetrate to deeper sections and heat the mass to pressure melting point. In

contrast to the most of polythermal Svalbard glaciers, no clear cold/temperate transition surface (CTS) was detected on radargrams (i.e. Jania et al. 1996; Moore et al. 1999; Pälli et al. 2003b), but 'blurred' bedrock reflection was interpreted in this study as temperate bed conditions. Weak scattering occurs close to the bottom continuously along the main valley. A schematic illustration of the polythermal structure of Svenbreen is presented on fig. 7.8.

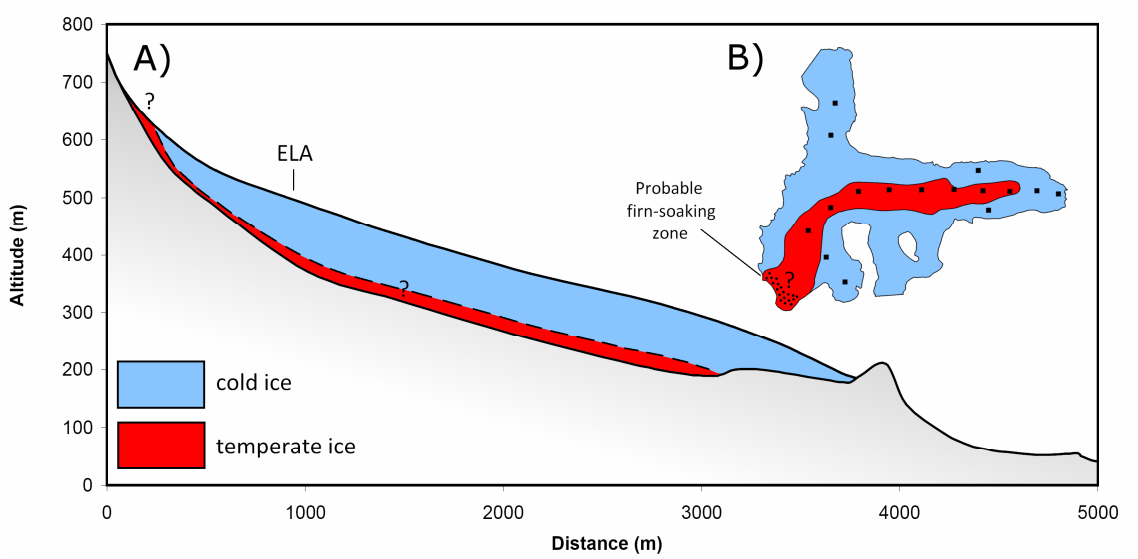

Fig. 7.8 Thermal structure of Svenbreen, A - a schematic longitudinal profile of the glacier; B - planimetric extent of temperate bed conditions with location of ablation stakes (dots)

7.2 Hydrology

Monitoring of water discharge is (after the GPR survey) another method to collect information about intraglacial conditions of Svenbreen. Water circulation on, within and beneath a glacier body is driven to a large extent by its temperature. Amount of water in a glacier basin is altered mainly by weather, mass balance, snow conditions and by hydrogeology of the valley. Therefore, the pattern of water outflow from the glacier may be used as an indicator of many of its characteristics.

7.2.1 Glacial drainage

The vast majority of water is transferred to the front of Svenbreen via supraglacial channel system (figs. 7.9 and 7.10A). Slope of the glacier is generally low and the surface is even, so network of supraglacial streams is well developed in the ablation zone. Length of the longest streams is comparable to the glacier length and in steeper front zone they tend to meander and incise up to 3-4 m into ice. Water from the highest reaches, if does not refreeze, forms locally narrow streams in snow or superimposed ice and join larger supraglacial streams in lower sections. Year after year meltwater follows the same channels on the surface. Comparison of available glacier topography data confirms that the whole system is very stable throughout the last decades and the shifts occurring due to geometry changes are relatively slow and of minor magnitude. A characteristic mark of the supraglacial stream network on Svenbreen is its asymmetry: because the southern zone of the snout is higher elevated and the general aspect is to the east, water flows to the north-eastern direction. A deep lateral channel has therefore

developed along the northern edge (meandering inside of an ice-cored lateral moraine in some sections), draining about half of the glacier surface. In this zone water reaches shallow bed (fig. 7.10C) and emerges at the front. The other half of Svenbreen area is drained by a stream system developed at the foot of the cirque and Nataliaskaret. No lateral channel occurs along the southern rim of the glacier, all the water from this zone is transferred directly to the front across the tongue. An interesting feature of supraglacial hydrology is a small lake (few tens of metres long) in the main cirque at ~550 m a.s.l. It is located in a depression at the foot of steep rock walls and is supplied by meltwater from the highest reaches of the glacier. The lake has been existing for at least the last five decades, as it is visible on aerial images from 1960 and 1990. The lake shows however highly variable shape and size, dependant on hydrological conditions and ice topography (fig. 7.10E and F). In the wintertime liquid water may still exist in the lake, as indicated by radar survey in April 2012 (section 7.1.2), or may be emptied during the ablation season.

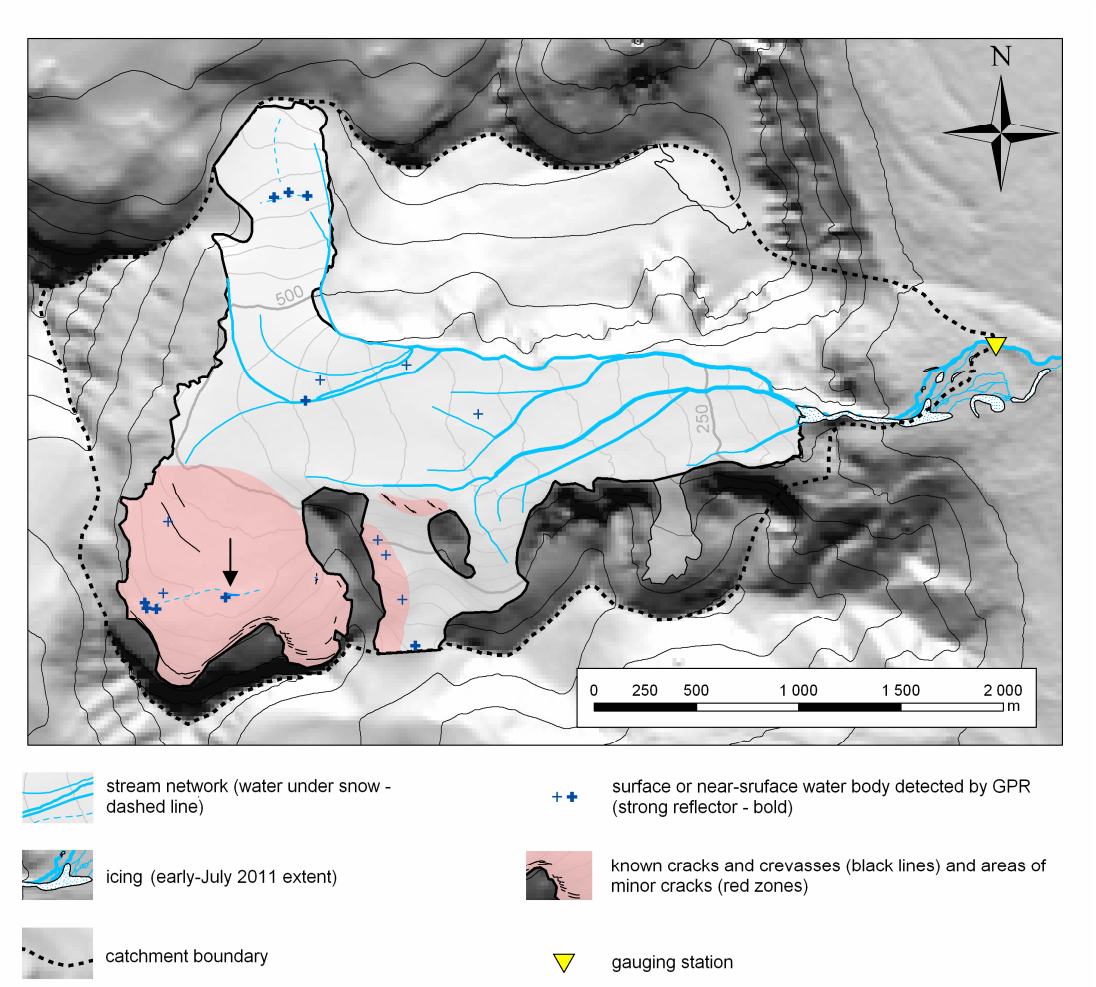

Fig. 7.9 Main surface elements of Svenbreen hydrology. Arrow indicates a small supraglacial lake mentioned in text. Contour lines (2009) are drawn every 25 m on the glacier and every 100 m on the surrounding terrain

Svenbreen has only few zones where water may penetrate to englacial and subglacial systems. These zones are restricted only to the highest areas, as e.g. no moulins or cracks occur in the ablation zone, as could be expected from a glacier with a cold surface layer with a low balance gradient (Baranowski 1977). Contact of the glacier with rocks of the cirque is well marked by bergschrund type crevasses, while feet of the steep rock walls of the cirque and

Nataliaskaret are occupied by multiple narrow transverse cracks (<50 cm width). Moreover, fractures of ~1 cm in width and measurable depth reaching 50 cm may be formed year after year in fresh superimposed ice in the glacier cirque, so water may penetrate to deeper layers in the second part of ablation season. Another process of vertical water transfer on Svenbreen is cut-and-closure of supraglacial channels, directly observed in higher zones of the glacier (fig. 7.10B). The slowest process of water transfer to deeper sections of Svenbreen is by percolation of water between firn grains. The possible firn zone on the glacier occupies only a small, shaded patch of the cirque, slightly up-glacier from the supraglacial lake. Radar survey revealed locally strong scattering in this area, interpreted as water storage and its percolation down to the bed (fig. 7.5G). Such situation was observed especially across a western extension of the lake, most likely being an incised channel or crevasse filled with water (fig. 7.9 and 7.10E).

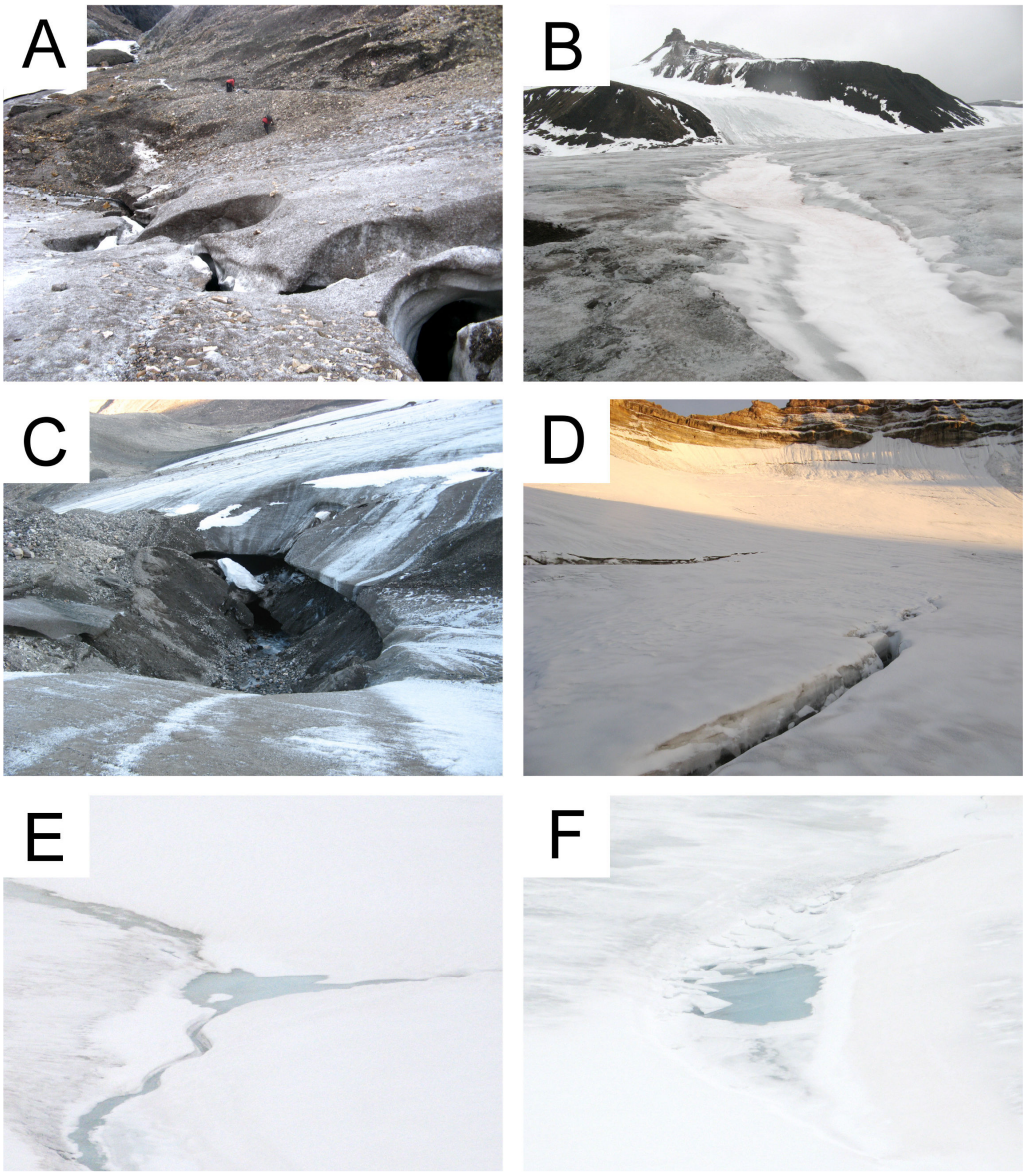

Fig. 7.10 Selected elements of Svenbreen hydrology. A - Supraglacial channel at Svenbreen front; B - closure of a supraglacial channel in the end of melt season; C - lateral channel reaching the bed in the front zone (ice and water flow is to the left); D - narrow cracks in the highest zone of Svenbreen (bergschrund visible in the far background); E, F - variable form of the supraglacial lake in the accumulation zone: 2/08/2010 (E) and emptied lake on 2/09/2012 (F)

7.2.2 Discharge, runoff and water balance

Water from all drainage systems (supra-, en- and subglacial) contributes to general glacier outflow. Discharge from glaciers and its variability is of top practical interest in populated areas in the Arctic and other regions. It is also a good indicator of widely understood state of glaciers, as it is influenced i.e. by weather, mass balance or thermal regime. The proglacial river (Svenelva) emerges from a lateral portal, flows between icing patches, in the canyon and braides in the moraine zone. Melting (and hence runoff) are expected to onset together with positive air temperature, usually in mid-May at the sea-level (see section 3.5). Data from the earliest period of ablation season are however very limited. Single observations of the stream zone in early-May 2011 revealed very slow water flow under the snow just after few days of positive T_a. Time-lapse photographs clearly show that until early-June Svenelva develops regular channels, yet in snow cover. When snow melts out from low elevated areas in late-June, Svenelva spreads on the flat inner outwash plain into two braiding streams: the northern, being currently the main branch, and episodic southern stream, activated during higher discharge periods in July-August (fig. 7.9). Both branches of the proglacial system tend to switch channels during a single melt-season. On multi-decadal timescale changes of the proglacial river network follow geomorphic processes, which act on fresh mineral surface of Svenbreen moraine zone. Debris-flows, land-slides, melting-out and erosion of ice-cored ridges and hills or draining of morainic ponds all have a key impact on the shape and functioning of proglacial river system. On aerial images from 1960 and 1990 several ponds along the main stream occur. At present, transfer of water and sediments out of the Svenbreen basin is relatively efficient, as the flowing water encounters no lakes, which could act as buffering reservoirs.

In the main branch of Svenelva, ~1 km from the glacier's front, a water-level recorder was operating during the warmest periods of four summer seasons (mainly July-August, 2009-2012). A rating curve is available for this data from several discharge measurements (fig. 4.4). Unfortunately, precipitation record from the sea-level sensor in the study area (PET station) is available only for summer seasons 2009 and 2010, while air temperature (T_a) from the glacier for 2011 and 2012. Hence, to obtain fundamental comparability, data from Svalbard Lufthavn station (SVL) is used as an air temperature background. Although T_a course is similar in the study area and at SVL (Rachlewicz & Styszyńska 2007; Láska et al. 2012), precipitation is mostly of local character. Hence, precipitation data from SVL is only given as total sums and daily means, to provide any idea of rainfall intensity in a given season.

Data for 2009 summer season is available for period 21/07-30/08 (fig. 7.11A), during which total rainfall was very low (6.2 mm or 0.15 mm d^{-1} measured at SVL). Average daily discharge, Q, has shown good correlation with air temperature at SVL ($R^2 = 0.66$) and even higher with T_a at PET ($R^2 = 0.75$). Discharge was the highest in July and has been progressively decreasing with lowering air temperature in August, showing a clear daily rhythm in the whole studied period. Total runoff from the basin was $2.5 \cdot 10^6$ m^3 ($60 \cdot 10^3$ m^3 d^{-1}) in the analysed time span. Next season was covered with the shortest dataset (24/07-22/08/2010). Precipitation was rather normal and reached 16.6 mm at SVL (0.54 mm d^{-1}), with a certain portion of snow. In the first part of the record Q was low and relatively stable, as well as T_a. Two summer snowfalls occurred in the middle of August: minor on 13/08 and major on 14/08, heavy enough to cover low-altitude terrain with thin snow cover. This summer accumulation event was considerably more pronounced on Svenbreen, as it covered the glacier (together with later snow-drift) with a fresh snow pack of 4.4 cm w.eq. (Małecki et al. 2011). Response of water outflow was immediate. High albedo of the surface and low T_a

almost completely stopped melting and surface runoff, so river discharge decreased dramatically. Hydrographs on fig. 7.11B and 7.12 show a near-zero Q between 16/08 and 19/08, caused by zero water level at the measuring sensor, but along the main axis of the stream the actual discharge was considerably higher than presented. River discharge started to rise suddenly in the afternoon of 18/08. Both fresh and winter snow survived in the higher zones of Svenbreen until the end of observations, decreasing the runoff considerably due to melt reduction and water storage. Total runoff in Svenelva was low ($1.6 \cdot 10^6$ m^3, $53 \cdot 10^3$ m^3 d^{-1}) and correlation between mean daily Q and T_a at SVL was lower in 2010 than in 2009, with $R^2 = 0.32$ ($R^2 = 0.53$ with T_a at PET).

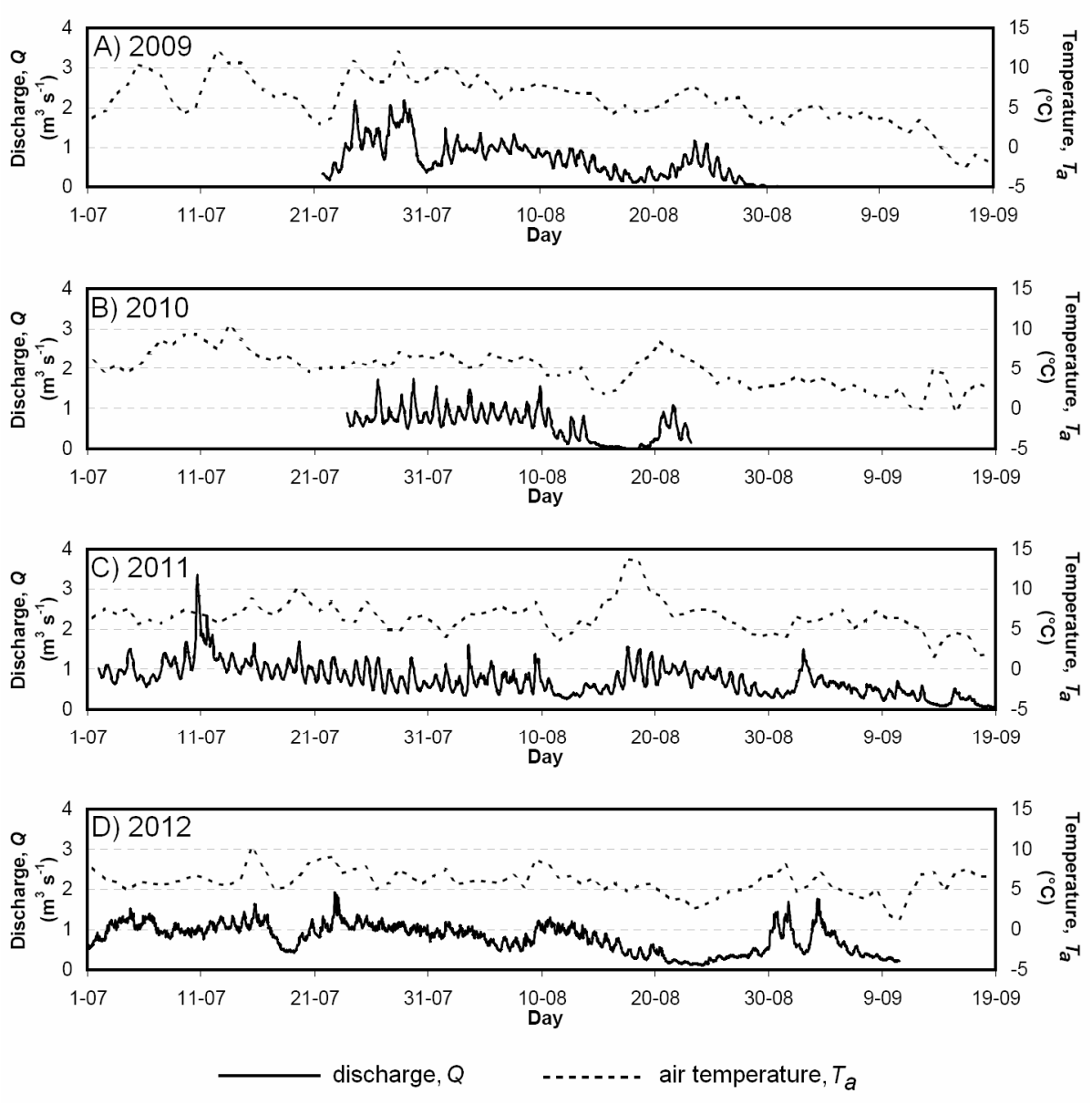

Fig. 7.11 Discharge from Svenbreen basin in 2009-2012 summer seasons against mean daily temperature at SVL

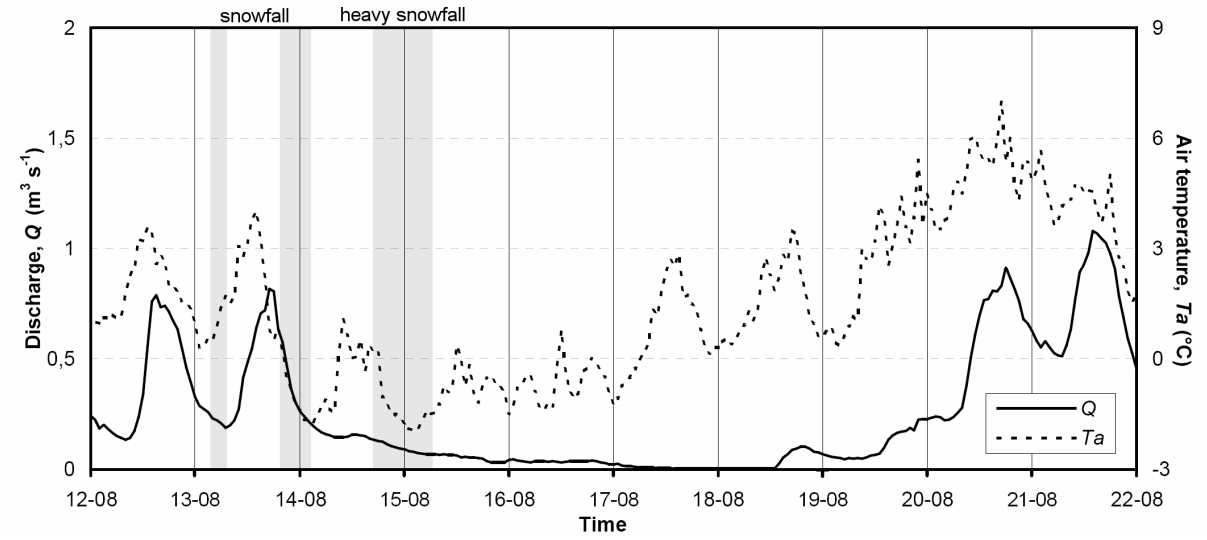

Fig. 7.12 Cessation of outflow from Svenbreen basin after heavy snowfalls in the summer of 2010 against air temperature in the middle of the glacier (S60, 358 m a.s.l.). Note different vertical scale than on figs. 7.11 and 7.13 and that zero-discharge on 17/08 is caused by zero-water level at the measuring sensor, while some discharge was still active

In 2011 water level sensor was operating since 2/07 until 18/09, covering the longest period of river discharge data. Precipitation measured at SVL was 43.5 mm in that period, corresponding to mean daily value of 0.55 mm d^{-1}. Two extreme events occurred in this season: heavy rainfall on 10/07 and an anomalously warm period between 16/08 and 20/08 (fig. 7.13). The first one, together with relatively high air temperature over the glacier (6°C), have caused the greatest flood ever observed on Svenelva, with peak discharge reaching nearly 4 $m^3 s^{-1}$. Soon after the rain has ceased, Q decreased to 2 $m^3 s^{-1}$, still being very high as for Svenbreen (compare with fig. 7.11). Until 12:00 of the next day, river discharge has been very slowly declining, but after, a step-like discharge increase was observed, from 1.6 to 2.9 $m^3 s^{-1}$. Flood waves observed during both days were most likely linked. While the wave from 10/07 may be fully explained by very intensive precipitation, hydrograph of the latter wave resembles glacial lake outburst floods, though in a small scale. There are however no proglacial lakes at the front of Svenbreen, so this minor flood is interpreted as an evidence for englacial (subglacial) drainage, originating from an outburst of pressurized water accumulated during the storm event. It is considered as an evidence for existence of intraglacial water drainage system. In August of 2011 few extremely warm days occurred, potentially increasing melt and runoff. Although the maximum T_a noted on Svenbreen reached as much as 12°C and the days were almost clear, Q has shown only minor increase and followed a normal daily cycle, with minima in the early morning and afternoon maxima of ~1.5 $m^3 s^{-1}$. As discussed in section 6.2, in this time of year net radiation has little impact on melt-energy and turbulent heat fluxes play the dominant role in melt process. Therefore, low meltwater production during the warm period 16-20/08/2011 could result from no-wind weather (minimal turbulent heat exchange between warm air and ice) and low solar angle, with associated shading of the glacier by the surrounding massifs. Overall correlation of Q and T_a in 2011 was only R^2 = 0.33, but if the two extreme events were to be excluded, the agreement increases to R^2 = 0.48. Outflow from the basin was $5.1 \cdot 10^6$ m^3, corresponding to $65 \cdot 10^3$ m^3 d^{-1}.

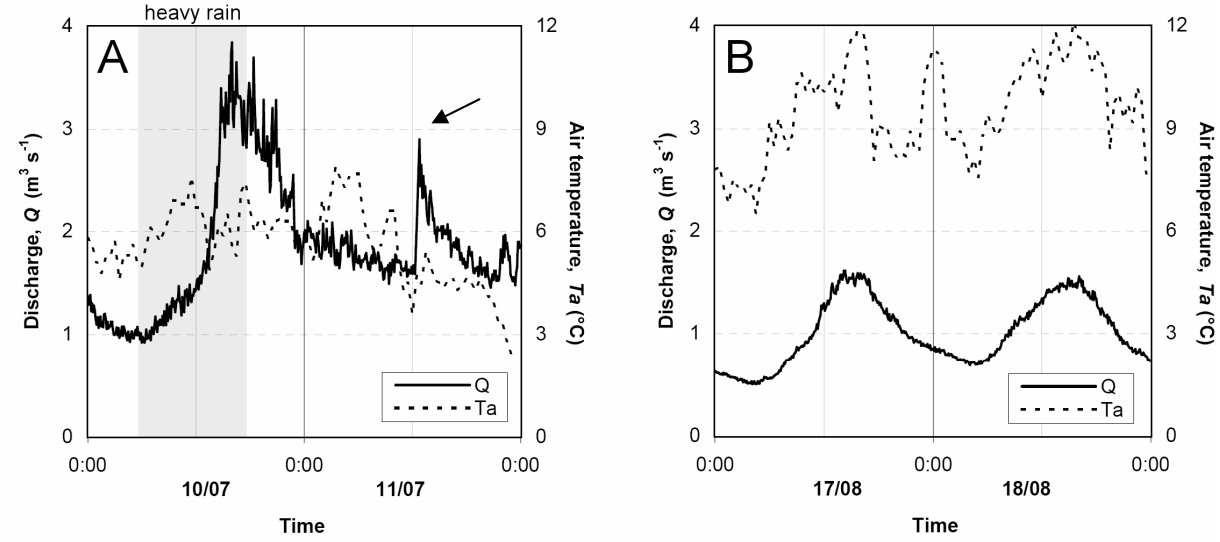

Fig. 7.13 5-min discharge values against air temperature in the middle of the glacier (S60, 358 m a.s.l.). A - rainfall-induced flood wave on 10/07/2011 and the secondary outburst flood on 11/07 (arrow); B - extremely warm air over the glacier and its no effect on discharge magnitude on 17-18/08/2011

The balance year 2011/12 was characterized by low summer melting and long snow cover presence (see section 6.3.2). However, relatively high precipitation (59.8 mm or 0.83 mm d^{-1} at SVL) compensated low meltwater runoff to a high level and overall river discharge was similar as in 2011. When compared to previous years, daily discharge cycle was poorly pronounced, being likely an effect of water storage in the snow pack. Overall day-by-day variability was the lowest from all investigated seasons. Energy balance station (AWS) in the middle of the glacier (stake S60, 358 m a.s.l.) gave reliable information about surface melting conditions (section 6.2.2). No extreme events in 2012 hydrograph are present, but data from AWS could be used to analyse discharge variability during periods of limited or no melt. Several short freeze-up events are visible on fig. 7.14. Clearly, response of river discharge to melt intensity is well pronounced at high Q levels. Sharp Q decrease from ~1 m^3 s^{-1} to ~0.5 m^3 s^{-1} accompanied melt cessation on 17/07, which has stabilized as soon as some melting occurred on the next day (fig. 7.14A). During the second event, no melting has been occurring at AWS site since evening of 22/08 for almost 2 days, having no distinct impact on Q (fig. 7.14B). Progressing cessation of melt in early September (fig. 7.14C) resulted in gradual decrease of discharge, but it has not dropped to zero, as even on the 10/09 some water was still flowing in supraglacial channels contributing to river discharge. In general, 2012 outflow correlated with T_a with $R^2 = 0.49$. During the campaign total runoff was similar as in 2011 with $5.0 \cdot 10^6$ m^3, resulting in the highest daily mean of $69 \cdot 10^3$ m^3 d^{-1}. It stays in contrast to low melting and steady-state mass balance of Svenbreen, but may be partly explained by higher precipitation and snowmelt input from the surrounding slopes (water balance discussed below).

In every record two distinct cycles of different periods are visible: seasonal and daily. A general seasonal trend of discharge decrease was observed since July, when the highest water level was observed, until the end of measurement periods. High discharge results from intensive melting during the warmest period of the year and is followed by a decrease in August and the lowest level in September. Daily discharge course corresponds to 24-hour melting cycle, which may be well represented by air temperature (fig. 7.15). A lag between air temperature extremes and discharge minimum and maximum is clearly visible. The minimal

air temperature above a glacier occurs around 4:00 o'clock, but the lowest water-level happens on average at 6:00-7:00. A similar shift occurs after the air reaches its maximal temperature (15:00 vs. 18:00) and is caused by travel-time of meltwater to the measuring site. The average lags observed are short (~3 hours), being an evidence that most of the water origins from supraglacial drainage, the most efficient from all drainage types. However, daily discharge cycle shows a clear evolution with progressing summer. In early-ablation season the lag is about 2 hours longer than average, due to water storage in snow, but also possibly due to temporal inefficiency of intraglacial drainage after the winter period. The response of discharge to surface melt is faster from mid-July onwards, in some periods occurring even before the T_a maximum. In early-September daily course of Q is hardly noticeable due to reduced melt, fresh snow, low solar angle and nearly permanent shading of the glacier.

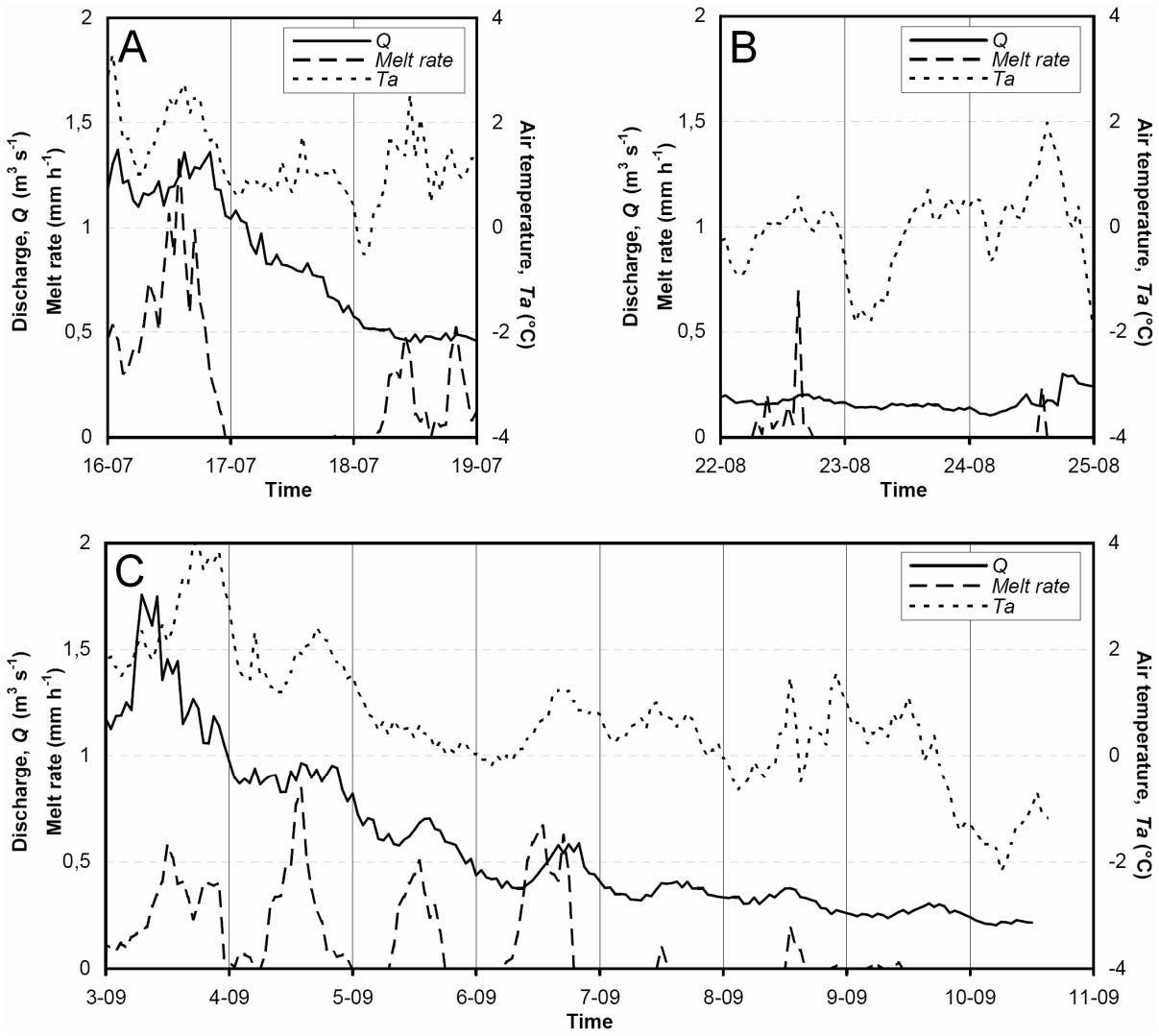

Fig. 7.14 Cessation of outflow from Svenbreen basin in the summer of 2012 during days of limited melt. Hourly values of melt rates and air temperature measured the middle of the glacier (S60, 358 m a.s.l.). Note different vertical scale than on figs. 7.11 and 7.13. Also note sharp Q decrease from high to low level on 17/07 (A) and poor Q response to melt cessation during low levels (B, C)

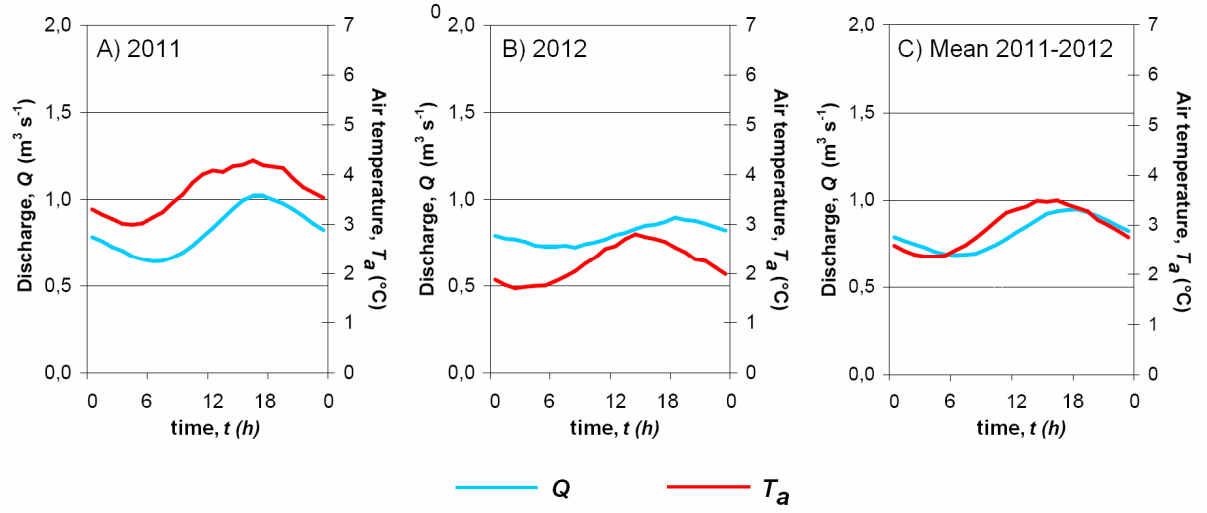

Fig. 7.15 Mean daily rhythm of water discharge against air temperature in the middle of Svenbreen (at S60, 358 m a.s.l.). Data are averaged for periods A) 2/07 - 10/09/2011; B) 1/07 - 10/09/2012, C) 1/07 - 10/09 2011 and 2012

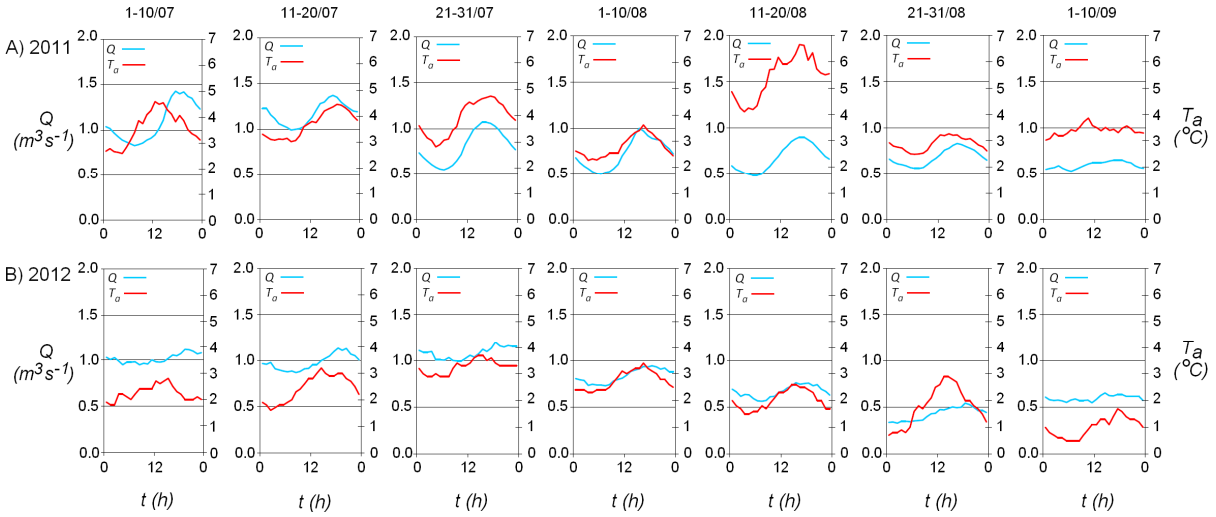

Fig. 7.16 Average cycle of air temperature and river discharge in 10-day intervals for A - 2011, B - 2012

Icing field observed at the front of the glacier is an evidence of its winter discharge, commonly attributed in Svalbard to polythermal structure (e.g. Gokhman 1987b; Bukowska-Jania & Szafraniec 2005), although some exceptions from this general rule exist (Bælum & Benn 2011). Most of the icing mass is accumulated between the front and entrance to the canyon (fig. 7.17). A new icing was formed during winter 2008/09 and in early-summer of 2009 water from the glacier has been flowing directly over the icing surface, covering it with a fan of fluvioglacial sediments. During the ablation season meltwater has been cutting a central channel making its way towards the canyon, while sediments accumulated on the icing conserved it from melting (fig. 7.17A). In the winter of 2009/10 only a small amount of icing mass filled the central channel, so no new icing was observed in early-summer of 2010. Meanwhile, the former fan has been transforming into ice-cored hummocks, with a distinct kettle in the middle (pitted outwash plain, fig. 7.17B). New icing was eventually produced during 2010/11 winter season and covered the entire discussed area with a thick layer of ice.

Most of this mass has survived the summer, even though it was extremely warm (fig. 7.17C). In the winter 2011/12 a fresh icing was spotted at the bottom of the canyon, but the photograph from early-summer 2012 shows no accumulation since the previous year, implying a very low winter discharge. Until late-summer 2012 most of the 2011 icing has melted out, exposing again the pitted outwash (fig. 7.17D). In the background of the information provided above, a preliminary statement seems to be justified, that winter discharge from Svenbreen has been experiencing a certain change in the recent years. Icing production cycle seemed to switch from annual to episodic, although this problem needs further, more detailed observations.

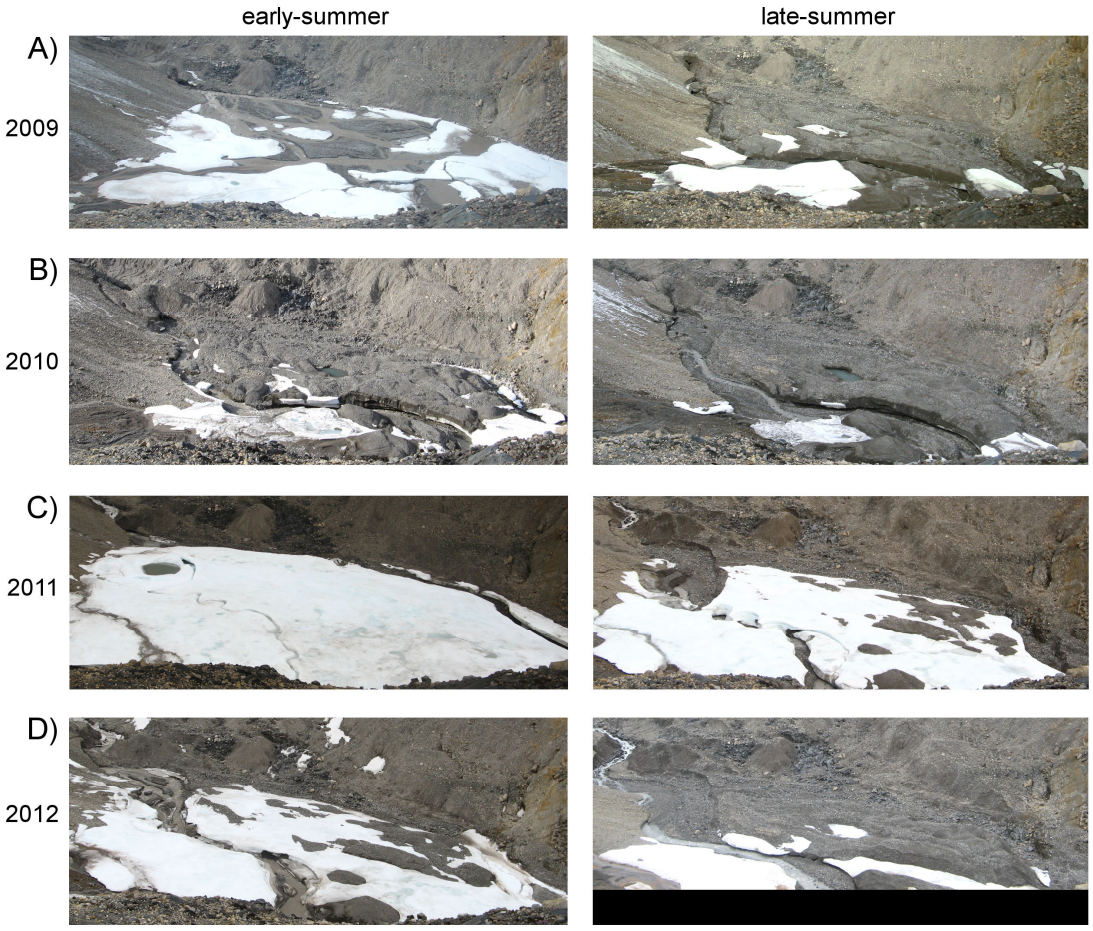

Fig. 7.17 Four years of form and degradation of Svenbreen icing field and an on-ice pitted outwash plain. Retreating glacier front is to the upper-left, water flows to the lower-right. Note no fresh icing in 2010 and 2012. 'Early-summer' photographs were taken in mid-July of each year, 'late-summer' in late-August or early-September. The scene is about 100 m wide from left to right

For balance years of 2010/11 and 2011/12 an attempt to approximate water balance components of Svenbreen basin was carried out (see section 4.3 for methods and full symbology). Investigated catchment closed by the gauging point is 8.66 km^2 and is covered with ice in 45%. The study covers two distinctly different balance years: 2010/11 (negative mass balance) and 2011/12 (steady-state balance). Total specific runoff from the basin (Q_{total}) in 2010/11 was 737 mm. Areal summer precipitation input (P_{summer}) was 130 mm, while meltwater production (P_{winter} - B_n) was 604 mm. Balance residual (water storage in the basin and an error term, $dS + \varepsilon$) calculated from these estimates was low with 14 mm. In 2011/12

season Q_{total} was very similar as in year before (711 mm), because higher P_{summer} (259 mm) partly balanced limited meltwater production (386 mm). A clear imbalance between Q_{total}, P_{summer} and melting must have been compensated by additional water input. $dS + \varepsilon$ was found to be significant with 77 mm. In the background of hydrological investigations and the radar survey described in the previous sections at least some of its share could result from a water release from subglacial environment, although it is impossible to separate dS from ε with the collected data. Nevertheless, water balance investigation does not exclude subglacial water presence.

Tab. 7.1 Approximated components of Svenbreen basin water balance

	2011		2012	
	specific (mm)	**volume (10^6 m^3)**	**specific (mm)**	**volume (10^6 m^3)**
Winter precipitation on the glacier, $B_w = s_{sven}$	232	2.01	262	2.27
Winter precipitation on slopes, s_{slope}	106*	0.91*	131*	1.13*
Winter precipitation total, P_{winter}	**338**	**2.92**	**393**	**3.40**
Melting of ice, M_{ice}	268	2.32	65	0.57
Melting of snow on the glacier, M_{snow}	230	1.99	190	1.65
Melting of snow on slopes, M_{slope}	106*	0.91*	131*	1.13*
Melting total, M_{total}	**604**	**5.23**	**386**	**3.34**
Net balance, B_n	**-266**	**-2.30**	**7**	**0.06**
Summer precipitation, P_{summer}	**130****	**1.12****	**259****	**2.24****
Condensation, C	**1**	**0.01**	**1**	**0.01**
Evaporation, E	**8***	**0.07***	**8***	**0.07***
Residuals, $dS + \varepsilon$	**14**	**0.12**	**77**	**0.67**
Winter runoff, Q_{winter}	14	0.12	14	0.12
Runoff in June, Q_{Jun}	130*	1.13*	126*	1.09*
Runoff in the period July-September, $Q_{Jul\text{-}Sep}$	593	5.14	572	4.95
Runoff total, Q_{total}	**737**	**6.38**	**711**	**6.16**

* assumption, no precise measurements
** approximated with measurements from SVL station

The available data made it possible to calculate relative contribution of individual components to summer runoff from the basin (fig. 7.18). In both investigated seasons snow melt was a major contribution to water runoff (45%). The absolute volume of water from melted snow (on the glacier and ice-free slopes) was $2.90 \cdot 10^6$ m^3 and $2.78 \cdot 10^6$ m^3, respectively for 2010/11 and 2011/12 balance years. In 2011 also a significant mass of ice has melted out from Svenbreen ($2.32 \cdot 10^6$ m^3, 36% of runoff), while in 2012 ice loss was four times lower ($0.57 \cdot 10^6$ m^3, 9%). Annual precipitation yields were estimated as $3.61 \cdot 10^6$ m^3 in 2010/11 and $4.99 \cdot 10^6$ m^3 in 2011/12, translating to 417 mm and 576 mm respectively. P_{winter} contributed to runoff with melting snow. P_{summer} was formed mostly by rain and accounted for $1.12 \cdot 10^6$ m^3 or 17% of runoff in 2011, while in 2012 volume of rain delivered to the basin was twice higher ($2.24 \cdot 10^6$ m^3 in 2012), as was its contribution to proglacial runoff (36%). Not much may be stated about the nature of water balance residuals, but their role may be significant as calculated by Hodson et al. (2005) for Midre Lovénbreen. On Svenbreen, the calculated residuals of the water balance were positive for 2012, allowing a subglacial water release. However, more detailed studies are necessary to exclude the balance error term.

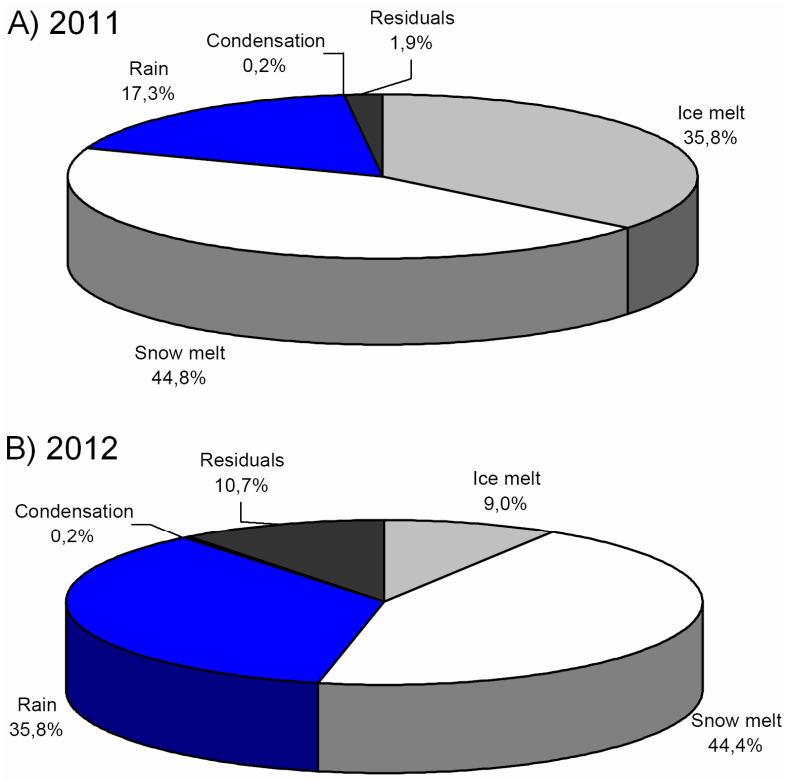

Fig. 7.18 Approximated contributors to summer river runoff from Svenbreen basin in A) negative mass balance year 2010/11; B) steady-state mass balance year 2011/12. Residuals denote water storage and error term

Concluding, hydrology of Svenbreen shows a clear dominance of supraglacial drainage, so river discharge reflects conditions on the surface and rainfall input to a high extent. In agreement with GPR investigations, there are some traces of intraglacial water routing, the role of which is variable in time, as suggested by observations of icing formation and water balance study. Water balance of the basin is highly dependant on weather and mass balance conditions and likely evolves with changing physical properties of the glacier.

8

Changes of physical properties of Svenbreen and their drivers

8.1 Topoclimatic controls of mass changes

Climate change fundamentally influences glacier's mass by altering its mass balance (fig. 1.1). Analysis of links between local climate (covering i.e. T_a, RH, u, SW_{in}) and individual components of mass balance equation (eq. 2.1) has a key meaning to understand response of glaciers to climate forcing. Results of glacio-meteorological investigations on Svenbreen are presented in section 6.1 and 6.2, while results of mass balance surveys are summarized in section 6.3. Here, implications of unique topoclimate of Svenbreen on its mass balance are discussed.

8.1.1 Increased winter balance - a snowdrift concept

Snow accumulation in Svalbard is generally low and potentially the lowest in arid interior of Spitsbergen (see section 3.4). Mass balance data from small central Spitsbergen glaciers is limited to few-year long records from three sites: Longyearbreen, Bogerbreen and Bertilbreen (glacier neighbouring Svenbreen from the south). In the period of measurements (1970's-1980's) mean B_w of the glaciers mentioned was 48, 52 and 41 cm w.eq. respectively, while on more maritime glaciers of western Svalbard accumulation in a similar period was significantly higher with ~75 cm w.eq. (Troitskiy 1988; Killingtveit et al. 2003). During the first season of winter studies on Svenbreen, 2009/10, snow depth probings gave mean snowpack thickness of 130 cm. Using an average snow density obtained from snow pit measurements from other years, it translates to approximate B_w of about 43 cm w.eq., though this figure is probably significantly underestimated (see section 6.3.1). In 2010/11 full winter balance parameters were measured directly and obtained B_w was 54 ± 10 cm w.eq., while in 2011/12 it was the highest with 61 ± 10 cm w.eq.

In the background presented above it may be stated, that during a short period 2010-2012 winter balance on Svenbreen was considerably higher than previously reported averages for other central Spitsbergen glaciers. A map by Gokhman and Khodakov (1986) supports the idea of increased snow supply, as it clearly shows that during winter 1982/83 Svenbreen experienced the greatest accumulation in the whole Pyramiden region (fig. 8.1). Additional snow source from avalanching is only restricted to narrow areas near the rock walls and applies also to i.e. Bertilbreen. Hence, it is certainly not responsible for greater overall accumulation on Svenbreen. The only reasonable mechanism for its increased B_w is a snow drift concept proposed below.

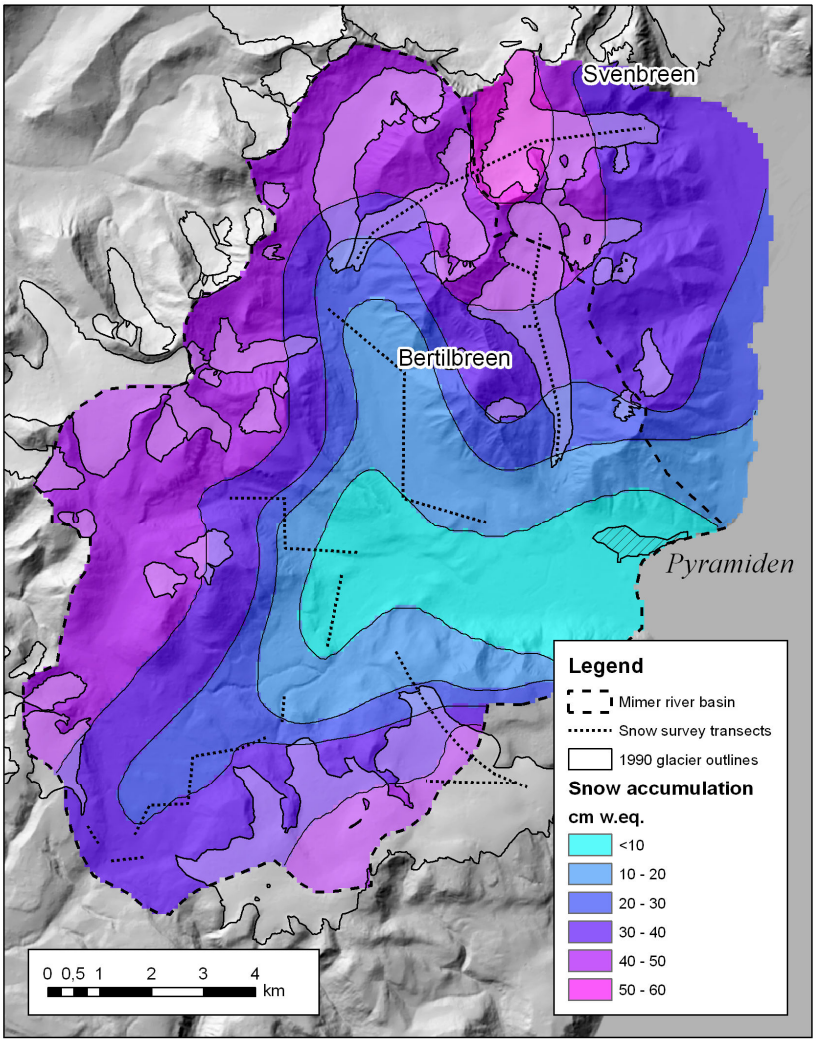

Fig. 8.1 Winter sow accumulation in Pyramiden area in April 1983. Note the highest accumulation on Svenbreen. After Gokhman & Khodakov (1986), modified

The glacier valley opens widely to the east, where vast, high elevated icefields of Mittag-Lefflerbreen and Olav V Land are located (fig. 3.6A). As mentioned in section 3.1, atmospheric circulation above Svalbard is dominated in the winter by air advection from the eastern sector (E, NE and NW, 51% days between October and April, 1951-2006, Niedźwiedź 2007). The associated winds, if strong enough to exceed the shear strength of the surface snow, carry great loads of particles suspended in the air at considerable altitudes. Eastern winds from Olav V Land are then canalized in valleys of Ragnarbreen and Ebbabreen,

transporting the snow to Svenbreen area. Some portion of this mass, when released above the glacier, contributes to its winter balance. Data from the glacier foreland underline the role of north-easterly winds from Ragnarbreen (Witoszová & Láska 2010; Láska et al. 2012), while data from Svenbreen show only a minor frequency of eastern winds. However, as discussed in section 6.1.3, wind speed and direction directly above Svenbreen surface do not reflect general synoptic situation. The associated low wind velocity in the glacier basin limits further snow redistribution. Such situation was directly observed in late-March 2010 and likely occurs frequently during winter seasons. This concept is supported by the mentioned low-altitude meteorological records and indirectly by relatively low snow density on Svenbreen (0.33 g cm^{-3} on average), likely to result from limited wind-compaction. Most authors reported snow density averaged for Svalbard basins of 0.36-0.38 g cm^{-3} (e.g. Gus'kov 1983; Winther et al. 1998; Sand et al. 2003; Neumann 2006; Nawrot 2011; Sobota 2010) and often even higher (e.g. Gus'kov 1983; Grześ & Sobota 2000; Nawrot 2011; Ignatiuk 2012).

The proposed mechanism of a additional topoclimatic snow input is very simple and built on very sparse winter data. Snow cover information is available only for three seasons, while short, expeditionary winter fieldworks do not allow continuous observations of snow cover evolution. Hence, the above concept needs validation by further research.

8.1.2 Reduced ablation as a result of low energy availability

In contrast to winter periods, there is a much greater understanding of summer balance controls, as it may be physically modelled with the available data (section 6.2). Mean summer balance of Svenbreen, measured during relatively warm ablation seasons 2011 and 2012, was only -88 cm w.eq. It is significantly lower than ablation of three other central Spitsbergen glaciers mentioned in the previous section. Longyearbreen, Bogerbreen and Bertilbreen have been experiencing much more negative mean summer balance (-103, -96 and -115 cm w.eq. respectively, Troitskiy 1988) during much cooler period (1970's and 1980's). On the western coast of Spitsbergen, on Midre Lovénbreen and Austre Brøggerbreen, similar summer balance values were observed in that time (-113 and -116 cm w.eq. respectively, 1975-1985). The reasons of low ablation rates on Svenbreen should be sought in its very local climatic features, having a fundamental influence on the amount of energy available for melt.

8.1.2.1 Individuality of Svenbreen's topoclimate

In section 3.5 it is argued that summer T_a in the study area (PET station) is higher by 0.5-1°C than at SVL station and by 1.5-2°C than at NYA on the western coast (tab. 3.1). Air temperature distribution higher in the mountains and on glaciers depends on thermal gradient and its commonly observed values range from -0.6 to -0.7°C · 100 m^{-1} (wet adiabatic lapse rate) up to about -1.0°C · 100 m^{-1} (dry adiabatic lapse rate). Both are met on Svalbard glaciers during the summer period. Average temperature gradient varying from about -0.5°C · 100 m^{-1} (in 1970 and 1979) to -1.0 °C · 100 m^{-1} (in 1983) was found for Werenskioldbreen (Baranowski 1975; Pereyma 1983; Pereyma & Piasecki 1988). A study by Nawrot (2011) revealed an average lapse rate of -0.6°C · 100 m^{-1} for Ariebreen. Polish researchers have been measuring air temperature gradient on Waldemarbreen of -0.6°C · 100 m^{-1} (e.g. Araźny 1999; Kejna 2002; Brykała & Araźny 2002). Piasecki & Gluza (1988) announced average lapse rates of -0.7 and -0.9°C · 100 m^{-1}, respectively for Scottbreen and Renardbreen. Krismer (2009) calculated very low multiannual summer lapse rates on Kongsvegen, ranging from -0.2

to -0.5°C · 100 m^{-1} between two stations on the glacier and about -0.8 to -0.9°C · 100 m^{-1} when measured from the coast to the ELA. Lapse rates noted on Svenbreen are presented in section 6.1.1 and are generally close to -1.0°C · 100 m^{-1} when measured along SVL-S60 transect and -0.7 to -1.0°C · 100 m^{-1} for the ablation zone.

Dry adiabatic gradient of air temperature often observed on Svenbreen (figs. 6.4 and 6.5) causes fast cooling of the air with increasing elevation. It implies, that high summer T_a at the sea-level is more efficiently decreased when moving up-glacier, so the thermal effect of climate continentality is reduced. Lapse rates on Svenbreen are expected to have a direct relation with air moisture. Relative humidity of the air (*RH*) in Svalbard is generally high, supported by ocean proximity and low air temperature. Average summer sea-level *RH* noted along the western coast of Spitsbergen mostly ranges from 85% to 90% (e.g. Wójcik et al. 1983; Piasecki & Gluza 1988; Kejna 2002; Kejna & Maszewski 2007; Przybylak et al. 2007b), while in the study area it is considerably lower due to significant distance from the open seas (70-75% at PET station, Rachlewicz 2003a; Małecki et al. 2011). In effect, summer air vapour pressure, e_a, at S60 typically oscillates around only 600 Pa. As a result of more negative lapse rate, elevation a.s.l. and cooling effect of snow and ice surfaces, mean JJA T_a in the middle ablation zone of Svenbreen is only about 2-3°C (tab. 6.1), being similar to summer T_a of other Svalbard glaciers (compare with tab. 8.1).

Another peculiarity of Svenbreen meteorology is a very low mean wind velocity during ablation season, typically of about 1.5 m s^{-1}. Average summer wind speed on other glaciers in Svalbard is generally higher: ~2.0 m s^{-1} on Waldemarbreen (e.g. Przybylak et al. 2007a; Kejna & Maszewski 2007; Kejna et al. 2010) and Midre Lovénbreen (Hodson et al. 2005), 2.0-4.5 m s^{-1} on Hansbreen (Migała et al. 2006; Araźny et al. 2009; Sikora et al. 2010, 2011), ~3.5 m s^{-1} on Scottbreen (Bartoszewski et al. 2004) and on Kongsvegen (Krismer 2009) and ~4.0 m s^{-1} on Austfonna (Østby 2010). On Ebbabreen, the largest glacier in Petuniabukta area, situated just 10 km east from Svenbreen, average summer wind velocity ranges from 2.6 to 4.1 m s^{-1} (2008-2010, Małecki, unpublished ms.). It underlines the local character of wind conditions in glacial environments, driven mainly by surrounding topography, with high rock walls having a fundamental protecting effect. All factors described above have a direct impact on energy balance of the glacier surface.

8.1.2.2 Energy balance of Svenbreen against other glaciers

Heat balance investigations are very rare on Svalbard glaciers, what is mainly linked to station maintenance difficulties in harsh polar conditions. AWS on Svenbreen, operated by Adam Mickiewicz University, is the first glacier energy balance station located in arid Dickson Land. Available data from Svalbard is hardly comparable to Svenbreen record due to different time and parameter coverage, size and type of a glacier, elevation, equipment and data treatment used, but also because many authors do not publish any averaged energy flux values. From all these reasons some studies could not have been used here (e.g. Baranowski 1977; Arnold et al. 2006; Van Pelt et al. 2012). Some papers were however suitable for comparisons with Svenbreen record and their findings are presented in tab. 8.1 as summer means.

The glaciers of comparison are situated along the western coast of Spitsbergen and on Nordaustlandet (Etonbreen). In all cases net radiation, Q_N, dominated their energy budget. It supported 72%-83% of total available energy. On Svenbreen this contribution was the lowest

with 70%, because Q_N was greatly reduced (21 W m^{-2}), mainly due to low SW_{in} (140 W m^{-2}). Sensible heat flux (Q_H) was very similar in ablation zones of each of the glaciers of comparison and ranged from 11 to 13 W m^{-2}. On Svenbreen Q_H was the lowest (7 W m^{-2}) due to the lowest wind speed on the glacier, but paradixically its relative contribution to the overall heat budget was the highest from the analysed glaciers (22%). Latent heat flux (Q_L) is the least important energy source in Svalbard, although very variable between the sites, as it either contributes to melting or decreases the melt energy by sublimation. Positive values of Q_L were found on Midre Lovénbreen (9%) and Hansbreen (6%), what may be partly attributed to humid air in these areas, whereas on Etonbreen, Kongsvegen and on Svenbreen Q_L was a sink. Total amount of average energy available for melt, Q_M, was different at each location, with definitely the lowest value on Svenbreen (only 25 W m^{-2}) and the highest on larger tidewater glaciers in Spitsbergen.

Tab. 8.1 Energy balance in ablation zones of Svalbard glaciers at given elevations (median glacier elevation in parentheses). T_a - air temperature, RH - relative humidity, u - wind speed, SW_{in} - shortwave incoming radiation, Q_N - net radiation, Q_H - sensible heat flux, Q_L - latent heat flux, Q_M - melt energy

	T_a °C	RH %	u m s^{-1}	SW_{in} W m^{-2}	Q_N W m^{-2}	Q_H W m^{-2}	Q_L W m^{-2}	Q_M W m^{-2}	Period	Reference
Svenbreen 358 m (med. 470 m)	**2.1**	**84.5**	**1.8**	**139.7**	**21.1 (70%)**	**6.7 (22%)**	**-2.5 (-8%)**	**25.0 (92%)**	**15/06-10/9 2012**	**This work**
Hansbreen 201 m (med. 350 m [1])	2.5	90.4	2.7	147.2	50.5 (76%)	12.1 (18%)	3.8 (6%)	66.5 (100%)	13/06-6/09 2004	Migała et al. (2006)
Midre Lovénbreen [2] 75 m (med. 330 m [1])	3.5	90.7	2.2	163.3	43.8 (72%)	11.7 (19%)	5.3 (9%)	60.8 (100%)	1/06-31/08 1997-2002 [3]	Hodson et al. (2005)
Kongsvegen [2] 170 m (med. 500 m [1])	1.5	83.8	3.4	203.7	77.3 (83%)	13.0 (14%)	-3.3 (-4%)	87.1 (96%)	1/06-31/08 2007	Krismer (2009)
Kongsvegen ELA [2] 550 m (med. 500 m [1])	0.0	85.6	3.5	224.7	41.9 (78%)	5.1 (9%)	-6.7 (-12%)	40.3 (88%)	1/06-31/08 2000-2007	Krismer (2009)
Etonbreen [4] 369 m (med. 420 m [1])	1.5	90	4	200	52 (81%)	12 (19%)	0 (0%)	53 (83%) [5]	15/06-10/9 2004	Østby (2010)

[1] after Hagen et al. (1993); [2] values recalculated from original data; [3] only for melt conditions; [4] values approximated from original diagrams; [5] negative ground heat flux included

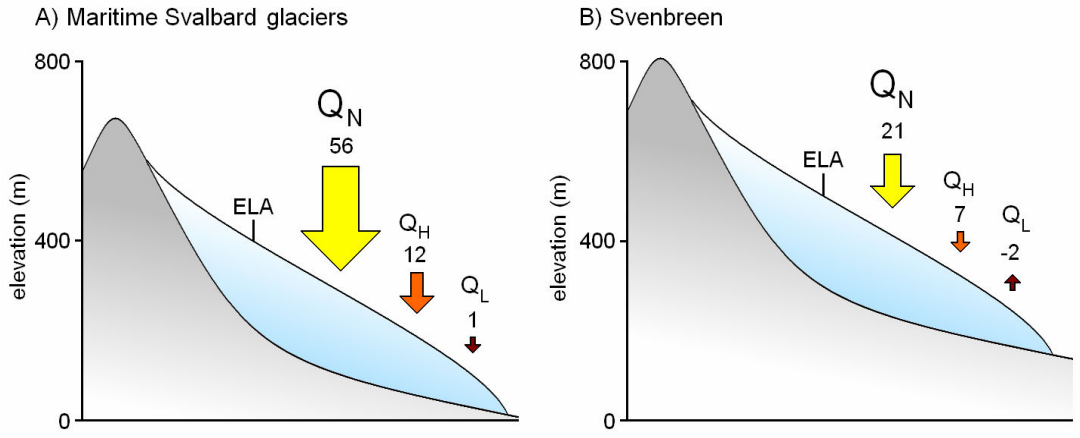

Fig. 8.2 Contribution of energy balance components to melting (in W m^{-2}) in ablation zones of A - maritime Svalbard glaciers (mean values from tab. 8.1) and B - Svenbreen. Symbology: Q_N - net radiation, Q_H - sensible heat flux, Q_L - latent heat flux

In the analysed ablation season surface energy balance of Svenbreen was significantly different from conditions found on other Svalbard glaciers (fig. 8.2). Its individuality was caused primarily by abnormally low Q_N and SW_{in}, linked mainly to cloudiness (typical for the whole archipelago) and topography. The glacier tongue flows to the east and is moreover gently inclined towards the north, what has a huge impact on its insolation. High rock walls surrounding the glacier protect it further from direct solar radiation, particularly since the latter half of August, when the glacier stays in the shadow for most of the day. Moreover, very low absolute values of turbulent heat fluxes were caused by low wind velocity, resulting in turn from a strong protective topographic influence. Negative Q_L is an effect of limited air moisture in central Spitsbergen. The main drivers of energy balance conditions on Svenbreen are therefore geometry of the valley and the glacier surface, as well as quasi-continental climate of Dickson Land.

Period of data averaging, field equipment, data processing procedures and obviously the chosen energy balance model have a huge impact on the results of investigations. Temporal coverage of data for Midre Lovénbreen and Kongsvegen in tab. 8.1 spans from the beginning of June until end of August, with the first two weeks of this period not necessarily being favourable for melt. It also has a huge impact e.g. on incoming shortwave radiation averages. If Svenbreen was to be analysed in a similar period, its mean SW_{in} would be 172 W m^{-2} - by 32 W m^{-2} higher than given in tab. 8.1. As described in chapter 'Methods and errors' (section 4.3), multiple corrections and assumptions were introduced in the energy balance model of Svenbreen. Those included elements that certainly are only partly valid, such as constant surface temperature at 0°C, logarithmic wind profile or constant surface roughness length of 5 mm. Most of estimates of surface roughness of melting snow and ice found in the literature range from 1 to 10 mm, but the energy balance model used here is only moderately sensitive to the chosen value in case of Svenbreen record. As an example, use of roughness of 2.53 mm (average found for Midre Lovénbreen, Hodson et al. 2005) slightly decreases mean summer Q_H from 6.7 W m^{-2} to 6.0 W m^{-2}, with insignificant impact on Q_L. Conversely, use of 10 mm surface roughness increases Q_H to 7.5 W m^{-2}. It needs therefore to be underlined, that results of heat budget investigations from Svenbreen presented in this work are approximations representing a simplified version of reality, rather than precise measurements (especially of turbulent heat fluxes), and may contain considerable errors.

Another issue of concern is related to interannual variability of weather and hence energy balance conditions presented in tab. 8.1. Few-year long records from glaciers in different climatic zones show that typical year-by-year variability of summer SW_{in} is within e.g. 2 W m^{-2} on a glacier in Norway (Andreassen et al. 2008), but may be also higher with ~20 W m^{-2}, as e.g. in Greenland (Van de Wal et al. 2005). LW_{in}, relative air humidity and wind speed are rather stable and the differences observed between individual seasons are mostly (though not always) lower than ~5 W m^{-2}, ~5% and ~0.5 m s^{-1} respectively. Differences between cool and warm summer periods on glaciers are typically on the order of ~1.5°C. In this context it must be stressed, that Svenbreen 2012 record represents a relatively cool season, when summer mass balance at AWS site was b_s = -89 cm w.eq. and overall glacier mass balance was near-zero. Energy balance conditions in other years must have been different to some extent, particularly during extremely warm 2011 summer season, when summer balance at the measuring point was b_s = -151 cm w.eq. On the other hand, years with low surface melting seem to be normal for the glacier of study and manifest its individuality in the background of other Svalbard ice masses. The presented meteorological and energy balance records clearly show the influence of arid climate of central Spitsbergen. They may be considered as representative for Svenbreen, as long as all the restrictions discussed above are concerned.

8.1.2.3 Temperature-index ablation reconstruction

Direct energy balance data from Svenbreen covers only one ablation season. It is however commonly accepted, that ablation in polar and temperate zones is correlated to air temperature, T_a, as it reflects variability of several energy balance components to a high extent (Ohmura 2001; Hock 2003). T_a is the fundamental parameter measured at meteorological stations, it is therefore very useful in mass balance calculations referring to present and past climate conditions. The available record for Svenbreen, consisting of meteorological data and 139 stake inspections, was used to draw the relationship between air temperature and ablation. Specifically, as sub-zero air temperature was excluded, ablation was correlated with positive degree-days (PDD). It could be then used to reconstruct melt intensity on Svenbreen for comparison with older mass balance records from other central Spitsbergen glaciers.

Temperature data used in this study origins from two different sources, including on-glacier T_a measurements at different altitudes. The other record origins from low-altitude SVL station and to calculate T_a on Svenbreen a constant lapse rate of -1.0°C · 100 m^{-1} was used. From these two sources, two alternative versions of positive degree-day sums for each point on the glacier were calculated: PDD_{obs} (from direct records) and PDD_{SVL} (from approximated T_a). Ablation was computed from stake measurements and included thickness changes of snow cover, superimposed ice and glacier ice. As clearly visible on fig. 8.3A, ablation showed better agreement with PDD_{SVL}. It may be related to the fact, that ice surface cannot be warmed up above 0°C, so on-glacier summer air temperature (PDD_{obs}) poorly reflects weather conditions (i.e. insolation) and potential ablation.

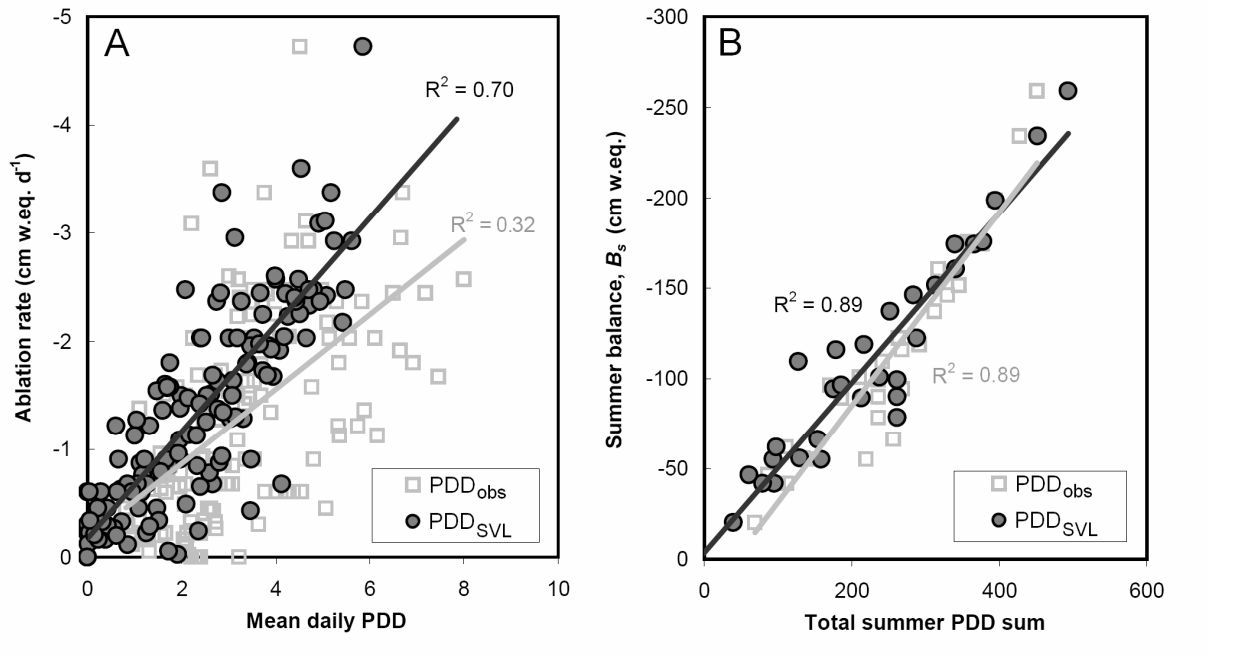

Fig. 8.3 A - relationship between daily ablation rates observed on Svenbreen (in 2010, 2011 and 2012) and mean daily PDD inferred from single stake inspections; B - relationship between summer balance and total summer PDD sums (2011/12 and 2011/12). Explanations: "PDD_{obs}" - relationship between ablation rates and PDD obtained from direct record; "PDD_{SVL}" - relationship between ablation rates and PDD approximated from Svalbard Lufthavn station. Note inversed vertical axes and a good correlation between ablation rates PDD_{SVL} on panel A

Data presented on fig. 8.3 confirm that ablation on Svenbreen may be reconstructed from low-altitude SVL air temperature data with reasonable accuracy. The only additional information needed to calculate a glacier-wide ablation estimate is geometry of the glacier for computations of PDD distribution. For this purpose 1990 and 2009 DEMs have been used, tuned to simulate year-by-year geometry evolution (see section 4.2). Reconstruction of summer balance on Svenbreen was carried out for the period starting with 1976, when measurements at SVL station begun. A simple temperature-index method was used, assuming a linear relationship between point b_s (in cm w.eq.) and PDDs, visualized on fig. 8.3B:

$$b_s = -0.47 \cdot PDD_{SVL} - 3.5 \qquad \text{(Eq. 8.1)}$$

Equation 8.1 was then applied to each cell of maps of PDD distribution for each summer season. From the resulting rasters average summer balance B_s was inferred by cell integration. Reliable error statistics for glacier-wide summer balance estimations of the model are obviously impossible to asses because of sparse reference data. Differences between modelled and observed B_s in 2011 and 2012 were respectively 0 and 19 cm. Conservative error bars have been therefore arbitrarily fixed at ± 25 cm w.eq.

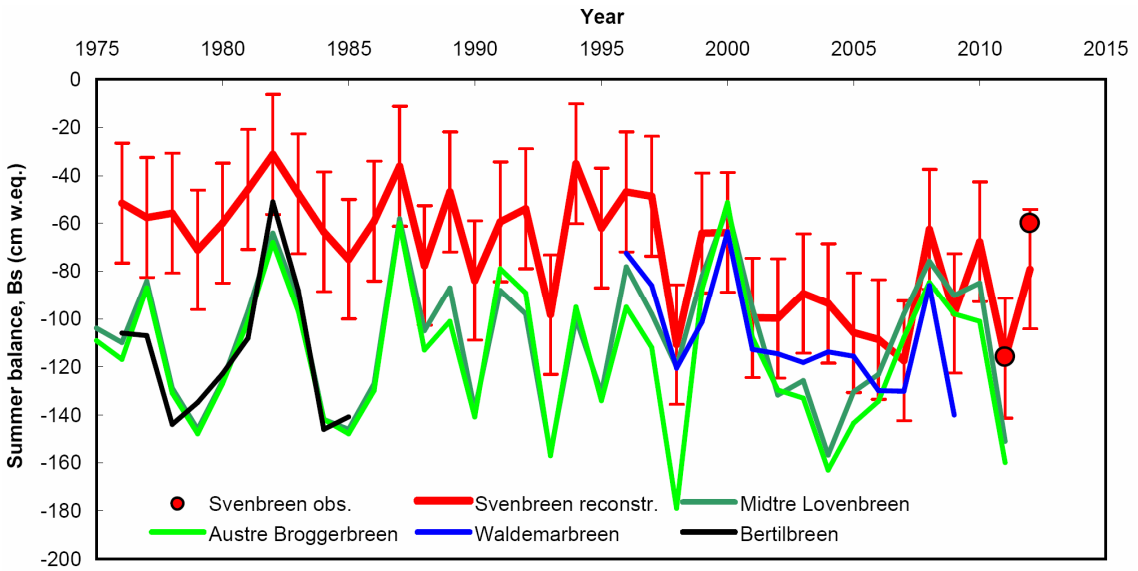

Fig. 8.4 Reconstructed summer mass balance of Svenbreen (with 25 cm w.eq. error bars) against summer balance of other selected Svalbard glaciers. Comparison data after Troitsky (1988), Sobota (2007a) and WGMS (2012)

Results of the model are showed on fig. 8.4. For the period 2008-2012 its performance is reasonable and is in agreement with direct observations (compare maps of late-summer snow cover, fig. 6.34). Modelled B_s values range from -31 ± 25 cm w.eq. in 1982 to -117 ± 25cm w.eq. in 2007. For year 2011 reconstructed summer balance was the same as measured in the field, with -116 ± 25 cm w.eq., while for 2012 it was -79 ± 25 cm w.eq. (measured B_s = -60 ± 15 cm w.eq.). The main purpose of the temperature-index modelling exercise was to investigate whether ablation on Svenbreen is normal as for a small land-terminating Svalbard glacier. Strikingly, fig. 8.4 clearly reveals that its reconstructed summer balance is by 20-50 cm w.eq. less negative than noted on other glaciers, including neighbouring Bertilbreen, even though error bars are wide.

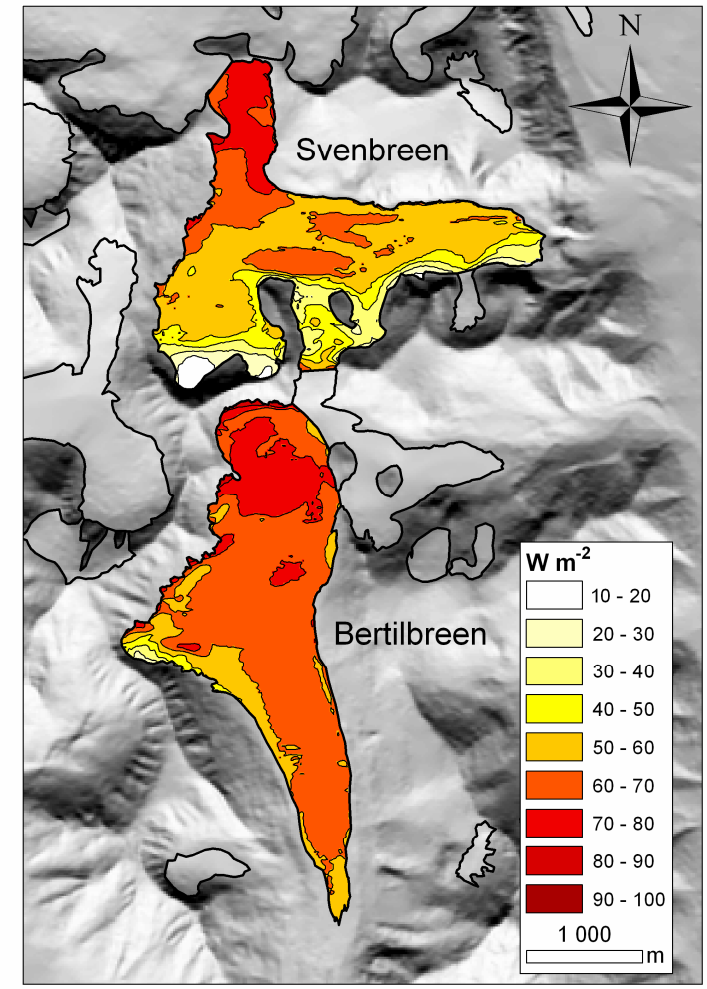

Fig. 8.5 Spatial variability of calculated potential direct solar radiation on Svenbreen and Bertilbreen based on 2009 geometry and averaged for period 15/06-15/09

Ablation data for Bertilbreen is available for the period 1976-1985, when summer T_a was significantly lower than in the last decade (4.1°C on average at SVL). Despite this fact Bertilbreen has shown high average ablation of B_s = -115 cm w.eq. Meanwhile, modelled ablation on Svenbreen was twice lower with B_s = -56 ± 25 cm w.eq. Both glaciers are characterized by a very similar area and hypsometry, but Bertilbreen receives far more solar radiation due to its southern aspect, being an additional source of heat in surface energy balance, thus enhancing melt processes (fig. 8.5). This simple comparison underlines the role of local topography, which in case of Svenbreen highly reduces melting and is confirmed by the energy balance study (section 6.2). Other factors also play role, as i.e. albedo of both glaciers. As discussed in section 8.1.1 snow accumulation on Svenbreen is most likely considerably higher than on Bertilbreen, so occurrence of highly reflective snow cover is longer, what further decreases melting. Moreover, as discussed in section 6.1.3, general wind speed and foehn-type wind events have not been observed on Svenbreen in the period of study, suggesting their negligible importance. On other Svalbard glaciers foehn winds are known to greatly enhance ablation (e.g. Leszkiewicz et al. 1999).

Both mass balance components of Svenbreen proved to be significantly influenced by local factors. Topoclimate of the glacier is manifested not only by meteorological parameters, such

as air temperature, relative humidity or wind speed, but also by exposition to snow-drifting winds during winter season. In effect, the topoclimate of Svenbreen is responsible for relatively high winter balance and low ablation rates during summer periods, having a key impact on its net mass changes.

8.1.3 Slow mass loss - evidence from geometry changes and field observations

For the last five decades geometry changes of glaciers in central Dickson Land have been unidirectional, as all seven investigated ice masses studied in section 5.1 have been thinning. This trend is similar to trends found in previous work in other Svalbard regions. Nuth et al. (2007; 2010) and Moholdt et al. (2010) found that Svalbard glaciers are generally thinning in all regions. Kohler et al. (2007) and Nuth et al. (2007) measured progressively increasing thinning rates of Svalbard glaciers since at least 1936, being in agreement with retreat of glaciers in the study area until 1960 (Rachlewicz et al. 2007). Kohler et al. (2007) and James et al. (2012) brought evidences of enhanced mass loss since the 1990's, which are now supported by results from central Dickson Land, where glacier thinning between 1990 and 2009 was on average by 58% faster than in the period 1960-1990 (tab. 5.1). Acceleration of mass loss correlates with a gradual increase of summer air temperature in Svalbard (fig. 3.2).

Unfortunately, literature suitable for interregional comparisons is limited, mainly due to differences in temporal coverage of earlier works and methods used, as here the focus is on thinning rates averaged for period 1960's - 2000's. Elevation changes of the largest ice fields in Svalbard in the considered time span were presented by Nuth et al. (2010). Their results clearly show glacier thinning (average dH/dt = -36 cm a^{-1}) and a regionalisation of the general mass loss, with the most negative dH/dt along the southern and western coast of Spitsbergen, decreasing towards north-east. Some works characterizing long-term geometry changes of individual small ice masses have been also published, i.e. by Kääb (2008), who announced elevation changes of -55 cm a^{-1} and -61 cm a^{-1} (1970-2000's) for two ice caps in eastern Svalbard. Barrand et al. (2010) computed mean dH/dt of two glaciers in NW Spitsbergen of -58 cm a^{-1} and -41 cm a^{-1} for epoch 1966-2005. Recently James et al. (2012) analysed six small glaciers in different parts of Svalbard (mostly close to the coasts) for a similar period and reported thinning rates of -25, -32, -44, -64 and -87 up to as much as -100 cm a^{-1}, though the latter case considered only the lowest part of a glacier and hence is not representative.

In central Dickson Land Vestre Muninbreen has been lowering by dH/dt = -80 ± 6 cm a^{-1}, making it one of the fastest thinning glaciers in Svalbard. From the investigated ice masses surface lowering of Svenbreen seems to be particularly slow (-43 ± 6 cm a^{-1}). Large discrepancy between dH/dt at both mentioned sites implies, that mass loss of glaciers in the study area is very sensitive to local factors, with topography (of a valley and of a glacier) being the dominant control. Average long-term glacier surface lowering in central Dickson Land was -61 ± 7 cm a^{-1}, what stays in contrast to results of Nuth et al. (2007), who argued that small central Spitsbergen ice masses are closer to being in balance due to their quasi-continental climate. Their results are however difficult to compare with those provided in section 5.1, as they considered different time span and region. In any case, mass loss in central Dickson Land is high, similarly as in other regions of the archipelago, but it may be significantly influenced by local factors. One of the reasons of relatively high average dH/dt in the study area is southern aspect of three relatively large glaciers. It coincides with their fastest mass loss, likely due to increased incoming shortwave radiation (compare with fig. 8.5). Such orientation is however exceptional in Dickson Land. In this background, it seems

probable that conditions on easterly-oriented, steadily-thinning Svenbreen better represent the general mass balance conditions of Spitsbergen interior than area-weighted mean of seven glaciers presented in section 5.1. The issue needs further studies.

Among small Svalbard glaciers, long-term (40-50 years) thinning rates lower than that of Svenbreen were announced in the literature only for three ice masses - Slakbreen, Gulfaksebreen (James et al. 2012) and Midre Lovénbreen (Barrand et al. 2010) - with the two first being by an order of magnitude larger and higher elevated than the studied glacier. Measurements of dynamic component of *dH/dt* on Svenbreen indicate that its elevation changes are driven mainly by its mass balance (section 5.2.3). Slow thinning suggests therefore lower overall ablation than on other ice masses, so the geodetic survey supports the findings inferred from direct energy balance and ablation investigations (see the previous sections). Field-based net balance information for Svenbreen is available for 3 distinctly different years (compare with section 6.3). In 2007/08 balance year the ELA was just at ~300 m a.s.l. and in late-August 85% of the glacier area was covered with last-winter snow, with depth ranging from 10 to 90 cm (obtained from only few random probings). Assuming a 15 cm thick superimposed ice underlying a snow cover of an average depth of 40 cm, reasonable net balance for this year would be highly positive, with about 30 cm w.eq., although it is only a rough estimate. Meanwhile, other similar glaciers have been experiencing net losses (fig. 8.6A). In 2010/11, after a very warm ablation season, much higher ELA position was documented on Svenbreen (560 m), resulting in a negative net balance of B_n = -62 ± 18 cm w.eq. and being the least negative from all small ice masses studied in the archipelago (fig. 8.6B). One year later, despite relatively warm summer of 2012, ELA was located just at 460 m and Svenbreen has experienced a mass balance equilibrium. Its B_n was 1 ± 18 cm w.eq., but no comparison data is available for this season yet.

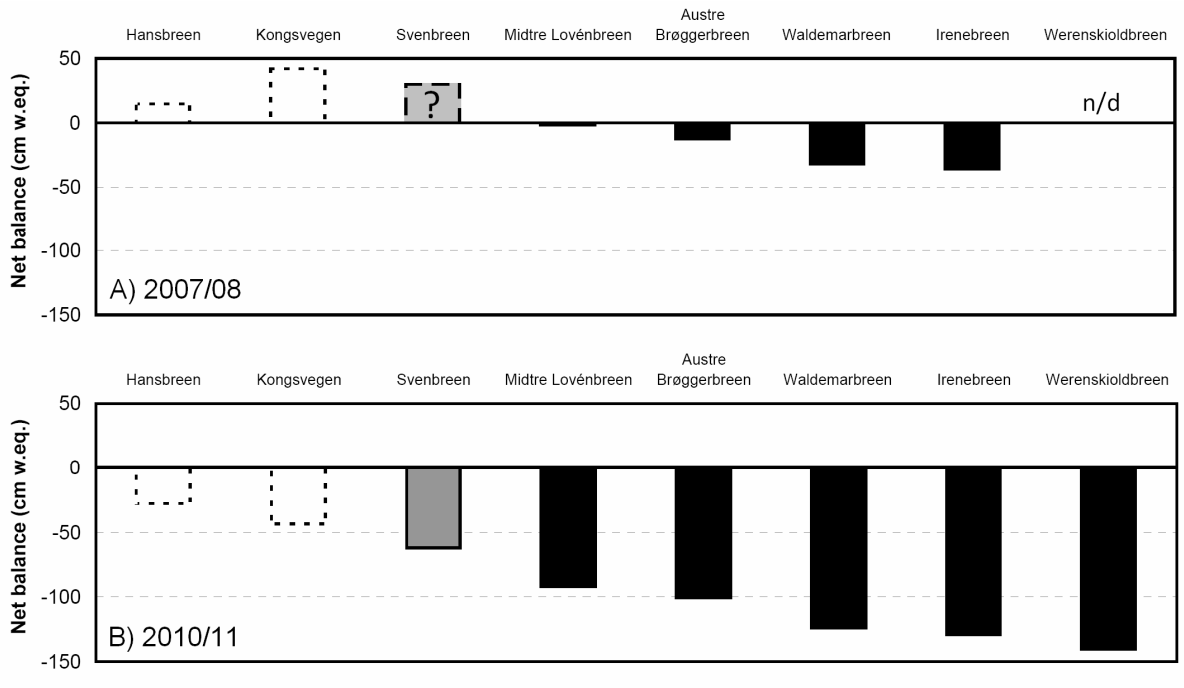

Fig. 8.6 Net mass balance of Svalbard glaciers in A) 2007/08 (with a rough estimate for Svenbreen) and B) 2010/11. Large tidewater glaciers are marked with dashed transparent columns. Note that mass balance of Svenbreen (grey column) is closer to being in balance than other land-terminating glaciers (black columns). After: WGMS (2012); Ignatiuk (2012)

After few years of observations, supported by geometry change study, it may be stated that net mass budget of Svenbreen is indeed less negative than observed on other similar land-terminating glaciers in the archipelago. Their mass budget records indicate that near-zero (B_n > -5 cm w.eq.) or positive net balances are very rare (excluding larger ice masses). As an example, small glaciers with the longest mass balance series, Austre Brøggerbreen and Midre Lovénbreen, have been experiencing such situation only very sporadically (respectively 4 and 9 times since 1960's). In contrast, positive B_n on Svenbreen occurred twice in only 5-year period of observation and resulted from unique topoclimatic conditions on the glacier. Its local climate is favourable for increased snow supply during winter and unfavourable for ablation during summer seasons, so net mass balance of Svenbreen is more similar to that of larger ice masses, as Hansbreen or Kongsvegen, than to other small land-terminating glaciers. Therefore, in the light of the facts from this and previous sections, Svenbreen may be considered as relatively resistant to general warming observed in Svalbard.

8.2 Hydrology, hydrothermal properties and their potential changes

8.2.1 Water balance and specific runoff

Structure of Svenbreen water balance (section 7.2.2) has shown a distinct difference when compared to other sites in Svalbard. It may be attributed to regional and local climate features. Annual areal precipitation for the basin was estimated using snow accumulation and SVL summer precipitation record, using a relatively high precipitation gradient of 30% · 100 m^{-1}, inferred from snow surveys. A similar gradient of 31% · 100 m^{-1} was used for Londonelva (Sand & Bruland 1999), though Killingtveit et al. (2003) listed several publications where slightly lower values are found (10-25% · 100 m^{-1}). Total annual precipitation obtained for Svenbreen basin was 416 and 576 mm for both studied years, being about 2-3 times higher than average sums measured at SVL station. It is however lower than in other Svalbard catchments. Sand & Bruland (1999) reported average precipitation for DeGeerdalen (central Spitsbergen) of 478 mm, for Londonelva (NW Spitsbergen) 595 mm and for Bayelva (NW Spitsbergen) 968 mm. For the latter basin Hodson et al. (2005) calculated average precipitation of 1088 mm. High overall precipitation was observed in glacierized basins of Hornsund region, the most maritime zone of Svalbard, where Jania & Pulina (1994) found annual precipitation of 1070-1340 mm. In the same region, Nawrot (2011) announced much lower value of 607 mm for one season of observation in a very small catchment of Ariebreen.

As could be expected, specific annual runoff from Svenbreen basin, estimated as 711 and 737 mm, was lower than value obtained for nearby Bertilbreen area (820 mm, Gokhman & Khodakov 1986), due to less intensive melting (see previous section). It was also significantly lower than runoff from similar basins in more maritime regions of Svalbard. Multiannual water balance studies in Bayelva (basin of Austre Brøggerbreen, NW Spitsbergen) gave total runoff of 1091-1261 mm (Sand & Bruland 1999; Hodson et al. 2005). Krawczyk & Bartoszewski (2005) estimated annual specific runoff of 1228 mm for Scottbreen basin (SW Spitsbergen). Pulina et al. (1984) and Jania & Pulina (1994) announced very high as for Svalbard annual runoff rates, ranging from 1680 mm to 1920 mm for S Spitsbergen. Little or no glacier-covered catchments in different regions of Svalbard have published records of runoff ranging from 411 mm to 823 mm (Gokhman & Khodakov 1986; Gokhman 1988; Jania & Pulina 1994; Sand & Bruland 1999; Killingtveit et al. 2003; Nawrot 2011). Specific runoff from heavily glacierized (<40%) Svalbard basins seems therefore to be significantly lower in

central Spitsbergen than in coastal regions, reflecting mainly limited precipitation, on which melt issues are superimposed only in the second order. Structure of water balance of Svenbreen basin is clearly dependant on prevailing weather conditions during the year. It is therefore expected to reflect the ongoing change of climate, glacier mass balance and its thermal structure to some extent. The current trend of rising summer air temperature will clearly lead to an increased role of glacier ice in river runoff.

Although the results of water balance investigations gave realistic values of its individual components, the error expected in this study is high. Several balance elements were not measured in the field, from which the most important are: summer precipitation P_{summer}, water reserves in winter snow cover resting on the slopes surrounding the glacier s_{slopes} and river runoff from the basin in June Q_{Jun}. Instead, arbitrary values were assumed for these parameters on the basis of the literature, field experience or (as in case of precipitation) record from SVL station. The estimate of the volume of the total runoff is affected by Q_{Jun} and an increase in assumed June runoff by 50% results in a rise of total runoff by only about 8%. Thereofre, estimates of Q_{total} are relatively resistant to erroneus assumptions, but the quality of actual water discharge measurements (and hence $Q_{Jul\text{-}Sep}$) remains questionable due turbulent water flow in the proglacial river.

8.2.2 Hydrothermal regime of Svenbreen and its changes

Svenbreen has been classified as a polythermal glacier, with thick cold surface layer and pressure-melting conditions at the bed (section 7.1). Borehole thermistors installed at 8 m depth in ablation zone (at stake S30) and accumulation zone (S100) have shown almost stable negative ice temperature (T_i) of -4.1°C at S30 and -4.5°C at S100. These T_i values are very similar to 10 m ice temperature observed in 1980 on Bertilbreen: -4.3°C at 325 m and -4.8°C at 475 m (Jania et al. 1996). Similar studies, as the one showed in section 7.1.1, have been previously performed by Sobota (2009, 2011) on Waldemarbreen and Irenebreen, two small glaciers in NW Spitsbergen. He reported 10 m temperature in accumulation areas of -2.3 for the first and -3.3°C for the latter glacier, higher than noted on Svenbreen. General subsurface temperature variability was similar as presented here (fig. 7.1), but in contrast to his findings higher sites on Svenbreen and Bertilbreen were even cooler than ice at the lower locations. It may be interpreted as an effect of a lack of a firn zone, where T_i at 10 m is driven by meltwater presence. Jania et al. (1996) presented a detailed study of thermal structure of Hansbreen using numerous borehole termistors. Near-surface T_i readings revealed melting point in the firn zone and -2°C to -4°C at 10 m depth elsewhere. They also report 10 m T_i from ablation zones of other Svalbard sites: -8.5°C on Vestfonna (NE Svalbard) and -4.8°C on Kongsvegen (NW Spitsbergen). Ice temperature in the higher zones of Svalbard glaciers ranged from 0 to -1°C on Kongsvegen and Amundsenisen (S Spitsbergen) and from -1 to -3°C on large icefields Vestfonna, Holtedahlfonna (NW Spitsbergen) and Lomonosovfonna (central Spitsbergen). On Nordenskiöldbreen, a large tidewater glacier close to the study area, T_i in the accumulation zone (670 m) was -5.0°C. The lowest T_i was measured in the highest zone of a small glacier Bogerbreen in central Spitsbergen (-7.5°C) and on Hoghetta at 1200 m (-11.0°C, N Spitsbergen). The wide spectrum of ice temperature observed in Svalbard underlines the complexity of the issue of glacier thermal structure. In the Svalbard context, Svenbreen is characterized by moderately cool ice in its accumulation area. However, it must be stressed that ice in other High Arctic glaciers is mostly significantly cooler, with e.g. -23°C at 10 m depth on White Glacier or on Devon Ice Cap in arctic Canada (Paterson, 1981).

Ground penetrating radar study, as well as observations of water runoff from the glacier, delivered strong traces for temperate conditions at the bottom of Svenbreen and in a small patch of firn (chapter 7). Internal reflecting horizon (which could be interpreted as cold/temperate transition surface, CTS) is however not visible on radargrams. Instead, a blurred bedrock reflection was interpreted as zone of a warm base, occurring continuously along the main axis of the glacier. A lack of CTS, together with temperate ice-bed interface was previously reported for Austre Brøggerbreen in NW Spitsbergen (Björnsson et al. 1996) and Svenbreen is most likely a similar case, making it one of the smallest glaciers in Svalbard to contain considerable zone of temperate ice.

Two main polythermal types prevail in Svalbard: the so called Canadian type (type A on fig. 2.3, with cold surface layer covering the whole glacier) and Scandinavian type (type E, cold surface layer only in the ablation zone). Glaciers smaller than ~5 km^2 have been mostly classified as entirely (or almost entirely) cold, e.g. Scott Turnerbreen (Hodgkins et al. 1999), Longyearbreen, Larsbreen (Etzelmüller et al. 2000), Tellbreen (Bælum & Benn 2011) or Ariebreen (Machío et al. 2007; Nawrot 2011). Medium sized and larger valley glaciers contain warm basal ice i.e. Austre Brøggerbreen (Björnsson et al. 1996), Werenskioldbreen (Pälli et al. 2003a) and Bertilbreen (Gokhman et al. 1982; Gokhman 1987a,b), or temperate ice at the bottom and in the accumulation zone, i.e. Erikbreen (Ødegård et al. 1992), Midre Lovénbreen, Kongsvegen, Uvérsbreen (Björnsson et al. 1996) or Hansbreen (Jania et al. 1996; Moore et al. 1999; Pälli et al. 2003a). Thermal structure of Svenbreen is interpreted as a mixture of types A and E (though closer to the Canadian type), with thin temperate basal layer along the axis of the greatest thickness, and a ~100 m thick cold surface layer, covering almost the whole glacier area, except for a small protected patch of temperate firn zone, close to the rock walls in the glacier cirque (fig. 7.8).

Hydrology of Svenbreen reflects well its thermal structure and is rather typical for small polythermal glaciers in Svalbard (e.g. Hodgkins 1997; Etzelmüller et al. 2000). There is a stable supraglacial drainage system, similarly as observed on other glaciers in the study area (Gokhman 1987; Kostrzewski & Zwoliński 1995). Surficial runoff dominates the glacier's hydrology, as indicated by a general agreement between river discharge and melting intensity, represented e.g. by air temperature. Correlation of average daily discharge Q with mean daily air temperature T_a (measured 60 km away at SVL) ranged from $R^2 = 0.32$ to $R^2 = 0.66$. However, the agreement between Q and T_a increased by 0.1-0.2 up to $R^2 = 0.75$ when T_a record from nearby PET station was used. Unfortunately, such data was only available for two out of four investigated seasons. The latter R^2 figure is similar to other values obtained for glaciers of the archipelago (e.g. Bartoszewski 1989; Leszkiewicz et al. 1999). The leading role of surface melt water in Svenbreen hydrology is confirmed by short average lag (3 hours) between maximum air temperature and maximum river discharge. Similar value was obtained e.g. for Werenskioldbreen (Pereyma & Piasecki 1988) or for Scottbreen (Bartoszewski 2007). Rachlewicz (2009a) reported much longer delays for three larger glaciers close to Svenbreen of 6-7 hours, 10 hours and 4-5 hours, but in their case gauging stations were located relatively far from their fronts.

The glacier cirque is the only zone on Svenbreen where water may reach to deeper layers by soaking (in the firn patch) or through narrow cracks in ice (1-50 cm in width). About 30-40 m underneath the accumulation zone multiple point-reflectors are visible on radargrams, interpreted (at least in part) as small englacial channels (fig. 7.4). Intraglacial drainage was confirmed by the character of summer and winter outflow from the glacier, the latter forming icing fields. Numerous previous works reported formation of proglacial icings in Svalbard,

what by most authors was attributed to water routing due to temperate ice conditions (e.g. Gokhman 1987; Bukowska-Jania & Szafraniec 2005; Rachlewicz et al. 2007), what is not always the case (Bælum & Benn 2011). Year after year some icing fields (variable in size) are formed in the winter in the forefield of Svenbreen, being in agreement with interpretations of intraglacial glacier drainage from GPR and hydrological data. A very interesting finding of this work is an episodic character of icings' formation in the last years (more specifically: formation of alternate large and insignificant icing fields). This observation, supported by greatly reduced icing volume than few decades ago, is most likely a sign of progressing freezing of the glacier and cessation of winter discharge, although this problem needs further studies to explain step-like changes in the character of winter outflow.

Transformation of polythermal glaciers into entirely cold-based was already reported for Svalbard. Russian works discussed changing thermal conditions of nearby Bertilbreen and progressive freezing of its temperate zone, linked to negative long-term mass balance. Gokhman et al. (1982) reported lack of firn accumulation since at least late 1960's. Gokhman (1987a) argued that increasing role of superimposed ice formation cools the glacier from the surface downwards. The same author have sketched a probable scenario of hydrothermal evolution of Bertilbreen under a warming climate and expected a complete freeze-up of the glacier until early 21st century and subsequent freezing of subglacial talik within next 10 years, resulting in complete cessation of intraglacial water routing (Gokhman 1987b). Hodgkins et al. (1999) investigated a small glacier Scott Turnerbreen with GPR and borehole thermistors and concluded that it has switched from a warm-based into an entirely cold-based glacier. Investigations on Midre Lovénbreen by different means concluded continuous reduction of its temperate basal layer (Hambrey et al. 2005; Willis et al. 2007). In this context, no CTS, but a blurred bedrock reflection recorded during 2012 GPR survey on both Svenbreen and Bertilbreen, may be another sign of their freezing and progressive transformation into cold glaciers. Negative mass balance of the studied glacier since at least 1960 (as calculated from geometry changes), together with observations mentioned earlier suggest, that such direction of evolution is very likely for Svenbreen and may carry important consequences for its further functioning.

8.3 Glacier dynamics - changes and geomorphological implications

Mass balance, motion pattern, geometry, past and present thermal structure and hydrology are keys for understanding geomorphological activity of a glacier and its forefield history. Advancing, retreating or stationary glaciers develop an own unique spectrum of landforms. Cold ice is generally frozen to the bed and has a very limited ability for landscape remodelling, in contrast to active temperate ice. The most prominent examples of glaciers' geomorphological activity are their valleys, being overdeepend to a degree dependant of the ice-bed conditions. GPR survey on Svenbreen clearly showed a V-shaped bedrock beneath cold-based Poznańskaret and Nataliaskaret (fig. 7.7). It indicates that these hanging valleys have been most likely entirely cold even during Little Ice Age, as they have not been remodelled by sliding ice. In contrast, the main valley, where present-day ice thickness reaches 130 m and the basal ice is at the pressure-melting point, is well exarated and resembles the U shape (fig. 7.6). Extent of temperate ice beneath Svenbreen is limited, so only in the deepest sections of the cirque and tongue remodelling and overdeepening of the bed may still occur, supported by subglacial water drainage. Denudation in Svenbreen basin, also reflecting subglacial erosion, has not been a subject of studies yet. Neighbouring larger polythermal glacier systems have been well investigated by researchers from Adam

Mickiewicz University, who obtained average rates ranging from 0.1 to 0.8 mm a^{-1} (e.g. Kostrzewski et al. 1989; Rachlewicz 2009a). Denudation rate in Svenbreen basin may be expected to be lower due to lower glacier activity.

Despite temperate ice-bed interface along its main axis, Svenbreen flows at present very slowly. Its maximum velocity is ~3 m a^{-1} close to the approximate ELA (section 5.2.3), as its lateral parts are frozen to the valley sides. Many other warm-based ice masses in Svalbard, mostly larger, move at a significantly faster rate, on the order of 10-15 m a^{-1} (e.g. Baranowski 1977; Nutall & Hodkins 2005; Rachlewicz 2009a), in extreme cases (during an active phase of a surge) being on the order of hundreds of m a^{-1} (e.g. Hagen 1988; Murray et al. 1998; Dowdeswell & Benham 2003). However, many other small glaciers (including Bertilbreen, Midre Lovénbreen and Austre Brøggerbreen) flow at a similar speed as Svenbreen, 1-5 m a^{-1} (e.g. Melvold & Hagen 1998; Etzelmüller et al. 2000; Hagen et al. 2003a; Sund & Eiken 2004; Neumann 2006; Mavlyudov 2010). Here it needs underlining that mass loss of Svenbreen observed in the last decades reduced its thickness considerably. According to Glen's flow law (section 2.5.1) flow velocity is strictly dependant on ice thickness (eq. 2.10), so Svenbreen must have been flowing at a significantly faster rate than at present, implying greater dynamics of sediment transport and relief remodelling.

The earliest observations of Slater (1925) revealed a completely different character of the glacier than it is at present. In these times the Svenbreen's front has been surpassing the riegel (figs. 5.4 and 5.7), steeply flowing downwards to the present moraine zone, hence showing great motion dynamics. The front zone was covered with a dense network of active thrust planes and contained significant amounts of sediments, composing multiple on-ice heaps. In response to the warming climate, since early-20th century Svenbreen has been continuously losing mass and retreating (section 5.2.1), producing a 1.5 km long marginal zone. It was generally formed until 1960, during rapid disintegration of the snout, with later remodelling by melting of ice-cores and action of proglacial waters. Detailed field investigations during summer of 2011 made it possible to sketch the main features of the present-day forefield geomorphology (fig. 8.7). From the north, south and east it is closed by huge terminal and lateral moraines, marking the maximum LIA extent. Inside of these boundaries three distinct landforms dominate: a complex of ice-cored hummocky moraine with multiple kettles, an inner outwash plain and washed-out remnants of an esker of uncertain origin (Karczewski & Kłysz 1994).

Diversity of the moraine zone stays in contrast to present-day front of Svenbreen, which is almost inactive. In accordance to radar investigations temperate bed conditions beneath Svenbreen are to be found only along the main axis of the valley, up-glacier from stake S30 (section 7.1.2), as shown in fig. 8.8. Stakes lying above temperate bed in the lower glacier section (S30-S50) move at average speed of 1.1-1.3 m a^{-1}, while stakes in the frontal zone are almost stagnant (section 5.2.3). Different ice velocities are also clearly visible from the foliations' pattern, as they are heavily distorted above temperate base, possibly due to enhanced sliding. On the surface, close to the zone where faster ice meets frontal part, frozen to its bed, a dense network of discontinuous thrust faults has developed in response to increased compressive stresses. A similar situation was found e.g. on Werenskioldbreen. With this glacier as an example, Baranowski (1977) and Bukowska-Jania & Jania (1988) presented general motion mechanisms of polythermal land terminating glaciers in Svalbard. Baranowski argued that at contact of active temperate mass with a cold frontal ice intensive thrusting occurs from the bed up to the surface. Bukowska-Jania and Jania modified his model, with thrusting occurring not at ice-bed interface, but at cold-temperate transition surface, to explain

lack of sediments along thrust faults on Werenskioldbreen. Observations from Svenbreen gave an opportunity to validate both concepts.

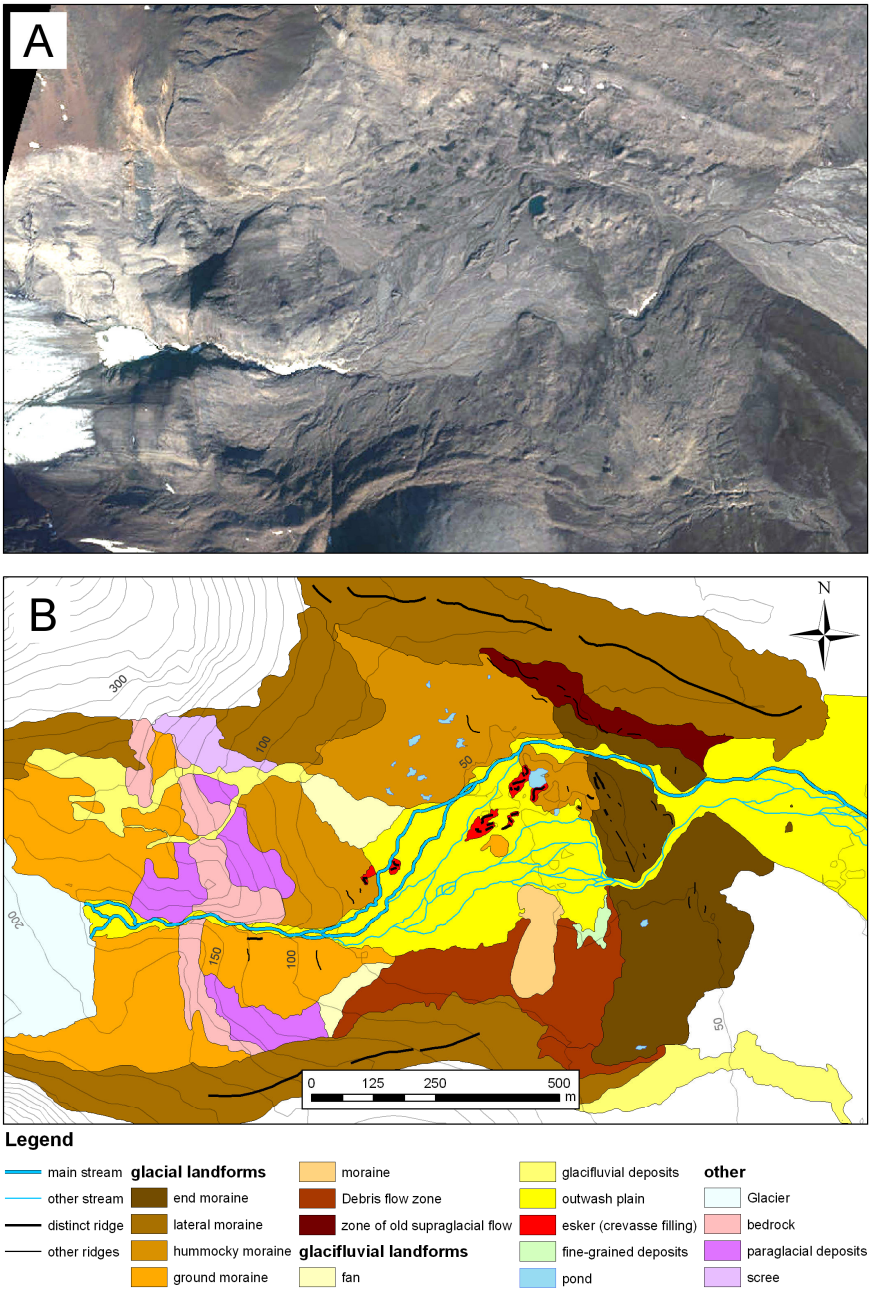

Fig. 8.7 A - Orthorectified aerial image of Svenbreen moraine zone (July 2011, courtesy of 'TopoSvalbard' by Norsk Polarinstitutt); B - Geomorphological sketch of the same area based on direct fieldworks by M. Ewertowski, A. Tomczyk and J. Małecki. Contour lines (2009) every 25 m

Similarly as on Werenskioldbreen, shear planes in the lower sections of Svenbreen show no sediment filling (fig. 8.9). Instead, only short debris bands parallel to general ice flow direction occur at the front. However, debris transportation to the surface is clearly visible on the radargram from longitudinal GPR transect (section 7.2, fig. 7.4). In opposition to Baranowski's model, traces of sediment up-lift are not focused at a point of transition from temperate to cold bed, but are elongated at a distance of ~500 m. With mostly debris-free shear planes the other model by Bukowska-Jania and Jania becomes advantageous.

Observations of recently exposed large sedimentary boulders at S20 also do not reject their concept. Petrography of the lower section of the valley is composed of dark Hecla Hoek metamorphic rocks, implying that the exposed soft blocks origin from the glacier cirque. They must have been transported englacially, as indicated by unchanged angular shape of the largest blocks, hence they could not be incorporated from basal sections.

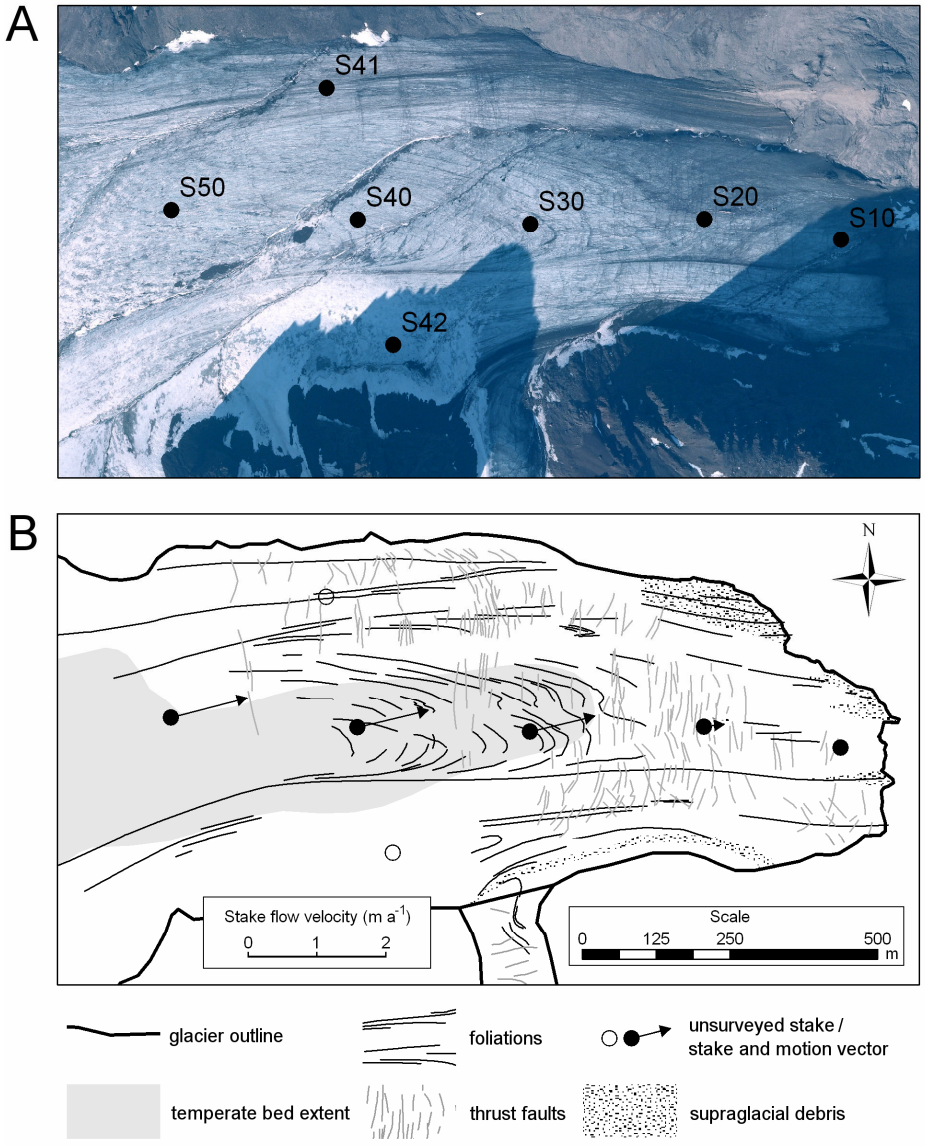

Fig. 8.8 A - aerial image of Svenbreen front zone (July 2009, courtesy of 'TopoSvalbard' by Norsk Polarinstitutt) with ablation stake positions; B - structure of the Svenbreen frontal ice, with foliations and thrust faults against thermal state of the bed. Note heavily distorted foliations above temperate ice and faults on cold front zone

Formation of new landforms at the actual front is vastly limited: melting ice accumulates a thin cover of deposits as a ground moraine in the northern part of the snout, while in its central zone a small medial moraine produces a 0.5 m high longitudinal ridge composed of ice and angular unsorted deposits (fig. 8.9). In the background of the discussion above, negligible diversity of present-day geomorphological processes at the front may be fully explained by low front dynamics due to negative changes of glacier physical properties.

Fig. 8.9 Panorama of Svenbreen front and its poorly diversified nearest forefield (on 19/08/2010) taken from the riegel. Note thrust planes and foliations underlined by fresh snow. Short medial moraine is in the middle of the picture. To the very right: an on-icing pitted outwash plain, a lateral moraine and a well-defined LIA trimline on the neighbouring slopes

In the system of retreating Svenbreen, the greatest geomorphological impact plays the proglacial water flow, by both washout of older landforms, as well as sediment transfer and its later accumulation. Washout is well visible in Svenbreen's marginal zone, where a large patch of inner outwash plain has developed by removing older hummocks. The same applies to disintegration of the former esker, almost completed in the last two decades (fig. 8.7). Sediments from glacier-covered basins in the study area are partly deposited on outwash plains and partly delivered to Billefjorden. Intensive downwasting of ice masses is well reflected in sediment accumulation rates in the fjord's bottom. For Billefjorden mean modern sediment accumulation rate was estimated as 10 times higher than during the LIA (Szczuciński et al. 2009), underlining wider impacts of a glacier decay. In a local scale, sediment transport and deposition may lead to formation or remodelling of individual landforms. As an example, deposition of fluvioglacial debris on the icing field is a fundamental contribution to formation of a small patch of a pitted outwash plain located between the present front and the canyon. Proximity of the glacier portal and geometric configuration of the surrounding topography drive a peculiar cycle of its evolution: it is alternately exposed for one or more years and buried (preserved) by a new icing (section 7.2.2, fig. 7.17). It is the zone showing the greatest dynamics of changes, controlled primarily by glacier's hydrological conditions and sediment availability, instead of degradation of its ice-core, as is the case of hummocks at the foot of the riegel.

Due to negative changes of glacier physical properties (i.e. mass, thickness, length, velocity) the glacier forefield has been shaped with a gradually decreasing diversity. Present-day properties of the glacier are insufficient to maintain high geomorphological activity, so no new distinct landforms are to be found in the closest front proximity. At this point, an important problem arises, concerning the future trends of Svenbreen evolution.

8.4 Trends of changes of physical properties of Svenbreen

Results of detailed investigations on Svenbreen presented in this work provide an insight into past and present-day state of the glacier. Also, the data give a sufficiently wide spectrum of recognized regularities to conclude about its general future behaviour. Since early 1900's it

has been decreasing its mass, thickness, length, velocity and most likely overall ice temperature. It may be directly linked to climate change, manifested in Svalbard as a distinct overall air temperature rise in the 20th and 21st centuries (section 3.1). Warming is predicted to continue in this sector of the Arctic in the coming decades (Benestad et al. 2002; Førland et al. 2012). As showed in section 8.1.2.3, summer balance is proportional to air temperature, so further warming will accelerate surface ablation. Winter balance evolution may not be predicted from the presented data alone. Model studies suggest increased precipitation in the Arctic in response to rising air temperature, but direct Svalbard observations of precipitation and winter balance on glaciers suggest no trend or even a certain decrease recently (Førland & Hanssen-Bauer 2003; Barrand et al. 2010). In any case, it seems justified to state that negative post-LIA changes of physical properties of Svenbreen will most likely continue in the coming years, although will be less pronounced than on other small glaciers in the archipelago. Front retreat to higher (cooler) sections of the valley is very slow and stable, while the bedrock is even, so only a modest acceleration of the retreat rate is expected in the coming 1-2 decades. Thermal structure of Svenbreen is likely to eventually turn to cold-based, as proposed for neighbouring Bertilbreen (Gokhman 1987a,b) and observed on e.g. Scott Turnerbreen (Hodgkins et al. 1999), but the glacier is still relatively thick along its main axis, so this process will be longer than on both glaciers mentioned. Formation of icing fields has been experiencing some fluctuations in the last years, interpreted as its gradual cessation, but further observations are needed to confirm this hypothesis. Increased melting will lead to greater runoff from the basin in the next decades and its decrease after the glacier reaches a certain critical size. Flow dynamics will progressively decline due to glacier thinning and decay of temperate bed. Englacial debris will steadily melt out from ice, forming thin sediment covers on the ground with poor relief diversity, later washed out by proglacial rivers.

9

Conclusions and research perspectives

Svenbreen, a small valley glacier from the interior of Svalbard, was a subject of detailed glaciological studies between 2009 and 2012. Their aim was to investigate response of a small glacier to climate change in an arid, quasi-continental region underrepresented in the literature - Dickson Land. This work also aimed to bring basic data, first from this area, which could be found interesting for wider scientific community, representing glaciology, hydrology, geomorphology, climatology and other sciences, e.g. ecology. Techniques from many fields of glaciological research were used: mass balance investigations, geometry change measurements, energy balance monitoring, radar surveys and others. The major findings of this work are as follows:

- The study confirmed that small glaciers are excellent indicators of contemporary landscape changes in polar areas. Similarly as other ice masses in Svalbard, Svenbreen is in a negative mass balance mode and has been experiencing mass loss in the 20th century, resulting in a well pronounced change of its extent. However, it has shown a very clear individuality with respect to other small Svalbard glaciers. Its present-day state, functioning pattern and behaviour in response to climatic impulses are clearly unique and result from peculiar climatic conditions, fundamentally modified by local environmental factors.

- The factor having the greatest impact on the observed state and functioning of Svenbreen is geometry of its valley, as it shapes vertical extent of the glacier and insolation regime of its individual parts. It also directly impacts exposition to prevailing wind directions and snow-drift. Bedrock relief fundamentally influences glacier dynamics and deglaciation process.

- Arid climate of central Spitsbergen is significantly modified above Svenbreen due to influence of complex topography and other factors. In result, a peculiar glacier topoclimate is formed, unique in scale of Svalbard. During summer periods, warmer than elsewhere in Svalbard, air temperature declines fast with elevation, from average of ~6°C at the sea-level to 2-3°C in the middle ablation zone of the glacier. Dry

adiabatic lapse rates of -1°C · 100 m^{-1} are typical for Svenbreen. Average wind velocity is among the lowest from Svalbard glaciers (~1.5 m s^{-1}). Relative humidity and air vapour pressure are limited (respectively ~80% and ~600 Pa) and incoming shortwave radiation is very low (140 W m^{-2}).

- Individuality of the glacier's topoclimate influences unique surface energy balance conditions of Svenbreen. Overall melt energy on Svenbreen, measured during the summer of 2012, was very low (25 W m^{-2}), similarly as all its components: net radiation (21 W m^{-2}), sensible heat flux (7 W m^{-2}) and latent heat flux (-2 W m^{-2}). On other Svalbard glaciers these figures are much higher, typically with ~50 W m^{-2}, ~12 W m^{-2} and ~2 W m^{-2}, respectively for net radiation, sensible and latent heat fluxes.

- Mass balance components are governed by local topoclimate peculiarities. Winter balance is higher than on other central Spitsbergen glaciers, likely due to intensive snow-drift. Summer balance is less negative than elsewhere, as revealed by direct measurements and temperature index 1976-2012 modelling.

- In result, mass loss of Svenbreen is greatly reduced, making it considerably more resistant to a warming climate than other glaciers in its neighbourhood and in the whole archipelago. Direct observations of mass budget suggest, that positive net balance years are rather normal for the glacier, as they occurred twice during short period between 2008 and 2012. Relatively slow mass loss is also suggested by energy balance (low melt energy) and geometry change studies (low long-term thinning rate of -43 cm a^{-1}, with average for the region of -61 cm a^{-1}).

- Climate warming observed in Svalbard since early 20th century had a fundamental impact on the present-day state of Svenbreen. Despite greater resistance to warming, the glacier has lost 34% of its LIA area and 28% of its maximum length.

- The present-day volume of the glacier is 0.22 km^3 (2009-2011). Since 1960 it has decreased by 28%, but the regional average is significantly higher (roughly 39%). Similarly as other studied glaciers, Svenbreen sharply accelerated its thinning after 1990, from -32 to -61 cm a^{-1}, due to rising air temperature. Its thinning rate is however still lower than of other ice masses in the area.

- In contrast to most of small Svalbard glaciers, Svenbreen is still polythermal, as revealed by GPR study. Lack of cold/temperate transition surface on radargrams is interpreted as a sign of low thickness of temperate basal layer. The surface layer is cold, with 8 m ice temperature of about -4.5°C. Radar data suggests that a small isolated patch of temperate firn has survived at least 5 decades of negative mass balance.

- Due to cold surface layer and only few narrow cracks on the surface, most of water is drained supraglacially. Intraglacial drainage is active and is confirmed by radar survey and observations of proglacial discharge. Annual runoff from Svenbreen basin (700-750 mm) is lower than from other similar catchments in Svalbard, reflecting quasi-continental climate of Dickson Land.

- Episodic formation of new icing fields is interpreted as a variability of winter discharge volume and hence a sign of the ongoing changes in hydrothermal regime of

Svenbreen. Likely, the temperate core of the glacier is freezing, although further observations are needed.

- Retreat of the glacier formed a 1.5 km long moraine zone. Geomorphological activity of the front has been however decreasing in the last decades. At present, ice motion is slow, with maximum velocity of 3.2 m a^{-1} close to the ELA and less than 0.5 m a^{-1} close to the front. Generally low activity of Svenbreen, as well as its stagnant front are the reasons that no distinct new landforms are formed in the forefield since ~1960.

- Negative changes of physical properties of Svenbreen are predicted to continue and accelerate in response to further climate warming. Its impact will be however less pronounced than on other small glaciers in Svalbard.

- Limitations of the study are associated with data errors and interpretation difficulties. Accuracy of fundamental parameters given in the work are within ± 17-19 cm a^{-1} for glacier-wide thinning rates of Svenbreen (being relatively high, with 28-59% of the estimated value), ± 7 cm a^{-1} for flow velocities, ± 10 cm w.eq. for winter balance, ± 15 cm w.eq. for summer balance and ± 18 cm w.eq. for net balance. Interpretation uncertainties apply mainly to the issues related to the thermal regime of the glacier. Results of the GPR investigations are unambiguous in some aspects.

Svenbreen is a unique Svalbard glacier, where the influence of local factors is extremely well visible in its response to climate change. This work provides a fundamental dataset for this glacier, but also rises many new questions. Comparison of Svenbreen with a greater sample of Dickson Land glaciers will help to recognize its unique character and the overall mass balance of the region. Revision of thinning rates of Svenbreen with higher-resolution data would be of great use for precise geodetic mass balance assessments. Continuation of direct glacier monitoring programme will bring more data on climate-glacier interactions and will make it possible to validate the concepts presented in this work. Rather a qualitative research on thermal evolution of the glacier should encourage for more detailed studies. Ideally, boreholes drilled down to the bed, together with surveys using different GPR antenna frequencies would give a more comprehensive view of the glaciers thermal structure, particularly in the probable firn patch. In the background of Svenbreen's thermal structure, the issue of its potential speed-ups in response to increased meltwater penetration seems to be very interesting and could be resolved with a continuous, automatic GPS monitoring system. Tracing experiments and investigations of water chemistry and sediment load would bring new light on the issue of intraglacial drainage of Svenbreen under changing mass balance and hydrothermal conditions. Interannual volume fluctuations of proglacial icings were observed from year to year and finding their driving mechanisms is a challenge for the next seasons. Finally, after obtaining longer datasets, modelling studies of glacier-wide energy balance, mass balance, hydrology and dynamics would be of the greatest value, as they are a perfect tool to comprehensively validate the gained knowledge and to extend the data to the past and the future.

Appendix

Tab. A1 Direct air temperature record from Svenbreen (S60, 358 m a.s.l.)

	2011										2012						
Date	**May**	**Jun**	**Jul**	**Aug**	**Sep**	**Oct**	**Nov**	**Dec**	**Jan**	**Feb**	**Mar**	**Apr**	**May**	**Jun**	**Jul**	**Aug**	**Sep**
1	-2.6	2.3	2.7	3.2	2.1	-4.5	-16.0	-5.7	-6.1	-4.0	-9.9	-17.9	-7.0	-1.9	2.1	4.2	1.6
2	-2.0	0.5	3.8	2.5	3.5	1.0	-14.4	-11.0	-2.3	-7.3	-17.5	-17.6	-10.6	-0.2	3.2	2.5	2.7
3	-2.9	-0.6	3.4	2.8	2.7	-1.6	-11.7	-11.5	-2.3	-6.0	-11.8	-18.2	-8.2	-2.9	2.6	2.5	2.6
4	-11.7	0.1	3.4	2.7	3.6	-4.7	-8.1	-16.9	-4.0	-6.2	-1.0	-16.6	-4.2	-2.1	2.1	1.6	1.8
5	-10.3	-0.1	1.9	2.9	4.6	-6.7	0.6	-18.8	-7.6	-1.6	-0.3	-21.3	-4.8	-1.6	2.1	1.3	0.5
6	-2.1	1.5	2.0	3.4	2.8	-9.4	1.5	-16.3	-10.6	-3.9	-2.9	-16.8	-5.2	-0.9	2.3	1.6	0.5
7	-1.0	0.1	2.9	3.5	3.0	-9.6	-0.1	-11.3	-15.2	-2.9	-4.2	-13.6	-9.6	0.1	2.7	2.4	0.5
8	-3.2	0.3	3.5	3.2	3.3	-11.9	-7.5	-5.2	-15.9	0.2	-2.8	-15.1	-11.4	-1.6	2.5	2.8	0.2
9	-8.9	0.5	5.4	2.8	3.3	-12.5	-9.7	-7.9	-11.4	-5.5	-2.3	-14.8	-7.3	0.7	1.4	3.6	0.2
10	-11.0	0.6	6.0	0.7	5.2	-11.2	-11.1	-11.8	-8.9	-14.7	-5.3	-13.1	-4.6	-0.7	1.4	5.0	-1.4
11	-10.3	1.1	5.2	0.4	3.1	-7.2	-11.2	-13.6	-6.0	-16.0	-10.3	-12.9	-5.8	-0.1	1.9	2.9	n/d
12	-4.1	2.8	2.5	1.3	2.1	-7.0	-4.9	-7.8	-8.2	-14.7	-10.6	-14.6	-4.6	-1.0	3.0	2.8	n/d
13	-2.2	3.9	3.1	3.1	-1.7	-7.3	-17.2	-9.4	-11.1	-17.4	-12.5	-13.4	-6.2	0.4	2.3	2.5	n/d
14	-0.9	4.4	2.7	2.9	1.3	-6.5	-18.1	-9.9	-6.2	-18.4	-15.2	-14.1	-7.4	1.3	3.0	2.0	n/d
15	-6.9	4.0	3.5	4.4	4.5	-2.4	-18.3	-10.1	-1.5	-18.5	-12.8	-14.6	-8.2	2.0	4.3	1.9	n/d
16	-12.6	2.6	2.9	7.6	2.0	-5.3	-8.3	-2.8	-8.0	-21.7	-5.0	-16.9	-10.0	1.8	2.0	1.6	n/d
17	-11.4	2.4	2.8	9.1	-1.4	-7.4	-11.5	-4.0	-4.3	-9.5	-6.0	-15.7	-7.6	1.0	0.9	1.2	n/d
18	-9.3	1.9	3.8	10.0	-2.3	-9.4	-14.7	-8.3	-4.6	-3.3	-11.4	-18.0	-3.5	1.3	1.0	1.8	n/d
19	-8.8	1.8	5.2	8.5	2.2	-7.8	-14.8	-7.9	-2.6	-5.5	-13.0	-16.6	-2.6	3.0	2.1	2.1	n/d
20	-7.6	2.4	4.9	7.2	1.3	-3.3	-9.8	-12.4	-5.0	-6.6	-12.8	-17.7	-4.0	2.8	3.9	1.3	n/d
21	-6.9	3.1	4.8	5.0	0.3	-5.7	-3.3	-14.0	-10.9	-12.2	-15.4	-18.6	-6.4	1.5	4.9	-0.1	n/d
22	-5.2	3.3	4.8	5.4	2.5	-6.9	0.0	-5.6	-11.2	-12.3	-16.0	-12.6	-3.9	1.1	5.5	-0.1	n/d
23	-3.2	2.6	3.1	3.6	1.6	-4.5	-2.6	-2.1	-15.2	-13.9	-10.4	-9.1	-1.7	1.8	3.7	-0.4	n/d
24	-1.9	2.4	3.3	3.0	1.4	-0.2	-6.2	-0.8	-13.9	-10.8	-12.1	-5.7	-0.2	0.9	3.4	0.4	n/d
25	-5.3	2.8	4.2	3.8	1.5	-5.2	-13.6	-6.1	-14.9	-9.8	-20.4	-6.8	-3.6	1.0	3.3	0.2	n/d
26	-5.6	4.0	4.9	2.8	2.4	-5.4	-15.1	-4.5	-4.4	-13.9	-14.6	-5.9	-3.7	0.4	2.2	1.5	n/d
27	-1.0	2.9	2.5	3.2	0.5	0.2	-15.4	-8.8	0.7	-14.6	-7.4	-7.6	-4.3	0.4	2.2	2.1	n/d
28	-0.6	3.8	2.7	1.6	0.7	1.0	-18.2	-18.2	-4.4	-7.2	-7.9	-8.3	-4.7	0.8	2.7	2.5	n/d
29	0.5	2.5	5.0	0.9	-2.3	-0.3	-12.0	-20.8	-0.6	-5.8	-13.1	-13.0	-5.0	1.3	3.1	3.5	n/d
30	2.2	3.1	3.7	1.2	-4.2	-9.7	-7.1	-22.5	0.5		-10.9	-10.1	-5.1	1.1	2.5	4.6	n/d
31	3.0		3.9	1.1		-16.6		-16.4	-1.8		-16.6		-2.2		2.3	5.6	n/d
Mean	**-5.0**	**2.1**	**3.7**	**3.7**	**1.7**	**-6.1**	**-10.0**	**-10.4**	**-7.0**	**-9.8**	**-10.1**	**-13.9**	**-5.6**	**0.4**	**2.7**	**2.2**	**0.9***

*1-10/09

Tab. A2 Surface energy balance at S60 (358 m a.s.l.) in April 2012 as averaged from hourly values

Date	T_a °C	RH %	e_a Pa	u m s^{-1}	SW_{in} W m^{-2}	SW_{out} W m^{-2}	SW_{bal} W m^{-2}	α %	LW_{in} W m^{-2}	LW_{out} W m^{-2}	LW_{bal} W m^{-2}	Q_N W m^{-2}	Q_H W m^{-2}	Q_L W m^{-2}	Q_M W m^{-2}
4-01	-17.9	83.4	123	3.4	80	65	15	82%			-22	-7.8			
4-02	-17.6	87.1	130	1.6	71	60	11	84%			-50	-39			
4-03	-18.2	74.9	107	2.5	97	81	17	83%			-52	-35			
4-04	-16.6	76.6	126	4.0	111	90	21	81%			-57	-36			
4-05	-21.3	86.5	93	2.1	97	79	19	81%			-55	-36			
4-06	-16.8	94.2	158	2.2	132	99	33	75%			-60	-26			
4-07	-13.6	85.7	177	1.6	142	113	29	80%			-46	-17			
4-08	-15.1	83.6	151	2.0	142	111	31	78%			-66	-34			
4-09	-14.8	89.9	168	1.3	115	90	25	78%			-56	-31			
4-10	-13.1	82.2	177	1.7	130	105	25	81%			-62	-37			
4-11	-12.9	82.9	181	2.0	141	112	28	80%			-68	-39			
4-12	-14.6	86.1	166	1.7	138	113	25	82%			-58	-32			
13-04	-13.4	91.0	193	1.4	110	94	15	86%			-36	-21			
14-04	-14.1	87.5	171	1.2	115	97	18	85%			-58	-40			
15-04	-14.6	85.2	162	1.2	127	107	21	84%			-62	-41			
16-04	-16.9	84.0	129	1.4	151	120	31	80%			-45	-14			
17-04	-15.7	82.5	142	1.4	138	108	31	78%			-38	-7.5			
18-04	-18.0	80.5	113	2.1	183	142	41	78%			-71	-30			
19-04	-16.6	76.5	121	1.5	180	143	37	79%			-39	-2.1			
20-04	-17.7	90.5	132	1.4	140	115	25	82%			-71	-46			
21-04	-18.6	88.0	118	2.2	181	141	41	78%			-73	-33			
22-04	-12.6	80.7	179	2.0	163	131	33	80%			-61	-28			
23-04	-9.1	76.4	229	1.7	183	145	39	79%			-41	-2.9			
24-04	-5.7	80.2	309	1.8	157	130	28	82%			-37	-9.3			
25-04	-6.8	71.6	254	2.9	208	162	45	78%			-58	-13			
26-04	-5.9	67.1	258	3.0	160	130	30	81%			-32	-2.4			
27-04	-7.6	84.0	275	1.3	174	140	34	81%			-46	-12			
28-04	-8.3	84.0	266	1.6	192	154	39	80%			-45	-5.7			
29-04	-13.0	88.8	194	2.1	192	155	36	81%			-41	-5.0			
30-04	-10.1	81.2	218	1.3	191	159	32	83%			-40	-8.4			
Mean	**-13.9**	**83.1**	**174**	**1.9**	**145**	**116**	**28**	**81%**			**-52**	**-23**			

Tab. A3 Surface energy balance at S60 (358 m a.s.l.) in May 2012 as averaged from hourly values

Date	T_a °C	RH %	e_a Pa	u m s^{-1}	SW_{in} W m^{-2}	SW_{out} W m^{-2}	SW_{bal} W m^{-2}	α %	LW_{in} W m^{-2}	LW_{out} W m^{-2}	LW_{bal} W m^{-2}	Q_N W m^{-2}	Q_H W m^{-2}	Q_L W m^{-2}	Q_M W m^{-2}
5-01	-7.0	88.3	298	0.9	151	134	17	89%			-74	-57			
5-02	-10.6	91.5	240	2.8	165	142	23	86%			-30	-6.6			
5-03	-8.2	83.8	256	0.4	203	168	35	83%			-52	-17			
5-04	-4.2	81.0	339	1.0	202	165	37	82%			-53	-16			
5-05	-4.8	90.1	360	0.6	174	145	29	83%			-32	-3.5			
5-06	-5.2	85.6	327	0.4	179	150	29	84%			-30	-0.8			
5-07	-9.6	83.7	233	1.6	244	193	52	79%			-41	10			
5-08	-11.4	81.4	190	1.8	275	213	62	77%			-66	-4.0			
5-09	-7.3	80.0	258	1.3	268	209	59	78%			-54	5.5			
5-10	-4.6	76.3	312	1.5	212	172	39	81%			-38	1.4			
5-11	-5.8	75.6	291	2.3	241	196	45	82%			-54	-9.4			
5-12	-4.6	70.7	302	3.1	180	154	26	85%			-33	-6.3			
13-05	-6.2	72.2	264	2.0	288	224	64	78%			-72	-7.9			
14-05	-7.4	63.3	204	2.0	318	244	73	77%			-89	-16			
15-05	-8.2	74.1	233	2.0	278	218	60	78%			-78	-18			
16-05	-10.0	74.7	195	1.8	319	243	75	76%			-84	-8.3			
17-05	-7.6	77.9	248	1.9	323	247	76	77%			-79	-3.4			
18-05	-3.5	76.4	340	1.6	230	189	42	82%			-36	5.8			
19-05	-2.6	71.4	355	3.4	174	148	26	85%			-22	4.1			
20-05	-4.0	73.7	323	3.3	277	215	62	78%			-55	7.4			
21-05	-6.4	79.8	277	1.9	303	231	73	76%			-75	-2.6			
22-05	-3.9	80.2	341	0.9	194	159	35	82%			-23	12			
23-05	-1.7	84.7	446	2.2	196	171	26	87%			-58	-32			
24-05	-0.2	90.0	500	1.0	209	175	33	84%			-76	-42			
25-05	-3.6	91.0	411	1.8	231	187	44	81%			-45	-1.4			
26-05	-3.7	80.3	347	1.0	208	171	37	82%			-38	-0.5			
27-05	-4.3	77.5	326	2.8	315	253	62	80%			-74	-12			
28-05	-4.7	78.8	334	4.3	246	209	37	85%			-24	13			
29-05	-5.0	75.3	313	4.9	229	194	35	85%			-22	13			
30-05	-5.1	73.1	301	3.9	222	185	37	83%			-26	11			
31-05	-2.2	78.5	392	2.1	246	211	34	86%			-33	1.1			
Mean	**-5.6**	**79.4**	**308**	**2.0**	**235**	**191**	**45**	**82%**			**-50**	**-5.8**			

Tab. A4 Surface energy balance at S60 (358 m a.s.l.) in June 2012 as averaged from hourly values

Date	T_a °C	RH %	e_a Pa	u m s^{-1}	SW_{in} W m^{-2}	SW_{out} W m^{-2}	SW_{bal} W m^{-2}	α %	LW_{in} W m^{-2}	LW_{out} W m^{-2}	LW_{bal} W m^{-2}	Q_N W m^{-2}	Q_H W m^{-2}	Q_L W m^{-2}	Q_M W m^{-2}
6-01	-1.9	83.5	417	1.9	285	228	57	80%			-64	-6.5			
6-02	-0.2	84.2	466	0.9	229	187	42	82%			-57	-15			
6-03	-2.9	87.7	413	1.7	244	199	45	82%			-47	-2.5			
6-04	-2.1	84.9	400	0.9	287	216	71	75%			-48	23			
6-05	-1.6	86.3	452	2.3	231	183	48	79%			-39	9.5			
6-06	-0.9	87.8	471	1.8	349	250	99	72%			-92	7.1			
6-07	0.1	79.4	451	1.0	261	190	72	73%			-46	26			
6-08	-1.6	84.2	436	2.5	292	212	79	73%			-72	6.8			
6-09	0.7	76.6	430	0.5	352	245	106	70%			-88	19			
6-10	-0.7	80.8	419	0.9	331	236	95	71%			-91	3.8			
6-11	-0.1	81.2	437	0.8	345	236	110	68%			-61	49			
6-12	-1.0	84.4	456	1.8	270	195	75	72%			-48	27			
13-06	0.4	80.5	462	0.8	272	196	76	72%			-41	35			
14-06	1.3	85.7	538	0.8	218	161	58	74%			-53	4.2			
15-06	2.0	79.5	513	1.1	318	215	103	68%	257	316	-59	44	2.2	-2.6	434
16-06	1.8	81.6	528	1.4	304	214	90	70%	256	316	-60	31	2.6	-4.2	29
17-06	1.0	86.4	536	1.1	201	142	59	71%	290	316	-26	33	1.5	-1.0	33
18-06	1.3	84.5	515	1.1	328	212	117	64%	259	316	-57	60	1.5	-0.7	61
19-06	3.0	81.5	598	1.5	136	97	39	71%	267	316	-48	-10	7.6	-0.1	-2.0
20-06	2.8	89.4	645	1.6	141	102	39	72%	282	316	-34	5.0	8.3	2.1	15
21-06	1.5	82.1	539	2.2	261	176	85	68%	280	316	-36	49	7.9	-4.6	52
22-06	1.1	87.8	563	1.4	139	102	37	74%	281	316	-34	2.7	3.2	-0.9	4.9
23-06	1.8	88.8	594	1.3	161	115	47	71%	296	316	-20	27	4.0	0.0	31
24-06	0.9	82.7	527	2.4	203	139	63	69%	267	316	-49	15	4.3	-11	8.3
25-06	1.0	76.3	467	1.3	264	190	74	72%	251	316	-65	9.2	2.5	-3.9	7.9
26-06	0.4	82.5	490	1.3	248	194	54	78%	246	316	-70	-16	2.2	-5.7	-20
27-06	0.4	81.2	474	1.1	224	172	53	77%	268	316	-47	5.1	0.0	-3.2	2.0
28-06	0.8	86.4	534	1.7	194	148	46	76%	260	316	-55	-9.1	1.4	-5.9	-14
29-06	1.3	80.5	522	2.0	234	159	74	68%	253	316	-63	12	6.8	-8.7	9.7
30-06	1.1	73.2	444	1.6	361	237	124	66%	217	316	-99	25	1.4	-5.5	21
Mean	**0.4**	**83.0**	**491**	**1.4**	**256**	**185**	**71**	**73%**	**n/d**	**n/d**	**-56**	**16**	**n/d**	**n/d**	**n/d**
Mean*	**1.4**	**82.8**	**531**	**1.5**	**232**	**163**	**69**	**71%**	**264**	**316**	**-51**	**18**	**3.6**	**-3.5**	**18**

*15/06-30/06

Tab. A5 Surface energy balance at S60 (358 m a.s.l.) in July 2012 as averaged from hourly values

Date	T_a °C	RH %	e_a Pa	u m s^{-1}	SW_{in} W m^{-2}	SW_{out} W m^{-2}	SW_{bal} W m^{-2}	α %	LW_{in} W m^{-2}	LW_{out} W m^{-2}	LW_{bal} W m^{-2}	Q_N W m^{-2}	Q_H W m^{-2}	Q_L W m^{-2}	Q_M W m^{-2}
7-01	2.1	76.7	506	1.5	329	215	115	65%	247	316	-69	46	3.1	-3.9	45
7-02	3.2	76.4	567	1.8	235	159	76	68%	292	316	-24	53	12	-1.4	63
7-03	2.6	95.5	687	1.4	101	73	28	72%	308	316	-8.1	20	4.6	2.9	28
7-04	2.1	92.0	635	2.2	155	107	48	69%	293	316	-22	25	10	1.4	37
7-05	2.1	86.8	588	1.4	194	129	65	66%	293	316	-22	43	6.1	0.6	49
7-06	2.3	72.1	518	4.6	152	102	51	67%	282	316	-33	17	23	-22	18
7-07	2.7	71.5	512	2.4	182	121	62	66%	283	316	-32	29	14	-8.3	36
7-08	2.5	72.3	514	2.4	272	171	101	63%	266	316	-49	51	16	-9.0	59
7-09	1.4	81.5	540	3.4	165	109	56	66%	284	316	-31	25	13	-12	27
7-10	1.4	82.8	547	2.4	197	129	68	65%	280	316	-36	32	8.6	-6.7	34
7-11	1.9	82.4	548	1.7	261	163	98	63%	284	316	-32	66	6.1	-2.3	70
7-12	3.0	85.1	616	1.4	186	121	65	65%	305	316	-10	55	5.3	0.8	61
13-07	2.3	88.5	607	0.9	194	125	69	65%	289	316	-26	42	1.4	0.3	44
14-07	3.0	86.1	621	1.6	289	175	114	61%	263	316	-53	61	7.0	1.1	69
15-07	4.3	81.7	651	1.7	250	159	90	64%	259	316	-56	34	12	3.2	49
16-07	2.0	83.7	567	1.7	238	147	91	62%	273	316	-42	49	7.7	-1.9	55
17-07	0.9	83.1	523	1.2	135	100	35	74%	254	316	-61	-26	1.5	-2.3	-27
18-07	1.0	87.4	553	0.9	125	88	37	70%	288	316	-27	10	0.0	-1.3	8.6
19-07	2.1	89.2	616	1.3	143	93	50	65%	312	316	-3.2	47	5.1	0.9	53
20-07	3.9	82.3	633	1.3	232	138	94	59%	273	316	-43	52	3.2	0.8	56
21-07	4.9	75.8	639	1.9	249	145	104	58%	283	316	-33	71	17	4.3	92
22-07	5.5	88.1	778	2.2	129	80	49	62%	293	316	-23	26	21	11	58
23-07	3.7	94.0	735	1.9	95	59	36	62%	302	316	-14	22	14	8.0	44
24-07	3.4	89.6	679	1.4	147	87	60	59%	287	316	-28	32	7.1	2.7	42
25-07	3.3	91.1	688	1.0	98	58	40	59%	307	316	-8.6	32	2.9	1.1	36
26-07	2.2	94.7	658	0.8	123	71	53	57%	288	316	-28	25	1.2	0.5	27
27-07	2.2	92.7	647	1.2	102	57	45	56%	294	316	-22	23	3.8	2.0	29
28-07	2.7	94.2	685	1.3	102	53	49	52%	296	316	-20	30	5.2	3.0	38
29-07	3.1	90.1	681	2.5	99	51	48	52%	298	316	-17	31	19	6.3	55
30-07	2.5	82.6	598	3.9	122	55	67	45%	270	316	-46	21	25	-3.5	42
31-07	2.3	84.8	594	1.4	155	78	77	50%	285	316	-31	46	4.9	0.0	51
Mean	**2.7**	**85.0**	**611**	**1.8**	**176**	**110**	**66**	**62%**	**285**	**316**	**-31**	**35**	**9.0**	**-0.8**	**43**

Tab. A6 Surface energy balance at S60 (358 m a.s.l.) in August 2012 as averaged from hourly values

Date	T_a °C	RH %	e_a Pa	u m s^{-1}	SW_{in} W m^{-2}	SW_{out} W m^{-2}	SW_{bal} W m^{-2}	α %	LW_{in} W m^{-2}	LW_{out} W m^{-2}	LW_{bal} W m^{-2}	Q_N W m^{-2}	Q_H W m^{-2}	Q_L W m^{-2}	Q_M W m^{-2}
8-01	4.2	82.8	662	1.6	189	100	89	53%	275	316	-40	49	7.7	2.0	59
8-02	2.5	97.5	700	1.2	76	40	37	52%	306	316	-9.4	27	3.4	2.3	33
8-03	2.5	92.5	664	0.9	83	43	40	51%	297	316	-19	21	0.6	0.2	22
8-04	1.6	89.4	605	1.3	85	43	43	50%	302	316	-14	29	4.2	0.2	33
8-05	1.3	85.2	562	1.2	97	53	43	55%	293	316	-22	21	2.2	-1.8	22
8-06	1.6	87.8	589	1.1	101	53	47	53%	280	316	-35	12	2.8	-0.3	15
8-07	2.4	88.3	628	1.1	94	48	45	52%	307	316	-8.3	37	2.0	0.4	39
8-08	2.8	81.8	602	2.3	128	64	64	50%	283	316	-33	31	16	-1.0	46
8-09	3.6	93.2	724	1.1	88	42	46	47%	288	316	-28	19	4.4	2.3	25
8-10	5.0	92.1	801	1.9	43	18	25	41%	300	316	-16	10	14	8.3	32
8-11	2.9	96.0	711	1.1	84	32	51	38%	299	316	-16	35	3.8	1.9	41
8-12	2.8	95.3	700	1.2	82	31	51	38%	298	316	-18	33	3.9	2.0	39
13-08	2.5	90.9	659	1.4	69	25	45	36%	288	316	-27	18	6.2	2.0	26
14-08	2.0	87.2	600	1.2	110	40	70	36%	291	316	-24	46	4.4	-0.3	50
15-08	1.9	87.0	600	1.7	90	31	59	34%	300	316	-15	44	6.7	0.3	50
16-08	1.6	91.9	623	1.5	69	24	45	35%	290	316	-26	19	3.8	0.1	23
17-08	1.2	80.4	525	1.3	88	31	57	35%	279	316	-36	21	2.7	-3.0	21
18-08	1.8	83.1	564	1.7	131	52	79	40%	257	316	-59	20	4.2	-4.2	20
19-08	2.1	86.6	610	1.7	84	31	53	37%	294	316	-22	31	8.5	-0.4	39
20-08	1.3	69.7	467	5.1	125	55	70	44%	252	316	-64	6.7	16	-32	-9.2
21-08	-0.1	77.3	461	2.0	86	36	50	42%	287	316	-29	21	-0.2	-12	8.8
22-08	-0.1	79.8	478	1.6	65	35	31	53%	294	316	-22	8.6	0.4	-6.3	2.6
23-08	-0.4	76.3	444	2.8	88	68	20	78%	274	316	-41	-22	-1.1	-21	-44
24-08	0.4	67.5	421	4.2	120	79	41	66%	248	316	-68	-26	5.3	-32	-54
25-08	0.2	72.4	444	2.7	105	58	47	55%	262	316	-53	-6.7	3.5	-17	-20
26-08	1.5	70.5	477	3.3	71	36	35	51%	279	316	-37	-1.5	16	-15	-0.3
27-08	2.1	75.4	535	2.4	27	12	15	45%	285	316	-30	-16	14	-7.9	-10
28-08	2.5	83.4	595	1.3	64	33	31	52%	268	316	-47	-16	6.0	-0.4	-11
29-08	3.5	76.6	599	1.5	47	16	31	35%	305	316	-10	20	7.5	0.9	29
30-08	4.6	85.6	725	2.5	31	7.1	24	23%	293	316	-22	1.6	25	9.8	37
31-08	5.6	78.0	710	2.7	30	6.6	24	22%	295	316	-20	3.5	28	9.1	40
Mean	**2.2**	**83.9**	**596**	**1.9**	**85**	**40**	**45**	**45%**	**286**	**316**	**-29**	**16**	**7.2**	**-3.7**	**20**

Tab. A7 Surface energy balance at S60 (358 m a.s.l.) in September 2012 as averaged from hourly values

Date	T_a °C	RH %	e_a Pa	u m s^{-1}	SW_{in} W m^{-2}	SW_{out} W m^{-2}	SW_{bal} W m^{-2}	α %	LW_{in} W m^{-2}	LW_{out} W m^{-2}	LW_{bal} W m^{-2}	Q_N W m^{-2}	Q_H W m^{-2}	Q_L W m^{-2}	Q_M W m^{-2}
9-01	1.6	80.4	548	2.0	37	9.7	27	26%	283	316	-33	-5.5	8.7	-5.6	-2.5
9-02	2.7	86.0	640	1.4	29	11	17	40%	285	316	-31	-14	7.7	2.0	-4.1
9-03	2.6	91.1	669	1.0	27	5.7	21	21%	306	316	-9.2	12	2.6	0.7	15
9-04	1.8	92.0	633	1.1	54	14	40	27%	289	316	-27	13	3.0	0.8	17
9-05	0.5	87.2	550	1.6	38	11	27	29%	296	316	-19	7.9	1.7	-2.6	6.9
9-06	0.5	87.2	547	1.8	51	17	34	33%	300	316	-16	18	2.9	-3.3	18
9-07	0.5	87.3	551	2.9	34	27	7.1	79%	286	316	-29	-22	4.1	-7.9	-26
9-08	0.2	91.2	553	1.6	71	57	14	80%	291	316	-24	-9.9	-0.6	-2.7	-13
9-09	0.2	94.5	578	0.7	44	34	10	77%	296	316	-20	-10	-0.4	-0.5	-11
9-10	-1.4	79.8	432	1.9	62	47	15	75%	287	316	-28	-13	-3.6	-6.3	-23
Mean	**0.9**	**87.7**	**570**	**1.6**	**45**	**23**	**21**	**49%**	**292**	**316**	**-24**	**-2.4**	**2.6**	**-2.5**	**-2.3**

Tab. A8 Locations of ablation stakes in 2010 and 2012. Datum: WGS84, UTM 33N. All values in metres

	27/07/2010			23/07/2012		
Stake	**Easting (52…)**	**Northing (87…)**	**Elevation**	**Easting (52…)**	**Northing (87…)**	**Elevation**
S10	9803.22	39871.00	188.51	9803.41	39870.99	184.83
S20	9571.38	39906.46	224.89	9572.13	39906.56	221.64
S30	9276.51	39898.43	279.42	9278.56	39898.87	276.98
S40	8984.16	39905.74	306.60	8986.56	39906.31	304.46
S41	n/d	n/d	n/d	8936.93	40152.58	301.97
S42	n/d	n/d	n/d	9051.44	39682.06	314.42
S50	8668.16	39921.81	332.55	8670.70	39922.46	330.90
S60	8314.90	39915.90	359.66	8318.44	39919.38	358.01
S70	7963.28	39916.99	391.00	n/d	n/d	n/d
S80	7629.74	39897.73	425.03	n/d	n/d	n/d
S90	7326.74	39723.52	464.90	7332.73	39725.81	463.32
S100	7081.99	39468.55	514.08	7084.47	39473.84	512.83
S110	7278.84	39177.69	541.32	7277.94	39179.97	540.92
S120	7483.54	38907.40	625.36	n/d	n/d	n/d
S130	n/d	n/d	n/d	7330.24	40508.54	507.10
S140	n/d	n/d	n/d	7371.74	40859.59	565.27

Tab. A9 Surface mass balance components at individual stakes. Symbology: r - potential direct solar radiation (averaged for 15/06-15/09); b_w, b_s, b_n - point specific winter, summer and net balance respectively

			2011			2012		
Stake	**Elev.**	r	b_w	b_s	b_n	b_w	b_s	b_n
	m	W m^{-2}	cm w.eq.	cm w.eq.	cm w.eq.	cm w.eq.	cm w.eq.	cm w.eq.
S10	185	42	26	-259	-233	31	-175	-145
S20	222	51	37	-234	-198	34	-160	-126
S30	277	56	40	-199	-158	46	-122	-77
S40	304	53	42	-174	-132	46	-90	-44
S41	302	58	n/d	n/d	n/d	39	-99	-60
S42	314	41	n/d	n/d	n/d	51	-78	-27
S50	331	58	45	-174	-129	58	-101	-43
S60	358	61	48	-151	-104	58	-89	-32
S70	391	60	47	-146	-99	59	-96	-37
S80	425	57	45	-137	-92	54	-55	-1
S90	463	61	49	-119	-70	58	-56	2
S100	513	55	49	-94	-45	61	-42	19
S110	541	55	72	-66	6	56	-42	14
S120	625	33	45	-55	-10	58	-20	38
S130	507	69	52	-116	-64	61	-62	-1
S140	565	72	40	-109	-69	56	-46	10

Tab. A10 Specific and volume winter, summer and net balance of Svenbreen calculated for 50 m elevation intervals in 2010/11 balance year

		Winter balance		Summer balance		Net balance	
Altitude	**Area**	**Specific**	**Volume**	**Specific**	**Volume**	**Specific**	**Volume**
(m a.s.l.)	(10^3 km^2)	(cm w.eq.)	(10^3 m^3 w.eq.)	(cm w.eq.)	(10^3 m^3 w.eq.)	(cm w.eq.)	(10^3 m^3 w.eq.)
700-750	10.8	51	5.5	-37	-4.0	14	1.5
650-700	67.6	53	35.7	-54	-36.8	-2	-1.1
600-650	291.6	60	173.6	-68	-197.7	-8	-24.1
550-600	458.0	69	318.2	-66	-304.1	3	14.1
500-550	705.2	61	431.7	-82	-576.6	-21	-144.9
450-500	528.8	53	282.1	-104	-550.7	-51	-268.6
400-450	413.6	51	210.5	-122	-506.2	-71	-295.6
350-400	511.6	50	254.6	-144	-735.5	-94	-481.0
300-350	360.4	45	160.8	-167	-601.0	-122	-440.2
250-300	210.4	39	82.9	-200	-421.1	-161	-338.2
200-250	140.0	33	46.8	-224	-314.0	-191	-267.1
150-200	26.4	29	7.7	-253	-66.8	-224	-59.1
150-750	**3724.4**	**54**	**2010.0**	**-116**	**-4314.3**	**-62**	**-2304.4**

Tab. A11 Specific and volume winter, summer and net balance of Svenbreen calculated for 50 m elevation intervals in 2011/12 balance year

		Winter balance		Summer balance		Net balance	
Altitude	**Area**	**Specific**	**Volume**	**Specific**	**Volume**	**Specific**	**Volume**
(m a.s.l.)	(10^3 km^2)	(cm w.eq.)	(10^3 m^3 w.eq.)	(cm w.eq.)	(10^3 m^3 w.eq.)	(cm w.eq.)	(10^3 m^3 w.eq.)
700-750	10.8	71	7.7	-7	-0.7	64	6.9
650-700	67.6	63	42.9	-15	-10.5	48	32.4
600-650	291.6	60	176.0	-25	-73.5	35	102.5
550-600	458.0	71	326.0	-28	-126.4	44	199.5
500-550	705.2	65	459.5	-38	-264.5	28	194.9
450-500	528.8	61	321.5	-48	-254.7	13	66.8
400-450	413.6	64	265.8	-60	-247.2	4	18.5
350-400	511.6	63	324.4	-76	-387.5	-12	-63.1
300-350	360.4	56	200.7	-93	-335.7	-37	-135.0
250-300	210.4	42	87.7	-122	-257.1	-81	-169.4
200-250	140.0	34	47.9	-148	-206.5	-113	-158.6
150-200	26.4	31	8.2	-177	-46.8	-146	-38.6
150-750	**3724.4**	**61**	**2268.0**	**-60**	**-2211.2**	**1**	**56.9**

Tab. A12 Monthly data from S30 and S100: air temperature T_a , relative humidity *RH* and ice temperature *Ti* (at 2, 4 and 8 m depth)

	S30					S100				
	T_a	*RH*	T_i at -2 m	T_i at -4 m	T_i at -8 m	T_a	*RH*	T_i at -2 m	T_i at -4 m	T_i at -8 m
Month	°C	%	°C	°C	°C	°C	%	°C	°C	°C
Sep 2011*	1.0	88.5	-1.7	-3.5	-4.4	-0.2	94.7	-1.9	-3.6	-4.8
Oct 2011	-5.3	83.1	-2.9	-3.4	-4.2	-7.0	93.5	-3.2	-3.5	-4.6
Nov 2011	-9.3	88.0	-3.8	-3.8	-4.0	-10.9	97.2	-4.4	-3.9	-4.3
Dec 2011	-9.7	84.3	-4.4	-4.1	-3.9	-11.4	95.1	-4.9	-4.3	-4.2
Jan 2012	-6.3	86.0	-5.0	-4.5	-3.9	-7.9	95.4	-5.5	-4.6	-4.3
Feb 2012	-8.9	89.6	-4.7	-4.7	-4.0	-11.0	98.2	-5.7	-4.9	-4.3
Mar 2012	-9.0	84.4	-4.6	-4.6	-4.0	-11.7	99.5	-5.7	-5.1	-4.4
Apr 2012	-12.7	87.5	-5.0	-4.7	-4.1	-15.0	97.9	-5.9	-5.2	-4.5
May 2012	-4.5	81.7	-5.3	-5.0	-4.2	n/d	n/d	-6.2	-5.4	-4.6
Jun 2012	1.3	84.5	-4.5	-5.0	-4.2	n/d	n/d	-5.8	-5.5	-4.7
Jul 2012	3.6	85.5	-2.6	-4.3	-4.3	n/d	n/d	-3.7	-5.0	-4.7
Aug 2012	2.9	85.3	-1.1	-3.3	-4.1	n/d	n/d	-2.5	-4.1	-4.5
Sep 2012**	1.6	88.6	-0.7	-2.7	-4.0	n/d	n/d	-2.1	-3.6	-4.4
Annual mean	**-4.8**	**85.6**	**-3.8**	**-4.2**	**-4.1**	**n/d**	**n/d**	**-4.7**	**-4.6**	**-4.5**

* 18-30/09
**1-10/09

Literature

ACIA 2005. Arctic Climate Impact Assessment Report. Symon C., Arris L. & Heal B. (eds.), Cambridge University Press, Cambridge.

Ahlmann H.W. 1933. Scientific results of the Swedish-Norwegian Arctic Expedition in the summer of 1931. Part 8. Geografiska Annaler 15.

Andreassen L.M. 1999. Comparing traditional mass balance measurements with long-term volume change extracted from topographical maps: A case study of Storbreen glacier in Jotunheimen, Norway, for the period 1940-1997. Geografiska Annaler, 81A (4), 467-476.

Andreassen L.M., van den Broeke M.R., Giesen R.H. & Oerlemans J. 2008. A 5 year record of surface enrgy and mass balance from the ablation zone of Storbreen, Norway. Journal of Glaciology, 54 (185), 245-258.

Araźny A. 1999. Differentiation of air temperature in the summer season 1998 on the Waldemar glacier and on the Kaffiøyra plain (Spitsbergen). Polish Polar Studies. 26th International Polar Symposium, Lublin, 18-20 June 1999.

Araźny A., Migała K., Sikora S., Budzik T. & Puczko D. 2009. Warunki meteorologiczne i biometeorologiczne w rejonie Hornsundu w ciepłej porze roku 2007 i 2008 (Biometeorological and meteorological conditions in Hornsund region during the warm season of 2007 and 2008). Problemy Klimatologii Polarnej, 19, 203-222.

Araźny A., Migała K., Sikora S. & Budzik T. 2010. Meteorological and biometeorological conditions in the Hornsund area (Spitsbergen) during the warm season. Polish Polar Research, 31 (3), 217-238.

Armstrong R.L. & Brun E. 2008. Snow and climate. Processes, surface energy exchange and modelling. Cambridge University Press, Cambridge, pp. 222.

Arnold N.S., Rees W.G., Hodson A.J. & Kohler J. 2006. Topographic controls on the surface energy balance of a high Arctic valley glacier. Journal of Geophysical Research, 111, doi:10.1029/2005JF000426.

Bahr D. B., Pfeffer, W. T., Sassolas, C. and Meier, M. 1998. Response time of glaciers as a function of size and mass balance: 1. Theory. Journal of Geophysical Research, 103 (B5), 9777–9782.

Baird P.D. 1964. The Polar World. Longmans, London, pp. 328.

Bamber J., Krabill W., Raper V. & Dowdeswell J. 2004. Anomalous recent growth of part of a large Arctic ice cap: Austfonna, Svalbard. Geophysical Research Letters, 30 (L12402), doi:10.1029/2004GL019667.

Baranowski S. 1975. Glaciological investigations and glaciomorphological observations made in 1970 on Werenskiold Glacier and in its forefield. In: Glaciological investigations of the Polish Scientific Spitsbergen Expeditions 1970-74, Acta Universitatis Wratislaviensis, 251, 69-94.

Baranowski S. 1977. Subpolarne lodowce Spitsbergenu na tle klimatu tego regionu (Subpolar Spitsbergen glaciers in the background of the climate of this region). Wydawnictwo Uniwersytetu Wrocławskiego, Wrocław, pp. 157.

Barrand N.E., James, T.D. & Murray T. 2010. Spatio-temporal variability in elevation changes of two high-Arctic valley glaciers. Journal of Glaciology, 56 (199), 771-780.

Bartoszewski S. 1989. Charakterystyka odpływu ze zlewni lodowca Scotta (Zachodni Spitsbergen) w 1988 r. (Characteristics of outflow of the Scott Glacier (Western Spitsbergen) in 1988. In: Wyprawy Geograficzne na Spitsbergen 1986-1988. Uniwersytet Marii Curie-Skłodowskiej, Lublin, 1989, 61-65.

Bartoszewski S. 2002. Odpływ ze zlewni lodowca Scotta (Spitsbergen) w sezonie letnim 2001 r. (Runoff from the Scott glacier catchment (Spitsbergen) in the summer season of 2001). In: Kostrzewski A. & Rachlewicz G. (eds.), Polish Polar Studies. Funkcjonowanie i monitoring geoekosystemów obszarów polarnych, Poznań, 65-72.

Bartoszewski S. 2007. The functioning of Scott Glacier in conditions of climate global changes. Landform Analysis, 5, 5-8.

Bartoszewski S., Gluza A. & Siwek K. 2004. Ablacja i odpływ rzeczny z lodowca Scotta na tle warunków meteorologicznych (Ablation and river outflow from Scott glacier in the background of meteorological conditions). XXX Międzynarodowe Sympozjum Polarne, 23-25 September 2004, Gdynia, 15-18

Bælum K. & Benn D.I. 2011. Thermal structure and drainage system of a small valley glacier (Tellbreen, Svalbard), investigated by ground penetrating radar. The Cryosphere, 5, 139-149.

Bednorz E. & Kolendowicz L. 2010. Summer 2009 thermal and bioclimatic conditions in Ebba Valley, central Spitsbergen. Polish Polar Research, 31 (4), 327-348.

Benestad R.E., Førland E.J. & Hanssen-Bauer I. 2002. Empirically downscaled temperature scenarios for Svalbard. Atmospheric Science Letters, 2002, doi:10.1006/asle.2002.0051

Benn D.I. & Evans D.J.A. 2010. Glaciers and glaciation. London, Hodder Education, pp. 816.

Bingham R.G., Nienow P.W., Sharp M.J. & Boon S. 2005. Subglacial drainage processes at a High Arctic polythermal glacier. Journal of Glaciology, 51, 15–24.

Bintanja R. 1998. The contribution of snowdrift sublimation to the surface mass balance of Antarctica. Annals of Glaciology, 27, 251–9.
Bintanja R., van Oldenborgh G.J., Drijfhout S.S., Wouters B. & Katsman C.A. 2013. Important role for ocean warming and increased ice-shelf melt in Antarctic sea-ice expansion. Nature Geoscience, 2013, doi:10.1038/ngeo1767
Björnsson H., Gjessing Y., Hamran S.-E., Hagen J.O., Liestøl O., Palsson F. & Erlingsson B. 1996. The thermal regime of sub-polar glaciers mapped by multi-frequency radio-echo sounding. Journal of Glaciology, 42 (140), 23–32.
Blatter H. & Hutter K. 1991. Polythermal conditions in arctic glaciers. Journal of Glaciology, 37, 261–9.
Błaszczyk M., Jania J.A. & Hagen J.O. 2009. Tidewater glaciers of Svalbard: Recent changes and estimates of calving fluxes. Polish Polar Research, 30 (2), 85-142.
Braithwaite R.J. 2009. Calculation of sensible-heat flux over a melting ice surface using simple climate data and daily measurements of ablation. Annals of Glaciology, 50, 9-15.
Brock B. & Arnold N.S. 2000. A spreadsheet-based (Microsoft Excel) point surface energy balance model for glacier and snow melt studies. Earth Surface Processes and Landforms, 25, 649-658.
Brock B., Rivera A., Casassa G., Bown F. & Acuña C. 2007. The surface energy balance of an active ice-covered volcano: Villarrica Volcano, Southern Chile. Annals of Glaciology, 45, 104-114.
Brotzge J.A. & Duchon C.E. 2000. A field comparison among a domeless net radiometer, two four-component net radiometers, and a domed net radiometer. Journal of Atmospheric and Oceanic Technology, 17, 1569-1582.
Brykała D. & Araźny A. 2002. Wpływ warunków meteorologicznych na kształtowanie się odpływu powierzchniowego na lodowcu Waldemara (NW Spitsbergen) latem 1997 roku (Influence of meteorological conditions to the surface run-off on the Waldemar glacier (NW Spitsbegen) in the summer of 1997). Problemy Klimatologii Polarnej, 10, 139-158.
Bukowska-Jania E. & Jania J. 1988. Zmiany geometrii czołowej części lodowca Werenskiold (Spitsbergen) w latach 1957-1983 (Changes of the geometry of the frontal part of Werenskiold Glacier (Spitsbergen) in the period of 1957-1983). Wyprawy Polarne Uniwersytetu Śląskiego 1980-1984, Prace Naukowe Uniwersytetu Śląskiego w Katowicach nr 910. Uniwersytet Śląski, Katowice, 1988, 64-91.
Bukowska-Jania E. & Szafraniec J. 2005. Distribution and morphometric characteristics of icing fields in Svalbard. Polar Research, 24 (1), 41-53.
Cazenave A., Dominh K., Guinehut S., Berthier E., Llovel W., Ramillien G., Ablain M. & Larnicol G. 2009. Sea level budget over 2003-2008: A reevaluation from GRACE space gravimetry, satellite altimetry and Argo. Global and Planetary Change, 65 (1-2), 83-88.
Chorley R.J. & Kennedy A. 1971. Physical geography, a systems approach. Prentice-Hall, London, pp. 370.
Church J.A., White N.J., Konikow L.F., Domingues C.M., Cogley J.G., Rignot E., Gregory J.M., van den Broeke M.R., Monaghan A.J. & Velicogna I. 2011. Revisiting the Earth's sea-level and energy budgets from 1961 to 2008. Geophysical Research Letters, 38 (L 18601), doi:10.1029/2011GL048794
Cogley J.G., Hock R., Rasmussen L.A., Arendt A.A., Bauder A., Braithwaite R.J., Jansson P., Kaser G., Möller M., Nicholson L. & Zemp M. 2011. Glossary of Glacier Mass Balance and Related Terms. IHP-VII Technical Documents in Hydrology No. 86, IACS Contribution No. 2, UNESCO-IHP, Paris.
Cox L.H. & March R.S. 2004. Comparison of geodetic and glaciological mass-balance techniques, Gulkana Glacier, Alaska, U.S.A. Journal of Glaciology, 50 (170), 363–370.
CPE (Centre for Polar Ecology) 2012. Report on Czech research activities in Petuniabukta, Billefjorden, Svalbard, performed in summer season 2012. University of South Bohemia, Česke Budejovice.
Cuffey K.M. & Paterson W.S.B. 2010. The Physics of Glaciers. Academic Press, pp. 704
Curry J.A. & Webster P.J. 1999. Thermodynamics of atmospheres and oceans. San Diego: Academic Press.
D'Andrea W.J., Vaillencourt D.A., Balascio N.L., Werner A., Roof S.R., Retelle M. & Bradley R.S. 2012. Mild Little Ice Age and unprecedented recent warmth in an 1800 year lake sediment records from Svalbard. Geology, 40 (11), doi:10.1130/G33365.1
Dowdeswell J.A. 1986. Drainage-basin characteristics of Nordaustlandet ice caps, Svalbard. Journal of Glaciology, 32 (110), 31-38.
Dowdeswell J.A. & Benham T.J. 2003. A surge of Perseibreen, Svalbard, examined using aerial photography and ASTER high resolution satellite imagery. Polar Research, 22 (2), 373-383.
Dowdeswell J.A., Hamilton G.A & Hagen J.O. 1991. The duration of the active phase on surge-type glaciers: contrasts between Svalbard and other regions. Journal of Glaciology, 37 (127), 388-400.
Dowdeswell J.A., Hodgkins R., Nuttall A.M., Hagen J.O. & Hamilton G.S. 1995. Mass balance change as a control on the frequency and occurrence of glacier surges in Svalbard, Norwegian High Arctic. Geophysical Research Letters, 22 (21), 2909–2912.

Dowdeswell J.A., Hagen J.O., Bjørnsson H., Glazovsky A., Harrison W. D., Holmlund P., Jania J., Koerner R., Lefauconnier B., Ommanney S. & Thomas B. 1997. The mass balance of circum-Arctic glaciers and recent climate change. Quaternary Research, 48, 1–14.

Dowdeswell J.A., Benham T.J., Strozzi T. & Hagen J.O. 2008. Iceberg calving flux and mass balance of the Austfonna ice cap on Nordaustlandet, Svalbard. Journal of Geophysical Research, 113 (F03022), doi:10.1029/2007JF000905.

Dunse T., Schuler T.V., Hagen J.O. & Reijmer C.H. 2012. Seasonal speed-up of two outlet glaciers of Austfonna, Svalbard, inferred from continuous GPS measurements. The Cryosphere, 6, 453-466.

Dyurgerov M.B. & Meier M.F. 1997. Mass balance of mountain and subpolar glaciers: a new global assessment for 1961–1990. Arctic and Alpine Research, 29, 379–391

Dyurgerov M.B. & Meier M.F. 2000. Twentieth century climate change: Evidence from small glaciers. Proceedings of National Academy of Sciences of the United States of America (PNAS), 97, 243-245.

Elsberg D.H., Harrison W.D., Echelmeyer K.A. & Krimmel R.M. 2001. Quantifying the effects of climate and surface change on glacier mass balance. Journal of Glaciology, 47 (159), 649–658.

Etzelmüller B., Vatne G., Ødegård R.S. & Sollid J.L. 1993. Mass balance and changes of surface slope, crevasse and flow pattern of Erikbreen, northern Spitsbergen: an application of a geographical information system (GIS). Polar Research, 12 (2), 131-146.

Etzelmüller B., Ødegård R.S., Vatne G., Mysterud R.S., Tonning T. & Sollid J.L. 2000. Glacier characteristics and sediment transfer system of Longyearbreen and Larsbreen, western Spitsbergen. Norsk Geografisk Tidskrift, 54, 157-168.

Evans D.J.A., Strzelecki M., Milledge D.G., Orton C. 2011. Hørbyebreen polythermal glacial landsystem, Svalbard. Jorunal of Maps, 8 (2), 146-156.

Ewertowski M., Kasprzak L., Szuman I. & Tomczyk I. 2010. Depositional processes within the frontal ice-cored moraine system, Ragnar glacier, Svalbard. Quaestiones Geographicae, 29 (1), 27-36.

Ewertowski M., Kasprzak L., Szuman I. & Tomczyk I. 2011. Controlled, ice-cored moraines: sediment and geomorphology. An example from Ragnarbreen, Svalbard. Zeitschrift für Geomorphologie, 56 (1), 53-74.

Førland E.J. & Hanssen-Bauer I. 2000. Increased precipitation in the Norwegian Arctic: true or false? Climate Change, 46, 485-509.

Førland E.J., Hanssen-Bauer I., Jónsson T., Kern-Hanssen C., Nordli P.Ø., Tveito O.E. and Vaarby Laursen E. 2002. Twentieth-century variations in temperature and precipitation in the Nordic Arctic. Polar Record, 38 (206), 203–210.

Førland E.J., Benestad R., Hanssen-Bauer I., Haugen J.E. & Skaugen T.E. 2012. Temperature and precipitation development at Svalbard 1900-2100. Advances in Meteorology, 2011, doi:10.1155/2011/893790

Fountain A.G. & Walder J. 1998. Water flow through temperate glaciers. Reviews of Geophysics, 36, 299–328.

Fowler A.C., Murray T. & Ng F.S.L. 2001. Thermally controlled glacier surging. Journal of Glaciology, 47 (159), 527-538.

Gibas J., Rachlewicz G. & Szczuciński W. 2005. Application of DC resistivity soundings and geomorphological surveys in studies of modern Arctic glacier marginal zones, Petuniabukta, Spitsbergen. Polish Polar Research, 26 (4), 239–258.

Glen A.R., Fleming W.L.S., Brough J., Robertson R.H.S., Gatty O., Benson J.S., Stott F.C. & Hartley C.H. 1934: The Oxford University Expedition to Spitsbergen, 1933. The Geographical Journal, 84 (2), 104-129.

Glen J.W. 1955. The creep of polycrystalline ice. Proceedings of the Royal Society, Series A, 228, 519–38.

Gokhman V.V. 1987a. Two types of intraglacial meltwater regime for the Bertil Glacier, Svalbard. Polar Geography, 11 (4), 241-248.

Gokhman V.V. 1987b. Distribution and conditions of formation of glacial icings on Spitsbergen. Polar Geography, 11 (4), 249-260.

Gokhman V.V. 1988. The runoff regime of rivers in Spitsbergen. Polar Geography, 12 (4), 285-296.

Gokhman V.V. & Khodakov V.G. 1983. Vopros analiza, prognoza i preobrazovaniya zimnego stoka vody iz lednika Bertil na Shpitsbergene (Problems of the analysis, prediction and transformation of the winter discharge of water from Bertil Glacier on Spitsbergen). Materialy glyatsiologicheskikh issledovaniy, 46, 185-193.

Gokhman V.V. & Khodakov V.G. 1986. Hydrological investigations in the Mimer river basin, Svalbard, in 1983. Polar Geography, 10 (4), 309-316.

Gokhman V.V., Troitskiy L.C. & Kotlyakov V.G. 1982. Gidrotermicheskiy rezhim i vodokhozyaystvennaya rol' lednika Bertil na Shpitsbergene (Hydrothermal regime of Bertil Glacier on Spitsbergen and its water-supply role). Materialy glyatsiologicheskikh issledovaniy, 45, 154-159.

Gordiyenko F.G., Kotlyakov V.M., Punning Ya.-K.M., Vairmae R. 1980. Study of a 200 m core from the Lomonosov Ice Plateau in Spitsbergen and the paleoclimatic implications. Polar Geography and Geology, 5, 242-251.

Grabiec M., Budzik T. & Głowacki P. 2012. Modelling and hindcasting of the mass balance of Werenskioldbreen (southern Svalbard). Arctic, Antarctic and Alpine Research, 44 (2), 164-179.
Greve R. & Blatter H. 2009. Dynamics of ice sheets and glaciers. Springer-Verlag Heidelberg, Berlin, pp. 287.
Grove J.M. 2001. The initiation of the "Little Ice Age" in regions round the north Atlantic. Climatic Change, 48, 53-82.
Grudd H. 1990. Small glaciers as sensitive indicators of climatic fluctuations. Geografiska Annaler. Series A. Physical Geography, 72 (1), 119-123.
Grześ M. & Sobota I. 2000. Winter snow accumulation and discharge from the Waldemar Glacier, northwestern Spitsbergen in 1996-1998. Polish Polar Research, 21 (1), 19-32.
Gulley J.D., Benn D.I., Muller D. & Luckman A. 2009. A cut-and-closure origin for englacial conduits in uncrevassed regions of polythermal glaciers. Journal of Glaciology, 55 (189), 66-80.
Gus'kov A.S. 1983. Vodno-ledoviy balans lednikov Shpitsbergena v 1979/80 balansovom godu (Water-ice balance of glaciers of Spitsbergen in the 1979/80 balance year). Materialy glyatsiologicheskikh issledovaniy, 46, 136-139.
Hagen J.O. 1987. Glacier surge at Usherbreen, Svalbard. Polar Research, 5 (2), 239-252.
Hagen J.O. 1988. Glacier surge in Svalbard with examples from Usherbreen. Norsk Geografisk Tidskrift, 42 (4), 203-213.
Hagen J.O., Lefauconnier B. & Liestøl O. 1991. Glacier mass balance in Svalbard since 1912. Glaciers-Ocean-Atmosphere Interactions (Proceedings of the International Symposium hel at St Petersburg, September 1990). IAHS Publ. no. 208, 1991.
Hagen J.O., Liestøl O., Roland E. & Jørgensen T. 1993. Glacier atlas of Svalbard and Jan Mayen. Oslo: Norwegian Polar Institute.
Hagen J.O., Melvold K., Eiken T., Isaksson E. & Lefauconnier B. 1999. Mass balance methods on Kongsvegen, Svalbard. Geografiska Annaler, Series A, Physical Geography, 81 (4), 593-601.
Hagen J.O., Kohler J., Melvold K. & Winther J.-G. 2003a. Glaciers in Svalbard: mass balance, runoff and freshwater flux. Polar Research, 22, 145–159.
Hagen J.O., Melvold K., Pinglot F. & Dowdeswell J.A. 2003b. On the net mass balance of the glaciers and ice caps in Svalbard, Norwegian Arctic. Arctic, Antarctic and Alpine Research, 35 (2), 264–270.
Hagen J.O., Eiken T., Kohler J. & Melvold K. 2005. Geometry changes on Svalbard glaciers: mass-balance or dynamic response? Annals of Glaciology, 42, 255-261.
Hambrey M.J., Murray T., Glasser N.F., Hubbard A., Hubbard B., Stuart G., Hansen S. & Kohler J. 2005. Structure and changing dynamics of a polythermal valley glacier on a centennial timescale: Midre Lovénbreen, Svalbard. Journal of Geophysical Research, 110 (F01006), doi:10.1029/2004JF000128.
Hamilton G.S. & Dowdeswell J.A. 1996. Controls on glacier surging in Svalbard. Journal of Glaciology, 42 (140), 157–168.
Hanaček M., Flašar J. & Nývlt D. 2011. Sedimentary petrological characteristics of lateral and frontal moraine and proglacial glaciofluvial sediments of Bertilbreen, Central Svalbard. Czech Polar Reports, 1 (1), 11-33.
Hanson B. & Hooke R. Le B. 2000. Glacier calving: a numerical model of forces in the calving speed-water depth relation. Journal of Glaciology, 46, 188–96.
Hanssen-Bauer I. & Førland E.J. 1998. Long-term trends in precipitation and temperature in the Norwegian Arctic: can they be explained by changes in atmospheric circulation patterns? Climate Research, 10, 143–153.
Harland W.B. 1953. The Cambridge Spitsbergen Expedition, 1949. The Geographical Journal, 118 (3), 309-329.
Hasnain S.I. 1999. Runoff characteristics of a glacierized catchment, Garhwal Himalaya, India. Hydrological Sciences, 44, 847–54.
Hock R. 2003. Temperature index melt modelling in mountain areas. Journal of Hydrology, 282, 104-115.
Hock R. 2005. Glacier melt: a review of processes and their modeling. Progress in Physical Geography, 29 (3), 362–391
Hodgkins R. 1994. The seasonal evolution of meltwater discharge quality and routing at a High-Arctic glacier. PhD thesis, University of Cambridge, Cambridge.
Hodgkins R. 1997. Glacier hydrology in Svalbard, Norwegian High Arctic. Quaternary Science Reviews, 16, 957-973.
Hodgkins R., Hagen J.O. & Hamran S.-E.1999. 20th century mass balance and thermal regime change at Scott Turnerbreen, Svalbard. Annals of Glaciology, 28 (1), 216-220.
Hodson A., Kohler J. & Brinkhaus M. 2005. Multi-year water and surface energy budget of a high-latitude polythermal glacier: evidence for overwinter water storage in a dynamic subglacial reservoir. Annals of Glaciology, 42, 42-46.
Holmgren B. 1971: Climate and energy exchange on a sub-polar ice cap in summer. Arctic Institute of North America Devon Island Expedition 1961-1963. Uppsala: Meteorologiska Institutionen, Uppsala Universitet. Meddelande 107 Part A–E.

Hooke R. Le B. 2005. Principles of Glacier Mechanics. Cambridge University Press, Cambridge, pp. 439.
Hooke R. Le B., Laumann T. & Kohler J. 1990. Subglacial water pressures and the shape of subglacial conduits. Journal of Glaciology, 36, 67–71.
Hubbard B. & Nienow P. 1997. Alpine subglacial hydrology. Quaternary Science Reviews, 16, 939-955.
Humlum O. 2002. Modelling late 20th-century precipitation in Nordenskiold Land, Svalbard, by geomorphic means. Norsk Geografisk Tidsskrift, 56 (2), 96–103.
Ignatiuk D. 2012. Bilans energetyczny powierzchni lodowca a zasilanie systemu drenażu glacjalnego Werenskioldbreen (Surface energy balance of a glacier against recharge of glacial drainage on Werenskioldbreen). PhD thesis, University of Silesia, Sosnowiec.
Immerzeel W.M., van Beek L.P.H. & Bierkens M.F.P. 2010. Climate change will affect the Asian water towers. Science, 328, 1382-1385.
Isaksson E., Pohjola V., Jauhiainen T., Moore J., Pinglot J.F., Vaikmäe R., van de Wal R.S.W., Hagen J.O., Ivask J., Karlöf L., Martma T., Meijer H.A.J., Mulvaney R., Thomassen M. & van den Brocke M. 2001. A new ice−core record from Lomonosovfonna, Svalbard: viewing the 1920–97 data in relation to present climate and environmental conditions. Journal of Glaciology 47: 335–345.
Isaksson E., Hermanson M., Hicks S., Igarashi M., Kamiyama K., Moore J., Motoyama H., Muir D., Pohjola V., Vaikmäe R., van de Wal R.S.W. & Watanabe O. 2003. Ice cores from Svalbard – useful archives of past climate and pollution history. Physics and Chemistry of the Earth, 28, 1217–1228.
Isaksson E., Kohler J., Pohjola V., Moore J., Igarashi M., Karlöf L., Martma T., Meijer H., Motoyama H., Vaikmäe R. & van de Wal R.S.W. 2005: Two ice-core δ18O records from Svalbard illustrating climate and sea-ice variability over the last 400 years. The Holocene, 15 (4), 501-509.
James T.D., Murray T., Barrand N.E., Sykes H.J., Fox A.J. & King M.A. 2012. Observations of enhanced thinning in the upper reaches of Svalbard glaciers. The Cryosphere, 6, 1369-1381.
Jania J. 1988. Dynamiczne procesy glacjalne na południowym Spitsbergenie w świetle badań fotointerpretacyjnych i fotogrametrycznych (Dynamic glacial processes in southern Spitsbergen in the background of photointerpretation and photogrammetry). Prace Naukowe Uniwersytetu Śląskiego w Katowicach, 92.
Jania J. 1997. Glacjologia. Wydawnictwo Naukowe PWN, Warsaw, pp. 358.
Jania J., Lipert C. & Mechliński Z. 1984. The ice mass loss in the front zone of the Werenskiold Glacier from 1957 to 1978 determined using terrestrial photogrammetry. Polish Polar Research, 5 (3-4), 207-216.
Jania J., Mochnacki D. & Gądek B. 1996. The thermal structure of Hansbreen, a tidewater glacier in southern Spitsbergen, Svalbard. Polar Research, 15 (1), 53-66.
Jania J. & Pulina M. 1990. Field investigations performed during the glaciological Spitsbergen expedition in 1989, Interim report, Uniwersytet Śląski, Katowice, pp. 13.
Jania J. & Pulina M. 1994. Polish hydrological studies in Spitsbergen, Svalbard: a review of some results. In: K. Sand & A. Killingtveit (eds.), Proceedings of the 10th International Northern Research Basins Symposium and Workshop, Spitsbergen, Norway. Trondheim, Norwegian Institute of Technology.
Jansson P., Hock R. & Schneider T. 2003. The concept of glacier storage: a review. Journal of Hydrology, 282, 116–29.
Jiskoot H., Boyle P. & Murray T. 1998. The incidence of glacier surging in Svalbard: evidence from multivariate statistics. Computers & Geosciences, 24 (4), 387–399.
Jiskoot H., Murray T. & Boyle P. 2000. Controls on the distribution of surge-type glaciers in Svalbard. Journal of Glaciology, 46 (154), 412-422.
Johannesson T., Raymond C.F., Waddington E. 1989. Time-scale for adjustment of glaciers to changes in mass-balance. Journal of Glaciology, 35, 355-369.
Jonsson S. & Hansson M. 1990. Identification of annual layers in superimposed ice Storoyjokulen in northeastern Svalbad. Geografiska Annaler. Series A, Physical Geography, 72 (1), 41-54.
Kääb A. 2008. Glacier Volume Changes Using ASTER Satellite Stereo and ICESat GLAS Laser Altimetry. A Test Study on Edgeøya, Eastern Svalbard. IEEE Transactions on Geoscience and Remote Sensing, 46 (10), 2823-2830.
Kamb B. 1987. Glacier surge mechanism based on linked-cavity configuration of the basal water conduit system. Journal of Geophysical Research, 92 (B9), 8083-9100.
Karczewski A. 1989: The development of the marginal zone of the Horbyebreen, Petuniabukta, central Spitsbergen. Polish Polar Research, 10 (3), 371-377.
Karczewski A. 1995: Contemporary glaciation of the Petuniabukta area against the background of late-vistulian and holocene deglaciation (western Olav V Land, Spitsbergen), Quaestiones Geographicae, Special Issue 4, 133-138.
Karczewski A. & Kłysz P. 1994. Lithofacies and structural analysis of crevasse filling deposits of the Svenbreen foreland (Petuniabukta, Spitsbergen). In: XXI Polar Symposium. 60 years of Polish Research of Spitsbergen. 23-24 September 1994, Warszawa, Instytut Geofizyki PAN, 123-133.

Karczewski A. & Rygielski W. 1989. The profile of glacial deposits in the Horbyedalen and an attempt at their chronostratigraphy, central Spitsbergen. Polish Polar Research, 10 (3), 401-409.
Karczewski A., Borówka M., Maćkowiak K., Rygielski W., Ulatowski P. & Wojciechowski A. 1987. Funkcjonowanie strefy marginalnej lodowca Horbye oraz udział jego wód proglacjalnych w rozwoju równi pływowej zatoki Petunia (Functioning of the marginal zone of Horbye glacier and contribution of its proglacial waters in the development of Petuniabukta tidal flat). XVI Sympozjum Polarne, Lublin, 80-83.
Karczewski A., Borówka M., Gonera P., Kasprzak L., Kłysz P., Kostrzewski A., Lindner L., Marks L., Rygielski W., Stankowski W., Wojciechowski A. & Wysokiński L. 1990. Petuniabukta, Billefjorden, Spitsbergen. Geomorfologia. Mapa geomorfologiczna 1:40 000 (Petuniabukta, Billefjorden, Spitsbergen. Geomorfologia. Geomorphological map 1: 40 000). Uniwersytet im. A. Mickiewicza, Poznań, 1990.
Kaser G., Fountain A. & Jansson P. 2002. A manual for monitoring the mass balance of mountain glaciers. IHP-VI Technical Documents in Hydrology No. 59, ICSI Constribution, UNESCO-IHP, Paris.
Kaser G., Cogley J.G., Dyurgerov M.B., Meier M.F. & Ohmura A. 2006. Mass balance of glaciers and ice caps: Consensus estimates for 1961 – 2004. Geophysical Research Letters, 33 (L19501), doi 10.1029/2006GL027511.
Kasprzak L. & Ewertowski M. 2007. Ice-cored moraines in the Petunia Bukta area – examples from Ragnar marginal zone. Landform Analysis, 5, 37–40.
Kehrwald N.M., Thompson L.G., Tandong Y., Mosley-Thompson E., Schotterer U., Alfimov V., Beer J., Eikenberg J. & Davis M.E. 2008. Mass loss on Himalayan glacier endangers water resources. Geophysical Research Letters 35 (L22503), doi:10.1029/2008GL035556
Kejna M. 2002. Warunki meteorologiczne na Kaffioyrze w okresie 13 lipca - 9 września 1999 roku (Meteorological conditions on Kaffioyra in the period 13th July - 9th September 1999). Problemy Klimatologii Polarnej, 10, 93-110.
Kejna M. & Maszewski R. 2007. Warunki meteorologiczne w rejonie lodowca Waldemara (NW Spitsbergen) w sezonie letnim 2006 r. (Meteorological conditions in the region of Waldemar glacier (NW Spitsbergen) in the summer season of 2006). In: Przybylak R., Kejna M., Araźny A. & Głowacki P. (eds.), Abiotyczne środowisko Spitsbergenu w latach 2005-2006 w warunkach globalnego ocieplenia. Uniwersytet Mikołaja Kopernika, Toruń, 2007: 165-178.
Kejna M., Przybylak R., Araźny A., Jankowska J., Maszewski R. & Wyszyński P. 2010. Warunki topoklimatyczne w sezonach letnich w rejonie Kaffioyry (NW Spitsbergen) w latach 2005-2009 (Topoclimatic conditions in summer seasons in the Kaffioyra region (NW Spitsbergen) in the years 2005-2009). Problemy Klimatologii Polarnej 20, 63-81.
Killingtveit Å., Pettersson L.-E. & Sand K. 2003. Water balance investigations in Svalbard. Polar Research, 22 (2), 161-174.
Kłysz P., 1985: Glacial forms and deposits of Ebba Glacier and its foreland (Petuniabukta region, Spitsbergen), Polish Polar Research, 10: 277-301.
Kłysz P., Lindner L., Marks L., Wysokiński L., 1987: Map of Quaternary landforms and sediments of the Ebbadalen-Nordenskioldbreen region (Olav V Land, Spitsbergen), 1:20 000. Wydawnictwo Geologiczne, Warszawa 1987.
Koerner R.M. 1968. Fabric analysis of a core from the Meighen ice cap, NWT, Canada. Journal of Glaciology, 7 (51), 421-430.
Kohler J., Nordli Ø., Brandt O., Isaksson E., Pohjola V., Martma T. & Aas H.F. 2002. Svalbard temperature and precipitation, late 19th century to the present. Final report on ACIA-funded project. Norwegian Polar Institute, Oslo, Norway
Kohler J., James T. D., Murray T., Nuth C., Brandt O., Barrand N. E., Aas H. F. & Luckman A. 2007. Acceleration in thinning rate on western Svalbard glaciers. Geophysical Research Letters, 34, L18502, doi 10.1029/2007GL030681.
Kostrzewski A. & Zwoliński Z. 1995. Hydraulic geometry of a supraglacial stream. Quaestiones Geographicae. Special Issue, 4, 165-176.
Kostrzewski A. & Zwoliński Z. (eds.). 2003. Funkcjonowanie dawnych i współczesnych geoekosystemów Spitsbergenu (Functioning of past and present-day geoecosystems of Spitsbergen). Stowarzyszenie Geomorfologów Polskich, Poznań-Longyearbyen, pp. 190.
Kostrzewski A., Kaniecki A., Kapuściński J., Klimczak R., Stach A. & Zwoliński Z. 1989. The dynamics and rate of denudation of glaciated and non-glaciated catchments, central Spitsbergen. Polish Polar Research, 10 (3), 317-367.
Kostrzewski A., Pulina M. & Zwoliński Z. (eds.). 2004. Glacjologia, geomorfologia i sedymentologia środowiska polarnego Spitsbergenu (Glaciology, geomorphology and sedimentology of polar environment of Spitsbergen). Stowarzyszenie Geomorfologów Polskich, Sosnowiec-Poznań-Longyearbyen, pp. 310

Kostrzewski A., Rachlewicz G. & Zwoliński Z. 2007a. Zmiany funkcjonowania geoekosystemów lądowych Arktyki. (Changes in functioning of terrestrial Arctic geoecosystems). In: Styszyńska A. & Marsz A. (eds.), Zmiany klimatyczne w Arktyce in Antarktyce w ostatnim pięćdziesięcioleciu XX wieku i ich implikacje środowiskowe.

Kostrzewski A., Rachlewicz G. & Zwoliński Z. 2007b. Present-day geomorphological activity in the Arctic. Landform Analysis, 5, 41-46.

König M., Nuth Ch., Kohler J., Moholdt G. & Pettersen R. 2013. A digital glacier database for Svalbard. In: Kargel J.S., Leonard G.J., Bishop M.P., Kääb A. & Raup B.H. (eds.), Global Land Ice Measurements from Space. Springer., 810 p., ISBN 978-3-540-79817-0

Krawczyk W. & Bartoszewski S. 2005. Crustal solute fluxes and transient carbon dioxide drawdown in the Scottbreen Basin, Svalbard, in 2002. Journal of Hydrology, 362 (3-4), 206-219.

Krimmel R.M. & Vaughn B.H. 1987. Columbia Glacier, Alaska: changes in velocity 1977–1986. Journal of Geophysical Research, 92 (B9), 8961–8.

Krismer T. 2009. Spatial and spatial mass balance modelling on an Arctic glacier, Kongsvegen, Spitzbergen. MSc. thsesis, University of Innsbruck, Innsbruck.

Kruszewski G. 2005. Wpływ zmian temperatury wód w głównym nurcie prądu Zachodniospitsbergeńskiego na temperaturę powietrza na Spitsbergenie Zachodnim (1982-2002) (The influence of the changes in sea surface temperature in the West Spitsbergen Current on the air temperature at West Spitsbergen (1982-2002)). Problemy Klimatologii Polarnej, 15, 53-63.

Kruszewski G. 2009. Zmiany prędkości wiatru w rejonie Svalbardu w latach 1948-2008 (Changes in surface wind speed in Svalbard area (1948-2008)). Problemy Klimatologii Polarnej 19, 159-168.

Kuhn M., Markl G., Kaser G., Nickus U., Obleitner F. & Schneider H. 1985. Fluctuations of climate and mass balance: different responses of two adjacent glaciers. Z. Gletscherkd. Glazialgeol., 21, 409-416

Kuhn M., Dreiseitl E., Hofinger S., Markl G., Span N. & Kaser G. 1999. Measurements and models of the mass balance of Hintereisferner. Geografiska Annaler 81A (4): 659-670.

Lagally M. 1932. Zur Thermodynamik der Gletscher (On the glacier thermodynamics). Zeitschrift fur Gletscherkunde, 20, p. 199-214.

Lankauf K.R. 2002. Recesja lodowców rejonu Kaffiøyry (Ziemia Oscara II – Spitsbergen) w XX wieku (Retreat of glaciers in the Kaffiøyra region (Oscar II Land - Spitsbergen) in 20th century). Prace Geograficzne IG i PZPAN, 183.

Láska K., Witoszová D. & Prošek P. 2012. Weather patterns of the coastal zone of Petuniabukta, central Spitsbergen in the period 2008-2010. Polish Polar Research, 33 (4), 297-318.

Lefauconnier B. & Hagen J.O. 1991. Surging and calving glaciers in eastern Svalbard. Meddelelser 116. Oslo: Norsk Polarinstitutt.

Lemke P., Ren J., Alley R., Allison I., Carrasco J., Flato G., Fujii Y., Kaser G., Mote P., Thomas R. & Zhang T. 2007. Observations: Changes in Snow, Ice and Frozen Ground. Climate Change 2007: The Physical Science Basis. Contribution of Working Group I to the Fourth Assessment Report of the Intergovernmental Panel on Climate Change. 1

Leszkiewicz J., Piasecki J. & Pulina M. 1999. Hydrology of the Werenskiold glacier catchment are (south Spitsbergen) in summer 1998. Polish Polar Studies. 26th International Polar Symposium, Lublin, 18-20 June 1999, 153-160.

Lewis K.J., Fountain A.G. & Dana G.L. 1998. Surface energy balance and meltwater production for a Dry Valley glacier, Taylor Valley, Antarctica. Annals of Glaciology, 27, 603–609.

Liestøl O. 1993. Glaciers of Europe - glaciers of Svalbard, Norway. U.S. Geological Survey Prof.. Pap. 1386-E, E127-E151.

Macheret Yu.Ya., Zhuravlev A.B. & Bobrova L.I. 1985. Thickness, subglacial relief and volume of Svalbard glaciers based on radio echo-sounding data. Polar Geography, 9 (3), 224-243.

Machío F., Lapazaran J., Dolnicki P., Petlicki M., Głowacki P. & Navarro F. 2007. Preliminary results from radio-echo sounding at Ariebreen, Hornsund, Spitsbergen. In: The Dynamics and Mass Budget of Arctic Glaciers. Extended abstracts. Workshop and GLACIODYN (IPY) meeting, 15-18 January 2007, Pontresina, Switzerland. Institute for Marine and Atmospheric Research, Utrecht University, the Netherlands.

Małecki J., Buchwał A., Rachlewicz G., Rymer K., Strzelecki M. & Wawrzyniak T. 2011. Environmental studies in northern Billefjorden – Institute of Geoecology and Geoinformation A. Mickiewicz University 15th Expedition – Svalbard 2010. In: G. Rachlewicz & J. Małecki (eds.), Institute of Geoecology and Geoinformation A. Mickiewicz University Polar Reports, vol. 1. Bogucki Wydawnictwo Naukowe, Poznań, 52 p., ISBN 978-83-62662-57-9.

Mann D.H. 1986. Reliability of a fjord glacier's fluctuations for paleoclimatic reconstructions. Quaternary Research, Volume 25, Issue 1, p. 10–24

Marciniak M., Szczucińska A. & Dragon K. 2007. Measurements of selected water balance components in Ebbaelva catchments, Svalbard - pilot study. Landform Analysis, 5, 51-54.
Mavlyudov B.G. 2010. Peshchera lednika Bertil, Shpitsbergen: historiya i sovremennost' (Cave of Bertil glacier, Spitsbergen: history and the present). Speleologiya i speleostologiya: Razvitiye i Vzaimodeystviye Nauk. Mezhdunarodnaya Nauchno-Prakticheskaya Konferentsiya, Nabrezhnyye Chelny, 2010, 9-12.
Mazurek M., Paluszkiewicz R., Rachlewicz G. & Zwoliński Z. 2012. Variability of water chemistry in tundra lakes, Petuniabukta coast, central Spitsbergen, Svalbard. The Scientific World Journal, 2012, ID 596516, 13 pp, doi:10.1100/2012/596516
Meier M.F., Dyurgerov M.B., Rick U.K., O'Neel S., Pfeffer W.T., Anderson R.S., Anderson S.P. & Glazovsky A.F. 2007. Glaciers dominate eustatic sea-level rise in the 21st century. Science, 317, 1064-1067.
Melvold K. & Hagen J.O. 1998. Evolution of a surge-type glacier in its quiescent phase: Kongsvegen, Spitsbergen, 1964 – 95. Journal of Glaciology, 44 (147), 394– 404.
Migała K., Piwowar B.A. & Puczko D. 2006. A meteorological study of the ablation process on Hans Glacier, SW Spitsbergen. Polish Polar Research, 27 (3), 243-258.
Migała K., Nasiółkowski T. & Pereyma J. 2008. Topoclimatic conditions in the Hornsund area (SW Spitsbergen) during the ablation season 2005. Polish Polar Research, 29 (1), 73-91.
Moholdt G., Nuth C., Hagen J.O. & Kohler J. 2010a. Recent elevation changes of Svalbard glaciers derived from ICESat laser altimetry. Remote Sensing of Environment, 114 (11), 2756-2767.
Moholdt G., Hagen J.O., Eiken T. & Schuler T.V. 2010b. Geometric changes and mass balance of the Austfonna ice cap, Svalbard. The Cryosphere, 4, 21−34.
Moore J.C., Pälli A., Ludwig F., Blatter H., Jania J., Gądek B., Głowacki P., Mochnacki D. & Isaksson E. 1999. High-resolution hydrothermal structure of Hansbreen, Spitsbergen, mapped by ground-penetrating radar. Journal of Glaciology, 45 (151), 524-532.
Müller F. & Iken A. 1973. Velocity fluctuations and water regime of Arctic valley glaciers. International Association of Hydrological Sciences Publication, 95, 165–82.
Murray T., Dowdeswell J.A., Drewry D.J. & Frearson I. 1998. Geometric evolution and ice dynamics during a surge of Bakaninbreen, Svalbard. Journal of Glaciology, 44 (147), 263-272.
Murray T., Stuart G.W., Miller P.J., Woodward J., Smith A.M., Porter P.R. & Jiskoot H. 2000. Glacier surge propagation by thermal evolution at the bed. Journal of Geophysical Research, 105 (B6), 13491-13507
Murray T., Strozzi T., Luckman A., Jiskoot H. & Christakos P. 2003. Is there a single surge mechanism? Constrasts in dynamics between glacier surges in Svalbard and other regions. Journal of Geophysical Research, 108 (B5), doi:10.1029/2002JB001906
Murray T., Booth A. & Rippin D.M. 2007. Water-content of glacier-ice: Limitations on estimates from velocity analysis of surface ground-penetrating radar surveys. Journal of Environmental and Engineering Geophysics, 12, 87–99.
Nawrot A.P. 2011. Operation of the small glaciated catchment geosystem (Arie, Spitsbergen). PhD thesis, Adam Mickiewicz University, Poznań.
Nesje A., Bakke J., Dahl S.O., Lie Ø. & Matthews J.A. 2008. Norwegian mountain glaciers in the past, present and future. Global and Planetary Change 60, 10-27.
Neumann U. 2006. Climate - glacier links on Bogerbreen, Svalbard. Glacier mass balance investigations in central Spitsbergen 2004/2005. MSc thesis, University of Oslo, Oslo.
Niedźwiedź T. 2004. Współczesne zmiany klimatyczne na Spitsbergenie (Contemporary climate changes in Svalbard). XXX Międzynarodowe Sympozjum Polarne, 23-25 September 2004, Gdynia, 131-134.
Niedźwiedź T. 2006. Główne cechy cyrkulacji atmosfery nad Spitsbergenem (XII.1950-IX.2006) (The main forms of atmospheric circulation above Spitsbergen. December 1950-September 2006). Problemy Klimatologii Polarnej, 16, 91-105.
Niedźwiedź T. 2007. Warunki cyrkulacyjne na Spitsbergenie w latach 2005-2006 (Atmospheric Circulation Conditions in 2005-2006 above Spitsbergen). In: Przybylak R., Kejna M., Araźny A. & Głowacki P. (eds.), Abiotyczne Środowisko Spitsbergenu w latach 2005-2006 w warunkach globalnego ocieplenia,UMK, Toruń, 17-32.
Niedźwiedź T. 2013. Kalendarz typów cyrkulacji atmosfery dla Spitsbergenu — zbiór komputerowy (Calendar of atmospheric circulation types for Spitsbergen - a digital dataset). Uniwersytet Śląski, Katedra Klimatologii, Sosnowiec.
Nienow P.W., Hubbard A.L., Hubbard B.P., Chandler D.M., Mair D.W.F., Sharp M.J. & Willis I.C. 2005. Hydrological controls on diurnal ice flow variability. Journal of Geophysical Research, 110 (F4), DOI: 10.1029/2003JF000112.
Nihoul J.C.J. & Kostianoy A.G. 2009. Influence of Climate Change on the Changing Arctic and Sub-Arctic Conditions. Proceedings of the NATO Advanced Research Workshop, Liège, Belgium 8-10 May 2008. Springer Verlag, Dordrecht, The Netherlands.

Nordli P.Ø. & Kohler J. 2003. The early 20th century warming. Daily observations at Green Harbour, Grønfjorden, Spitsbergen. DNMI KLIMA Rapp. 12/03. Oslo: Det Norske Meteorologiske Institutt.
Nussbaumer S.U., Zumbühl H.J. & Steiner D. 2007. Fluctuations of the 'Mer de Glace' (Mont Blanc area, France) AD 1500–2050: an interdisciplinary approach using new historical data and neural network simulations. Zeitschrift für Gletscherkunde und Glazialgeologie, 40, 5–175.
Nutall A.-M. & Hodgkins R. 2005. Temporal variations in flow velocity at Finsterwalderbreen, a Svalbard surge-type glacier. Annals of Glaciology, 42, 71-76.
Nuth C. & Kääb A. 2011. Co-registration and bias corrections of satellite elevation data sets for quantifying glacier thickness change. The Cryosphere, 5, 271-290.
Nuth C., Kohler J., Aas H. F., Brandt O. & Hagen J. O. 2007. Glacier geometry and elevation changes on Svalbard (1936– 90): a baseline dataset. Annals of Glaciology, 46, 106-116.
Nuth C., Moholdt G., Kohler J., Hagen J. O. & Kääb A. 2010. Svalbard glacier elevation changes and contribution to sea level rise. Journal of Geophysical Research, 115, F01008, doi 10.1029/2008JF001223.
Nuttall A.-M., Hodgkins R. 2005. Temporal variations in flow velocitiy at Finsterwalderbreen, a Svalbard surge-type glacier. Annals of Glaciology, 42, 71-76.
Nye J.F. 1957. The distribution of stress and velocity in glaciers and ice sheets. Proceedings of the Royal Society, A 239, 113–33.
Nye J.F. 1960. The response of glaciers and ice sheets to seasonal and climatic changes. Proceedings of the Royal Society of London, Serie A, 256 (1287), 559-584.
Oerlemans J. 1986. Glaciers as indicators of a carbon dioxide warming. Nature, 320 (6063), 607-609.
Oerlemans J. 1994. Quantifying Global Warming from the Retreat of Glaciers. Science, 264 (5156), 243 - 245.
Oerlemans J. 2005. Extracting a climate signal from 169 glacier records. Science, 308 (5722), 675–677.
Oerlemans J. & Fortuin J.P.F. 1992. Sensitivity of Glaciers and Small Ice Caps to Greenhouse Warming. Science, 258 (5079), 115-117.
Oerlemans J. & Grisogono B. 2002. Glacier winds and parameterisation of the related surface heat fluxes. Tellus, A 54, 440–452.
Oerlemans J. & Nick F.M. 2005. A minimal model of a tidewater glacier. Annals of Glaciology, 42, 1-6.
Ohmura A. 2001. Physical basis for the temperature-based melt-index model. Journal of Applied Meteorology, 40, 753– 761.
Overpeck J., Hughen K., Hardy D., Bradley R., Case R., Douglas M., Finney B., Gajewski K., Jacoby G., Jennings A., Lamoureux S., Lasca A., MacDonald G., Moore J., Retelle M., Smith S., Wolfe A. & Zielinski G. 1997. Arctic environmental change of the last four centuries. Science, 278 (5341), 1251-1256.
Ødegård R.S., Hamran S.E., Bø P.H., Etzelmüller B., Vatne G. & Sollid L. 1992. Thermal regime of a valley glacier, Erikbreen, northern Spitsbergen. Polar Research, 11 (2), 69-79.
Øestby T.I. 2010. Distributed energy and surface mass balance modeling of Austfonna, Svalbard. MSc thesis, University of Oslo, Oslo.
Østrem G. & Brugman M. 1991. Glacier mass-balance measurements. A manual for field and office work. Norwegian Water Resources and Energy Administration, and Environment Canada, National Hydrology Research Institute Science Report no. 4, Saskatchewan, Canada.
Østrem G. & Haakensen N. 1999. Map comparison or traditional mass balance measurements: which method is better? Geografiska Annaler, 81A (4), 703-711.
Pälli A., Moore J.C., Jania J., Kolondra L. & Głowacki P. 2003a. The drainage pattern of Hansbreen and Werenskioldbreen, two polythermal glaciers in Svalbard. Polar Research, 22 (2), 355-371.
Pälli A., Moore J.C. & Rolstad C. 2003b. Firn-ice transition-zone features of four polythermal glaciers in Svalbard seen by ground-penetrating radar. Annals of Glaciology, 37, 298-304.
Paterson W.S.B. 1981. The physics of Glaciers. Pergamon Press, Oxford, pp. 380.
Paterson W.S.B. 1994. The Physics of Glaciers. Pergamon Press, Oxford, pp.480.
Pelicciotti F., Brock B., Strasser U., Burlando P., Funk M. & Corripio J. 2005. An enhanced temperature-index glacier melt model including the shortwave radiation balance: development and testing for Haut Glacier d'Arolla, Switzerland. Journal of Glaciology, 51 (175), 573-587.
Pelto M., Higgins S.M., Hughes T.J. & Fastook J.L. 1990. Modeling mass-balance charges during a glaciation cycle. Annals of Glaciology, 14, 238-241.
Pereyma J. 1983. Climatological problems of the Hornsund area. Acta Universitatis Wratislaviensis, 714, 1-131.
Pereyma J. & Piasecki J. 1988. Warunki topoklimatyczne i hydrologiczne w rejonie lodowca Werenskiold na Spitsbergenie w sezonie letnio-jesiennym 1983 roku (Topoclimatic and hydrological conditions in Werenskiold glacier area in summer-autumn season of 1983). Wyprawy Polarne Uniwersytetu Śląskiego 1980-1984, Prace Naukowe Uniwersytetu Śląskiego w Katowicach nr 910. Uniwersytet Śląski, Katowice, 1988, 107-122.

Petlicki M., Lapazaran J., Navarro F., Głowacki P., Machio F., 2008: Ice volume changes of Ariebreen, Spitsbergen, during 1936-1990-2007. In: The dynamics and mass balance of Arctic glaciers. Extended abstracts, workshop and GLACIODYN (IPY) meeting, IASC

Pettersson, R. 2004. Dynamics of the Cold Surface Layer of Polythermal Storglaciären, Sweden. PhD thesis, Stockholm University, Stockholm.

Piasecki J. & Gluza A. 1988. Wybrane cechy topoklimatu płd. Bellsundu w sezonie wiosenno-letnim 1987 r. (SW Spitsbergen) (Selected elements of topoclimate of S Bellsund in spring-summer season of 1987 (SW Spitsbergen)). XV Sympozjum Polarne, Wrocław, 19-21 May 1988, 217-225.

Pinglot J. F., Pourchet M., Lefauconnier B., Hagen J. O., Isaksson E., Vaikmäe R. & Kamiyama K. 1999. Accumulation in Svalbard glaciers deduced from ice cores with nuclear tests and Chernobyl reference layers. Polar Research, 18, 315– 321.

Pinglot J.F., Hagen J.O., Melvold K., Eiken T. & Vincent C. 2001. A mean net accumulation pattern derived from radioactive layers and radar soundings on Austfonna, Nordaustlandet, Svalbard. Journal of Glaciology, 47, 555−566.

Przybylak R. 2007. Współczesne zmiany klimatu w Arktyce (Contemporary climate change in the Arctic). In: Styszyńska A. & Marsz A. (eds.), Zmiany klimatyczne w Arktyce in Antarktyce w ostatnim pięćdziesięcioleciu XX wieku i ich implikacje środowiskowe.

Przybylak R., Araźny A., Gluza A., Hojan M., Migała K., Sikora S., Siwek K. & Zwoliński Z. 2006. Porównanie warunków meteorologicznych na zachodnim wybrzeżu Spitsbergenu w sezonie letnim 2005 r. (Diversification of meteorological conditions on the western coast of Spitsbergen during summer season of 2005.) Problemy Klimatologii Polarnej 16, 125-138.

Przybylak R., Araźny A. & Ćwiklińska K. 2007a. Warunki meteorologiczne w rejonie lodowca Waldemara (NW Spitsbergen) w sezonie letnim 2005 r. (Meteorological conditions in the region of Waldemar glacier (NW Spitsbergen) in the summer season of 2005). In: Przybylak R., Kejna M., Araźny A. & Głowacki P. (eds.), Abiotyczne środowisko Spitsbergenu w latach 2005-2006 w warunkach globalnego ocieplenia. Uniwersytet Mikołaja Kopernika, Toruń, 51-65.

Przybylak R, Kejna M, Araźny A., Maszewski R., Gluza A., Hojan M., Migała K., Sikora S., Siwek K. & Zwoliński Z. 2007b. Zróżnicowanie warunków meteorologicznych na zachodnim wybrzeżu Spitsbergenu w sezonie letnim 2006 r. (Diversification of meteorological conditions on the western coast of Spitsbergen during summer season of 2006.) In: Przybylak R., Kejna M., Araźny A. & Głowacki P. (eds.), Abiotyczne środowisko Spistbergenu w latach 2005-2006 w warunkach globalnego ocieplenia. (Abiotic environment of Spitsbergen in years 2005-2006 under conditions of global warming.). Uniwersytet Mikołaja Kopernika, Toruń, 179-194.

Pulina M., Pereyma J., Kida J. & Krawczyk W. 1984. Characteristics of the polar hydrological year 1979/80 in the basin of Werenskiold glacier, SW Spitsbergen. Polish Polar Research, 5, 165-182.

Rachlewicz G. 2003a. Warunki meteorologiczne w zatoce Petunia (Spitsbergen środkowy) w sezonach letnich 2000 i 2001 (Meteorological conditions in Petunia Bay (central Spitsbergen) in 2000 and 2001 summer seasons). Problemy Klimatologii Polarnej, 13, 127-138.

Rachlewicz G. 2003b. Uwarunkowania środowiskowe obiegu wody w systemie lodowca Hørbye (środkowy Spitsbergen) (Environmental controls of water routing in Hørbye glacier system (centra Spitsbergen). In: Kostrzewski A. & Szpikowski J. (eds.), Funkcjonowanie geoekosystemów zlewni rzecznych, tom III. Obieg wody – uwarunkowanie i skutki w środowisku przyrodniczym. Bogucki Wydawnictwo Naukowe, Poznań: 353–365.

Rachlewicz G. 2007. Geomorphology outline of the vicinity of Petuniabukta. Landform Analysis, 5, 216-220.

Rachlewicz G. 2009a. Contemporary sediment fluxes and relief changes in high Arctic glacierized valley systems (Billefjorden, Central Spitsbergen). Uniwersytet im. Adama Mickiewicza w Poznaniu, seria geografia nr 87. Wydawnictwo Naukowe UAM, Poznań 2009.

Rachlewicz G. 2009b. River floods in glacier-covered catchments of the High Arctic: Billefjorden-Wijdefjorden, Svalbard. Norsk Geografisk Tidsskrift, 63, 115-122.

Rachlewicz G. & Styszyńska A. 2007. Porównanie przebiegu temperatury powietrza w Petuniabukta i Svalbard Lufthavn (Isfjord, Spitsbergen) w latach 2001-2003 (A comparison of air temperature course in Petuniabukta and Svalbard Lufthavn (Isfjorden, Spitsbergen) in 2001-2003). Problemy Klimatologii Polarnej, 17, 121-134.

Rachlewicz G., Szczuciński W. & Ewertowski M. 2007. Post -"Little Ice Age" retreat rates of glaciers around Billefjorden in central Spitsbergen, Svalbard. Polish Polar Research, 28 (3), 159-186.

Raper V., Bamber J. & Krabill W. 2005. Interpretation of the anomalous growth of Austfonna, Svalbard, a large Arctic ice cap. Annals of Glaciology, 42, 373-379.

Röthlisberger H. & Lang H. 1987. Glacial hydrology. In: Gurnell A. M. & Clark M. J. (eds.), Glacio-fluvial Sediment Transfer. Wiley, New York, 207–84.

Rutter N., Hodson A., Irvine-Fynn T. & Kristensen Solas M. 2011. Hydrology and hydrochemistry of a deglaciating high-Arctic catchment, Svalbard. Journal of Hydrology, 410, 39-50.
Sand K. & Bruland O. 1999. Water balance of three High Arctic river basins in Svalbard. In: J.Eliasson (ed.), Proceedings of the 12th International Northern Research Basins Symposium and Workshop. Reykjavik, Kirkjubaejarklaustur and Hofn, Iceland, 23-27 August 1999. Engineering Institute, University of Iceland.
Sand K., Winther J.-G., Marechal D., Bruland O. & Melvold K. 2003. Regional variations of snow accumulation on Spitsbergen, Svalbard in 1997-99. Nordic Hydrology, 34, 17-32.
Schaefli B., Hingray B. & Musy A. 2007. Climate change and hydropower production in the Swiss Alps: quantification of potential impacts and related modelling uncertainties. Hydrology and Earth System Science 11 (3), 1191-1205.
Schuler T.V. & Melvold K. 2004. Melt water production at Gruvefonna and subglacial water intrusions into Svea Nord Gruva. Technical Report, Department of Geosciences, University of Oslo, Norway. pp. 37.
Schulson E.M. & Duval P. 2009. Creep and fracture of ice. Cambridge University Press, Cambridge.
Schytt V. 1969. Some comments on glacier surges in eastern Svalbard. Canadian Journal of Earth Sciences, 6 (4), Part 2, 867-873.
Sikora S., Araźny A., Budzik T., Migała K. & Puczko D. 2010. Warunki meteorologiczne i biometeorologiczne okolic Hornsundu (Spitsbergen zachodni) w roku 2009 (Meteorological and biometeorological conditions in the Hornsund region (western Spitsbergen) in 2009). Problemy Klimatologii Polarnej, 20, 83-101.
Sikora S., Budzik T., Migała K. & Puczko D. 2011. Warunki meteorologiczne i biometeorologiczne południowego-zachodniego Svalbardu w 2010 roku (Meteorological and biometeorological conditions of south-west Svalbard in 2010). Problemy Klimatologii Polarnej, 21, 213-228.
Skidmore M.L. & M. Sharp. 1999. Drainage system behaviour of a High-Arctic polythermal glacier, Annals of Glaciology, 28, 209–215.
Slater G. 1925. Observations on the Nordenskiold and neighboring glaciers of Spitsbergen, 1921. Journal of Geology, 33, 408-446.
Sobota I. 2007a. Selected methods in mass balance estimation of Waldemar Glacier, Spitsbergen. Polish Polar Research, 28 (4), 249–268.
Sobota I. 2007b. Mass balance monitoring of Kaffiøyra glaciers, Svalbard. In: The Dynamics and Mass Budget of Arctic Glaciers. Extended abstracts. Workshop and GLACIODYN (IPY) meeting, 15-18 January 2007, Pontresina, Switzerland. Institute for Marine and Atmospheric Research, Utrecht University, the Netherlands.
Sobota I. 2007c. Ablation and outflow of Kaffioyra glaciers in 1996-2006, Svalbard. In: The Dynamics and Mass Budget of Arctic Glaciers. Extended abstracts. Workshop and GLACIODYN (IPY) meeting, 15-18 January 2007, Pontresina, Switzerland. Institute for Marine and Atmospheric Research, Utrecht University, the Netherlands.
Sobota I. 2009. The near-surface ice thermal structure of the Waldemarbreen, Svalbard. Polish Polar Research, 30 (4), 317-338.
Sobota I. 2010. Badania glacjologiczne współczesnych zmian lodowca Ireny, Svalbard (Glaciological investigations of contemporary changes of the Irene glacier, Svalbard). Problemy Klimatologii Polarnej, 20, 143-159.
Sobota I. 2011. Snow accumulation, melt, mass loss, and the near-surface ice temperature structure of Irenebreen, Svalbard. Polar Science, 5 (3), 321-336.
Solheim A. 1991. The depositional environment of surging sub-polar tidewater glaciers: a case study of the morphology, sedimentation and sediment properties in a surge-affected marine basin outside Nordaustlandet, northern Barents Sea. Norsk Polarinstitutt Skr. 194.
Solovyanova I. & Mavlyudov B.R. 2007. Mass balance observations on some glaciers in 2004/2005 and 2005/2006 balance years, Nordenskiold Land, Spitsbergen. In: The Dynamics and Mass Budget of Arctic Glaciers. Extended abstracts. Workshop and GLACIODYN (IPY) meeting, 15-18 January 2007, Pontresina, Switzerland. Institute for Marine and Atmospheric Research, Utrecht University, the Netherlands.
Strzelecki M. 2007. The dynamics of suspended and dissolved transport in a High-Arctic glaciated catchment in ablation seasons 2005 and 2006, Bertram River, Central Spitsbergen. Landform Analysis, 5, 82-84.
Strzelecki M. 2009. Suspended and solute transport in a small glaciated catchment Bertram River, Central Spitsbergen, in 2005–2006. Norsk Geografisk Tidskrift, 63 (2), 98-106.
Styszyńska A. & Marsz A. (eds.). 2007. Zmiany klimatyczne w Arktyce i Antarktyce w ostatnim pięćdziesięcioleciu XX wieku i ich implikacje środowiskowe (Climate change in the Arctic and Antarctic and its environmental implications). Wydawnictwo Akademii Morskiej, Gdynia.
Sugden D.E. & John B.S. 1976. Glaciers and Landscape. Arnold, London, pp. 376.
Sund M. & Eiken T. 2004. Quiescent-phase dynamics and surge history of a polythermal glacier: Hessbreen, Svalbard. Journal of Glaciology, 50 (171), 547-555.

Sund M., Eiken T., Hagen J.O. & Kääb A. 2009. Svalbard surge dynamics derived from geometric changes. Annals of Glaciology, 50 (52), 50-60.
Svendsen J.I. & Mangerud J. 1997. Holocene glacial and climatic variations on Spitsbergen, Svalbard. The Holocene, 7, 145-157.
Szczuciński W., Zajączkowski M. & Scholten J. 2009. Sediment accumulation rates in subpolar fjords - Impact of post-Little Ice Age glaciers retreat, Billefjorden, Svalbard. Estuarine, Coastal and Shelf Science, 85 (30), 345-356.
Szuman I. & Kasprzak L. 2010. Glacier ice structures influence on moraines developement (Hørbye glacier, Central Spitsbergen). Quaestiones Geographicae, 29 (1), 65-73.
Troitsky L.S. 1988. O balanse massy lednikov raznykh typov na Shpitsbergene (On the mass balance of different types of glaciers on Spitsbergen). Materialy glyatsiologicheskikh issledovaniy, 63, 117-121.
Ueda H. & Talalay P. 2007. Fifty years of Soviet and Russian drilling activity in polar and non-polar ice. A chronological history. US Army Corps of Engineers. Engineer Research and Development Center, October 2007.
Van de Wal R.S.W. & Oerlemans J. 1995. Response of valley glaciers to climate change and kinematic waves: a study with a numerical ice-flow model. Journal of Glaciology, 41, 142–52.
Van de Wal R.S.W., Greuell W., Van den Broeke M.R., Reijmer C.H. & Oerlemans J. 2005. Surface mass-balance observation and automatic weather station data along a transect near Kangerlussuaq, West Greenland. Annals of Glaciology, 42, 311-316.
Van den Broeke M., van As D., Reijmer C. & van de Wal R. 2004. Assessing and improving the quality of unattended radiation observations in antarctica. Journal of Atmospheric and Oceanic Technology, 21(9), 1417–1431.
Van Pelt W.J.J., Oerlemans J., Reijmer C.H., Pohjola V.A., Pettersson R. & van Angelen J.H. 2012. Simulating melt, runoff and refreezing on Nordenskioldbreen, Svalbard, using a coupled snow and energy balance model. The Cryosphere, 6, 641-659.
Vieli A., Jania J., Blatter H. & Funk M. 2004. Short-term velocity variations on Hansbreen, a tidewater glacier in Spitsbergen. Journal Of Glaciology, 50 (170), 389–398.
WGMS (World Glacier Monitoring Service) 2012. Digital mass balance database. WGMS website, http://www.geo.uzh.ch/microsite/wgms/index.html
Willis I.C., Rippin D.M. & Kohler J. 2007. Thermal regime changes of the polythermal Midre Lovenbreen, Svalbard. In: The Dynamics and Mass Budget of Arctic Glaciers. Extended abstracts. Workshop and GLACIODYN (IPY) meeting, 15-18 January 2007, Pontresina, Switzerland. Institute for Marine and Atmospheric Research, Utrecht University, the Netherlands.
Winther J.-G., Bruland O., Sand K., Killingtveit Å. & Marechal D. 1998. Snow accumulation distribution on Spitsbergen, Svalbard, in 1997. Polar Research, 17(2), 155–164.
Witoszová D. & Láska K. 2011. Klimatické poměry zátoky Petunia, Billefjorden (Špicberky) v období 2008-2010 (Climate conditions of the coastal zone of Petuniabukta, Billefjorden (Spitsbergen) in the period 2008-2010). In: Středová H., Rožnovský J. & Litschmann T. (eds.), Mikroklimat a mezoklimat krajinnych struktur a antropogennich prostredi. Skalni mlyn, 2-4 February 2011.
Wójcik G., Marciniak K. & Przybylak R. 1983. Wilgotność powietrza w sezonie letnim na nizinie nadmorskiej Kaffiøyra i lodowcu Waldemara (NW Spitsbergen) (Air humidity in the summer season on a coastal plain Kaffiøyra and Waldemar glacier (NW Spitsbergen)). Polskie Badania Polarne 1970-1982. X Sympozjum Polarne, Uniwersytet Mikołaja Kopernika, Toruń, 187-199.
Zagórski P., Siwek K., Gluza A. & Bartoszewski S.A. 2008a. Changes in the extent and geometry of the Scott Glacier, Spitsbergen. Polish Polar Research, 29 (2), 163-185.
Zagórski P., Siwek K. & Gluza A. 2008b. Zmiany zasięgu czoła i geometrii lodowca Renarda (Spitsbergen) na tle zmian klimatycznych XX wieku (Changes in the front extent and geometry of Renard Glacier (Spitsbergen) in the background of the 20th century climate changes). Problemy Klimatologii Polarnej, 18, 113-125.
Zemp M., Hoelzle M. & Haeberli W. 2009. Six decades of glacier mass-balance observations: a review of the worldwide monitoring network. Annals of Glaciology, 50, 101-111.
Zhuravlev A.B., Macheret Yu.Ya. & Bobrova. L.I. 1983. Radiolokalitsyonniye issledovaniye na polyarnom lednike s zimnym stokom (Radio-echo sounding investigations on a polar glacier with winter discharge). Materialy glyatsiologicheskikh issledovaniy, 46, 143-149.
Ziaja W. & Pipała R. 2007. Glacial recession 2001-2006 and its landscape effects in the Lindströmfjellet-Håbergnuten mountain ridge, Nordenskiöld Land, Spitsbergen. Polish Polar Research, 28 (4), 237-243.
Zwally H.J., Abdalati W., Herring T., Larson K., Saba J. & Steffen K. 2002. Surface melt-induced acceleration of Greenland ice-sheet flow. Science, 297 (5579), 218-222, 10.1126/science.1072708

Zwoliński Z., Kostrzewski A. & Rachlewicz G. 2008. Environmental changes in the Arctic. In: Singh S., Starkel L. & Syiemlieh H.J. (eds.), Environmental Changes and Geomorphic Hazards. North-Eastern Hill University, Shillong, Bookwell, New Delhi 2008: 23-36.